Evaluation of spore wall chemistry as a novel biochemical proxy for UV·B radiation

Thesis

UNRESTRICTED

Evaluation of spore wall chemistry as a novel biochemical proxy for UV-B radiation

A thesis submitted for the degree of Doctor of Philosophy

August 2008

Wesley T. Fraser

BSc. Hons. (University of Birmingham)

BSc. (University of Glamorgan)

MSc. (University of East Anglia)

Volcano Dynamics Group, Department of Earth & Environmental Sciences,

The Open University, Milton Keynes,

MK7 6AA, UK

Submission date: 29 August 2008

Date of award 21 January 2009

Abstract

The stratospheric ozone layer provides protection for Earth's land-based organisms against harmful ultraviolet (UV) radiation, but the past century has seen the ozone layer compromised as a result of human activity, resulting in commensurate variations in surface UV-B flux. Despite the importance of UV radiation to the well-being of life, reliable records of surface UV-B flux only exist for a short period of time (20-30 years). In order to gain a deeper understanding of the behaviour of ozone and UV-B flux in the past, an alternative method of determining UV-B is required. Changes in spore chemistry have been proposed as a palaeo-monitor of UV-B flux, which can then be related to stratospheric ozone abundance. By employing the rapid and inexpensive technique of FTIR microspectroscopy to investigate changes in spore chemistry, a large dataset spanning seven different spatial and temporal UV regimes has been generated in order to evaluate the feasibility of routine usage of a spore-based UV-B proxy. Exploring contemporary samples grown under controlled UV conditions and spores preserved in historical archives reveals that modern-day and recent spore chemistry show a positive relationship with known and calculated UV-B flux, with additional environmental factors such as cloudiness and vegetation canopy cover superimposed on these results. Examination of fossil spores obtained from sediments and experimentally matured specimens provides an insight into the chemical changes that occur in organic matter after incorporation into sediments, even under mild burial conditions. This thesis explores the potential of spore chemistry to act as a proxy monitor of past UV-B flux and is the first concerted attempt at applying FTIR spectroscopy to the investigation of spore chemistry in this way.

Acknowledgements

I would like to thank the following people and organisations, without whom this work would not have been possible:

My supervisors Mark Sephton, Steve Self, Charles Wellman, Dave Beerling and David James for providing me with the opportunity to conduct this research, as well as continued guidance and assistance throughout my time at the OU. NERC, Thermo Fisher Scientific and EU-ATANS grant are kindly thanked for providing me with financial support. In addition to my official supervisors, I would also like to thank Barry Lomax, Jon Watson, Sarah Sephton and Terry Callaghan and all at ANS for their invaluable help.

Peter Edwards (Kew Gardens) and Adele Smith (Royal Botanical Gardens, Edinburgh) provided access to sample collections and excellent advice.

I owe a debt of gratitude to my fellow PhD students at the OU; I fear my time in Milton Keynes would not have been so much fun without you all! Particular mention should go to Dave, Chris and Josh for being excellent housemates – my capacity for video game playing, spud-cannon construction and whisky consumption have all improved immeasurably. Carl for allowing me to drive various vans on his behalf, providing fun fieldwork and knowledge of horse avoidance tactics. RocSoc and PGSS for all non-work-related activities, and The Reelers, Sparta, No Balls, Etna All-Stars, A bunch of flankers, The Hookers and The OU touch-rugby club for providing me with enough sport to keep me occupied and perpetually tired.

Finally, a big thank you to my family for providing unfaltering support, not only throughout the course of my PhD, but for enabling me to follow whichever path I so wished. And thanks to Sam for putting up with me – it's a tough job!

Contents

Figures

Tables

Equations

Plates

Notes

This thesis is presented as a series of papers, and as such each chapter may be read as a stand-alone piece of work.

At the time of writing Chapter 2 is ready for submission to *Photochemistry & Photobiology* and Chapter 6 is ready for submission to *Organic Geochemistry*. In addition, an article based on Chapter 3 is in preparation for submission to *Journal of Experimental Botany*.

Prof. Mark Sephton performed GC-MS analysis for Chapter 2. Dr. Jon Watson performed GC-MS analysis and provided experimental assistance in Chapter 6.

1 Introduction

1.1 Our Atmosphere

A remarkably thin layer of gas (~90% of gas less than 60km altitude) envelopes Earth - our atmosphere - an internally dynamic, yet relatively stable mass that sustains life on our planet. Our atmosphere is a vital component of the Earth system; it provides us with air to breath, stores and distributes water to grow crops, and provides protection against the harmful effects of incoming solar radiation.

In recent decades it has been found that the natural state of balance of the atmosphere can be compromised in a number of ways. Human activity has been identified as a key factor in the present-day, but natural events have also severely impacted upon the state of the atmosphere. Ozone depletion induced by both natural and anthropogenic modification of the atmosphere has been of particular concern due to the consequent changes in incoming solar ultraviolet radiation. The work presented here evaluates the potential of plant chemistry to act as a proxy for measuring ultraviolet radiation, and ultimately stratospheric ozone. The following sections review the background for this topic.

1.2 Origin and composition of the atmosphere

1.2.1 Ancient atmospheres

Early Earth lacked the atmosphere we know today; initially the newly formed planet was shrouded in a cloud of primordial hydrogen and helium, but could not sustain such an atmosphere due to greater vigour of the solar wind than at present, which swept away any gas surrounding the Earth (Figure 1.1). Once the strength of the solar wind had subsided, gases began to accumulate at the surface of the earth (Lunine, 1999). The resultant atmosphere is

most likely to have been the product of both outgassing from volcanic activity (Warr & Smith, 1995) (mainly CO_2, $H_2O_{(v)}$ and SO_2, with minor amounts of H_2S, CO, HCl, HF, H_2, N_2 and noble gases; Delmelle & Stix, 2000) and input from meteoritic/cometary impacts (Owen & Bar-Nun, 1995), although which of these factors is of greatest importance is still a hotly debated topic. With time this proto-atmosphere evolved, mediated by physical, chemical and eventually biological influence.

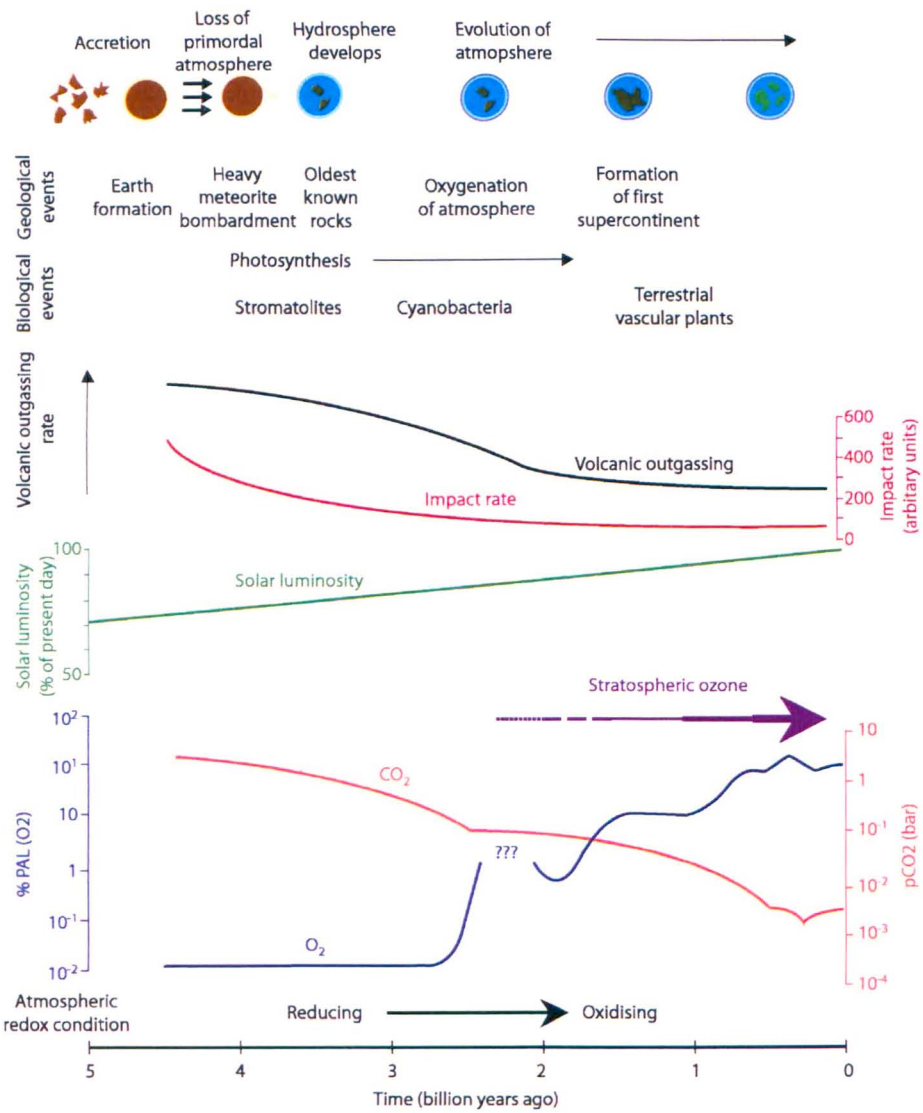

Figure 1.1 Summary of origin and evolution of Earths' atmosphere since the accretion of Earth ~4.5 Ga. Geological events summarised from: Lunine (1999). Biological events summarised from: Canfield (2005); Rozema *et al.* (1999). Volcanic outgassing history based on Catling & Claire (2005); Kump & Barley (2007). Cometary impact rates from: Shoemaker (1983); Lunine (1999). Solar luminosity calculated based on information from: Shaviv (2003); Bard & Frank (2006). Atmospheric gas concentrations and oxidation state from: Rozema *et al.* (1999); Canfield (2005); Sheldon (2006); Kump & Barley (2007).

One of the most significant events in the development and evolution of Earths atmosphere is the period of oxygenation that occurred approximately 2.5 Ga (billion years ago). Oxygenation of the atmosphere is thought to be the result of water-borne photosynthetic activity, thus the Earth-atmosphere system was modified by early life (Catling & Claire, 2005). Evidence for this shift from anoxic conditions to an oxygenated atmosphere (Figure 1.1) is provided by the presence of banded iron formations that contain iron in its reduced state (Fe^{2+}). The presence of reduced iron indicates there must have been a period where the atmosphere lacked oxygen. Up-sequence of these banded iron formations the existence of oxidised iron (Fe^{3+}) indicates conditions are no longer anoxic; Fe^{2+} has been oxidised to Fe^{3+}. The accumulation of oxygen in the atmosphere was certainly not a rapid process; a period of approximately 1 billion years elapsed between the first evidence of photosynthesising lifeforms and the build up of oxygen in the atmosphere (Figure 1.1). Recent work has suggested that oxygenation of the atmosphere took so long because there were vast oxygen sinks that needed to be oxidised before free atmospheric oxygen could exist (Kump & Barley, 2007).

1.2.2 The modern atmosphere

Modern atmospheric composition (Table 1.1) is dominated by the relatively stable diatomic nitrogen molecule (N_2) comprising ~78 % (0.78 mol/mol) of the total atmosphere, oxygen (O_2) accounts for ~20 %, argon (Ar) <0.1 %; $H_2O_{(v)}$ is subject to considerable local and regional variations, thus is not included in the mixing ratios quoted here. The remainder of the gases present are referred to as trace gases because of their extremely low concentration (Jacob, 1999). Although the trace constituents are in very low concentrations, their atmospheric impact is certainly not negligible. One such trace constituent is ozone.

Table 1.1 Modern day composition of Earths' atmosphere (from Visconti, 2001).

Gas	Mixing ratio
Nitrogen (N_2)	0.781
Oxygen (O_2)	0.209
Argon (Ar)	0.0093
Carbon dioxide (CO_2)	0.0034
Methane (CH_4)	$1.7\text{-}3\times10^{-6}$
Nitrous oxide (N_2O)	3.1×10^{-7}
Carbon monoxide (CO)	$0.4\text{-}2\times10^{-7}$
Ozone (O_3)	$0.1\text{-}1\times10^{-7}$
Nitrogen oxides (NO, NO_2)	$0.2\text{-}5\times10^{-10}$
Sulphur dioxide (SO_2)	3×10^{-10}

1.3 Ozone

Ozone (O_3) is a triatomic form of molecular oxygen that occurs naturally in the atmosphere, with approximately 90% occurring between 10-50 km altitude (i.e. the stratosphere) (Staehelin *et al.*, 2001). The majority of ozone is concentrated in the lower stratosphere, with greatest abundance centred at approximately 22 km (Barry & Chorley, 1998) giving rise to the popular reference the "ozone layer", although the exact altitude is subject to considerable latitudinal variation. The stratospheric ozone layer can be defined using a vertical temperature profile of the atmosphere (Figure 1.2). A temperature inversion is observed across the region of the ozone layer; reaching a maximum at approximately the altitude of the stratopause (~ 45-50 km). The inversion occurs near the stratopause because the process of ozonogenesis is mildly exothermic, ozone abundance is high enough to allow photochemical interactions and solar ultraviolet radiation is still relatively high in order to drive ozonogenesis (Barry & Chorley, 1998).

The remaining 10% of ozone in the atmosphere is found in the troposphere where it not only leads to the warming of the troposphere (i.e. as a greenhouse gas), but is also a toxic pollutant. Ozone is present in the troposphere due to: i) downward transport from the overlying

stratosphere, and ii) *in situ* production in the troposphere *via* cycling of NO_x in reactions with peroxy radicals (Equations 1.1 to 1.3):

Equation 1.1 Formation of NO_x; mechanism 1.

$$HO_2 + NO \longrightarrow OH + NO_2$$

Equation 1.2 Formation of NO_x; mechanism 2.

$$CH_3O_2 + NO \longrightarrow CH_3O + NO_2$$

then,

Equation 1.3 Generation of tropospheric ozone.

$$NO_2 + h\nu \xrightarrow{O2} NO + O_3$$

where HO_2 = peroxy radicals, NO = nitric oxide molecules, OH = hydroxyl radicals, CH_3O_2 = methylperoxy radicals, $h\nu$ = incoming solar radiation.

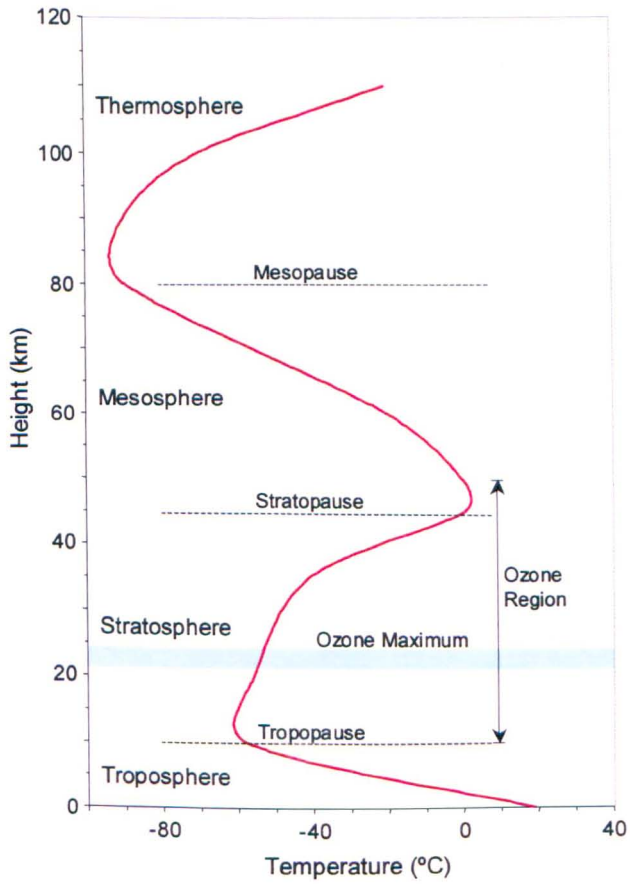

Figure 1.2 Temperature profile of the atmosphere. Temperature inversion within the stratosphere is evident from ~ 15km to ~ 45 km altitude (adapted from: Oke, 1987 and Barry & Chorley, 1998).

Ozone is produced in the tropical stratosphere *via* photochemical interaction between diatomic oxygen (O_2) and incoming solar radiation – the so-called Chapman cycle:

Equation 1.4 Production of oxygen free radicals.

$O_2 + h\nu \longrightarrow O\bullet + O\bullet$

Equation 1.5 Generation of stratospheric ozone.

$O\bullet + O_2 + M \longrightarrow O_3 + M$

where diatomic oxygen (O_2), the chemical precursor to ozone, is broken down homolytically into monatomic oxygen radicals ($O\bullet$) by the absorption of solar radiation ($h\nu$ – in fact, ultraviolet-C radiation (UV-C); λ = 100-280 nm) (Equation 1.4). In the presence of other atmospheric molecules, M, such as nitrogen (N_2), excess energy can be dissipated to the surrounding environment, and $O\bullet$ reacts with more O_2 to form O_3 (Equation 1.5) (Barry & Chorley, 1998). It is apparent from this mechanism that ozone cannot exist without the chemical precursor O_2; hence in geological history during periods of anoxic conditions, O_3 could not have been present in the atmosphere (Figure 1.1). The lack of stratospheric O_3 in the past has serious ramifications for Earth's biota, as will be discussed in later sections.

Atmospheric ozone is measured as the total amount in a vertical column (total column ozone) and quoted in Dobson Units (DU) (1 DU = 2.69 x 10^{16} molecule cm^{-2}) (UNEP, 2006). Ozone measurements were first conducted on a regular basis using ground-based instruments at Arosa in Switzerland, where a continuous record exists since 1927 (Staehelin *et al.*, 1998a, 1998b). However, it was not until the 1950's that well distributed ground-based measurements provided reasonable global coverage. Ground-based measurements are complemented by ozonesonde recordings; ozonesonde measurements are obtained *via* weather balloon-mounted instruments. The advantage of data obtained from ozonesonde is that it provides not only total column ozone measurements, but also ozone profiles vertically through the atmospheric column. Regular ozonesonde release programs have enabled the monitoring of changes in atmospheric ozone profiles through time. Recent reviews show that

during the period 1980-1990 total column ozone decreased by approximately 3 to 4% from the 1964-1980 mean value and has remained relatively stable at this level (3 to 5% reduction) since the latter half of the 1990's in all regions except the tropics (WMO, 2002, 2006). Tropical regions are highlighted as an area of interest because a small decrease (~3%) has been observed in the lowermost stratosphere, yet the total column ozone remains essentially unchanged. This discrepancy has been attributed to increases in tropospheric ozone equal to the decrease seen in the stratosphere (WMO, 2006).

Possibly the greatest technological advance in atmospheric observation was the advent of satellite-borne instruments. Since the launch of the Nimbus-7 satellite in 1978, essentially global-wide measurements of total column ozone have been available from the Total Ozone Mapping Spectrometer (TOMS) instruments (http://jwocky.gsfc.nasa.gov/). The later satellites Meteor-3 and Earth Probe progressively superseded Nimbus-7; both of these instruments also provided 1° x 1.25° (latitude/longitude) resolution gridded daily TOMS datasets. The latest instrument is the ozone monitoring instrument (OMI) aboard the Aura satellite. Compilation of data from all of these missions results in a continuous satellite-based record from 1979 to the present day.

Total column ozone varies greatly with latitude; equatorial regions are found to have the lowest amounts of total column ozone (~200 DU), whilst polar regions, particularly the Arctic, often experience ozone column thicknesses of up to 500 DU (Rex *et al.*, 2004). Although equatorial regions experience the lowest ozone column thickness, this part of the globe has the most stable ozone column. Polar regions are subject to large variability in total ozone, as evident by the now regular occurrence of the Antarctic "ozone hole" that has been known to reach total column ozone values of just 100 DU in recent years (WMO, 2006). The process of ozonogenesis takes place in the stratosphere at tropical latitudes and the ozone produced is rapidly transported polewards *via* the so-called Dobson-Brewer circulation (also

known as the Lagrangian-mean meridional circulation) (Figure 1.3). This transport of ozone leads to the distribution pattern observed, where the tropics can be regarded as an ozone 'source' and polar regions as an ozone 'reservoir' (Visconti, 2001).

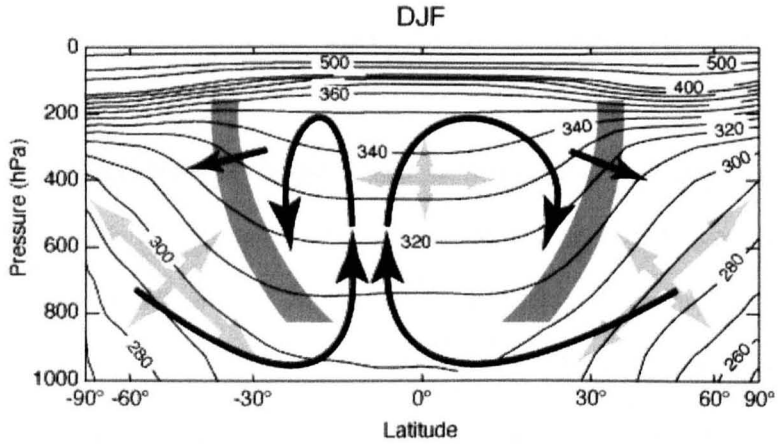

Figure 1.3 Generalised global-scale zonal-mean transport circulation for December-February (From: Bowman & Erukhimova, 2004).

Under unperturbed atmospheric conditions ozone production would be in equilibrium with ozone destruction. As already discussed, O_2 molecules in the stratosphere absorb UV-C radiation and dissociate to form O• radicals, which then react with other O_2 molecules to form O_3. Once formed, O_3 absorbs radiation in the UV-B band (λ = 280-315 nm), which leads to the photolytic decomposition of O_3, again forming various configurations of O_2 and O• radicals (Visconti, 2001) (Equations 1.6 and 1.7). The decomposition of ozone is facilitated by the presence of other radical species (X) in the atmosphere:

Equation 1.6 Mechanism of ozone destruction; stage 1.

$O_3 + X \rightarrow O_2 + XO$

Equation 1.7 Mechanism of ozone destruction; stage 2.

$XO + O \rightarrow X + O_2$

X, the catalyst is conserved throughout this mechanism, therefore can be cancelled in the net reaction:

Equation 1.8 Net reaction of ozone destruction.

$O + O_3 \rightarrow 2O_2$

As can be seen from Equations 1.4, 1.5 and 1.8, the formation and destruction of O_2 and O_3 in the stratosphere is a continual and globally balanced dynamic process driven by ultraviolet radiation in the middle atmosphere. It is most likely that such a balance has been maintained throughout the oxygenated period of Earth's history; however this has not been the case in recent times, where the rate of ozone destruction has outweighed the rate of ozone production.

1.3.1 Ozone Depletion

Observations of significant reductions in total column ozone above Antarctica on an annual basis triggered concern about the effect that human activity has upon the atmosphere (Farman *et al.*, 1985; Solomon, 1999). Molina & Rowland (1974) highlighted anthropogenic emissions of halogenated compounds as contributing to the regular decline in ozone abundance. The cyclical nature of ozone depletion above Antarctica caused by the interaction of ozone depleting substances (ODS) and incoming solar radiation is modulated by circulatory conditions pertaining to the region. Atmospheric circulation patterns essentially isolate Antarctica for part of the year, preventing exchange of air masses with higher latitudes, thus ozone-destroying reactions occur within the Antarctic air mass without ozone levels being replenished by adjacent, ozone-rich air masses. The net result is that the Antarctic air mass has a relative deficiency of ozone, hence an "ozone hole". Whilst Antarctica is a special case due to the isolating atmospheric circulation effects and therefore not truly representative of the rest of the globe, it serves to exemplify the impact of ozone destruction within our atmosphere.

Globally, total column ozone is found to have reduced by approximately 3.5 % for the period 2002-2005, compared with the mean value for 1964-1980 (WMO, 2006). Three factors are thought to cause to variations in total column ozone: 1) natural fluctuations in O_3 abundance, either a) due to varying rates of ozone production linked to incoming solar flux (Bard &

Frank, 2006) and physical catalysis of ozone destruction reactions, or b) on geological timescales, due to changes in atmospheric abundance of O_2 (Rozema, *et al.*, 1999; Harfoot *et al.*, 2007); 2) anthropogenic emissions that ultimately lead to an enhanced rate of ozone destruction (Molina & Rowland, 1974); and 3) stratospherically significant volcanic eruptions have been shown to alter total column ozone for a period of 2-4 years after eruption *via* heterogeneous surface chemistry effects on sulphate aerosol particles (Coffey, 1996; Robock, 2000; UNEP, 2006; WMO, 2006).

1.3.1.1 Natural fluctuations

Prior to Earth possessing an oxygenated atmosphere (~2.5 Ga) it would not have been possible for ozone to freely exist anywhere in the atmosphere because O_2 is required as the chemical precursor to O_3 (as outlined above). Thus on geological timescales the occurrence and abundance of O_3 is intrinsically linked to the oxidation state of the atmosphere (Harfoot *et al.*, 2007).

Near decadal variations in ozone abundance are observed and have been linked to the eleven-year solar cycle. Evidence suggests that in-phase modulation of total column ozone occurs due to increased solar input, therefore increased photochemical production of ozone *via* absorption of UV-C radiation in the stratosphere (Equations 1.1 and 1.2) (WMO, 2006).

Superimposed upon the long-term decreasing trend of stratospheric ozone is seasonal variability. Polar regions are greatly affected by the wide variation in diurnal solar flux, ranging from essentially 24-hour daylight to 24-hour darkness (polar winter). The formation of ice particle-bearing polar stratospheric clouds (PSCs) during the dark polar winter provide a catalytic surface for the heterogeneous destruction of ozone, but the process of ozone destruction does not occur until energy is provided in the form of ultraviolet radiation. When polar spring occurs, the sudden input of energy drives the rapid ozone depleting reactions

because of the significant availability of catalytic sites (PSCs) and a large ozone 'reservoir' that has built up. As already mentioned above, Antarctica is a prime example of this due to the isolating atmospheric vortex that occurs during polar winter and spring. Not until polar summer is reached does the isolating circulation pattern dissipate and free exchange with surrounding air masses begins to replenish ozone levels (Hofmann *et al.*, 1997). PSCs form more readily, are more extensive and persist longer when middle stratospheric temperatures are colder. Again, the isolating vortex surrounding Antarctica enables low temperatures to occur on a regular basis. The Arctic atmosphere is subject to weaker winter vortices, with a greater degree of influx from lower latitudes, resulting in generally warmer conditions. In recent years (1990's onwards) the Arctic air mass has experienced lower temperatures, allowing greater persistence and larger volume of PSCs to exist during some winter-spring periods, thus leading to higher than average springtime ozone depletion (Rex *et al.*, 2004; WMO, 2006).

1.3.1.2 Ozone depleting substances

Ozone Depleting Substances (ODS) have been defined as "...chemical substances of natural and anthropogenic origin... thought to have the potential to modify the chemical and physical properties of the ozone layer" (UNEP, 1985). Only ODS regarded as "long-lived compounds" are discussed here because "very short-lived substances" (VSLS) do not remain in the atmosphere long enough to be of considerable importance to this study (with the exception of some of the brominated VSLS), generally having an atmospheric lifetime of 6 months or less (WMO, 2006).

Anthropogenic sources of ODS have received the most attention relating to ozone depletion due to the rapid and significant effect such emissions have upon on ozone, evident in the many records of decreasing ozone from around the globe (WMO, 2006). It should be noted that there are also many natural sources for most groups of ODS (Table 1.2).

Table 1.2 Common ozone depleting substances and their source. FHAs = fully halogenated alkanes; PHAs = partially halogenated alkanes. Primary source of NO_x is N_2O. Tick marks in brackets indicate minor sources. Compiled from WMO 2002; 2007.

Core element	Compound	Formula	Anthropogenic	Natural
Carbon	Carbon monoxide	CO	✓	✓
	Carbon dioxide	CO_2	✓	✓
	Methane	CH_4	✓	✓
	Hydrocarbons	variable	✓	✓
Nitrogen	Nitrous oxide	N_2O	(✓)	✓
	Nitrogen oxides	NO_x	-	-
Halogens	FHAs	variable	✓	
	PHAs	variable	✓	(✓)
Hydrogen	Hydrogen	H_2	✓	✓
	Water	H_2O		✓

The only ODS groups that do not have significant natural sources are the fully halogenated alkanes (FHAs), partially halogenated alkanes (PHAs) and nitrogen oxides (NO_x). FHAs are solely anthropogenic in origin, either as a final product (chlorofluorocarbons (CFCs), halons) or as a by-product of the formation of CFCs and halons (i.e. carbon tetrachloride - CCl_4). PHAs have a predominantly anthropogenic source; the exceptions to this rule are methyl chloride (CH_3Cl) and methyl bromide (CH_3Br). It has been proposed that methyl chloride is released in significant quantities from a number of natural sources, the greatest contributions from tropical and sub-tropical plants and corresponding dead vegetation, oceans, salt marshes and fungi. In total, natural sources of methyl chloride account for ~80-90 % of total global emissions (WMO, 2006). The major net source of methyl bromide is thought to be coastal waters, although the data are sparse and have considerable associated errors. Other sources are recognised, such as the open ocean, but are balanced by acting as approximately equal-sized sinks for methyl bromide (WMO, 2006). Nitrogen oxides are a different case because they are not directly emitted from natural or anthropogenic sources; they are the product of photochemical reactions in the atmosphere involving N_2O. NO_x catalytically destroys ozone, with the end result of forming NO_2 and O_2 species (Portmann *et al.*, 1999).

Ozone depletion occurs when ODS are photolytically degraded to form free radical species. The energy required to dissociate and form radical species is provided by the incoming far-ultraviolet wavelength radiation of solar input (Molina & Rowland, 1974). One source of highly reactive radicals is halogenated compounds; these generate halogen radicals (i.e. Cl•, F•, I•, Br•) upon breakdown that go on to readily react with O_3 molecules following the generalised mechanism outlined by Equations 1.4 and 1.5, where X is replaced by one of the halogen radicals.

1.3.1.3 Volcanic eruptions

Explosive volcanic eruptions have been observed to have an impact on atmospheric chemistry *via* the injection of sulphur dioxide (SO_2) into the stratosphere that can lead to the formation of sulphate aerosols (WMO, 2006). Stratospheric aerosols exist as a loosely defined layer (P = 20-100 hPa; T = 200-240 K; pH_2O = $5x10^{-2}$-$1x10^{-3}$ Pa) and primarily consist of sulphate species in an unperturbed atmosphere (Visconti, 2001). Recent work has found no significant trend in non-volcanic stratospheric aerosol over the period 1970-2004 (Deshler *et al.*, 2006), suggesting that the stratospheric aerosol layer column depth is relatively constant on the order of decades. This aerosol layer is replenished by sulphur input from volcanic eruptions and is an integral part of the middle atmosphere. Sulphate aerosols play a vital role in atmospheric ozone chemistry as the aerosol surface provides a catalytic site for the production of active forms of chlorine from chlorine nitrate (Visconti, 2001). Catalysis of reaction is achieved by gas molecules colliding with the aerosol where they temporarily adhere for a longer period of time than would be expected by such a collision. The increased residence on the surface of the aerosol increases the probability of collision with another gas molecule, hence overall increasing the occurrence of reactions.

The impact of volcanic eruptions on stratospheric chemistry was clearly demonstrated by the eruption of Mt. Pinatubo (Indonesia, 15° 08'N 120° 21'E) on 15th June 1991. Ozone

measurements recorded just months after the eruption showed a decrease of 5-8% at tropical latitudes. By early 1993 the globally averaged total ozone column had reduced by up to 10% with the northern hemisphere experiencing the greatest ozone deficit; some more localised regions experienced much greater than 10% reduction (Hoffman *et al.*, 1994; Randel *et al.*, 1995; Coffey, 1996; see also Francis & Oppenheimer, 2004).

1.4 Ultraviolet radiation

Ultraviolet (UV) radiation is the region of the electromagnetic spectrum between visible and X-rays, and can be further divided into three wavelength bands. Ultraviolet-A (UV-A) has the longest wavelength (315-400 nm), ultraviolet-B (UV-B) has a range of 280-315 nm, and ultraviolet-C (UV-C) has the shortest wavelength (100-280 nm). The source of all UV that reaches Earth is the Sun, which typically emits radiation in the range of 150-3000 nm (UV to near-infrared) (Oke, 1987). UV radiation accounts for approximately 5% of terrestrial solar radiation energy input (Diffey, 2004).

All wavelengths of UV radiation are found to be harmful to living organisms, with increasing severity moving from long to shorter wavelengths, thus UV-A is relatively less harmful than UV-B, which in turn is relatively less harmful than UV-C. The relative harmfulness of UV is in accordance with fundamental physics, where shorter wavelengths possess greater energy than longer wavelength radiation.

UV radiation has been associated with a number of detrimental health issues, including skin cancer, ocular damage and immunosuppression in humans (Madronich *et al.*, 1998; Diffey, 2004), as well as deleterious effects observed in animal populations (Kiesecker *et al.*, 2001). Increased levels of UV have been linked with reduction in crop yield (Caldwell *et al.*, 1998) and may possibly influence the carbon cycle by altering decomposition rates of dead vegetative matter (Paul *et al.*, 1999). It should be emphasised that the greatest risk posed by UV radiation

to all life that underlies the above-mentioned effects, is the potential to cause genetic mutations by damaging DNA sequences.

1.4.1 Natural protection from UV radiation

Presently, humans have the capacity to provide themselves with a degree of protection from the harmful effects of UV radiation by the application of epidermal sunscreens. However, our fellow terrestrial-bound lifeforms do not enjoy such a luxury; they simply have to rely upon naturally occurring shielding from UV radiation. Natural UV filters are thought to have been an important factor in the development of life on Earth, particularly the transition from marine to terrestrial environs. It is proposed that much earlier in Earth's history UV flux incident upon Earth's surface was much higher than at present despite the faint sun paradox, thus UV-protection mechanisms would been an important evolutionary development (Towe, 1996; Rozema *et al.*, 1997; Rettberg *et al.*, 1998). Natural protection from UV is provided in one of two ways, external filtering of UV or internal defence mechanisms; these will be dealt with in turn below.

1.4.1.1 External filters

An external UV filter is one that attenuates or completely blocks incoming UV radiation, and is a natural consequence of the environment under consideration, rather than being under any direct biological control. The result of an external filter is an environment with equable UV conditions whereby the detrimental effects of UV no longer pose a threat to life.

The most important external UV filter for early life was the overlying water column in marine environments. Water is found to strongly attenuate UV radiation even at relatively shallow depths, thus creating an environment with sufficiently low UV-B flux to sustain life, whilst allowing photosynthesis to proceed (Rozema *et al.*, 1999). Such an external filter would have

been of paramount importance to the survival of early life because internal UV-protection mechanisms would not have developed at this stage of evolution (see below, Section 1.4.1.2).

Ozone, although only a minor constituent of atmospheric composition, plays a vital role in the reduction of UV flux to Earth's surface. As already discussed, the mechanisms that produce and destroy ozone in the stratosphere are driven by energy gained *via* the absorption of incoming UV radiation (Section 1.3). Absorption of UV in the stratosphere prevents it from reaching Earth's surface; hence stratospheric ozone, or "the ozone layer" provides external protection from UV. The dissociation of diatomic oxygen is driven by UV-C, which is found to be completely absorbed in the atmosphere, therefore does not reach Earth's surface. This is important as UV-C is by far the most harmful wavelength of UV radiation, and terrestrial life would most likely not exist if UV-C were to be encountered at Earth's surface. Energy to breakdown ozone is provided by the absorption of UV-B. Comparison of ground-based and satellite measurements of UV-B reveals just 9-10% of UV-B measured at the top of Earth's atmosphere eventually reaches Earth's surface, therefore the atmosphere must absorb ~90% of all incoming UV-B (WHO, 2007). The vast majority of absorption of UV-B is attributed to ozone, although sulphur dioxide (SO_2) has also been identified as absorbing a small proportion of UV-B (Björn, 1999). Combination of these processes results in no UV-C and very little UV-B reaching Earth's surface. UV-A flux is not absorbed by any component of the atmosphere, therefore essentially 100% of solar UV-A reaches Earth's surface. UV-A is deemed to be not as dangerous as UV-B or UV-C, although it can still be harmful if exposure is for a sufficiently long duration. In addition, it has been suggested that the development of some skin cancers are the result of cumulative exposure to UV radiation over the course of a lifetime, rather than occasional high intensity doses (Diffey, 2004).

1.4.1.2 Internal UV defence mechanisms

The sessile nature of plants has likely been a determining factor in the development of the array of internal defences available against the harmful effects of UV-B. Some defences are simply an adaptation of habit, whilst others are of a physiological nature. It is the physiological changes that are to be the focus here.

Numerous studies (Caldwell *et al.*, 1998, 2003; Searles *et al.*, 2001) find physical changes in structural components of plants. Leaf cuticle wax and epidermal thickness have been commonly used as indicators of incident UV-B flux. Leaf cuticle wax is the uppermost layer of a leaf with the primary function of preventing water loss from the top face of the leaf. Surprisingly cuticular wax offers only a poor level of protection against UV-B (Rozema *et al.*, 1999). The epidermis underlying the waxy cuticle is found to provide a substantial amount of protection against UV-B (Sullivan *et al.*, 1996).

Leaf area has frequently been found to show a negative relationship with UV-B flux (Sullivan & Rozema, 1999; Searles *et al.*, 2001; Caldwell *et al.*, 2003). The reason for reduced leaf growth is not entirely known, although it has been linked to suppressed growth rates induced by exposure to UV-B, causing changes in secondary chemistry. Reduced growth rates coincide with observations of 'dwarf' vegetation inhabiting regions of naturally high UV-B flux (Flenley, 2007). It is proposed that slower growth rates enable photorepair mechanisms to operate (Sullivan & Rozema, 1999).

Photorepair mechanisms act within cells to mitigate the effects of damage caused by UV. The primary targets for such self-repair mechanisms are proteins and DNA (Stapleton, 1992; Jansen *et al.*, 1998) in order to maintain the correct functioning of the cell. One of the most common defects caused by UV radiation is the formation of DNA dimmers, where identical bases bond to each other (i.e. thymine-thymine) (Rozema *et al.*, 1999). Mismatches within

DNA such as this are rectified by the enzyme DNA-photolyase (Stapleton, 1992), which cleaves, for example, thymine-thymine linkage and restores the thymine-adenine coupling that should normally exist.

Secondary metabolite chemistry in plants provides a very effective internal UV-screen and forms the basis for the remainder of the work presented here; secondary plant chemistry and its relationship with UV radiation will be discussed below (Section 1.5).

1.4.2 UV-active pigments in plants

Secondary metabolites are widely reported to possess significant UV-B screening properties (Rozema *et al.*, 1997, 2001a, 2001b; Caldwell *et al.*, 1998; Chapter 3) and are found to occur in many plant tissues, including leaves and pollen/spores (Blokker *et al.*, 2005; Watson *et al.*, 2007). UV-B stimulates the synthesis of secondary metabolites that are predominantly phenolic compounds. Phenolic compounds are based on a phenol ring (Figure 1.4a) and can be either single-ringed, or polyphenolics, i.e. containing more than one ring linked together (Figure 1.4b). The synthesis of secondary metabolites originates with the Shikimate pathway, which links sugar metabolism with phenolic metabolism (Meijkamp *et al.*, 1999). The result of the Shikimate pathway is the amino acid phenylalanine; this acts as the precursor to a variety of complex phenolics *via* the phenylpropanoid pathway (PPP). Products of the PPP include cinnamic acid derivatives (CAD), flavonones, flavonols, flavonoids and anthocyanin. Of these products, the CAD are single-ringed compounds whilst the rest are complex polyphenolics. The stimulation of the PPP by UV-B radiation and resultant enhanced production of UV-B absorbing phenolic compounds suggests an active protective response to adverse UV conditions exists.

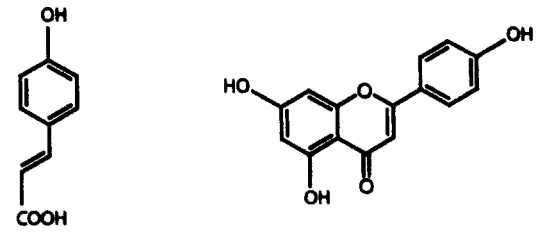

a) *para*-coumaric b) flavone

Figure 1.4 Example of a) a single-ringed phenolic compound, and b) a polyphenolic compound formed at different stages of the phenylpropanoid pathway.

1.5 Phenolic compounds as a proxy for past UV-B flux

Much attention has been paid to the possibility that the secondary metabolites of plants may be exploited as a palæo-monitor of past changes in UV-B flux (Rozema *et al.*, 2001b). The majority of studies that have measured UV-B absorbing compounds use leaf tissue, however leaves are highly susceptible to degradation and decomposition on relatively short timescales. In addition, the question as to whether leaf tissue secondary metabolites reliably record changes in UV-B flux has been raised (Phoenix *et al.*, 2002; Fedina *et al.*, 2005).

Recently the potential of pollen and spores to record long-term changes has been explored due to the resilience of these entities (Rozema *et al.*, 2001a, 2001b; Blokker *et al.*, 2005; Descolas-Gros & Schölzel, 2007). Spores and pollen that can be reliably identified to genus level are prevalent throughout a substantial part of the geological record (Visscher *et al.*, 2004) and can be recovered from sediments using standard laboratory techniques (Jones & Rowe, 1999). The longevity of spores and pollen remnants in the fossil record is due to the physical and chemical resistance to attack provided by the outermost shell of the gamete, the exine.

1.5.1 Biopolymers

The exine of pollen and spores is thought to consist predominantly of the biopolymer sporopollenin (Wittborn *et al.*, 1998; Jahren, 2004; Descolas-Gros & Schölzel, 2007). Biopolymers can be described as large molecules that comprise of a suite of smaller

monomers, which are chemical entities in their own right. The monomeric entities are most likely to possess similar functional group arrangements in order to allow them to be successfully linked into the final biopolymer. A simple example of a polymer is the man-made plastic polyethylene ("polythene"), which is a series of ethene monomeric units linked together *via* a backbone of carbon-carbon bonds, although this is not entirely analogous to sporopollenin because it consists of only one type of monomer. Two examples of biopolymers (also referred to as macromolecules) with multiple units contributing to the structure are DNA and proteins. Using DNA as an example here, the backbone is constructed from alternating, covalently bonded sugar and phosphate monomers, attached to this backbone are the genetic coding bases (adenine, thymine, guanine, and cytosine). The monomeric units are linked together by ester bonds. Another feature of DNA that exemplifies some of the behaviour of biopolymers is the existence of hydrogen-bonding binding two single chains of DNA together to form a double-helix structure (secondary structure), and ultimately the three-dimensional contortion of the double-helix (tertiary structure) (Loughlin, 2004). Molecular structure controlled by hydrogen-bonding plays a vital role in the form and function of biological polymers because it is the key to whether the biopolymer is biochemically active; this is particularly important for proteins and enzymes. Wittborn *et al.* (1998) observe nanoscale rod-like helical structures in the substructure of pollen of *Fagus sylvatica* and spores of *Lycopodium clavatum.* Using DNA and other macromolecular structures as structural analogues, the secondary and/or tertiary structures of sporopollenin, for example the multi-helical arrangement observed by Wittborn *et al.* (1998), may well be prove to be controlled by hydrogen-bonding.

1.5.2 Structural components of sporopollenin

The molecular composition of sporopollenin remains uncertain, but recent work (including this study) has employed the use of *in-situ* solid phase spectroscopic techniques to investigate molecular structure (see Descolas-Gros & Schölzel, 2007 for an overview). Early analyses

suggested ester-linked carotenoids and carotenoid derivatives comprised the major components of sporopollenin; this is now disputed and a copolymer structure consisting of aliphatic and aromatic (phenolic) monomeric units is favoured (Descolas-Gros & Schölzel, 2007). Numerous studies (Guildford *et al.*, 1988; Hemsley *et al.*, 1992; Blokker *et al.*, 2005; Watson *et al.*, 2007) have identified products of the phenylpropanoid pathway (see Section 1.4.2 above) as aromatic constituents, whilst fatty acids are thought to represent the aliphatic fraction of sporopollenin. Further detailed analysis of sporopollenin composition is presented in Chapter 2.

1.6 Rationale

Rozema *et al.* (2001a, 2001b) propose that pollen and spores may hold the potential to act as palæo biochemical monitors of changes in UV-B flux, accessible *via* the determination of relative abundances of structural aromatic (phenolic) compounds. As outlined in Section 1.4.2, phenolic compounds are already recognised for playing a role in UV-B protection in plants, thus the analysis of natural biochemical UV-B screens in records of pollen and spores to provide an historical context is the next logical step.

The above proposition of using pollen and spores as a palæo-proxy of UV-B raises a number of questions: Can these biochemical monomers of sporopollenin be readily identified/quantified with current analytical instrumentation? Does the chemical composition of spore/pollen exine vary in relation to UV-B flux? Can the proposed chemical proxy be successfully applied to determine past UV-B flux? How far back in time can this proxy be reliably used?

1.7 Aims, Objectives & Outline

It is the aim of this study to evaluate the feasibility of using sporopollenin chemistry as a proxy for UV-B radiation through space and time. The success of sporopollenin chemistry as a proxy will be assessed by application to three situations where UV-B radiation is expected to vary. This will be achieved by addressing modern-day UV-B flux, recent spatial and temporal UV-B variations, and the potential for reconstruction of geological UV-B flux.

Chapter two presents a novel, rapid technique for semi-quantitative *in-situ* analysis of the structural components of the spore exine.

Chapter three examines the effect of experimentally manipulated UV-B flux on spore wall chemistry via field experiments conducted in Arctic Sweden (2004-2006).

Chapter four investigates spore wall chemistry changes in response to spatial and temporal changes in UV-B flux.

Chapter five attempts to apply this spore-based proxy to geological material in order to determine whether UV-B flux was an influential climatic variable in geological history.

Chapter six follows on from Chapter five providing a detailed study into diagenetic effects upon sporopollenin chemistry.

1.8 References

Bard, E. & Frank, M. (2006) Climate change and solar variability: What's new under the sun? *Earth and Planetary Science Letters* **248**, 1-14.

Barry, R.G. & Chorley, R.J. (1998) *Atmosphere, weather and climate (7th edition).* Routeldge, London, UK.

Björn, L-O. (1999) Ultraviolet radiation, the ozone layer and ozone depletion, in; *Stratospheric ozone depletion: The effects of enhanced UV-B radiation on terrestrial ecosystems* (ed. J. Rozema). Backhuys publishers, Leiden, The Netherlands. pp. 21-37.

Blokker, P., Yeloff, D., Boelen, P., Broekman, R.A. & Rozema, J. (2005) Development of a proxy for past surface UV-B irradiation: A thermally assisted hydrolysis and methylation py-GC/MS method for the analysis of pollen and spores. *Analytical Chemistry* **77**, 6026-6031.

Bowman, K.P. & Erukhimova, T. (2004) Comparison of global-scale Lagrangian transport properties of the NCEP reanalysis and CCM3. *Journal of Climate* **17**, 1135-1146.

Caldwell, M.M., Björn, L-O., Bornmann, J.F., Flint, S.D., Kulandaivelu, G., Teramura, A.H. & Tevini, M. (1998) Effects of increased solar ultraviolet radiation on terrestrial ecosystems. *Journal of Photochemistry and Photobiology B: Biology* **46**, 40-53.

Canfield, D.E. (2005) The early history of atmospheric oxygen. *Annual Review of Earth and Planetary Sciences* **33**, 1-36.

Catling, D.C. & Claire, M.W. (2005) How Earth's atmosphere evolved to an oxic state: A status report. *Earth and Planetary Science Letters* **237**, 1-20.

Coffey, M.T. (1996) Observations of the impact of volcanic activity on stratospheric chemistry. *Journal of Geophysical Research* **101**(D3), 6767-6780.

Descolas-Gros, C. & Schölzel, C. (2007) Stable isotope ratios of carbon and nitrogen in pollen grains in order to characterise plant functional groups and photosynthesis pathway types. *New Phytologist* **176**, 390-401.

Deshler, T., Anderson-Sprecher, R., Jäger, H., Barnes, J., Hofmann, D.J., Clemesha, B., Simonich, D., Osborn, Grainger, R.G. & Godin-Beekman, S. (2006) Trends in the nonvolcanic component of stratospheric aerosol over the period 1971-2004. *Journal of Geophysical Research* **111**, D01201, doi:10.1029/2005JD006089.

Delmelle, P. & Stix, J. (2000) Volcanic gases, in; *Encyclopaedia of Volcanoes* (*eds.* Sigurdsson, H., Houghton, B.F., McNutt, S.R., Rymer, H. & Stix, J.). Academic Press, London, UK. pp. 803-815.

Diffey, B. (2004) Climate change, ozone depletion and the impact on ultraviolet exposure of human skin. *Physics in Medicine and biology* **49**(1), R1-R11.

Farman, J.C., Gardiner, B.G. & Shaklin, J.D. (1985) Large losses of total ozone in Antarctica reveal seasonal ClOx/NOx interaction. *Nature* **315**, 207-210.

Fedina, I., Velitchkova, M., Georgieva, K. & Grigorova, I. (2005) UV-B-induced compounds as affected by proline and NaCl in *Hordeum vulgare* L. cv. Alfa. *Environmental and Experimental Botany* **54**, 182-191.

Flenley, J.R. (2007) Ultraviolet insolation and the tropical rainforest: altitudinal variations, Quaternary and recent change, extinctions, and biodiversity, in: *Tropical rainforest responses to climatic change* (eds. M.B. Bush & J.R. Flenley). Springer Publishing, Berlin, Germany.

Francis, P. & Oppenheimer, C. (2004) *Volcanoes (2nd edition).* Oxford University Press, Oxford, UK.

Guildford, W.J., Schneider, D.M., Labovitz, J. & Opella, S.J. (1988) High resolution solid state ^{13}C NMR spectroscopy of sporopollenins from different plant taxa. *Plant Physiology* **86**, 134-136.

Harfoot, M.B.J., Beerling, D.J., Lomax, B.H. & Pyle, J.A. (2007) A two-dimensional atmospheric chemistry modelling investigation of Earth's Phanerozoic O_3 and near-surface ultraviolet radiation history. *Journal of Geophysical Research* **112**, D07308, doi:10.1029/2006JD007372.

Hemsley, A.R., Chaloner, W.G., Scott, A.C. & Groombridge, C.J. (1992) Carbon-13 solid state nuclear magnetic resonance of sporopollenins from modern and fossil plants. *Annals of Botany* **69**, 545-549.

Hofmann, D.J., Oltmans, S.J., Komhyr, W.D., Harris, J.M., Lathrop, J.A., Langford, A.O., Deshler, T., Johnson, T., Torres, A. & Matthews, W.A. (1994) Ozone loss in the lower stratosphere over the United States in 1992-1993: Evidence for heterogeneous chemistry on the Pinatubo aerosol. *Geophysical Research Letter* **21**(1), 65-68.

Hofmann, D.J., Oltmans, S.J., Harris, J.M., Johnson, B.J. & Lathrop, J.A. (1997) Ten years of ozonesonde measurements at the south pole: Implications for recovery of springtime Antarctic ozone. *Journal of Geophysical Research* **102** (D7), 8931-8943.

Jacob, D.J. (1999) *Introduction to atmospheric chemistry.* Princeton University Press, Chichester, UK.

Jahren, A.H. (2004) The carbon stable isotope composition of pollen. *Review of Palæobotany & Palynology* **132**, 291-313.

Jansen, M.A.K., Gaba, V. & Greenberg, B.M. (1998) Higher plants and UV-B radiation: balancing damage, repair and acclimation. *Trends in Plant Science* **3**(4), 131-135.

Jones, T.P., & Rowe, N.P (Eds.) (1999) Fossil plants and spores: Modern techniques. Geological Society Publishing House, London, UK. pp. 396.

Kiesecker, J.M., Blaustein, A.R. & Belden, L.K. (2001) Complex causes of amphibian population declines. *Nature* **410**, 681-684.

Kump, L.R. & Barley, M.E. (2007) Increased subaerial volcanism and the rise of atmospheric oxygen 2.5 billion years ago. *Nature* **448**, 1033-1036.

Loughlin, J. (2004) Proteins, in; *From molecules to cells* (ed. J. Loughlin). Open University Press, pp. 79-148.

Lunine, J.I. (1999) *Earth: Evolution of a habitable world.* Cambridge University Press, Cambridge, UK.

Madronich, S., McKenzie, R.L., Björn, L-O. & Caldwell, M.M (1998) Changes in biologically active ultraviolet radiation reaching the Earth's surface. *Journal of Photochemistry and Photobiology B: Biology* **46**, 5-19.

Meijkamp, B., Aerts, R., van de Staaij, J., Tosserams, M., Ernst, W.H.O. & Rozema, J. (1999) Effects of UV-B on secondary metabolites in plants, in; *Stratospheric ozone depletion: The effects of enhanced UV-B radiation on terrestrial ecosystems* (ed. J. Rozema). Backhuys publishers, Leiden, The Netherlands. pp. 71-99.

Oke, T.R. (1987) *Boundary Layer Climates (2nd edition).* Routledge, London, UK.

Owen, T. & Bar-Nun, A. (1995) Comets, impacts and atmospheres. *Icarus* **116**, 215-226.

Paul, N., Callaghan, T.V., Moody, S., Gwynn-Jones, D., Johanson, U. & Gehrke, C. (1999) UV-B impacts on decomposition and biogeochemical cycling, in; *Stratospheric ozone depletion: The effects of enhanced UV-B radiation on terrestrial ecosystems* (ed. J. Rozema). Backhuys publishers, Leiden, The Netherlands. pp. 117-133.

Phoenix, G.K., Gwynn-Jones, D., Lee, J.A. & Callaghan, T.V. (2002) Ecological importance of ambient solar ultraviolet radiation to a sub-arctic heath community. *Plant Ecology* **165**, 263-273.

Portmann, R.W., Brown, S.S., Gierrczak, T., Talukdar, R.K., Burkholder, J.B. & Ravishankara, A.R. (1999) Role of nitrogen oxides in the stratosphere: A re-evaluation based on laboratory studies. *Geophysical Research Letters* **26**(15), 2387-2390.

Rampino, M.R. & Self, S. (1992) Volcanic winter and accelerated glaciation following the Toba super-eruption. *Nature* **359**, 50-52.

Randel, W.J., Wu, F. & Russell, J.M. (1995) Ozone and temperature changes in the stratosphere following the eruption of Mount Piantubo. *Journal of Geophysical Research* **100**(D8), 16753-16764.

Rettberg, P., Horneck, G., Strauch, W., Facius, R. & Seckmeyer, G. (1998) Simulation of planetary UV radiation climate on the example of the early Earth. *Advances in Space Research* **22**(3), 335-339.

Rex, M., Salawitch, R.J., von der Gathen, P., Harris, N.R.P., Chipperfield, M.P. & Naujokat, B. (2004) Arctic ozone loss and climate change. *Geophysical Research Letters* **31**, L04116, doi:10.1029/2003GL018844.

Rozema, J., van de Staaij, J., Björn, L-O. & Caldwell, M. (1997) UV-B as an environmental factor in plant life: stress and regulation. *Trends in Ecology and Evolution* **12**(1), 22-28.

Rozema, J., van de Staij, J., Björn, L-O. & de Bakker, N. (1999) Depletion of stratospheric ozone and solar UV-B radiation: Evolution of landplants, UV-screens and functions of

polyphenolics, in; *Stratospheric ozone depletion: The effects of enhanced UV-B radiation on terrestrial ecosystems* (ed. J. Rozema). Backhuys publishers, Leiden, The Netherlands. pp. 1-19.

Rozema, J., Broekman, R.A., Blokker, P., Meijkamp, B.B., de Bakker, N., van de Staaij, J., van Beem, A., Ariese, F. & Kars, S.M. (2001a) UV-B absorbance and UV-B absorbing compounds (para-coumaric acid) in pollen and sporopollenin: the perspective to track historic UV-B levels. *Journal of Photochemistry and Photobiology B: Biology* **62**, 108-117.

Rozema, J., Noordijk, A.J., Broekman, R.A., van Beem, A., Meijkamp, B.M., de Bakker, N.V.J., van de Staaij, J.W.M., Stroetenga, M., Bohncke, S.J.P., Konert, M., Kars, S., Peat, H., Smith, R.I.L. & Convey, P. (2001b) (Poly)phenolic compounds in pollen and spores of Antarctic plants as indicators of solar UV-B: A new proxy for the reconstruction of past solar UV-B? *Plant Ecology* **154**, 11-26.

Searles, P.S., Flint, S.D. & Caldwell, M.M. (2001) A meta-analysis of plant field studies simulating stratospheric ozone depletion. *Oecologia* **127**, 1-10.

Shaviv, N.J. (2003) Toward a solution to the early faint sun paradox: A lower cosmic ray flux from a stronger solar wind. *Journal of Geophysical Research* **108**(A12), article 1437.

Sheldon, N.D. (2006) Precambrian paleosols and atmospheric CO_2 levels. *Precambrian Research* **147**, 148-155.

Shoemaker, E. (1983) Asteroid and comet bombardment of the Earth. *Annual Review of Earth and Planetary Sciences* **11**, 461-494.

Solomon, S. (1999) Stratospheric ozone depletion: A review of concepts and history. *Review of Geophysics* **37**(3), 275-316.

Staehelin, J., Renaud, A., Bader, J., McPeters, R., Viatte, P., Hoegger, B., Bugnion, V., Girous, M. & Schill, H. (1998a) Total ozone series at Arosa (Switzerland): Homogenisation and data comparison. *Journal of Geophysical Research* **103** (D3), 5827-5841.

Staehelin, J., Kegel, R. & Harris, N.R.P. (1998b) Trend analysis of the homogenised total ozone series of Arosa (Switzerland), 1926-1996. *Journal of Geophysical Research* **103** (D7) 8389-8399.

Staehelin, J., Harris, N.R.P., Appenzeller, C. & Eberhard, J. (2001) Ozone trends: A review. *Review of Geophysics* **39**(2), 231-290.

Stapleton, A.E. (1992) Ultraviolet radiation and plants: Burning questions. *The Plant Cell* **4**, 1353-1358.

Sullivan, J.H., Howells, B.W., Ruhland, C.T. & Day, T.A. (1996) Changes in leaf expansion and epidermal screening effectiveness in *Liquidambar styraciflua* and *Pinus taeda* in response to UV-B radiation. *Physiologia Plantarum* **98**, 349-357.

Sullivan, J.H. & Rozema, J. (1999) UV-B effects on terrestrial plant growth and photosynthesis, in; *Stratospheric ozone depletion: The effects of enhanced UV-B radiation on terrestrial ecosystems* (ed. J. Rozema). Backhuys publishers, Leiden, The Netherlands. pp. 39-57.

Towe, K.M. (1996) Environmental oxygen conditions during the origin and early evolution of life. *Advances in Space Research* **18**(12), 7-15.

UNEP (United Nations Environmental Program) (1985) *The Vienna convention for the protection of the ozone layer.* UNEP, Nairobi, Kenya.

UNEP (United Nations Environmental Program) (2006) *Environmental effects of ozone depletion and its interactions with climate change: 2006 assessment.* UNEP, Nairobi, Kenya.

Visconti, G. (2001) *Fundamentals of physics and chemistry of the atmosphere.* Springer-Verlag, Berlin, Germany.

Visscher, H., Looy, C.V., Collinson, M.E., Brinkhuis, H., van Konijnenburg-van Cittert, J.H.A., Kürschner, W.M. & Sephton, M.A. (2004) Environmental mutagenesis during the end-Permian ecological crisis. *Proceedings of the National Academy of Sciences of the United States of America* **101**, 12952-12956.

Warr, K. & Smith, S. (1993) Science maters: Changing climate. Open University Educational Enterprises, Milton Keynes, UK.

Watson, J.S., Sephton, M.A., Sephton, S.V., Self, S., Fraser, W.T., Lomax, B.H., Gilmour, I., Wellman, C.H., Beerling, D.J. (2007) Rapid determination of spore chemistry using thermochemolysis gas chromatography-mass spectrometry and micro-Fourier transform infrared spectroscopy. *Photochemical & Photobiological Sciences* **6**, 689-694.

WHO (2007) Ultraviolet radiation and the INTERSUN programme, http://www.who.int/uv/en/ Date accessed: 22/10/2007.

Wittborn, J., Rao, K.V., El-Ghazaly, G. & Rowley, J.R. (1998) Nanosclae similarities in the substructure of the exines of Fagus pollen grains and Lycopodium spores. *Annals of Botany* **82**, 141-145.

WMO (World Meteorological Organisation) (2002) *Scientific assessment of ozone depletion: 2002.* Global ozone research and monitoring project – Report No. 47. Geneva, Switzerland

WMO (World Meteorological Organisation) (2007) *Scientific assessment of ozone depletion: 2006.* Global ozone research and monitoring project – Report No. 50. Geneva, Switzerland.

2 A novel technique for the rapid determination of spore wall aromaticity

2.1 Introduction

The investigation of recalcitrant geopolymers and associated biopolymers found in the sedimentary record has been the focus of a number of recent studies (see de Leeuw *et al.*, 2006 and Vandenbroucke & Largeau, 2007, and references therein). In particular the elucidation of the molecular composition of certain extant, highly-resistant biopolymers that form parts of microscopic entities (spores and pollen) often preserved in the geological record has proven a challenge. Analytical interrogation of such bio- and geo-polymers may reveal valuable information about the environmental conditions at the time of their formation.

Pollen and spores are a widely abundant source of bio- and geo-polymers in sediments owing to the prolific nature of the reproductive cycle of plants and the high dispersal potential brought about by their amenability to aeolian and hydrological transport mechanisms. As a result pollen analysis has been used extensively for qualitative palaeo-climatic reconstructions (e.g. Bradley, 1999). An important aspect of the reproductive cycle of plants is the annual production and release of pollen and spores, which provide the potential for the reconstruction of past climates and environments on annual scales, although such high resolution may not be achieved due to variable transport times and reworking of sediment. Combination of well-preserved pollen and spore records with organic geochemical analysis techniques offers the opportunity for high-temporal resolution analysis to investigate past short-term changes in environmental conditions, whereby the vegetation-derived material is acting as a biochemical monitor of the environment.

This Chapter presents the development of FTIR microspectroscopy as a rapid and inexpensive tool for the investigation of variations in spore wall chemistry in relation to UV-B flux as an environmental stress factor.

2.2 History of Research

It is well known that plants respond to exogenous stress and stimuli, in particular temperature (Kumar *et al.*, 2004; Wahid *et al.*, in press), light, water availability and salinity (Roy *et al.*, 1999; Reynolds *et al.*, 2005), atmospheric CO_2 (Visser *et al.*, 1997) and nutrients (Kumar *et al.*, 2004). Other environmental factors are also suggested to have an important influence on plants, such as herbivory (Gwynn-Jones *et al.*, 1997) and ultraviolet radiation (Rozema *et al.*, 1997).

The phenylpropanoid pathway (PPP) is found to be stimulated by ultraviolet-B (UV-B) radiation and, as a result, phenolic products of the PPP increase in abundance within plant tissues (Meijkamp *et al.*, 1999). There are two broad groups of products formed *via* the PPP. An initial step utilises phenylalanine that is catalysed by phenylalanine lyase (PAL) to form cinnamate, which is then converted to a number of single-ringed cinnamic acid derivatives (CAD) *via* simple substitution reactions on the aromatic ring. Complex polyphenolics are then synthesised from the CAD *via* chalcone synthase (CHS), resulting in multi-ringed flavanones, flavonols, flavones, flavonoids and anthocyanins (Meijkamp *et al.*, 1999) (Figure 2.1).

Previous studies have investigated methanol-soluble phenolic compounds in leaves to assess the extent to which plants respond to UV-B input as it is found that specific compounds are effective absorbers of UV-B (Ballaré *et al.*, 2001; Searles *et al.*, 2001). Compounds with UV-B absorbing properties are prevalent throughout plant tissues performing numerous roles, including structural rigidity, chemical and physical defence, and scavenging of free radicals, i.e. reactive oxygen species (ROS) (Grace & Logan, 2000; Pourcel *et al.*, 2006). Such UV-B absorbing properties of these compounds have given rise to them being referred to as UV-B

absorbing compounds (UACs) (Rozema *et al.*, 2001). Whilst flavonoids, anthocyanins, flavonols and other related complex polyphenolic compounds are the most common UV-B absorbing compounds in leaf tissues, or simpler phenolic UACs comprise the basic building blocks of structural biomacromolecules (or biopolymers) in other plant tissues, such as lignin, tannin, suberan, algaenan and sporopollenin (Rozema *et al.*, 2001; de Leeuw *et al.*, 2006; Vandenbroucke & Largeau, 2007).

Sporopollenin is the major constituent of the exine of spores and pollen grains. The exact structure of sporopollenin remains elusive and, as a result, debate over the nature of sporopollenin continues (Guildford *et al.*, 1988; de Leeuw *et al.*, 2006; Vandenbroucke & Largeau, 2007). Current understanding suggests there are a number of different extant types of sporopollenin throughout the plant kingdom (Guildford *et al.*, 1988; de Leeuw *et al.*, 2006); however there are two compositional end-member models that are held to be the most favoured possibilities. The first model of sporopollenin consists entirely of oxygenated aromatic monomers, in particular ferulic acid (FA) and *para*-coumaric acid (pCA) (Scott, 2002; de Leeuw *et al.*, 2006). The opposing end-member model is of an exclusively aliphatic biomacromolecule, akin to those found in fossilised pollen and spore material (Scott, 2002; de Leeuw *et al.*, 2006). Both end-member models are derived from data obtained using a variety of incomparable, chemically harsh sample preparation techniques that have the potential to inadvertently alter the chemistry of sporopollenin, thus affecting results (Hemsley *et al.*, 1992). The potential for a third model exists whereby modern sporopollenin is a mix of unbranched aliphatic chains (fatty acids) and phenolic-based monomers linked to form a copolymer, thus representing a mid-point between the two end-member models (Killops & Killops, 2005; Vandenbroucke & Largeau, 2007).

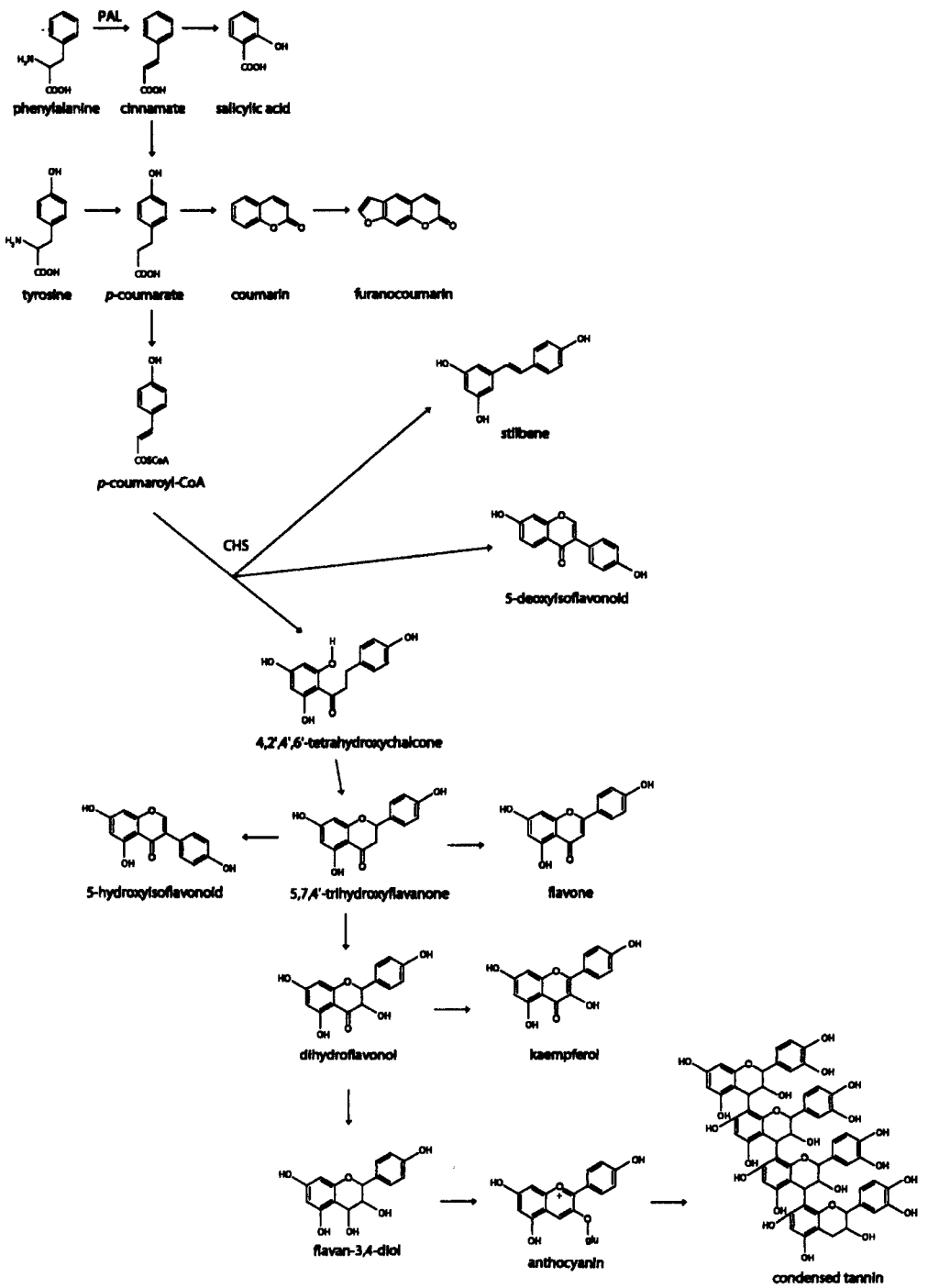

Figure 2.1 Phenylpropanoid pathway showing formation of simple and complex phenolic compounds derived from amino-acid phenylalanine. Production of simple (single-ringed) phenolics is mediated by PAL. Cinnamate is central to further reactions that produce the variety of CAD observed in plant tissues primarily via substitutions around the aromatic ring. All of the substituents during this first stage of the pathway are 'activating' groups, thus enabling the aromatic ring to readily undergo further reactions. The second stage of the PPP results in the formation of complex polyphenolics. This step is mediated by CHS and coenzyme-A (CoA). Further structural modifications of the polyphenolics proceed via dehydrogenation reactions and substitutions, where hydroxyl groups are the primary substituent. Modified from: Meijkamp *et al.* (1999).

Studies investigating ancient spores and pollen consistently find fossilised sporopollenin that has undergone only low-grade alteration to be an aliphatic biopolymer with little or no evidence of aromatic components; this has led to the conclusion that modern-day sporopollenin is also likely to be an aliphatic biopolymer. However, whether fossilised material is truly analogous to modern-day material is still a contested issue (see Chapters 6 & 7). It is likely that diagenesis and catagenesis play a significant role in post-depositional alteration of the chemical composition of sporopollenin from its original state, even at relatively early stages of alteration (Yule *et al.*, 2001; Watson *et al.*, 2007b). A solely aliphatic composition is the least likely model in the majority of cases because of the numerous reports of the occurrence of FA and pCA when investigating modern-day sporopollenin (Rozema *et al.*, 2001a, 2001b; Blokker *et al.*, 2005; Killops & Killops, 2005; Vandenbroucke & Largeau, 2007). FA and pCA, plus their associated derivatives are recurrent in the literature as constituents of sporopollenin and are thus considered likely to be the most significant UV-B absorbing compounds occurring within sporopollenin (Watson *et al.*, 2007a).

Rozema *et al.* (2001a) proposed that tracking UACs contribution to sporopollenin chemistry as a data source may afford the opportunity to reconstruct past UV-B regimes, and, as such, link UV-B flux to ozone column depth (Björn, 1999; Boelen *et al.*, 2006). Pollen and spores are ideal material for such an investigation because of their longevity and prominent representation in modern-day, recent and geological records. Herbaria (collections of preserved plant specimens) are cited as being a potentially valuable source of sample material (Blokker *et al.*, 2005) due to the detailed information recorded by the collectors regarding location, time of year, growth position/environment, habitat and coordinates.

Pyrolysis-GC-MS (py-GC-MS) has been used in an attempt to develop the potential of pollen and spores as proxies of UV-B flux (Rozema *et al.*, 2001a; Blokker *et al.*, 2005) by characterising and quantifying the abundances of UACs. A greater relative abundance of

UACs in sporopollenin is predicted to reflect a higher incident of ambient UV-B prior to spore and pollen production. Identification of sporopollenin constituents by py-GC-MS reveals further details of the production of phenolic-based components for each sample and their relationship to UV-B. The response of the PPP is thought to differ in the production for pCA and FA, with preferential increase in pCA production in response to UV-B stimulus, hence the ratio of pCA/FA has been suggested as a method for assessing the influence of UV-B on plant chemistry (Blokker *et al.*, 2005). Irrespective of which chemical species is increasing in abundance as a result of environmental stimuli, the net result will be that sporopollenin is likely to have a greater proportion of phenolic-based compounds within its structure when exposed to enhanced UV-B radiation.

Blokker *et al.* (2005) found that the detection limit for FA and pCA is 12 and 57 grains, respectively, when analysing *Alnus glutinosa* (Alder) pollen grains. However, when taking into account counting errors and variations in pyrolysis efficiencies these values are more likely to be 253 and 101 pollen grains for FA and pCA, respectively. This finding defines a substantial lower limit on sample size for the analytical capacity of GC-MS studies. Such a 'bulk' analysis technique is time-consuming due to the need to hand pick and count individual grains, and potentially impossible when using very small samples, such as those obtained when harvesting from herbaria.

FTIR microspectroscopy is a technique that enables rapid analysis and provides compositional and structural information. Only a limited number of studies have employed micro-FTIR for the analysis of pollen and spore material to date (Yule *et al.*, 2000), however FTIR opens up the potential for large quantities of data to be generated relatively quickly, typically with ~ 50 to ~ 200 scans being collected per analysis (Yule *et al.*, 2000; Marga *et al.*, 2003; Pappas *et al.*, 2003; Xuguang, 2005). Other studies favour a higher number of scans (~ 1000 scans) in order to reduce spectral noise (Walker & Mastalerz, 2004; Pšenička *et al.*, 2005), but an increasingly

greater number of scans are required for every incremental reduction in peak-to-peak noise, resulting in a significant trade-off between analytical time and spectral noise (King *et al.*, 2004; Appendix A). Typically a single scan with micro-FTIR takes between 0.5-2.0 seconds, depending on the mirror velocity used; as a result a single spectrum can be obtained in less than 5 minutes.

2.3 Experimental

2.3.1 Sample description

A set of *Lycopodium annotinum* samples harvested in 2006 from an area just west of Abisko, northern Sweden (68° 25'N, 18° 40'E), are used to demonstrate the principle underlying the analysis of all samples within this thesis, and the interpretation of data are applicable to data chapters that discuss modern and recent spore samples (Chapters 2, 3 and 4); Chapters 5 and 6 investigate fossil spores that require a different interpretation. Samples were selected to display the applicability of using micro-FTIR to track changes in spore wall chemistry. *L.annotinum* were the chosen study species because they have a broad geographical occurrence, provide great quantities of spores on an annual basis and *via* analogous species, are represented throughout a substantial proportion of the geological record.

2.3.1.1 Sample preparation

All samples were subject to sequential solvent extraction with acetone prior to analysis to remove any labile (non-sporopollenin bound) components within the spores, thereby isolating the sporoderm. 1 ml of acetone was added to the sample then agitated to ensure thorough mixing and subsequent extraction. After agitation the samples were centrifuged and 80 % of the acetone (i.e. 0.8 ml) drawn off, thus removing any solvent extractable moieties along with the acetone whilst leaving 0.2 ml surrounding the spore sample. This procedure was repeated

three times to ensure minimal labile components remained in the sample, resulting in a calculated labile component residence of approximately 0.8 % (1 ml - 80 % = 0.2 ml; 0.2 ml - 80 % = 0.04 ml; 0.04 ml - 80 % = 0.008 ml = 0.8%). Samples were then left to air-dry at room temperature for 24 hours in a clean-air fume hood before analysis to allow any residual acetone to evaporate. When samples were required to be stored for a prolonged period prior to analysis (up to 1 or 2 weeks), a sealed desiccator loaded with silica desiccant was used for storage to prevent the absorption of atmospheric moisture by the samples.

2.3.2 Pyrolysis gas chromatography-mass spectrometry (py-GC-MS)

Full characterisation of spore wall chemistry was achieved using py-GC-MS at Imperial College, London using an Agilent 5973 GC-MS. Samples were introduced into the GC-MS *via* a CDS AS-2500+ pyrolysis autosampler. Pyrolysis was conducted at 610 °C, with an initial temperature of 310 °C and a ramping rate of 20 °C per millisecond (Appendix A). To improve derivatisation, 10 µl of 25% tetramethylammoniumhydroxide (TMAH) in methanol was added to each sample; the methanol was allowed to evaporate over the course of a twelve-hour period prior to analysis. Helium was used as the carrier gas at a flow rate of 1.1 ml min^{-1}.

2.3.3 Fourier transform infrared (FTIR) microspectroscopy

Chemical functionality of the spore wall was determined by FTIR microspectroscopy at The Open University using a Thermo Nicolet FTIR bench unit fitted with a KBr beamsplitter. A Continuum IR-enabled microscope fitted with a 15x reflachromat objective lens and nitrogen-cooled MCT-A detector is interfaced with the bench unit to provide microscopic analysis capability. Atmospheric H_2O and CO_2 interference within spectra is countered by purging the entire system (bench unit, microscope and sample stage) with air that has been dried and scrubbed of CO_2 using a Peak Scientific ML85 purge unit. Analysis was conducted using a microscope aperture of 100 x 100 µm at 500 scans per sample with a resolution of 4 data

points per reciprocal centimetre (cm^{-1}). An aperture size of 100 x 100 μm enables between 6-12 spores to be analysed as a single analysis to give a 'bulk' spectrum, thus being comparable with data obtained *via* other techniques, such as pyro-GC-MS (Blokker *et al.*, 2005). Background spectra were collected immediately after every sample spectrum (Appendix A). FTIR analysis offers a rapid, non-destructive technique for obtaining equivalent information to pyro-GC-MS, thus enabling a greater throughput of samples within an equivalent amount of time, hence increasing the statistical rigour of the results. With this in mind, each analysis was replicated five times per sample.

2.3.4 Spectrophotometry

UV absorption for a selection of compounds found to be present in sporopollenin was assessed using a Philips PU8720 UV/Vis (ultra-violet/visible) scanning spectrophotometer at the University of Sheffield. A wavelength range of 200-400 nm, corresponding to the mid-UV-C through to far-UV-A range was selected for investigation. Samples were dissolved in either a 50:50 mix of methanol:MilliQ (MilliQ resistivity = >18.2 MΩ) water or dichloromethane (DCM) depending on their immiscibility with water.

2.4 Results and Discussion

2.4.1 Pyrolysis-GC-MS of *L. annotinum* spores

Py-GC-MS analysis of *L. annotinum* spores reveals a suite of compounds consisting of aliphatic carbon chains and aromatic compounds (Figures 2.2 and 2.3). All compounds are described as the carboxylic acids monomers released from sporopollenin by heat assisted fragmentation and derivatisation with TMAH. The results of this analysis are consistent with those of Rozema *et al.* (2001a), Blokker *et al.* (2005) and Watson *et al.* (2007a) even though these studies investigated other species. Solvent extraction prior to analysis ensures that only the outer

exine of the spore remains, effectively isolating sporopollenin in its natural form, therefore all compounds detected in the analysis must be structurally bound components (monomers) of sporopollenin. No nitrogen-containing compounds were identified with py-GC-MS; this is confirmed by independent analysis for nitrogen that found <1 wt % nitrogen (analysis by M.A. Gilmour, Planetary & Space Science Research Institute, The Open University).

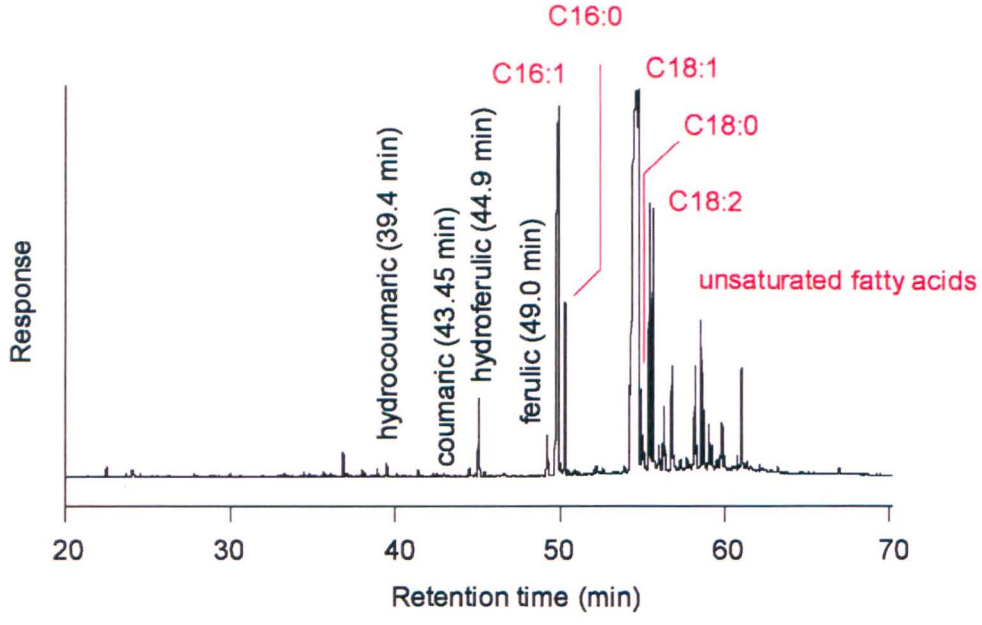

Figure 2.2 Pyrolysis-Gas Chromatography-Mass Spectrometry chromatogram of typical *L.annotinum* spores. Compounds present can be grouped into two categories: 1) phenolic, and 2) aliphatic. Phenolic fraction is exclusively CAD compounds formed via the PPP. Aliphatic fraction comprises unbranched fatty acids with varying degrees of unsaturation. Palmitoleic acid (C16:1) and oleic acid (C18:1) are the most abundant aliphatic constituents.

2.4.1.1 Aliphatics

The aliphatic carbon chains are all identified as unbranched carboxylic acids (fatty acids) by spectra obtained using Agilent MSD Chemstation software, ranging in length from C8 to C22, and exhibit saturated, mono- and poly-unsaturated forms. The most abundant fatty acids are highlighted in Figure 2.2. The mono-unsaturated compounds palmitoleic acid (9-hexadecenoic acid, C16:1) and oleic acid (9-octadecenoic acid, C18:1) are found to dominate the aliphatic fraction in abundance, with palmitic acid (hexadecanoic acid, C16:0) and linoleic

acid (9,12-octadecadieonic acid, C18:2) also making a significant contribution to the aliphatic composition. The remainder of the aliphatic fraction (> 55 minutes column retention time, Figure 2.2) appears to be a complex mixture of a variety of unsaturated fatty acids.

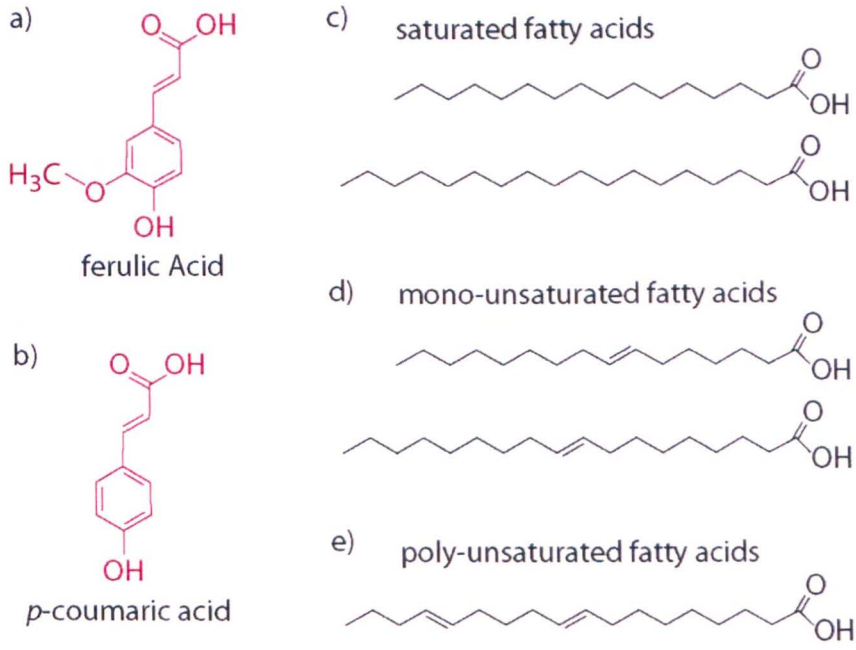

Figure 2.3 Structure of typical components of *L. annotinum* sporopollenin. Ferulic acid (a) and *para*-coumaric acid (b) constitute phenolic fraction. A suite of unbranched aliphatics are evident from chromatogram, however, those in greatest abundance are saturated fatty acids (c) palmitic acid (C16:0) and stearic acid (C18:0), mono-unsaturated fatty acids (d) palmioleic acid (C16:1) and oleic acid (C18:1), and (e) poly-unsaturated linoleic acid (C18:2).

2.4.1.2 Aromatic compounds

The aromatic compounds are identified as the phenol-based hydroxycinnamic acids *para*-coumaric acid and ferulic acid (m/z = 164 and 194, respectively) (Figures 2.2 and 2.3), belonging to the group of compounds referred to as cinnamic acid derivatives (CADs) (Edreva, 2005). No other components of sporopollenin are found to contain aromatic ring structures, thus the aromatic ring is a distinguishing feature of FA and pCA. The GC-MS chromatograms show FA to be the more abundant of the aromatic compounds, with pCA playing a relatively minor role. This is consistent with the results of Rozema *et al.* (2001a) who noted that FA could be detected in a single spore; pCA required at least three spores before

detection was reliable, suggesting a greater relative abundance of FA bound into the structure of sporopollenin. As noted above, Blokker *et al.* (2005) found the minimum pollen grain number for statistically significant quantification of FA and pCA abundance to be 12 and 57, respectively, further suggesting that FA may be the more abundant aromatic compound.

2.4.2 Spectrophotometry of sporopollenin components

Spectrophotometric analysis of pCA and FA reveals that both compounds are UV-active, i.e. they both absorb within the UV range of the electromagnetic spectrum. Specifically both are found to have high absorbencies in the UV-B band (Figure 2.4). Previous workers (Bornman, 1999; Meijkamp *et al.*, 1999; Rozema *et al.*, 2001a, 2001b) have also reported the capacity of flavonoids and related compounds (e.g. CADs) to absorb UV radiation. Figure 2.4 shows pCA to have an overall greater absorbtivity within the UV-B range than FA, with peak absorbance of ~0.23 at 285 nm.

Edreva (2005) proposed that the UV absorbing properties were due to the presence of the aromatic ring and its ability to dissipate the energy input from the UV radiation *via* the cloud of delocalised π-electrons associated with the aromatic structure, whereby a π electron is promoted to a higher energy orbital. In this situation excitation of the electron will cause a π → π* transition.

A selection of aliphatic compounds representative of those identified to be present in spore walls by GC-MS techniques were also analysed using UV/Vis spectrophotometry. Figure 2.4 demonstrates that none of the aliphatic components absorb in the UV region. The main groups of aliphatic components are all represented in this selection (saturated, mono-unsaturated, poly-unsaturated), thus is it reasonable to make the assumption that none of the other aliphatic compounds will absorb in the UV region because the only difference from the selection analysed is the carbon-chain length.

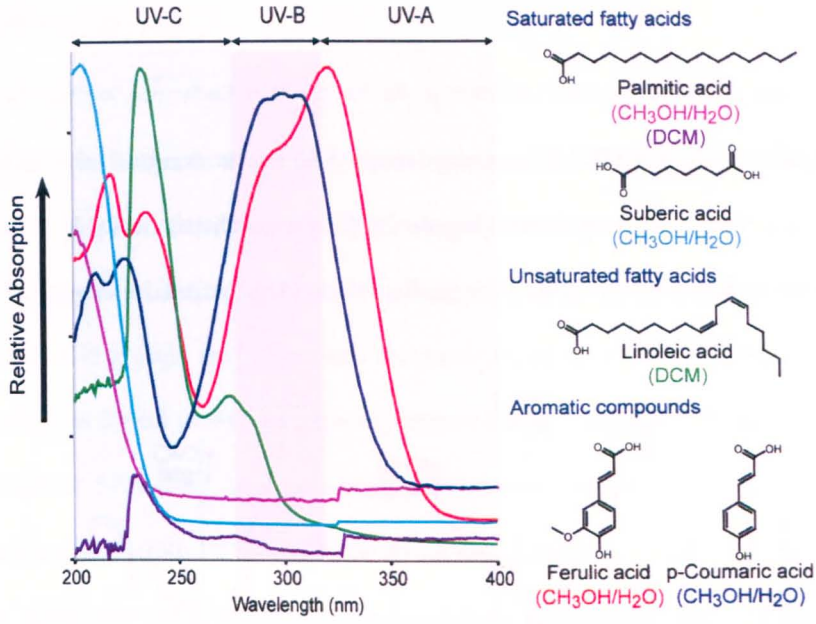

Figure 2.4 UV-visible spectra of compounds representative of sporopollenin compound groups identified by pyrolysis-Gas Chromatography-Mass Spectrometry. All compounds were dissolved in a 50:50 mixture of methanol:MilliQ water, except linoleic acid which is immiscible in water: linoleic acid was dissolved in DCM for analysis. In order to ensure comparable results from compounds analysed in different substrates palmitic acid was dissolved in both 50:50 methanol:MilliQ water and DCM. Spectra clearly show that only the phenolic compounds pCA and FA absorb within the UV-B region. Aliphatic compounds represented here do not show any evidence of UV-B absorption. A small shift in spectral lines at ~330 nm is due to switching of radiation sources within the instrument. Compounds dissolved in DCM show 'blocking effects' due to DCM at wavelengths below 250 nm, thus for these samples this region should be disregarded.

2.4.3 FTIR microspectroscopy of *L. annotinum* spores

As previously proposed by Rozema *et al.* (2001a), the relative abundance of hydroxycinnamic acids in sporopollenin has the potential to be exploited as a proxy measure for the incident surface UV-B. However, in order to obtain a reliable assessment of the aromatic response to UV-B a large number of samples with multiple repetitions would be required. To use py-GC-MS in such a situation would be prohibitively time-consuming and expensive; therefore a quicker, cheaper technique would be better suited. This study is the first to propose FTIR microspectroscopy as an effective technique to provide a short-cut to equivalent information about the chemistry of sporopollenin as that obtained using py-GC-MS. Pyrolysis techniques need only be used for regular confirmation of the organic units giving rise to the FTIR bands.

Spectra obtained using FTIR microspectroscopy identify a number of functional groups within the structure of sporopollenin (Figure 2.5); these are listed in Table 2.1. The primary features of the spectra are described in detail below, divided by functional group.

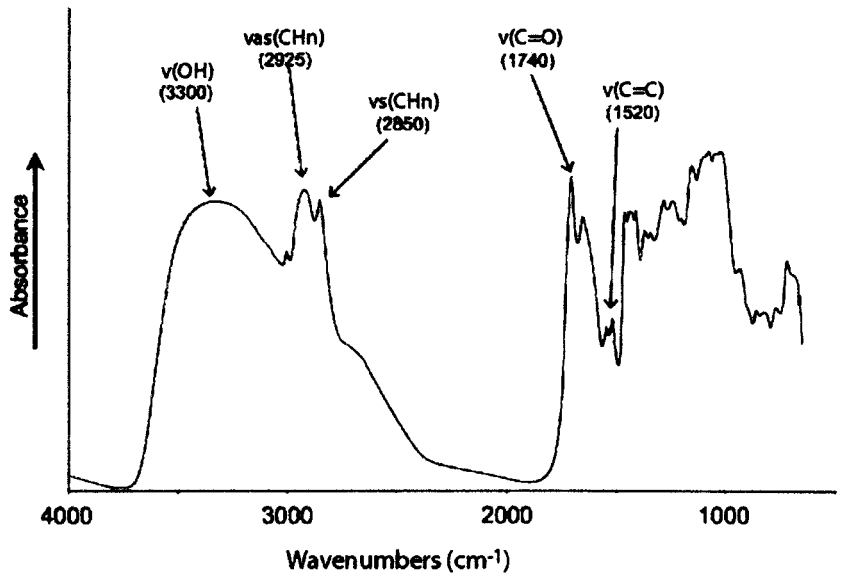

Figure 2.5 Micro-FTIR spectrum of a typical *L.annotinum* spore. Functional groups of greatest significance are highlighted. V(OH) = hydroxyl; vas(CH_n) = asymmetrical stretching of CH_2 and CH_3 groups; vs($C-H_n$) = symmetrical stretching of CH_2 and CH_3 groups; v(C=O) = carbonyl group in ester linkages; v(C=C) = carbon double bonds in aromatic ring structure (phenolics). See Table 2.1 for full interpretation of spectrum.

Table 2.1 Typical absorbance frequencies of functional groups found in sporopollenin monomers. From: Rouxhet et al. (1980), Williams & Fleming (1980).

Wavenumber (cm^{-1})	Bond	Functional group
3300	O-H	Hydroxyl
3006	C=C	Aliphatic chain
2925	C-H	Asymmetric stretching (CH_2 & CH_3)
2850	C-H	Symmetric stretching (CH_2 & CH_3)
1740	C=O	Ester linkage
1640	O-H	Hydroxyl
1520	C=C	Aromatic ring
1460	C-H	Asymmetric bending (CH_2 & CH_3)
1375	C-H	Symmetric bending (CH_3)
720	C=C	Aromatic ring or aliphatic chain

2.4.3.1 Hydroxyl groups

The most prominent absorbance band of all spectra is centred at 3300 cm^{-1}, this region corresponds to stretching vibrations of hydroxyl groups (OH) (Figure 2.5). All spectra show the OH band to be particularly broad, with greatest absorbance ranging between 3650 cm^{-1} to 3050 cm^{-1}, tailing off as far as 2500 cm^{-1}. The positioning of the broad absorbance band suggests that all OH groups are bound into the structure of sporopollenin, and are not due to free OH groups, as found in water or non-hydrogen-bonded groups. OH groups of water in solution absorb at 3710 cm^{-1}, and non-hydrogen bonded groups absorb at 3650-3590 cm^{-1} (Williams & Fleming, 1980). There may be some non-hydrogen-bonded OH groups present (absorbance 3650-3590 cm^{-1}), but this is not possible to determine in this analysis because the broad nature of the OH band obscures spectral detail in this region. The wavenumber range observed (3650-2500 cm^{-1}) points towards hydroxyl groups forming hydrogen bonds (H-bonds). Two types of H-bonds appear to be present; simple intermolecular H-bonded -OH groups (3600-3200 cm^{-1}), and intermolecular H-bonded -OH groups in chelate form (3200-2500 cm^{-1}) (Williams & Fleming, 1980). The fact that the tail of the OH band continues to 2500 cm^{-1} indicates the presence of stronger hydrogen bonding, suggested by Rouxhet *et al.* (1980) to be attributable to the OH contained with carboxyl groups.

Figure 2.3 demonstrates that sporopollenin monomers contain, or at least have the potential to contain, a single carboxyl group; in addition the CAD monomers are phenol-based with the hydroxyl group at C4 of the aromatic ring, further adding to the overall potential OH abundance. The strong influence that H-bonding appears to be having on the OH absorbance region suggests hydrogen-bonding may play an important role in the tertiary and/or quaternary structure of sporopollenin. It should be noted that most sporopollenin monomers are unlikely to contain terminal carboxyl or hydroxyl groups because these are the most probable bonding sites in order to construct a biopolymer (see Section 2.4.3.5). Only those monomers situated on the biopolymer perimeter will possess carboxyl and hydroxyl

groups that are not removed by covalent bonding, but may contribute to hydrogen-bonding. Thus the total hydroxyl/carboxyl content of sporopollenin should remain fairly constant irrespective of the balance of aromatic and aliphatic monomers because the tertiary/quaternary structure of sporopollenin needs to be maintained through correct hydrogen-bonding alignment. These findings corroborate the proposed exine substructure of Wittborn *et al.* (1998) who conclude that *Lycopodium* exines are constructed from multi-helical, rod-shaped units. Hydrogen-bonding is the most probable candidate for the maintenance of such a helix structure.

Vibrations due to bending of the OH group give rise to absorbance in the region 1410-2160 cm^{-1} (Williams & Fleming, 1980), however it is not possible to assign any of the absorbance bands in the sample spectra to OH bending with confidence due to considerable overlap with other functional groups.

2.4.3.2 Alkyl groups

A distinct doublet superimposed on the lower wavenumber tail of the hydroxyl band is attributed to stretching of alkyl groups (Figure 2.5). In particular, information about the relative proportions of CH_2 (within chain) and CH_3 (chain termination) groups can be determined. CH_2 group stretching vibrations occur at 2926cm^{-1} and 2853 cm^{-1} $\pm$10 cm^{-1}, indicating asymmetric and symmetric stretching, respectively, whereas CH_3 group stretching vibrations occur at 2962 cm^{-1} and 2872 cm^{-1}, again representing asymmetric and symmetric stretching modes, respectively (Rouxhet *et al.*, 1980). It is evident from the IR spectra that CH_2 groups dominate the alkyl signal from the positions of the absorbance bands at 2920 cm^{-1} and 2850 cm^{-1} (Figure 2.5). However, CH_3 groups still appear to be contributing a significant signal, demonstrated by the slight shouldering effect on the higher wavenumber flank of the 2920 cm^{-1} absorbance band, assignable to asymmetric stretching of CH_3 groups, and the relatively shallow trough between the CH_2 asymmetric and symmetric bands. Rouxhet *et al.*

(1980) suggest the shallow depth of trough is due to the positioning of the symmetric stretching band of the CH_3 groups. The monomeric composition identified by pyro-GC-MS has already demonstrated the abundance of long-chain aliphatic compounds; the IR data strongly agree with this evidence - longer C-chains will have a greater relative abundance of CH_2 groups than CH_3, hence the alkyl IR signal will be dominated by CH_2 vibrational modes.

A pair of alkyl vibrational bands occur at ~1460 cm^{-1} for asymmetric bending of both CH_2 and CH_3 groups, and at ~1375 cm^{-1} for symmetric bending of CH_3 groups; CH_2 groups are found to make a negligible contribution to the absorbance band at ~1375 cm^{-1} (Rouxhet *et al.* 1980). Again, the relative absorptions exhibited by these two bands suggest that CH_2 groups are more abundant than CH_3 groups because the CH_2 + CH_3 absorption band is significantly larger than the band due to CH_3 groups; if CH_2 groups were a only a minor component of sporopollenin monomers the CH_2 + CH_3, and CH_3-only bands would be of approximately equal intensity.

The final spectral feature related to the alkyl group is to be found at 720 cm^{-1}. Absorbance at 720 cm^{-1} is attributed to the rocking vibrational mode of CH_2 (Williams & Fleming, 1980), moreover, this group generally only gives a weak spectral response. Rouxhet *et al.* (1980) also assign the band at 720 cm^{-1} to CH_2 groups, suggesting that this absorption is associated with skeletal vibrations of straight carbon-chains greater than 4 x CH_2 in length. Within the sample set presented here it is feasible to assign a contribution towards the band at 720 cm^{-1} to CH_2, but reference to any standard IR spectroscopy assignment table shows that other groups of stronger absorbance also contribute to this region, thus probably overprint any signal from the CH_2 groups (see Section 2.4.3.4).

2.4.3.3 Aromatics

Pyro-GC-MS identified the cinnamic acid derivatives, ferulic acid and *para*-coumaric acid as being the only compounds to contain an aromatic ring, thus marking pCA and FA as distinct from the other monomers of sporopollenin. Figure 2.3 shows the division between the aromatic-based and aliphatic components, which coincides with the UV-activity of the compounds, where aromatics (phenols) are UV-active, and aliphatics are UV-inactive. Phenols commonly show a single band around 3030 cm^{-1}, two or three medium strength absorption bands between 1500-1600 cm^{-1}, a number of bands between 1225 and 950 cm^{-1}, a series of weak bands at 2000-1600 cm^{-1}, and a group of bands below 900 cm^{-1} (Williams & Fleming, 1980). The data presented here show a clear absorbance band at 1520-1510 cm^{-1} and a group of bands below 900 cm^{-1} (Figure 2.5). Bands at 3030 cm^{-1}, 2000-1600 cm^{-1} and 1225-950 cm^{-1} are not evident due to the presence of other functional groups within the same spectral regions, thus any aromatic signal in these regions would be overprinted and/or suffer interference. The group of bands below 900 cm^{-1} is often indicative of the substitution pattern on the aromatic ring caused by out-of-plane C-H bending vibrations (Williams & Fleming, 1980), which would be expected to be present in the samples of this study due to the presence of pCA and FA. Both pCA and FA are substituted structures and most likely contribute to the absorbance bands below 900 cm^{-1}, particularly as aromatic ring out-of-plane C-H bending vibrations are strong absorbers. It may be the case that other functional groups are also contributing to this spectral region (see Section 2.4.3.4) thus reducing reliability of using this region for investigation of the aromatic components.

The band at 1510-1520 cm^{-1} appears to be solely due to the aromatic ring as the only other functional group that is found to absorb in this region is the amide II group. Yule *et al.* (2000) have previously assigned this band to a N-containing functional group, however an amide group here must be discounted as making a significant contribution to this absorption band

because these samples contain only a negligible abundance (< 1 wt %) of nitrogen (see Section 2.4.1).

2.4.3.4 Unsaturated compounds

Section 2.4.1.1 identifies the presence of unsaturated carbon bonds within the fatty acid fraction. The IR spectra show three absorption bands (peaks) that relate to C=C bonds at 3006 cm^{-1}, 1650 cm^{-1} and 720 cm^{-1}. Absorption at 3006 cm^{-1} is due to a single C-H bond stretch immediately adjacent to a C=C bond (Figure 2.3) within a chain (Williams & Fleming, 1980), as is present in the unsaturated fatty acids and the propenoic side group of pCA and FA. Spectra show a clear peak in the region of 1650 cm^{-1} that can be attributed to a non-conjugated C=C bond. The band at 1650 cm^{-1} appears to be fairly strong suggesting the double bond is not symmetrically substituted; symmetrically substituted C=C bonds give only weak absorption and probably would not be distinguishable in these spectra. Absorption at 720 cm^{-1}, as mentioned above in Section 2.4.3.2, has already partly been assigned to the weakly absorbing rocking vibrations of CH_2 groups within long C-chains. However, this band also provides information about the configuration of C=C bonds and hence some of the structure of the compounds, in particular this wavenumber corresponds to *cis*-double bonds. Two lines of evidence are used to deduce this *cis*-double bond formation, firstly *cis*-bonds absorb in the region 730-675 cm^{-1}, and secondly *cis*-bonds show medium strength absorbance peaks, contrary to *trans*-double bonds that show only weak absorbance (Williams & Fleming, 1980).

2.4.3.5 Ester linkages

The final prominent feature of *Lycopodium* IR spectra (Figure 2.5) is the strong absorbance at 1740 cm^{-1}. Absorption within the tightly constrained region 1750-1735 cm^{-1} is assigned to the strongly absorbing carbonyl group as part of a saturated ester link (Williams & Fleming, 1980). The presence of an ester group provides information about the way in which the monomeric

components of sporopollenin are linked; this information is obtainable using FTIR microspectroscopy because of the use of essentially *in-situ* measurements of the intact spore exine. Py-GC-MS analysis has already shown that the methylated derivatives of sporopollenin monomers contain carboxyl groups, and in the case of CADs, phenolic groups too. The easiest manner in which carboxylic acids can polymerise is *via* esterification and such a model has previously been suggested by Edreva (2005).

2.5 Sporoderm aromaticity variation

FTIR spectra can be used to provide a semi-quantitative assessment of the relative abundance of aromatic UV-active compounds. Absorbance bands appear as peaks when displayed in 'absorbance' units (y-axis, Figure 2.5); absolute absorbance is related to amount of sample as well as strength of absorbance of the particular bonds. However, to isolate a specific number/mass of spores for each individual analysis is highlighted as being too labour intensive for large scale surveys (Blokker *et al.*, 2005), hence an alternative method of extracting information about the aromaticity of the sporoderm is required. Watson *et al.* (2007a) use a ratio of aromatic vs. hydroxyl (OH) groups, which alleviates the need for known quantities of sample to be analysed. In order to calculate this ratio, the heights of IR spectral peaks relating to the aromatic ring (i.e. UV-active components; ~1520 cm^{-1}) and hydroxyl bonds (i.e. ~3300 cm^{-1}) are measured using the software TQ Analyst. The aromatic-related peak height is then normalised to the hydroxyl peak height (Equation 2.1) :

Equation 2.1 Absorbance band normalisation.

$$UV_{ab} = aro_{1520} / OH_{3300}$$

Where UV_{ab} is the abundance of UV-B absorbing compounds, aro_{1520} is the FTIR response of single aromatic rings and OH_{3300} is the FTIR response of hydroxyl groups. All analysis results will be quoted in aro_{1520}/OH_{3300} ratio values from here on. As this is a ratio, all values are devoid of units.

2.5.1 Chemical responses detected using FTIR microspectroscopy

Figure 2.6 shows the variation in OH-normalised aromatic component abundance detected using FTIR microspectroscopy. It is apparent that aromatic absorbance (at ~1520 cm^{-1}) varies in relation to degree of UV-B shading demonstrating the applicability of using micro-FTIR analysis. Semi-quantitative analysis of the peak heights of the aromatic absorption bands reveals significant differences in the relative abundance of aromatic structures between sample groups (Figure 2.6). The details regarding why this change in aromatic abundance occurs will be discussed in Chapter 4.

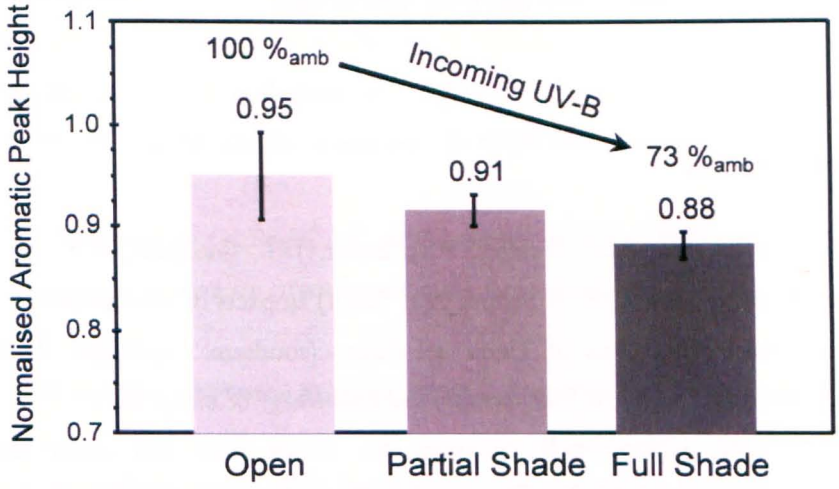

Figure 2.6 OH-normalised aromatic response of three sample groups. This figure demonstrates the ability of FTIR microspectroscopy to track differences in abundance of phenolic compounds via IR-absorbance of aromatic rings. Error bars are standard error.

2.6 Summary

It is apparent from the analysis presented above (Figure 2.6) that the fundamental building blocks for constructing a complex biopolymeric structure such as sporopollenin are present in *Lycopodium* spores, and, by using a distinctive feature of one or both of the classes of monomer (aliphatic and aromatic), it is possible to determine relative abundances of each, and thus

identify any changes in such abundances. FTIR microspectroscopy is a powerful and rapid technique that is well suited to the task.

If the hypothesis of Rozema *et al.* (2001a, 2001b) that increased CAD production within plants is a response to UV-B stimulation is correct, the relative height of the aromatic absorbance band (peak) would be expected to alter in accordance with relative abundance of aromatic groups. It is this proposition that forms the basis of the present work. The following three chapters will test this hypothesis by applying the rapid analytical technique detailed here to a selection of situations where UV-B flux is thought to vary.

2.7 References

Ballaré, C.L., Rousseaux, M.C., Searles, P.S., Zaller, J.G., Giordano, C.V., Robson, T.M., Caldwell, M.M., Sala, O.E. & Scopel, A.L. (2001) Impacts of solar ultraviolet-B radiation on terrestrial ecosystems of Tierra del Fuego (southern Argentina): An overview of recent progress. *Journal of Photochemistry and Photobiology B: Biology* **62**, 67-77.

Björn, L-O. (1999) Ultraviolet-B radiation, the ozone layer and ozone depletion, in; *Stratospheric ozone depletion: The effects of enhanced UV-B radiation on terrestrial ecosystems* (ed. J. Rozema). Backhuys publishers, Leiden, The Netherlands. pp. 21-37.

Blokker, P., Yeloff, D., Boelen, P., Broekman, R.A. & Rozema, J. (2005) Development of a proxy for past surface UV-B irradiation: A thermally assisted hydrolysis and methylation py-GC/MS method for the analysis of pollen and spores. *Analytical Chemistry* **77**(18) 6026-6031.

Boelen, P., de Boer, M.K., de Bakker, N.V.J. & Rozema, J. (2006) Outdoor studies on the effects of solar UV-B on bryophytes: overview and methodology. *Plant Ecology* **182**, 137-152.

Bornman, J.F. (1999) Localisation and functional significance of flavonoids and related compounds, in; *Stratospheric ozone depletion: The effects of enhanced UV-B radiation on terrestrial ecosystems* (ed. J. Rozema). Backhuys publishers, Leiden, The Netherlands. pp. 59-69.

Bradley, R.S. (1999) Paleoclimatology: Reconstructing climates of the Quaternary (2nd edition). Harcourt academic press, Burlington, MA, USA.

Burchard, P., Bilger, W. & Weissenböck, G. (2000) Contribution of hydroxycinnamates and flavonoids to epidermal shielding of UV-A and UV-B radiation in developing rye

primary leaves as assessed by ultraviolet chlorophyll fluorescence measurements. *Plant, Cell and Environment* **23**, 1373-1380.

Caldwell, M.M., Björn, L.O., Bornman, J.F., Flint, S.D., Kulandaivelu, G., Teramura, A.H. & Tevini, M. (1998) Effects of increased solar ultraviolet radiation on terrestrial ecosystems. *Journal of Photochemistry and Photobiology B: Biology* **46**, 40-52.

Edreva, A. (2005) The importance of non-photosynthetic pigments and cinnamic acid derivatives in photoprotection. *Agriculture, Ecosystems and Environment* **106**, 135-146.

Grace, S.C. & Logan, B.A. (2000) Energy dissipation and radical scavenging by the plant phenylpropanoid pathway. *Philosophical Transactions of the Royal Society of London B* **355**, 1499-1510.

Guildford, W.J., Schneider, D.M., Labovitz, J. & Opella, S.J. (1988) High resolution solid state ^{13}C NMR spectroscopy of sporopollenins from different plant taxa. *Plant Physiology* **86**, 134-136.

Gwynn-Jones, D., Lee, J.A. & Callaghan, T.V. (1997) Effects of UV-B radiation and elevated carbon dioxide concentrations on a sub-arctic forest heath ecosystem. *Plant Ecology* **128**, 243-249.

Hemsley, A.R., Chaloner, W.G., Scott, A.C. & Groombridge, C.J. (1992) Carbon-13 solid state nuclear magnetic resonance of sporopollenins from modern and fossil plants. *Annals of Botany* **69**, 545-549.

Hsiao, T.C. (1973) Plant responses to water stress. *Annual Reviews in Plant Physiology* **24**, 51-570.

Killops, S.D. & Killops, V.J. (2005) Introduction to organic geochemistry (2nd edition). Blackwell Publishing, Oxford, UK.

King, P.L., Ramsey, M.S., McMillan, P.F. & Swayze, G. (2004) Laboratory fourier transform infrared spectroscopy methods for geologic samples, in: *Infrared spectroscopy in geochemistry, exploration geochemistry and remote sensing* (eds. P.L. King, M.S. Ramsey & G.A. Swayze). Mineralogical Association of Canada short course series, volume 33. pp. 57-91.

Kumar, D., Singh, B.P. & Kumar, P. (2004) An overview of factors affecting sugar content of potatoes. *Annals of Applied Biology* **145**, 247-256.

de Leeuw, J.W., Versteegh, G.J.M. & van Bergen, P.F. (2006) Biomacromolecules of algae and plants and their fossil analogues. *Plant Ecology* **182**, 209-233.

Marga, F., Gallo, A. & Hasenstein, K.H. (2003) Cell wall components affect mechanical properties: studies with thistle flowers. *Plant Physiology and Biochemistry* **41**, 792-797.

Meijkamp, B., Aerts, R., van de Staaij, J., Tosserams, M., Ernst, W.H.O. & Rozema, J. (1999) Effects of UV-B on secondary metabolites in plants, in; *Stratospheric ozone depletion: The*

effects of enhanced UV-B radiation on terrestrial ecosystems (ed. J. Rozema). Backhuys publishers, Leiden, The Netherlands. pp. 71-99.

Pappas, C.S., Tarantilis, P.A., Harizanis, P.C. & Polissiou, M.G. (2003) New method for pollen identification by FTIR spectroscopy. *Applied Spectroscopy* **57**(1), 26-27.

Pourcel, L., Routaboul, J-M., Cheyner, V., Lepiniec, L. & Debeaujon, I. (2006) Flavanoid oxidation in plants: from biochemical properties to physiological functions. *Trends in Plant Science* **12**(1), 29-36.

Pšenička, J., Zodrow, E.L., Mastalerz, M. & Bek, J. (2005) Functional groups of fossil marattialeans: chemotaxonomic implications for Pennsylvanian tree ferns and pteridophylls. *International Journal of Coal Geology* **61**, 259-280.

Reynolds, M.P., Mujeeb-Kazi, A. & Sawkins, M. (2005) Prospects for utilising plant-adaptive mechanisms to improve wheat and other crops in drought – and salinity-prone environments. *Annals of Applied Biology* **146**, 239-259.

de la Rosa, T.M., Julkunen-Titto, R., Lehto, T. & Aphalo, P.J. (2001) Secondary metabolites and nutrient concentrations in silver birch seedlings under five levels of daily UV-B exposure and two relative nutrient addition rates. *New Phytologist* **150**, 121-132.

Rouxhet. P.G., Robin, P.L & Nicaise, G.B. (1980) Characterisation of kerogens and their evolution by infrared spectroscopy, in; *Kerogen*, (ed. B. Durand), Editions Techniq, Paris. pp. 163-190.

Roy, B.A., Stanton, M.L. & Eppley, S.M. (1999) Effects of environmental stress on leaf hair density and consequences for selection. *Journal of Evolutionary Biology* **12**, 1089-1103.

Rozema, J., van de Staaij, J., Björn, L-O. & Caldwell, M. (1997) UV-B as an environmental factor in plant life: stress and regulation. *Trends in Ecology and Evolution* **12**(1), 22-28.

Rozema, J., Broekman, R.A., Blokker, P., Meijkamp, B.B., de Bakker, N., van de Staaij, J., van Beem, A., Ariese, F. & Kars, S.M. (2001a) UV-B absorbance and UV-B absorbing compounds (para-coumaric acid) in pollen and sporopollenin: the perspective to track historic UV-B levels. *Journal of Photochemistry and Photobiology B: Biology* **62**, 108-117.

Rozema, J., Noordijk, A.J., Broekman, R.A., van Beem, A., Meijkamp, B.M., de bakker, N.V.J., van de Staaij, J.W.M., Stroetenga, M., Bohncke, S.J.P., Konert, M., Kars, S., Peat, H., Smith, R.I.L. & Convey, P. (2001b) (Poly)phenolic compounds in pollen and spores of Antacrtica plants as indicators of solar UV-B: A new proxy for the reconstruction of past solar UV-B? *Plant Ecology* **154**, 11-26.

Searles, P.S., Flint, S.D. & Caldwell, M.M. (2001) A meta-analysis of plant field studies simulating stratospheric ozone depletion. *Oecologia* **127**, 1-10.

Scott, A.C. (2002) Coal petrology and the origin of coal macerals: a way ahead? *International Journal of Coal Geology* **50**, 119-134.

Sephton, M.A. (1997) Organic compounds in meteorites. PhD thesis, The Open University.

Vandenbroucke, M. & Largeau, C. (2007) Kerogen origin, evolution and structure. *Organic Geochemistry* **38**, 719-833.

Visser, A.J., Tosserams, M., Groen, M.W., Kalis, G., Kwant, R., Magendans, G.W.H. & Rozema, J. (1997) The combined effects of CO_2 concentration and enhanced UV-B radiation on faba bean. 3. Leaf optical properties, pigments, stomatal index and epidermal cell density. *Plant Ecology* **128**, 209-222.

Wahid, A., Gelani, S., Ashraf, M. & Foolad, M.R. (in press) Heat tolerance in plants: An overview. *Environmental and Experimental Botany* doi:10.1016/j.envexpbot.2007.05.011

Walker, R. & Mastalerz, M. (2004) Functional groups and individual maceral chemistry of high volatile bituminous coals from southern Indiana: controls on coking. *International Journal of Coal Geology* **58**, 181-191.

Watson, J.S., Sephton, M.A., Sephton, S.V., Self, S., Fraser, W.T., Lomax, B.H., Gilmour, I., Wellman, C.H., Beerling, D.J. (2007a) Rapid determination of spore chemistry using thermochemolysis gas chromatography-mass spectrometry and micro-Fourier transform infrared spectroscopy. *Photochemical & Photobiological Sciences* **6**, 689-694.

Watson, J.S., Fraser, W.T., Self, S. & Septhon, M.A. (2007b) Formation of an aliphatic polymer during heating experiments with Lycopodium spores. IMOG 2007 conference abstract, Torquay, UK.

Williams, D.H. & Fleming, I. (1980) Spectroscopic methods in organic geochemistry. McGraw-Hill, London.

Wittborn, J., Rao, K.V., El-Ghazaly, G. & Rowley, J.R. (1998) Nanosclae similarities in the substructure of the exines of Fagus pollen grains and Lycopodium spores. *Annals of Botany* **82**, 141-145.

Xuaguang, S. (2005) The investigation of chemical structure of coal macerals via transmitted-light FTIR microspectroscopy. *Spectrochimica Acta: part A* **62**, 557-564.

Yule, B.L., Roberts, S. & Marshall, J.E.A. (2000) The thermal evolution of sporopollenin. *Organic Geochemistry* **31**, 859-870.

3 Experimental verification of proxy

3.1 Introduction

Numerous attempts have been made in recent years to constrain the physiological and chemical responses of plants to changes in UV-B flux in order to understand the effects that an anthropogenically-altered atmosphere might have upon Earth's biota (Searles *et al.*, 2001). The majority of studies have focussed on the flora of polar and sub-polar regions due to the stratospheric ozone 'holes' that develop over these areas. In order to isolate UV-B as a stress factor, experiments have been conducted whereby UV-B flux is artificially manipulated to simulate environmental conditions equivalent to those experienced during times of stratospheric ozone depletion. These experiments aim to provide an insight into how quickly plants respond to UV-B, what physiological and chemical changes are induced by UV-B radiation, and how detection of these induced changes may be applied to collections of natural material for the development of a successful UV-B flux proxy.

3.2 History of research

3.2.1 UV-B impact on plants

UV-B is recognised as an environmental stress factor (Rozema *et al.*, 1997; Stratmann, 2003) that stimulates the Shikimate and phenylpropanoid pathways (PPP) within terrestrial flora (Caldwell *et al.*, 1989; Meijkamp *et al.*, 1999) (as summarised in Chapters 1 and 2). The result of stimulating these pathways is the production and incorporation into tissues of UV-B absorbing compounds (UACs). The majority of studies that investigate UV-B photoprotection provided by UACs focus on UV-B absorption of leaf tissue (Searles *et al.*, 2001, Kotilainen *et al.*, 2008), although Stratmann (2003) indicates that changes in abundance of UAC in leaves may also be induced by herbivory *via* genetically controlled co-opted defence

pathways. If the same chemical response in leaves can be triggered by both herbivory and UV-B radiation any study investigating the phenolic content of leaves is susceptible to anomalous results due to interference with phenolic production.

Another problem posed by analysis of leaf phenolic content is that leaves are an "active" part of a living plant, thus are liable to change rapidly in response to changing stimuli. Rapid changes in chemical response to UV-B (both increases and decreases) would render leaf phenolic content as a proxy unviable.

Pollen/spores have much greater potential to act as UV-B monitors as they are the reproductive material of plants, thus investment in protecting the enclosed genetic information is likely in order to perpetuate the species (Santos *et al.*, 1998). Pollen/spores are ultimately to become detached from the plant, thus repair processes will not operate as the entity will no longer be an "active" part of the plant, and as a result a passive protection mechanism would be beneficial, if not essential.

Increased UV-B irradiance has been found to result in morphological changes and reduced growth, particularly in studies involving crop plants (Searles *et al.*, 2001). Overall decreases in leaf area and shoot biomass are observed under enhanced UV-B conditions (Sisson & Caldwell, 1976), whilst other parameters such as plant height or leaf mass per unit area, experience only minor changes, if any at all (Searles *et al.*, 2001). Confirmation of these relationships is provided by UV-B exclusion experiments conducted by Lingakumar *et al.* (1999). These experiments demonstrated increases in fresh mass (leaf mass and total mass), leaf area and height of seedlings under reduced UV-B regimes, suggesting a linear response both above and below present ambient UV-B levels.

Photosynthetic processes are reported to be adversely affected by increased UV-B *via* a number of mechanisms. Direct effects that impact upon photosynthesis include damage to chloroplast ultrastructure (Brandle *et al.*, 1977; Van *et al.*, 1977; Greenberg *et al.*, 1989; Allen *et al.*, 1998) and a resultant reduction in photosynthetic rate occurs (Sisson & Caldwell, 1976). In addition, indirect effects operate to decrease photosynthetic rate such as the alteration of the optical properties of leaves *via* changes in pigment content and anatomical effects, thus disrupting the distribution of photosynthetically active radiation (PAR) within the leaf (Bornman & Vogelmann, 1991).

As numerous reviews of the effects of UV-B on plants have summarised in recent years (Teramura, 1983; Teramura & Sullivan, 1994; Rozema *et al.*, 1997; Sullivan & Rozema, 1999) induction of UACs is cited as the most commonly observed effect of UV-B treatment (Caldwell & Flint, 1994; Searles *et al.*, 2001). Growth and morphological changes are the next most common effects, and finally impacts on photosynthesis are regarded as the least observed effect (Searles *et al.*, 2001).

3.2.1.1 Experimental approaches

Previous work on the impact of UV-B on plants has been conducted *via* a two-pronged approach; laboratory experiments have been conducted in growth cabinets, where artificial radiation sources are used to provide the entire radiative input enabling close control of all experimental variables (Ålenius *et al.*, 1995; Flint & Caldwell, 1996; Santos *et al.*, 1998; Rozema *et al.*, 2002; van de Staaij *et al.*, 2002). The second approach entails the manipulation and/or supplementation of natural incoming solar radiation in field studies (Teramura, 1983; Beggs & Wellman, 1985; Campbell *et al.*, 1999; Gwynn-Jones *et al.*, 1999; Huiskes *et al.*, 1999; Lingakumar *et al.*, 1999; Rozema *et al.*, 1999; Searles *et al.*, 1999; Ballaré *et al.*, 2001; Day *et al.*, 2001; Rousseaux *et al.*, 2001; Searles *et al.*, 2001; Rozema *et al.*, 2002; van de Staaij, *et al.*, 2002). Both types of experiment may be further sub-divided by the level of UV-B experienced by the

growing plants; exclusion experiments reduce the amount of UV-B reaching the plants, representing an increase in total column ozone depth (e.g Lingakumar *et al.*, 1999), whilst enhancement experiments supplement incoming UV-B, representing a depleted ozone column (e.g. Sisson & Caldwell, 1976).

Outdoor experiments that exploit the natural balance of the solar spectrum have become favoured because issues of disproportionate fluxes of UV-B and PAR associated with artificial radiation input are intrinsically negated by the use of natural sunlight (Teramura & Sullivan, 1991). But such field studies are not without their drawbacks. Musil *et al.* (2002) consider the effectiveness of UV-B enhancement regimes in field experiment set-ups by comparing the two types of radiation supplementation systems in use: square-wave (SQW) systems, and modulated (MOD) systems. Square-wave systems supply a predetermined constant UV-B flux appropriate for the geographical position of the field site that represents a specified ozone depletion scenario, as calculated by a spectral model with the assumption of clear-sky conditions (Björn & Murphy, 1985). Modulated delivery systems incorporate a feedback loop whereby natural UV-B is constantly measured and supplementation lamp output is adjusted accordingly to maintain a constant relative relationship between solar and supplemental radiation inputs. The key advantage of MOD systems over SQW systems is that less reliance on computer modelling is required in order to achieve the desired supplemental UV-B scenario; equally, this is also the basis of the primary criticism of SQW systems. As a consequence it is claimed that SQW systems may results in exaggerated input to experiments by up to 30% in some cases (Musil *et al.*, 2002). Such large discrepancies are likely to occur mostly on cloudy days because the spectral models upon which SQW input parameters are based assume clear-sky conditions, thus clouds are not accounted for in these calculations. Despite this criticism of SQW systems, they still remain in greater use because of the ease of operation of this type of delivery system; MOD systems are reported to be technically and

economically more demanding, whilst SQW systems can generally be left running for entire growing seasons without any additional operator input (Musil *et al.*, 2002).

Field studies involving UV-B treatments (particularly enhancement) generally show significantly less morphological and physiological responses to UV-B stress than expected from the results of growth chamber or greenhouse studies (Laakso & Huttunen, 1998; Sullivan & Rozema, 1999). The reasons for this are unclear; however, it may be that other environmental stress factors also play important roles that reduce the observed impact of UV-B in field studies. Inadequate replication of the natural balance between UV and PAR lighting conditions in growth chambers has been cited as a prominent factor that may lead to exaggeration of UV-B responses, thus increasing the difference between indoor and outdoor experiment results (Teramura, 1983; Searles *et al.*, 2001).

The field experiments described below investigate the most commonly observed plant response – changes in the chemistry of plant tissues.

3.2.2 Abisko-Naturvetenskapliga Station, Sweden

Abisko-Naturvetenskapliga Station (ANS) is situated approximately 200 km north of the arctic circle, northern Sweden (68° 21' N 18° 49' E) within an area forested almost exclusively by birch trees (*Betula pubescens* ssp. *tortuosa*; Ovhed & Holmgren, 1996) constituting part of the Abisko national park (77 km^2). ANS lies on the southern shore of Lake Torneträsk at an elevation of 385 m above sea level (a.s.l.).

The region around Abisko is bounded to the west and south by the Scandinavian (Scandes) Mountain range marking the Norwegian-Swedish border, with peaks reaching up to ~1500 m a.s.l. forming a physical barrier between the two countries.

3.2.2.1 Meteorology

Strong westerly winds are dominant along the northern Norwegian coast, sweeping moist maritime air across Norway giving rise to a dominant maritime climate, thus precipitation is high in this area (e.g. Svolvær, Lofoten Islands =~1500 mm yr^{-1}; Andenes ~1060 mm yr^{-1}; Narvik = ~830 mm yr^{-1}). However Abisko lies sheltered on the leeward side of the Scandinavian Mountains within a rain shadow (Berglund *et al.*, 1996; Hammarlund *et al.*, 2002; Ridefelt & Boelhouwers, 2006). As a result ANS and the surrounding area experiences significantly lower annual precipitation (e.g. Abisko = ~300 mm yr^{-1}; Torneträsk = ~472 mm yr^{-1}; Kiruna = ~500 mm yr^{-1}) and a more continental-style climate (Figure 3.1).

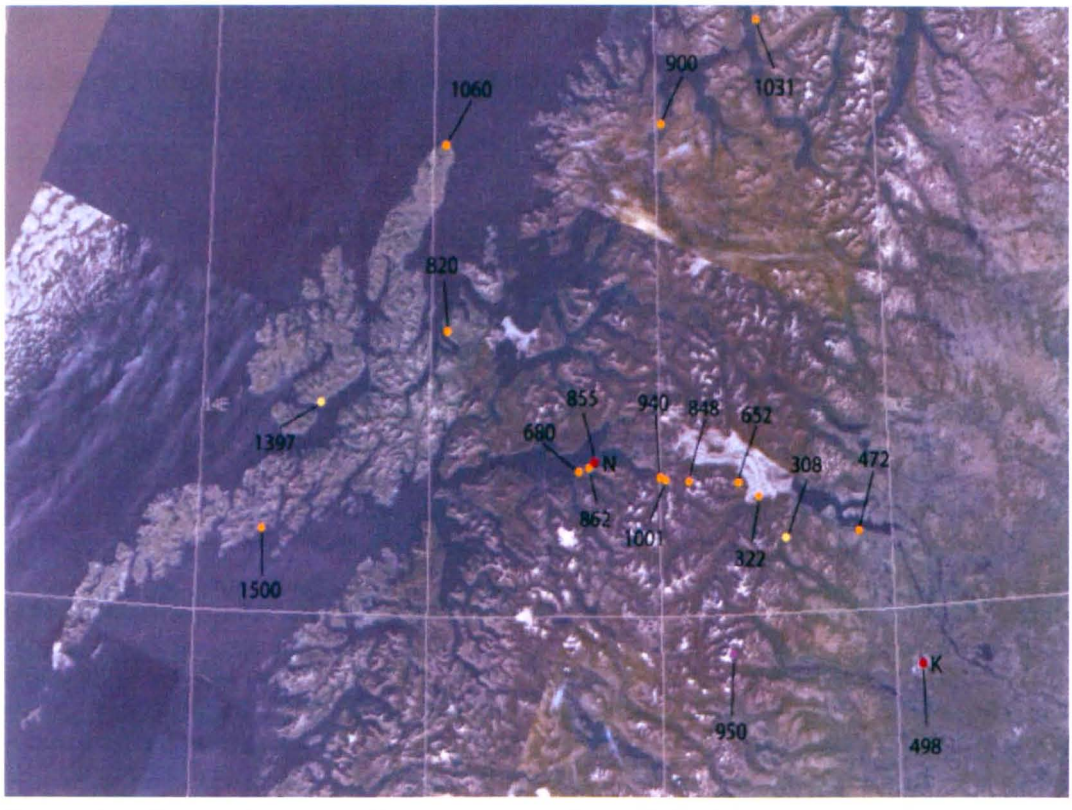

Figure 3.1 Regional map with mean annual precipitation (mm/year) indicated for various locations. Red circles represent main towns; orange circles indicate villages and small towns; purple circle indicate locations of research stations; yellow circles are locations with available records of precipitation data. K = Kiruna, N = Narvik. Data compiled from multiple sources, see table 8.5 in Appendix B for references. Map captured from GoogleEarth™.

Mean annual precipitation at ANS has increased over the past eight decades by an average of ~4 mm per decade for the period 1920-2000 (Figure 3.2a). The greatest proportion of precipitation falls as rain during the summer months (June, July, August), accounting for ~40 % of annual precipitation. Autumn and winter experience almost equal quantities of precipitation (~ 24 % and ~ 22 %, respectively); spring is the driest season (~15 %) (Figure 3.2b). These values agree with those reported elsewhere (Kohler *et al.*, 2006). Precipitation throughout autumn, winter and spring falls predominantly as snow (October to May) resulting in a long snowy season.

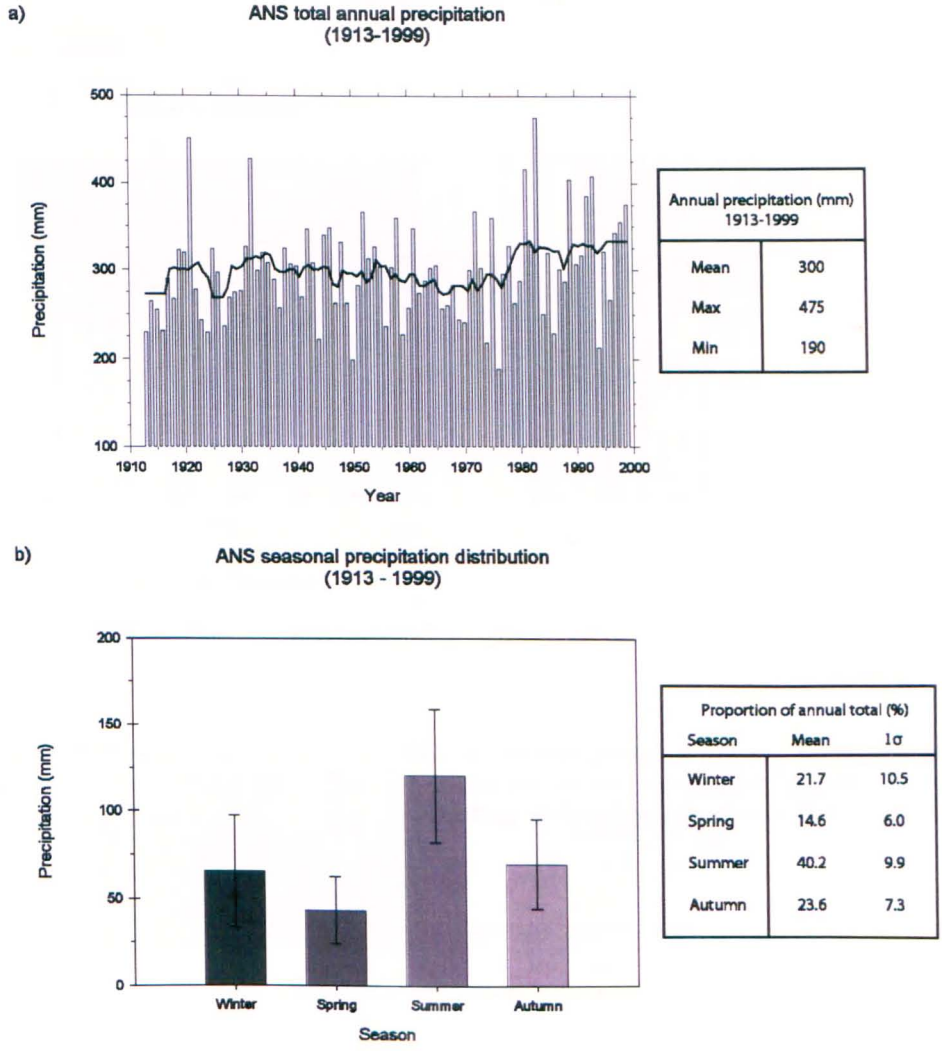

Figure 3.2 Precipitation record at Abisko-Naturvetenskapliga Station. a) Annual precipitation at ANS for the period 1913-1999. Trend line is 5 year running mean. b) Average seasonal distribution of precipitation at ANS for the period 1913-1999. Winter = Dec-Feb; spring = Mar-May; summer = Jun-Aug; autumn = Sep-Nov. Error bars are one standard deviation.

Mean annual air temperature at ANS has increased during the 130 years that records have been kept (Figure 3.3) rising by ~1 °C overall. Investigation of seasonal temperatures reveals that spring has been subject to the greatest change of ~2 °C. Both summer and autumn have also increased by approximately 1 °C. Mean winter temperatures appear to have remained stable since 1869 (Figure 3.4).

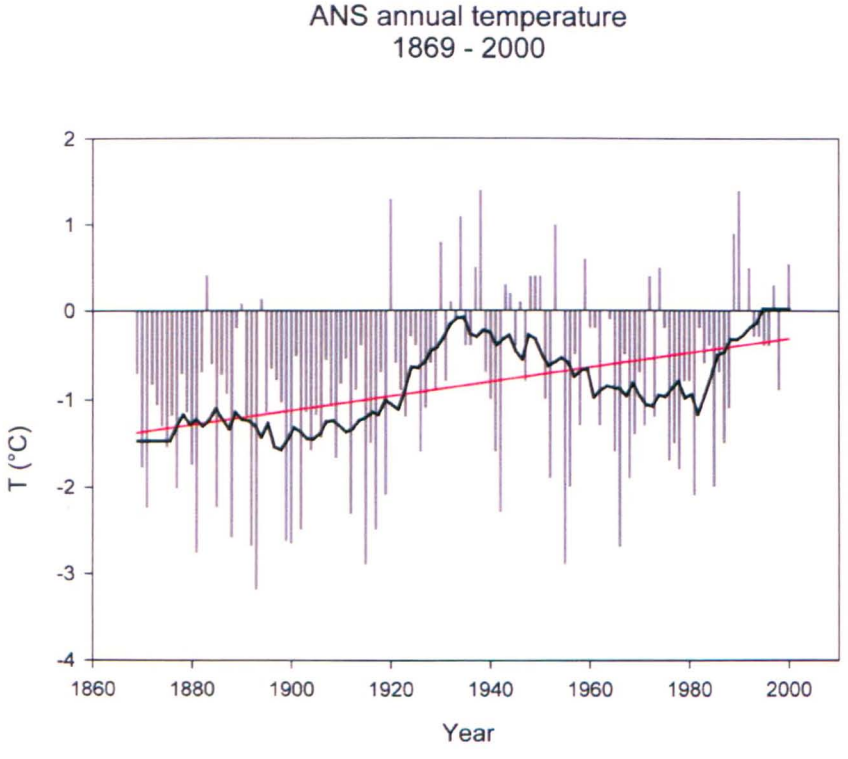

Figure 3.3 Mean annual air temperature at ANS for the period 1869-2000. Black line is 5 year running mean; red line is the linear trend for the entire period. An overall increase of ~1 ºC is observed for this period.

A combination of a prolonged snowy season and mean seasonal temperatures $\leq$ 0 °C from autumn until spring results in persistent snow-cover until early May. Snow-cover has a two-fold impact upon low-level flora; firstly by blocking out any available sunlight, and secondly by insulating the ground for up to seven months per year. The effect of snow cover and air temperature on soil temperature is demonstrated by using 2004 temperature records from ANS as an example (Figure 3.5). The shallowest layers of soil (5 cm) are at the interface between soil and air, thus respond the most rapidly to changes in air temperature, evident by

the greatest temperature range (Min = -3.85 °C, Max = 12.78 °C) and an annual trend that resembles the air temperature trend. It should be noted that this close temperature relationship between the uppermost layers of soil and air temperature is most strongly exhibited during the summer months; during the autumn-spring months the insulating effect of snow cover moderates soil temperature, preventing it from becoming as cold as the air temperature. At depth (100 cm), soil temperatures show the least variance throughout a single year (Min = 0.04 °C, Max = 7.19 °C) due to the insulation provided by the overlying soil layers. Interestingly, thermal inertia at this depth results in temperatures remaining above freezing for the entirety of the year, whereas overlying layers are found to drop below 0 °C during the winter.

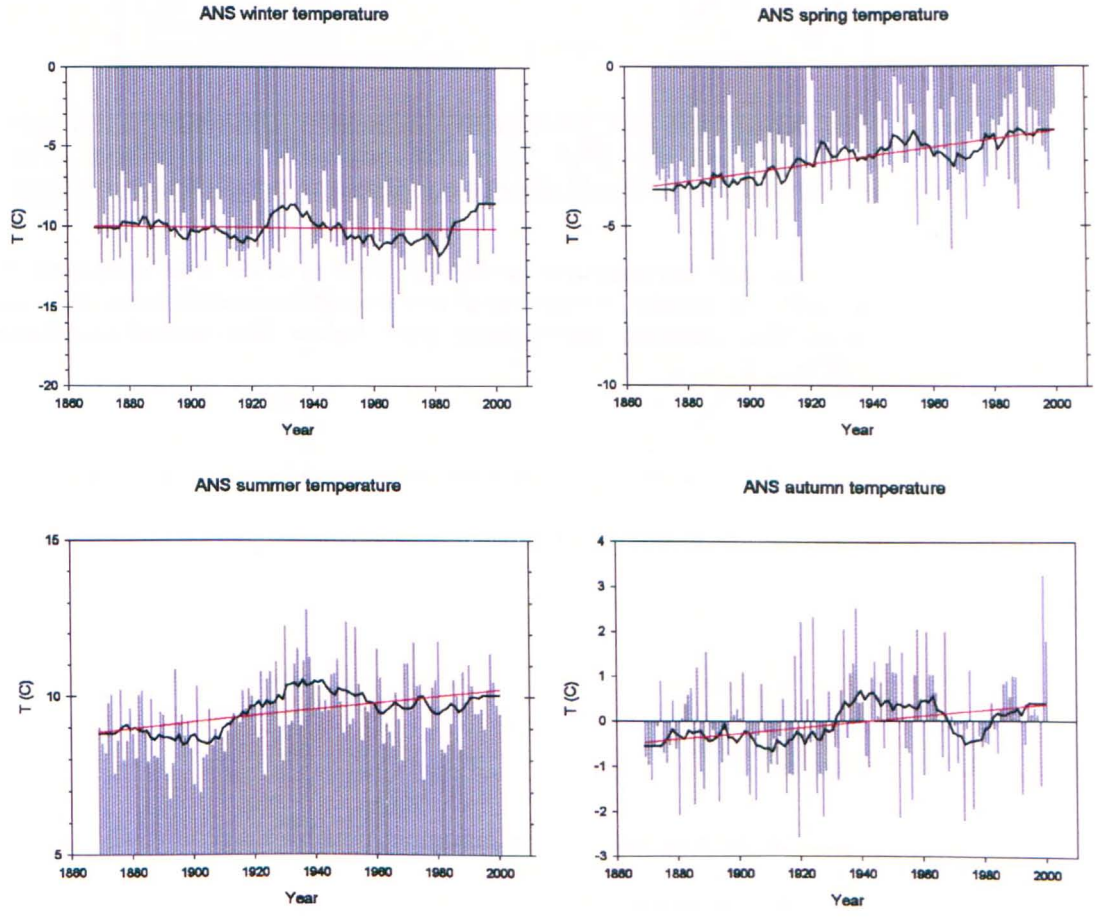

Figure 3.4 Seasonal mean air temperatures recorded at ANS for the period 1869-2000. Black line is 5 year running mean; red line is the linear trend for the entire period. Winter remains essentially stable throughout the recorded period, summer and autumn exhibit increases of ~1ºC, and spring shows the greatest increase of ~2ºC. Division of seasons is the same as for precipitation (Figure 3.2b).

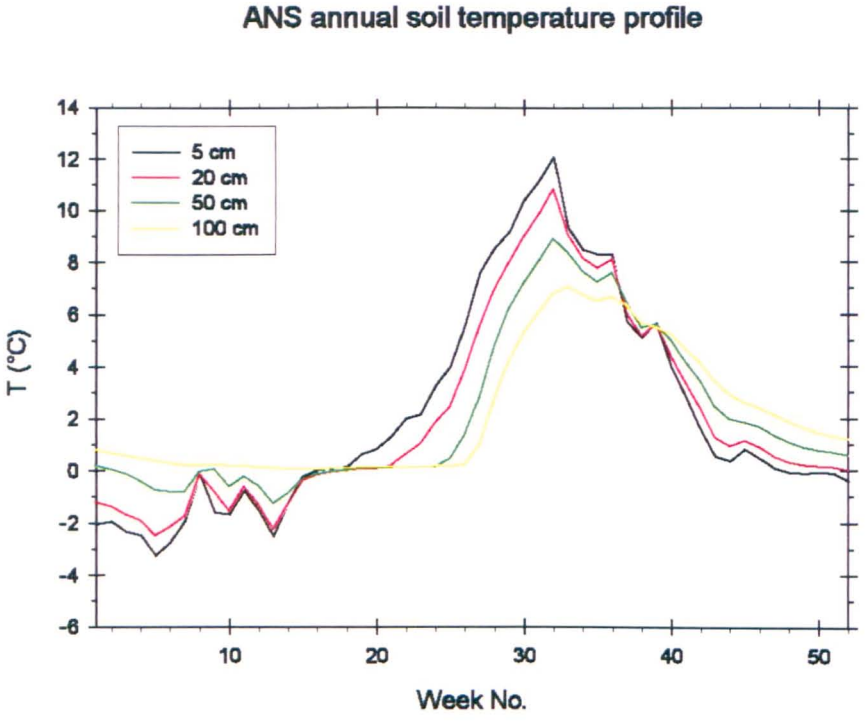

Figure 3.5 Weekly mean soil temperature profile for 2004 at ANS. Soil temperature is recorded at four different depths. Coupling of soil and atmospheric temperatures is greatest at shallower depths, particularly just below the soil-atmosphere interface (5 cm depth).

In summary, the persistence of snow cover for a considerable proportion of the year is a significant limiting factor on the length of the growing season, constraining ground-level plant growth to the months May through to October.

3.2.2.2 UV-B and ozone

Due to northern extremity, ANS experiences the maximum possible range in daylight hours throughout the year from total darkness during winter months, to 24-hour sunlight during summertime (Figure 3.6). Hence in summer months UV-B irradiance will be highest (0.77 ± 0.32 W m^{-2} (mean of peak daily irradiances for clear skies)) whilst winter months receive virtually no solar radiation whatsoever (UV-B = 0.001 ± 0.003 W m^{-2}) (Häder *et al.*, 2007). This intra-annual distribution of UV-B flux concentrates the annual UV-B input into those months that experience daylight, particularly the continuous daylight hours of the summer

months. Higher UV-B fluxes correlate well with photosynthetically active radiation (PAR; λ = 400-700 nm) (Figure 3.7), which coincide with the annual growing season. Ongoing UV-B measurements are being conducted at ANS; publicly accessible data via the ELDONET program (http://www.eldonet.org/) is available from 1997 to present (Häder *et al.*, 2007).

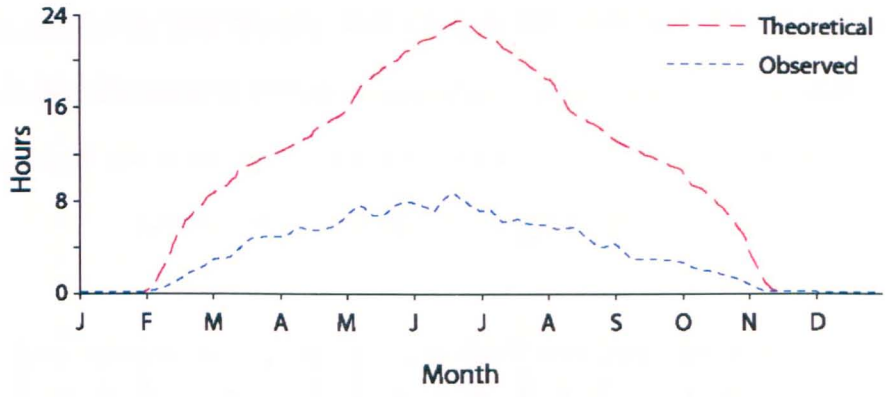

Figure 3.6 Theoretical maximum (red dashed line) and diurnal average of observed (blue dotted line) sunshine hours at ANS for the period 1961-1990. From: http://www.ans.kiruna.se/weather/y-shours.htm Date accessed: 20/08/2007.

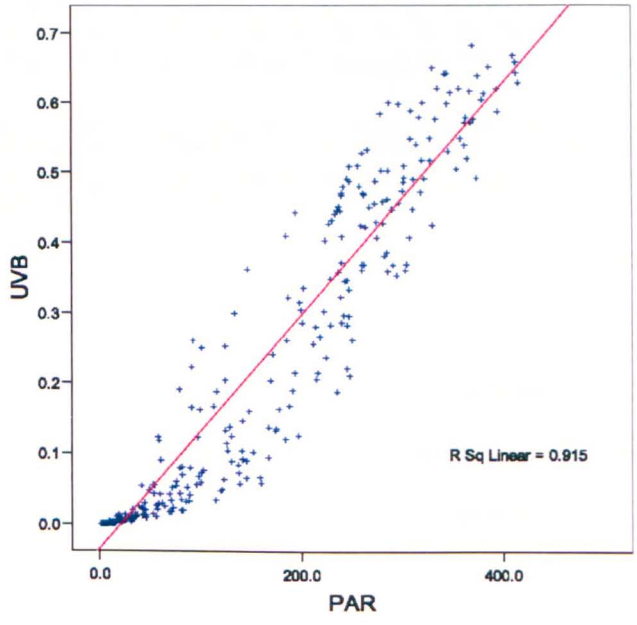

Figure 3.7 Linear regression of ELDONET UV-B and PAR measurements for 2004 at ANS. Both PAR and UV-B flux measured in W m^{-2}. Pearson correlation coefficient = 0.957 significant at the 0.01 level; F = 3664.161, p = <0.01.

ANS maintains an automated meteorological station on site that records high temporal resolution data (hourly) for precipitation, relative humidity, soil profile temperature, air temperature, wind speed/direction, incoming radiation (longwave, global and PAR), and sunshine duration (i.e. clear sky). The station is also equipped with spectroradiometers that provide regular UV-B measurements. Unfortunately the UV-B spectroradiometers at ANS were out of operation for most of the experimental period reported in this thesis (2004-2006) due to technical faults, followed by instrument calibration in Switzerland.

As a result of technical difficulties UV-B flux records are not available from the ANS meteorological station. Investigation of ELDONET data reveal that only 2004 is adequately recorded for the experimental period under consideration; both 2005 and 2006 appear to be incomplete (Appendix C). In order to rectify this gap in UV-B flux data Lindfors *et al.* (2006) have developed a model using total ozone, sunshine duration and snow depth as input parameters to determine past UV-B dosage (Lindfors *et al.*, 2003, 2005). Whilst this model extends UV dosage estimates back in time to 1913, it only provides a temporal resolution of seasonal variation. As discussed above (Section 3.2.2.1), the growing season at ANS is limited to a maximum period of May to October, encompassing the two seasons of spring (March to May) and summer (June to August). Thus it is the UV-B input during these months that is important for this study, particularly at the sub-seasonal scale in order to gain an insight into the duration of exposure required to initiate the chemical response under investigation. In order to investigate the sub-seasonal UV-B flux, UV-B must be reconstructed using an alternative method.

ANS have a near-continuous record of full-year PAR for the period 1985-2006 and is used in this study to attempt to reconstruct estimated UV-B flux using a rudimentary model based on a linear relationship observed between PAR and UV-B flux in the ELDONET data (see Appendix C for details of this model and a brief discussion of performance in relation to the

model of Lindfors *et al.*, 2006). The reconstruction of UV-B for the period 1985-2006 is presented in Figure 3.8. Whilst PAR and UV-B may exhibit a very strong linear relationship under clear-sky conditions, this is unlikely to hold true for cloudy conditions as is often the case with UV-B modelling (Musil *et al.*, 2002), thus UV-B flux generated by the model of the present study must be regarded as an estimate, however in the absence of any other high-resolution UV-B flux measurements for the period 2004-2006 the output from this model is likely to be the best equivalent data.

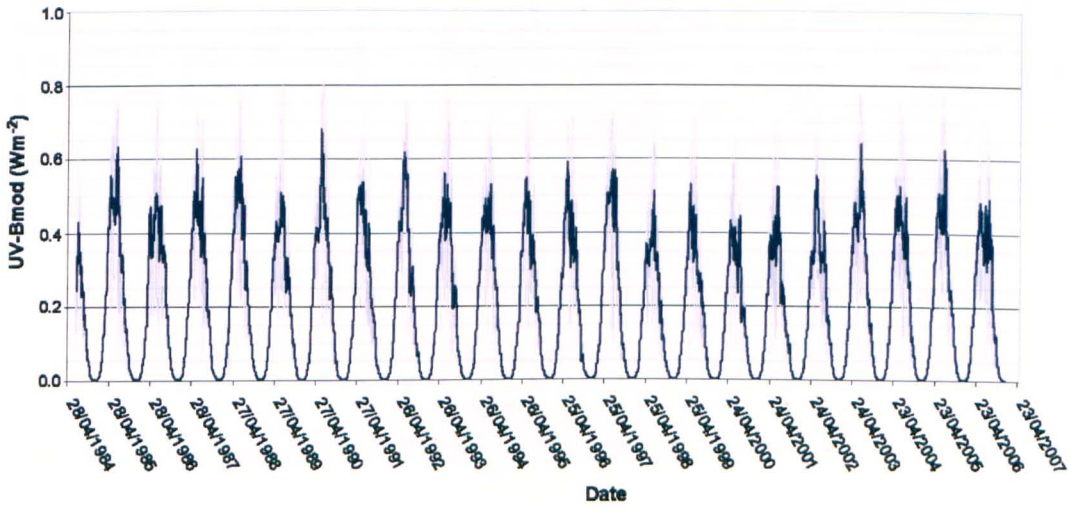

Figure 3.8 Reconstruction of UV-B flux from ANS PAR records for the period 1985-2006. Grey lines are daily values, thick blue line is the 14 day running mean in order to remove any short-term cloud effects.

Häder *et al.* (2007) also consider total ozone column data derived from the total ozone mapping spectrometer (TOMS) and find a mean column depth of 333 DU above ANS (1997-2005) (Min = 218 DU, Max = 495 DU). The data of Häder *et al.* (2007) include only days that experienced clear-sky conditions. Less sophisticated analysis of the raw TOMS data (i.e. without removal of non-clear days) returns a mean value of 327 DU (Min = 240 DU, Max = 448 DU) over the same period, which is in very close agreement with the published data (Appendix D). Analysis of monthly means reveals ozone is most abundant in early spring

(March-April) due to ozone build-up prior to polar sunrise and tapers off to ~71% of the spring maximum in autumn (October) (Figure 3.9).

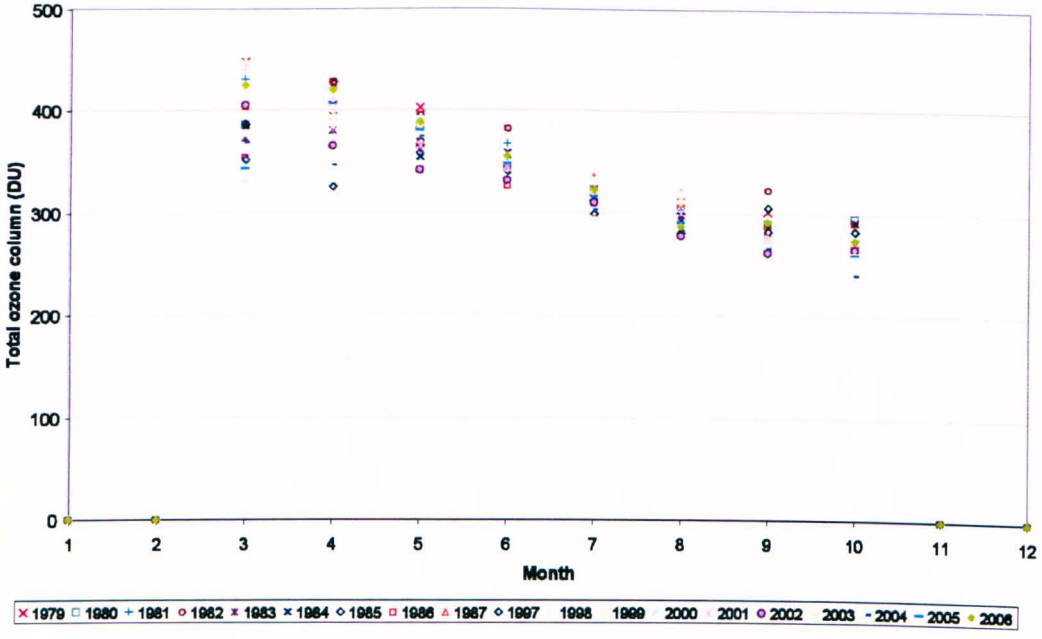

Figure 3.9 Monthly mean stratospheric ozone trend for the periods 1979-1987 and 1997-2006. Taken from the Nimubus7 TOMS (N7T; 1979-1987), Earth Probe TOMS (EPT; 1997-2004) and Ozone Monitoring Instrument (OMI; 2005-2006). Data from: http://toms.gsfc.nasa.gov/ Date accessed: 07/09/2007.

3.3 Sample description and experimental

Fresh *Lycopodium annotinum* spores were harvested from six pre-existing growth experiments located within the ANS research gardens (similar to those used in Phoenix *et al.*, 2000 and Gwynn-Jones, 2001). The experimental growth conditions used were designed to manipulate UV-B input to the plants throughout the growing season. Two UV scenarios were selected for investigation (Table 3.1). *L. annotinum* were analysed for reasons outlined in Chapter 2 (Section 2.3.1), and grow in abundance in the Abisko Valley surrounding ANS.

Table 3.1 Experimental growth conditions at ANS for years 2004-2006. UV-B measurements in µmol m^{-2} s^{-1}.

	UV-B measurements		% of ambient
	Ambient	Experimental	
Exclusion			
Treatment			
Mean	0.373	**0.029**	8.1
Std Dev	0.070	0.013	4.2
Count	18	18	18
Std Er	0.016	0.003	1.0
Control			
Mean	0.328	**0.170**	52.5
Std Dev	0.057	0.022	5.7
Count	18	18	18
Std Er	0.013	0.005	1.3
Ambient			
Mean	0.396	**0.367**	93.3
Std Dev	0.049	0.047	11.3
Count	18	18	18
Std Er	0.012	0.011	2.7

	UV-B measurements		% of ambient
	Ambient	Experimental	
Enhancement			
Treatment			
Mean	0.536	**0.554**	103.4
Std Dev	0.040	0.047	6.4
Count	15	15	15
Std Er	0.010	0.012	1.6
Control			
Mean	0.507	**0.489**	97.1
Std Dev	0.038	0.035	11.4
Count	15	15	15
Std Er	0.010	0.009	2.9
Ambient			
Mean	0.409	**0.400**	97.9
Std Dev	0.044	0.041	5.6
Count	15	15	15
Std Er	0.011	0.011	1.4

Length of growing season for this experiment is time-limited by the environmental factors outlined above. Growth does not begin until the snow cover has melted during May, and effectively ends when the spore-bearing strobili are harvested for analysis in the following September.

3.3.1 UV-B Exclusion

The first scenario deals with varying degrees of exclusion of UV-B radiation, simulating an increase in total ozone column depth (Table 3.1). Exclusion of UV-B was achieved via a UV-B specific filter (226 Lee UV, Lee filters, UK), supported by a metal frame (Plate 3.1). This reduced UV-B radiation reaching the plant to approximately 8 % of measured incipient ambient UV-B; this plot is termed the treatment plot. In addition two control set-ups were conducted in the same location; a control plot incorporated the same style of metal frame as the treatment plot, but without a UV-B filter. Due to shading effects and close proximity of the metal frame to the growing plants, control plots experienced approximately 52 % of

measured incident ambient UV-B. The filter was replaced with cellulose acetate that does not possess UV-B filtering properties. An ambient plot was simply a plot of undisturbed vegetation in the vicinity of the treatment and control plots; ambient plots received approximately 93 % incoming UV-B. All exclusion, control and ambient plots were replicated six times, totalling eighteen plots. For improved statistical confidence, 3 samples were taken from each experimental plot, equalling a potential maximum of 54 individual samples for analysis in total. In practice this total number of samples is unlikely due to variable success of growth within each plot in any particular year. The exclusion experiment was located in a small wooded area predominantly populated by birch trees typical of the natural habitat of *L. annotinum* in the region. Due to the presence of the birch trees the entire exclusion experiment was subject to variable amounts of shading of UV-B, equal to approximately 74 % of incident UV-B in an equivalent open area.

Plate 3.1 Experimental UV-B exclusion frame at ANS.

3.3.2 UV-B Enhancement

The second scenario is designed to model depletion of the ozone layer by enhancing the amount of UV-B to a level equivalent to 2.5 % total ozone column depletion (Table 3.1). Enhancement is achieved *via* UV lamps suspended from 1.6 m tall frames; this set-up allows a

large proportion of natural light to reach the *Lycopodium*, whilst the UV-B spectrum is supplemented by the lamps (Plate 3.2). Treatment plots were grown beneath frames with fully operational lamps, control plots had an identical set-up to the treatment plots, but the lamps were never operated. The ambient plots comprised of plants growing beneath open sky. The incident UV-B experienced under each experimental regime was 97%, 98% and 103%, for control, ambient and enhancement plots, respectively. All plots within the enhancement experiment were replicated five times, totalling fifteen plots altogether. Three samples were collected from each of the experimental plots, totalling a potential maximum of 45 individual samples overall. Again, this value represents the upper limit of harvestable samples, in reality samples number is likely to be less than this.

Plants for the enhancement experiment were transplanted from their natural growing sites in the surrounding area to gravel trays in order to allow them to be easily positioned under the enhancement frames. The enhancement site is situated approximately 60 m NE of the exclusion site on top of a small hillock, where the influence of shading from birch trees is almost non-existent.

Plate 3.2 Experimental UV-B enhancement frame at ANS.

3.3.3 UV-B measurements

All measurements of UV-B within the experimental plots at ANS were taken on the 13th and 14th of September 2006 at approximately midday (13:10-13:50 and 12:05-13:03, respectively), coinciding with peak daily levels of incident radiation (Figure 3.7). A Skye Instruments SKU400 handheld meter was used attached to a SKU430 UV-B specific detector, with an operational range of either 0.000-2.000 μmol m^{-2} s^{-1}, or 00.00-20.00 μmol m^{-2} s^{-1}. Natural levels of UV-B were found to be < 2 μmol m^{-2} s^{-1} therefore the smaller range was chosen in order to gain better precision (3 decimal places). Every measurement of UV-B experienced within a single plot was immediately followed by a measurement of ambient UV-B in an equivalent, adjacent position, i.e. similar shading, slope gradient and facing, vegetation cover. This allows any short-term effects to be removed by normalising the measurement to the pertaining ambient UV-B, quoted as a percentage of ambient UV-B ($UV\text{-}B_{amb}$).

Additional measurements of UV-B were conducted for the exclusion experiment to investigate whether incident UV-B beneath the frame was uniformly distributed. A single frame randomly selected from each of the control and treatment plots was investigated as a representative example of the experimental set-up. The area beneath each frame was divided into a four by four grid, resulting in sixteen segments and the UV-B sensor positioned in each grid segment in turn to record the incident UV-B flux at that position. After each measurement of beneath-frame UV-B, a measurement of ambient UV-B directly above the frame at an equivalent grid position was taken. Exclusion frames of dimensions of 17cm by 22cm were positioned in the field so that they slope towards the position of the midday sun (i.e. greatest zenith angle); frames slope downwards along the short edge, with a height from the ground of ~7cm at the front legs and ~12cm at the rear legs. Beneath-frame UV-B distribution measurements were all conducted on 14th September 2006 at 14:00-14:37, with the frame orientation sloping approximately towards the sun position.

3.3.4 FTIR microspectroscopy of *Lycopodium* spores

After harvesting and drying to release spores from strobili, samples were analysed in accordance with the method detailed in Appendix A. A Continuum IR-enabled microscope fitted with a 15x reflachromat objective lens and nitrogen-cooled MCT-A detector was interfaced with the bench unit to provide microscopic analysis capability. Analysis was conducted using a microscope aperture of 100 x 100 μm at 500 scans per sample with a resolution of 4 data points per reciprocal centimetre (cm^{-1}). Background spectra were collected immediately after every sample spectrum. Each analysis was replicated five times per sample.

3.4 Results

3.4.1 UV-B exclusion frames

Control and treatment frames from the exclusion experiment show considerable variation of incident UV-B within each frame (Figure 3.10). However, the average values agree well with those measured for all plots in each section of the experiment; treatment (i.e. frame fitted with UV-B filter) mean incident UV-B = 10.2 $\%_{amb}$, whilst control (i.e. frame with non-UV-B excluding 'filter') mean incident UV-B = 53.2 $\%_{amb}$, compared with 8 $\%_{amb}$ and 52 $\%_{amb}$, respectively, as measured across the entire exclusion experiment. The treatment frame shows a range of 28.4 $\%_{amb}$ across the entire frame, whilst the control frame exhibits a range of 22.5 $\%_{amb}$. Both treatment and control frames show the highest UV-B measurements towards the rear of the frame where UV-B flux reaches 30 $\%_{amb}$ and ~60 $\%_{amb}$ in one rear corner (Figure 3.10). Such an effect is likely due to a combination of the height of frame above the ground and the diffuse nature of UV-B radiation. The result of this variation in UV-B within single frames is that the plants will receive variable UV-B fluxes within a single frame, probably leading to a corresponding variability in the chemical response to UV-B.

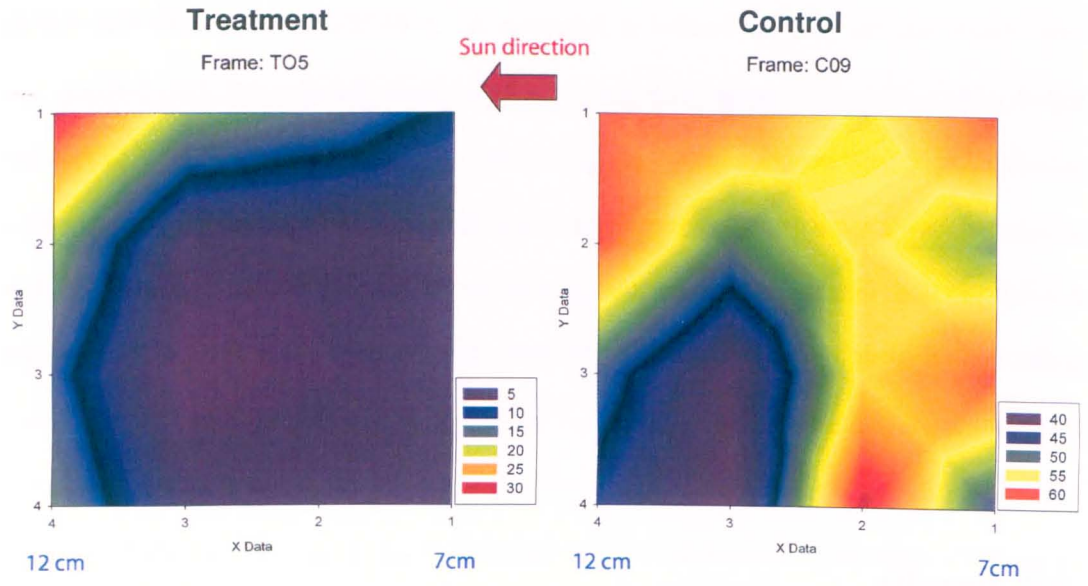

Figure 3.10 Distribution of UV-B under treatment and control exclusion frames. Sun direction perpendicular to "Y data" axis (i.e. from right). Distances in cm (in blue text) are height of frame above flat ground, thus top of frame slopes towards sun direction, representing situation at midday (maximum) radiation input. Note change in colour scale of plots between frames T05 and frame C09, as indicated by respective keys.

3.4.2 Field Experiments

A total of three complete growing seasons occurred during the course of the experiment conducted at ANS, beginning in May 2004. The results from each growing season are discussed year-by-year below. UV-B absorbing compounds are all quoted as mean ratios normalised to the peak height of the OH absorbance band in each individual spectrum (see Chapter 2 for details).

3.4.2.1 Abisko 2004

The 2004 dataset is based on the measurement of 34 samples in total, comprising 22 samples from the enhancement experiment and 12 samples from the exclusion experiment (Table 3.2).

Table 3.2 Number of samples harvested from each experiment for each year of experiment. T = treatment (exclusion or enhancement), C = control, and A = ambient.

Enhancement	2004	2005	2006	2007
T	5	13	4	0
C	7	15	8	0
A	10	9	12	0
	22	37	24	0
Exclusion				
T	4	14	11	0
C	4	12	10	0
A	4	12	13	0
	12	38	34	0
Total	34	75	58	0

Samples from the exclusion experiment show the greatest response of UAC in the ambient plots (0.808), whilst the treatment plots have the lowest relative abundance of UAC (0.764). Samples collected from the control plots fall between the ambient and treatment plots with respect to abundance of aromatic-based compounds (0.786) (Figure 3.11). Exclusion plots show a decreasing trend in UAC that correspond to the experimental UV-B regimes that the plants were subjected to, with highest UAC content found in plants that experienced the highest UV-B flux. However, as clearly demonstrated by the error bars (1σ) in Figure 3.11, the difference between experimental conditions are well within error.

Samples harvested from the enhancement experiment show control plots to have the lowest UAC abundance (0.660), whilst ambient plots have a slightly greater abundance (0.688). Treatment plots where supplemental UV-B has been imposed upon the growing plants exhibit the highest UAC content (0.702). The trend across the enhancement experiment corresponds with the measured UV-B input where ambient and control plots receive 97 $\%_{amb}$ and 98 $\%_{amb}$

UV-B, respectively, whilst the enhancement plots receive ~103 $\%_{amb}$. Similar to the exclusion experiment, these results are within error across the experiment.

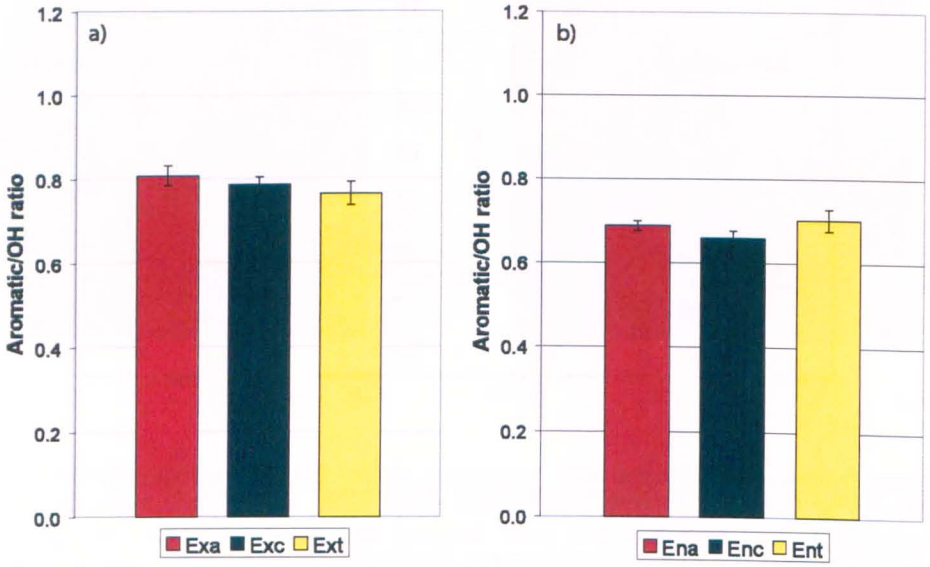

Figure 3.11 Experimental results from a) exclusion experiment, and b) enhancement experiment in 2004. Where prefix "Ex" refers to exclusion experimental frames, prefix "En" refers to enhancements experimental frames and a, c or t refers to ambient, control and treatment experiments, respectively. Error bars are standard error.

An additional factor to consider with these data is that 2004 saw a regional devastation of vegetation due to larvae (caterpillar) of the autumn moth (*Epirrita autumnata*) (Tenow, 1996) in the month of August (ACIA, 2004), and as a result the experimental plots had to be restarted with surviving plants. Restarting the experiments meant that the plants only had one month of growing under the manipulated UV-B conditions, which may not be long enough for a detectable response to develop in the spores.

3.4.2.2 Abisko 2005

The 2005 dataset is based on the measurement of 75 samples in total, comprising 37 samples from the enhancement experiment and 38 samples from the exclusion experiment (Table 3.2).

All plants were grown-on from the restarted experiment in 2004, therefore the same individuals (plants) were used in 2005.

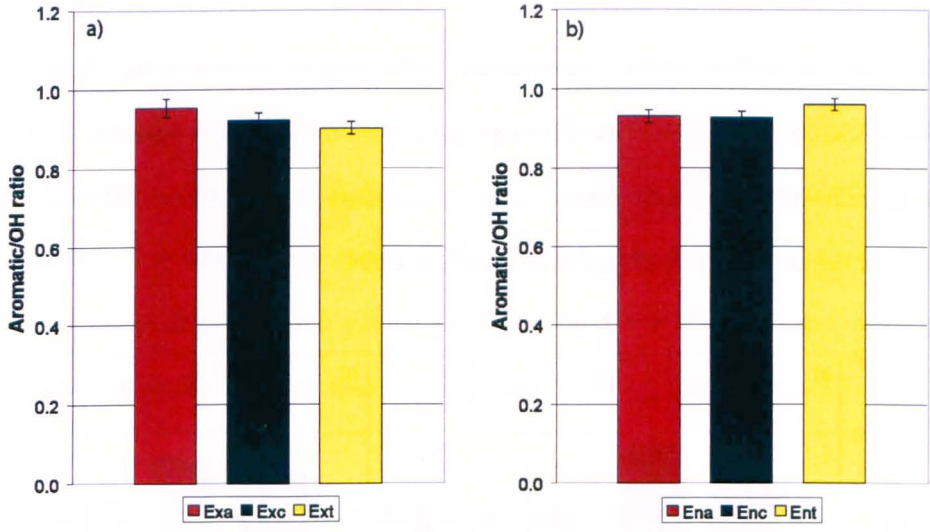

Figure 3.12 Experimental results from a) exclusion experiment, and b) enhancement experiment in 2005. Where prefix "Ex" refers to exclusion experimental frames, prefix "En" refers to enhancements experimental frames and a, c or t refers to ambient, control and treatment experiments, respectively. Error bars are standard error.

The exclusion plots show a decreasing trend that correlates well with a decreasing trend in received UV-B (Figure 3.12). Ambient plot aromatic/OH ratio = 0.955, control plots = 0.923 and treatment plots = 0.902.

Spore samples harvested from the treatment plots of the enhancement experiment exhibit the greatest UAC response (0.962), whilst control and ambient plots are almost equal, 0.929 and 0.931, respectively. Overall, the 2005 results suggest confirmation of the hypothesis of a positive UAC response to varying levels of incident UV-B flux, although, as with the 2004 results, the error bars (1σ) show considerable overlap.

3.4.2.3 Abisko 2006

The 2006 dataset is based on the measurement of 58 samples in total, comprising 24 samples from the enhancement experiment and 34 samples from the exclusion experiment (Table 3.2). Again, all individuals continued growing in the same plots under identical UV-B conditions as in 2005 and the latter part of the growing season of 2004.

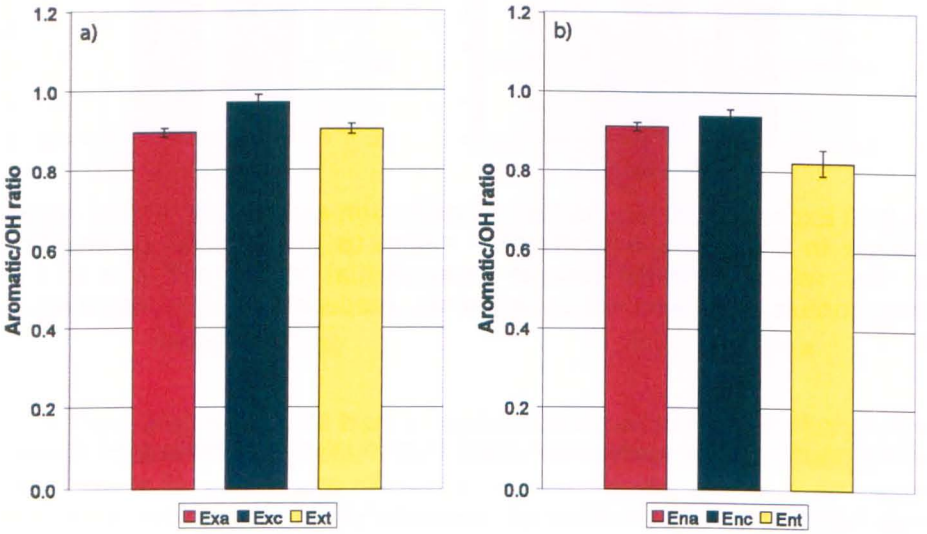

Figure 3.13 Experimental results from a) exclusion experiment, and b) enhancement experiment in 2006. Where prefix "Ex" refers to exclusion experimental frames, prefix "En" refers to enhancements experimental frames and a, c or t refers to ambient, control and treatment experiments, respectively. Error bars are standard error.

Ambient plots from the exclusion experiment show the lowest abundance of UAC (0.894), treatment plot values are next highest (0.902), with the control plots having the greatest abundance of UAC (0.970) (Figure 3.13). Enhancement plots display a similar pattern – control plots have the highest aromatic/OH response (0.939), ambient plots are lower (0.911), and treatment plots show the lowest response (0.823). There were no obvious extraneous conditions or events in 2006 that may have detrimentally affected the UAC response to UV-B to give rise to these results that stand out as different to previous years.

3.4.3 Interpretation

In 2004 and 2005 the mean spore wall chemistry trends follow the pattern hypothesised (Rozema *et al.*, 1997; 2001) whereby higher UV-B flux results in greater abundance of UAC. Interestingly the control plots in the enhancement experiment exhibit UAC content that is slightly lower than the ambient plots when, by design, there should be no difference between the two sets of plots. These control plots are subject to a mean UV-B flux of 97 $\%_{amb}$, which is very similar to that of the ambient plots (98 $\%_{amb}$ ±5.6), but the slightly lower mean UAC content may be attributed to the greater variability in UV-B flux at these plots due to additional shading by the UV lamp frames (UV-B flux = 97$\%_{amb}$ ±11.4; Table 3.1).

Results from 2006 do not fit the trend of 2004 and 2005. There is no obvious cause for 2006 results to be anomalous; however it may be that the individual plants are acclimatising to their UV environment, with the result that other environmental factors are playing a proportionally greater role in influencing spore chemistry.

A notable feature throughout all experimental years is that the enhancement plots do not show greater UAC responses compared with the exclusion plots from the same year, as would be expected if the relationship between UV-B and UAC content held true throughout the entire experiment. This discrepancy may be attributed to the potential that the enhancement plots are gradually becoming nutrient deficient and may have restricted access to water due to growing in gravel trays rather than in a natural position and substrate, as in the exclusion experiment.

3.4.4 Inter-annual variability

If the mean aromatic/OH ratios are taken for each year of the experiment across all experimental plots, inter-annual variations are revealed (Figure 3.14). 2004 samples exhibit the

lowest mean aromatic/OH ratio of 0.735 (1σ = 0.060), 2005 the highest ratio (0.934; 1σ = 0.022), and 2006 falls just below 2005 values (0.906; 1σ = 0.050). Closer examination of modelled UV-B flux for these three years shows coincident variability of UV-B flux and total number of sunshine hours with aromatic content of spores (Figure 3.14). Fourteen day averages of UV-B and sunshine hours are used in order to eliminate any short-term effects that may occur on a daily basis, providing a more representative picture of growing season UV-B regime. In particular, the latter half of the growing season is of interest because this is most likely the time when spores are developing ready for sporolation in September. Data presented here suggest that UV-B received during the final c. 2.5 months of the growing season is reflected in the changes in abundance of aromatic compounds in spore walls (Figure 3.14).

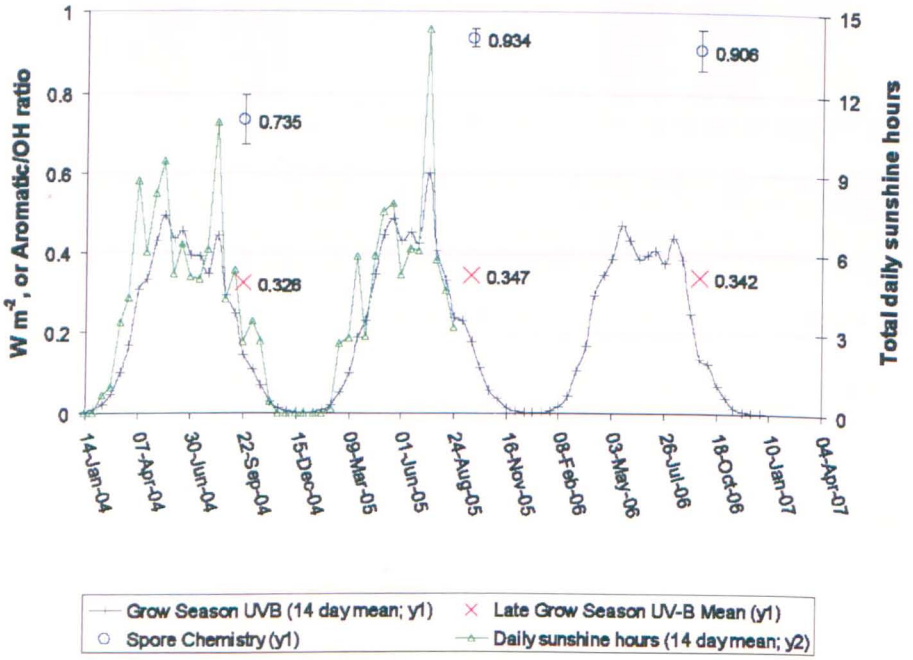

Figure 3.14 Relationship between growing season UV-B, sunshine hours and spore aromaticity across three years of data from ANS experiments.

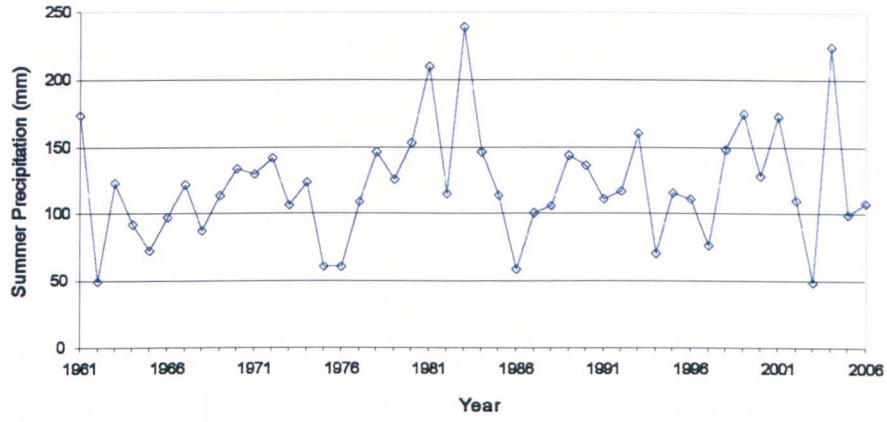

Figure 3.15 Summer precipitation measured at ANS for the period 1961-2006.

3.5 Discussion & Conclusions

Experimental manipulation of UV-B flux within a single growing season is not found to significantly influence spore wall aromaticity based on the data presented here; inter-annual variations appear to dominate the aromatic signal. However, the data do suggest that a trend may well be present, particularly evident in the results from 2004 and 2005, which is superimposed upon the inter-annual variability, but technique sensitivity is not high enough to distinguish such changes with statistical confidence. These results agree with recent work that has found experimental manipulation of UV-B in a long-term experiment on Svalbard does not cause significant changes in a range of plant growth parameters, and is attributed to an inherent tolerance to the extreme environmental conditions experienced at such high latitudes (Rozema *et al.*, 2006). All plants used in the experiment at ANS were native to the region, thus may well have an inherited tolerance to local UV-B conditions. Such an hypothesis can also account for the apparently anomalous data from 2006; if these plants acclimatise to UV-B flux over time, then it is reasonable to expect them to adjust to any manipulations of UV-B over the duration of the experiment.

Inter-annual shifts in UV-B flux received at the field site are observed and are likely due to changes in summertime cloud cover. This link is made by examination of the climatic data for

the region during the experimental period; reduced sunshine hours and UV-B flux correspond to increased summer precipitation, and vice versa (Figures 3.14 and 3.15). Precipitation is intimately linked with cloudiness, thus an increase in precipitation should indicate an increase in cloud cover, resulting in scattering and absorption of incoming solar radiation and as a consequence less radiation is experienced at ground-level. Summer precipitation in 2004 is the highest measured since 1983 (Figure 3.15), corresponding with the lowest late-growing season UV-B and lowest aromatic/OH ratio of the experimental period, as well as an overall reduction in sunshine hours (Figure 3.14). Conversely, 2005 received just 99.3 mm of precipitation (Figure 3.15), notably greater sunshine hours and the highest average late-growing season UV-B flux (Figure 3.14). Aromaticity across the 2005 experiment is the highest of the experimental period. The relationships between UV-B, precipitation and spore UAC abundance are represented graphically in Figure 3.16; both UAC abundance and UV-B show negative relationships with precipitation, whilst a positive relationship exists between UV-B and UAC abundance, suggesting that cloudiness may be playing a vital role. It is not possible to investigate the relationship of sunshine hours with these variables because there are less than two years of data available for the experimental period (see Figure 3.14).

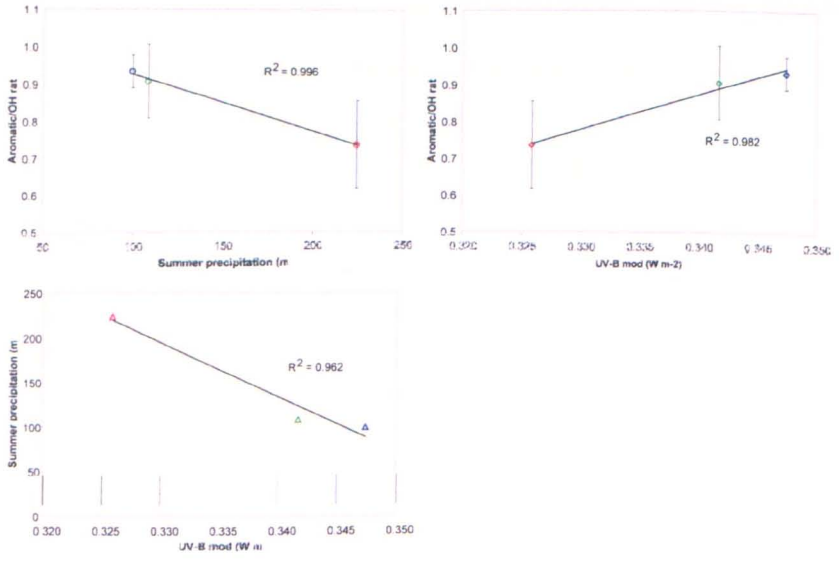

Figure 3.16 Linear regression of a) spore aromaticity vs. summer precipitation, b) summer precipitation vs. modelled UV-B, and c) spore aromaticity vs. modelled UV-B. Spore aromaticity is average aromatic/OH ratio across all experimental plots for each year; 2004 in red, 2005 in blue, 2006 in green. Error bars are two standard deviations.

While the relationship with inter-annual variation of precipitation, hence cloudiness, with modelled UV-B is promising, it should be noted that due to the modelling procedure of UV-B flux using PAR as a defining parameter, UV-B and PAR are now intrinsically linked. Thus it may be that changes in UAC abundance are in fact driven by PAR flux rather than UV-B, or a combination of both; however it is not possible to disentangle these data with the available information. Although PAR cannot be disregarded as a potential influence, it is less likely to be driving changes in UAC because there is an established link between incident UV-B and the production of UAC in plants (Meijkamp *et al.*, 1999), whilst no link with PAR exists. In order to isolate the effects of UV-B and/or PAR the experiment should be repeated with continuous simultaneous UV-B and PAR monitoring, preferably at the experimental scale using data loggers and UV-B/PAR sensors to obtain within-plot records. Such an approach would also provide an insight into the longer term effectiveness of the different manipulation scenarios.

3.6 Summary of Findings

• Experimental manipulation of incoming radiation results in a positive trend with UV-B absorbing compounds, although the statistical errors associated with measurements of the chemistry are greater than the variability between UV treatments.

• Inter-annual variations of radiation flux appear to have a greater influence on spore aromaticity than individual manipulation experiments.

• Whilst these chemical shifts in spores are attributed to a UV-B response mechanism, PAR cannot be ruled out as an important factor due to short-falls in suitable available environmental data, i.e. no independent records of UV-B and PAR for the entire experimental period.

• *Lycopodium annotinum* may acclimatise to local environmental conditions over the duration of the three year experiment.

Given the potential limitations of field studies of UV-B manipulation evident in this study and others (Rozema *et al.*, 2006), an alternative approach is to investigate natural samples that have been collected from regions subject to changes in UV-B flux as a result of spatial or temporal variability. The use of natural samples as UV-B monitors is explored in the next chapter.

3.7 References

ACIA (2004) Impacts of a warming Arctic: Climate impact assessment. Cambridge University Press, Cambridge, UK.

Ålenius, C.M., Vogelmann, T.C. & Bornman, J.F. (1995) A three-dimensional representation of the relationship between penetration of UV-B radiation and UV-screening pigments in leaves of *Brassica napus*. *New Phytologist* **131**, 297-302.

Allen, D.J., Nogués, S. & Baker, N.R. (1998) Ozone depletion and increased UV-B radiation: is there a real threat to photosynthesis? *Journal of Experimental Botany* **49**, 1775-1788.

Ballaré, C.L., Rousseaux, M.C., Searles, P.S., Zaller, J.G., Giordano, C.V., Robson, T.M., Caldwell, M.M., Sala, O. & Scopel, A.L. (2001) Impacts of solar ultraviolet-B radiation on terrestrial ecosystems of Tierra del Fuego (southern Argentina): An overview of recent progress. *Journal of Photochemistry and Photobiology B: Biology* **62**, 67-77.

Beggs, C.J. & Wellman, E. (1985) Analysis of light-controlled anthocyanin formation in Coleoptiles of *Zea mays* L.: The role of UV-B, blue, red and far-red light. *Photochemistry & Photobiology* **41**(4), 481-486.

Berglund, B.E., Barnekow, L., Hammarlund, D., Sandgren, P. & Snowball, I.F. (1996) Holocene forest dynamics and climate changes in the Abisko area, northern Sweden – the Sonesson model of vegetation history reconsidered and confirmed. *Ecological Bulletins* **45**, 15-30.

Björn, L-O. & Murphy, T.M. (1985) Computer calculations of solar radiation at ground level. *Physiologie Vegetale* **23**(5), 555-561.

Björn, L-O. (1999) Ultraviolet-B radiation, the ozone layer and ozone depletion, in; *Stratospheric ozone depletion: The effects of enhanced UV-B radiation on terrestrial ecosystems* (ed. J. Rozema). Backhuys publishers, Leiden, The Netherlands. pp. 21-37.

Bornman, J.F. & Vogelmann, T.C. (1991) Effect of UV-B radiation on leaf optical properties measured with fibre optics. *Journal of Experimental Botany* **42**, 547-554.

Brandle, J.R., Campbell, W.F., Sisson, W.B. & Caldwell, M.M. (1977) Net photosynthesis, electron transport capacity, and ultrastructure of *Pisum sativum* L. exposed to ultraviolet-B radiation. *Plant Physiology* **60**, 165-169.

Caldwell, M.M. Teramura, A.H. & Tevini, M. (1989) The changing solar ultraviolet climate and the ecological consequences for higher plants. *Trends in Ecology and Evolution* **4** (12), 363-367.

Campbell, B.D., Hofman, R.W. & Hunt, C.L. (1999) UV-B effects on New Zealand pasture ecosystems, in; *Stratospheric ozone depletion: The effects of enhanced UV-B radiation on terrestrial ecosystems* (ed. J. Rozema). Backhuys publishers, Leiden, The Netherlands. pp. 227-249.

Day, T.A., Ruhland, C.T. & Xiong, F.S. (2001) Influence of solar ultraviolet-B radiation on Antarctic terrestrial plants: results from a 4-year field study. *Journal of Photochemistry and Photobiology B: Biology* **62**, 78-87.

Flint, S.D. & Caldwell, M.M. (1996) Scaling plant ultraviolet spectral responses from laboratory action spectra to field spectral weighting factors. *Journal of Plant Physiology* **148**(1-2), 107-114.

Greenberg, B.M., Gaba, V., Canaani, O., Malkin, S., Mattoo, A.K. & Edelman, M. (1989) Separate photosensitizers mediate degradation of the 32-kDa photosystem II reaction centre protein in the visible and UV spectral regions. *Proceedings of the National Academy of Sciences* **86**, 6617-6620.

Gwynn-Jones, D., Johanson, U., Phoenix, G.K., Gehrke, C., Callaghan, T.V., Björn, L-O., Sonnesson, M & Lee, J.A. (1999) UV-B impacts and interactions with other co-occurring variables of environmental change: An Arctic perspective, in; *Stratospheric ozone depletion: The effects of enhanced UV-B radiation on terrestrial ecosystems* (ed. J. Rozema). Backhuys publishers, Leiden, The Netherlands. pp. 187-201.

Gwynn-Jones, D. (2001) Short-term impacts of enhanced UV-B radiation on photo-assimilate allocation and metabolism: a possible interpretation for time-dependent inhibition of growth. *Plant Ecology* **154**, 67-73.

Häder, D-P., Lebert, M., Schuster, M., del Ciampo, L., Helbling, E.W. & McKenzie, R. (2007) ELDONET – A decade of monitoring solar radiation on five continents. *Photochemistry and Photobiology* **83**, 1-10.

Hammarlund, D., Barnekow, L., Birks, H.J.B., Buchardt, B. & Edwards, T.W.D. (2002) Holocene changes in atmospheric circulation recorded in the oxygen-isotope stratigraphy of lacustrine carbonates from northern Sweden. *The Holocene* **12**(3), 339-351.

Huiskes, A.H.L., Lud, D., Moerdijk-Poortvliet, T.C.W. & Rozema, J. (1999) Impact of UV-B radiation on Antarctic terrestrial vegetation, in; *Stratospheric ozone depletion: The effects of*

enhanced UV-B radiation on terrestrial ecosystems (ed. J. Rozema). Backhuys publishers, Leiden, The Netherlands. pp. 313-337.

Jansen, M.A.K., Gaba, V. & Greenberg, B.M. (1998) Higher plants and UV-B radiation: Balancing damage, repair and acclimation. *Trends in Plant Science* **3**(4), 131-135.

Kohler, J., Brandt, O., Johansson, M. & Callaghan, T. (2006) A long-term Arctic snow depth record from Abisko, northern Sweden, 1913-2004. *Polar Research* **25**(2), 91-113.

Kotilainen, T., Tegelberg, R., Julkunen-Titto, R., Lindfors, A. & Aphalo, P.J. (2008) Metabolite specific effect of solar UV-A and UV-B on alder and birch leaf phenolics. *Global Change Biology* **14**, 1-11.

Laakso, K. & Huttunen, S. (1998) Effects of the ultraviolet-B radiation (UV-B) on conifers: A review. *Environmental Pollution* **99**, 319-328.

Lindfors, A.V., Arola, A., Kaurola, J., Taalas, P. & Svenøe, T. (2003) Long-term erythemal UV doses at Sodankylä estimated using total ozone, sunshine duration and snow depth. *Journal of Geophysical Research* **108**(D16)

Lindfors, A.V. & Vuilleumier, L. (2005) Erythemal UV at Davos (Switzerland), 1926-2003, estimated using total ozone, sunshine duration, and snow depth. *Journal of Geophysical Research* **110**(D2)

Lindfors, A., Holmgren, B. & Hansen, G. (2006) Long-term erythemal UV at Abisko and Helsinki estimated using total ozone, sunshine duration, and snow depth. *Proceedings of SPIE*, **6362**. doi: 10.1117/12.689742.

Lingakumar, K., Amudha, P. & Kulandaivelu, G. (1999) Exclusion of solar UV-B (280-315 nm) radiation on vegetative and photosynthetic activities in *Vigna unguiculata* L. *Plant Science* **148**, 97-103.

Meijkamp, B., Aerts, R., van de Staaij, J., Tosserams, M., Ernst, W.H.O. & Rozema, J. (1999) Effects of UV-B on secondary metabolites in plants, in; *Stratospheric ozone depletion: The effects of enhanced UV-B radiation on terrestrial ecosystems* (ed. J. Rozema). Backhuys publishers, Leiden, The Netherlands. pp. 71-99.

Musil, C.F., Björn, L-O., Scourfield, M.W.J. & Bodeker, G.E. (2002) How substantial are the ultraviolet-B supplementation inaccuracies in experimental square-wave delivery systems? *Environmental and Experimental Botany* **47**, 25-38.

Ovhed, M. & Holmgren, B. (1996) modelling and measuring evapotranspiration in a mountain birch forest. *Ecological Bulletins* **45**, 31-44.

Phoenix, G.K., Gwynn-Jones, D., Lee, J.A. & Callaghan, T.V. (2000) The impacts of UV-B radiation on the regeneration of a sub-arctic heath community. *Plant Ecology* **146**, 67-75.

Ridefelt, H. & Boelhouwers, J. (2006) Observations on reginal variation in solifluction landform morphology and environment in the Abisko region, northern Sweden. *Permafrost and Periglacial Processes* **17**, 253-266.

Rousseaux, M.C., Scopel, A.L., Searles, P.S., Caldwell, M.M., Osvaldo, E.S. & Ballaré, C.L. (2001) Responses to solar ultraviolet-B radiation in a shrub-dominated natural ecosystem of Tierra del Fuego (southern Argentina). *Global Change Biology* **7**, 467-478.

Rozema, J., van de Staaij, J., Björn, L-O. & Caldwell, M. (1997) UV-B as an environmental factor in plant life: stress and regulation. *Trends in Ecology and Evolution* **12**(1), 22-28.

Rozema, J., Oudejans, A., Houter, N., Schoonheim, H., Walraven, I., van't Klooster, C., van de Staaij, J., Tosserams, M., de bakker, N., van Beem, A., Stroetnga, M., Broekman, R., van Heerwaarden, L., Neilssen, H. & Aerts, R. (1999) Responses of plants from a dune grassland ecosystem in the Netherlands to solar UV-B: UV-B filtration and supplementation experiments, in; *Stratospheric ozone depletion: The effects of enhanced UV-B radiation on terrestrial ecosystems* (ed. J. Rozema). Backhuys publishers, Leiden, The Netherlands. pp. 203-225.

Rozema, J., Broekman, R.A., Blokker, P., Meijkamp, B.B., de Bakker, N., van de Staaij, J., van Beem, A., Ariese, F. & Kars, S.M. (2001) UV-B absorbance and UV-B absorbing compounds (para-coumaric acid) in pollen and sporopollenin: the perspective to track historic UV-B levels. *Journal of Photochemistry and Photobiology B: Biology* **62**, 108-117.

Rozema, J., Björn, L-O., Bornman, A., Gaberščik, A., Häder, D-P., Trošt, T., Germ, M., Klisch, M., Gröniger, A., Sinha, R.P., Lebert, M., He, Y-Y., Buffoni-Hall, R., de Bakker, N.V.J., van de Staaij, J. & Meijkamp, B.B. (2002) The role of UV-B radiation in aquatic and terrestrial ecosystems – an experimental and functional analysis of the evolution of UV-absorbing compounds. *Journal of Photochemistry and Photobiology B: Biology* **66**, 2-12.

Rozema, J., Boelen, P., Solheim, B., Zielke, M., Buskens, A., Doorenbosch, M., Fijn, R., Herder, J., Callaghan, T., Björn, L-O., Gwynn-Jones, D., Broekman, R., Blokker, P. & van de Poll, W. (2006) Stratospheric ozone depletion: high arctic tundra plant growth on Svalbard is not affected by enhanced UV-B after 7 years of UV-B supplementation in the field. *Plant Ecology* **182**, 121-135.

Santos, A., Almeida, J.M., Santos, I. & Salema, R. (1998) Biochemical and ultrastructural changes in pollen of *Zea mays* L. grown under enhanced UV-B radiation. *Annals of Botany* **82**, 641-645.

Searles, P.S. Flint, S.D. Diaz, S.B., Rousseaux, M.C., Ballaré, C.L. & Caldwell, M.M. (1999) Solar ultraviolet-B radiation influence on *Sphagnum* bog and *Carex* fen ecosystems: first field season findings in Tierra del Fuego, Argentina. *Global Change Biology* **5**, 225-234.

Searles, P.S., Flint, S.D. & Caldwell, M.M. (2001) A meta-analysis of plant field studies simulating stratospheric ozone depletion. *Oecologia* **127**, 1-10.

Sisson, W.B. & Caldwell, M.M. (1976) Photosynthesis, dark respiration, and growth of *Rumex patientia* L. exposed to ultraviolet irradiance (288 to 315 nanometres) simulating a reduced atmospheric ozone column. *Plant Physiology* **58**, 563-568.

Van de Staaij, J., de Bakker, N.V.J., Oosthoek, A., Broekman, R., van Beem, A., Stroetenga, M., Aerts, R. & Rozema, J. (2002) Flavonoid concentrations in three grass species and a sedge grown in the field and under controlled environment conditions in response to enhanced UV-B radiation. *Journal of Photochemistry and Photobiology B: Biology* **66**, 21-29.

Stratmann, J. (2003) Ultraviolet-B radiation co-opts defense signalling pathways. *Trends in Plant Science* **8**(11), 526-533.

Sullivan, J.H. & Rozema, J. (1999) UV-B effects on terrestrial plant growth and photosynthesis, in; *Stratospheric ozone depletion: The effects of enhanced UV-B radiation on terrestrial ecosystems* (ed. J. Rozema). Backhuys publishers, Leiden, The Netherlands. pp. 39-57.

Tenow, O. (1996) Hazards to a mountain birch forest – Abisko in perspective. *Ecological Bulletins* **45**, 104-114.

Teramura, A.H. (1983) Effects of ultraviolet-B radiation on the growth and yield of crop plants. *Physiologia Plantarum* **58**, 415-427.

Teraumra, A.H. & Sullivan, J.H. (1991) Potential impacts of increased solar UV-B on global plant productivity, in: *Photobiology* (ed. E. Riklis). Plenum Press, New York, USA. pp. 625-635.

Teramura, A.H. & Sullivan, J.H. (1994) Effects of UV-B radiation on photosynthesis and growth of terrestrial plants. *Photosynthetic Research* **39**, 463-473.

Van, T.K., Garrard, L.A. & West, S.H. (1977) Effect of 298nm radiation on photosynthetic reactions of leaf discs and chloroplast preparation of some crop species. *Environmental and Experimental Botany* **17**, 107-112.

4 Determination of spatial and temporal variations in surface UV-B radiation flux

4.1 Introduction

Natural variations in UV-B flux at Earth's surface afford the opportunity to perform natural experiments that are not subject to the same methodological uncertainties and limitations of field or laboratory UV manipulation experiments. UV-B is known to vary under the influence of a number of factors, including spatial positioning, atmospheric composition and chemistry, and temporal fluctuations thereof.

This chapter evaluates the application of the UV-B proxy presented in Chapter 2 to known natural changes in UV-B flux by exploiting historical collections of plants from regions that are expected to have been subject to variations in UV-B flux through time and space.

4.2 History of research and causes of surface UV-B variation

4.2.1 Natural variations of UV-B flux

Spatial and temporal variations in UV-B flux observed at the Earth's surface and their causes are summarised below.

4.2.1.1 Latitude

UV-B radiation is subject to natural variations on both local and global spatial scales. A much-documented spatial effect on UV-B flux is that of latitudinal position (Frederick *et al.*, 1989; Long *et al.*, 1995; Rigel *et al.*, 1999; Levelt *et al.*, 2006; Tanskanen *et al.*, 2006; WMO, 2007). It is related to the solar beam intensity received at Earth's surface. Solar beam

intensity is greatest at low latitudes and weakest at high latitudes because of the systematic change in angle of incidence of solar radiation with latitude, whereby an equal radiation flux is spread over differing sizes of surface area, thus altering radiation intensity at any location (Figure 4.1). Equatorial and tropical latitudes consistently receive UV-B flux ≥ 6 kJ m^{-2} throughout the year, whilst higher latitudes (greater than 45°) generally experience UV-B flux ≤ 6 kJ m^{-2} (Figure 4.2), although this is subject to substantial local variability due to surface type (albedo) and atmospheric composition (ozone), see Sections 4.2.1.3 and 4.2.2.1 below.

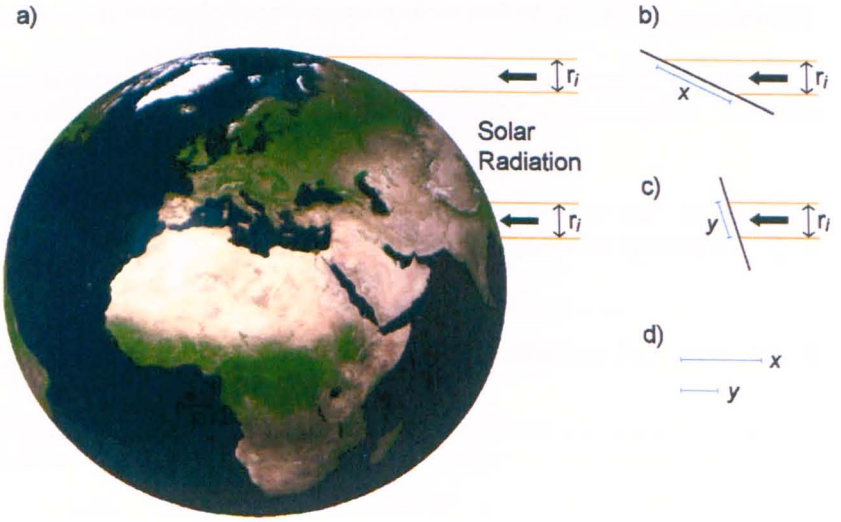

Figure 4.1 Localised surface distribution of solar radiation due to variations in angle of incidence in relation to latitude (a). Sections b) and c) show the difference in the spread of solar beam between high and low latitudes, respectively. d) compares the difference in diameter of the solar beam from b) and c).

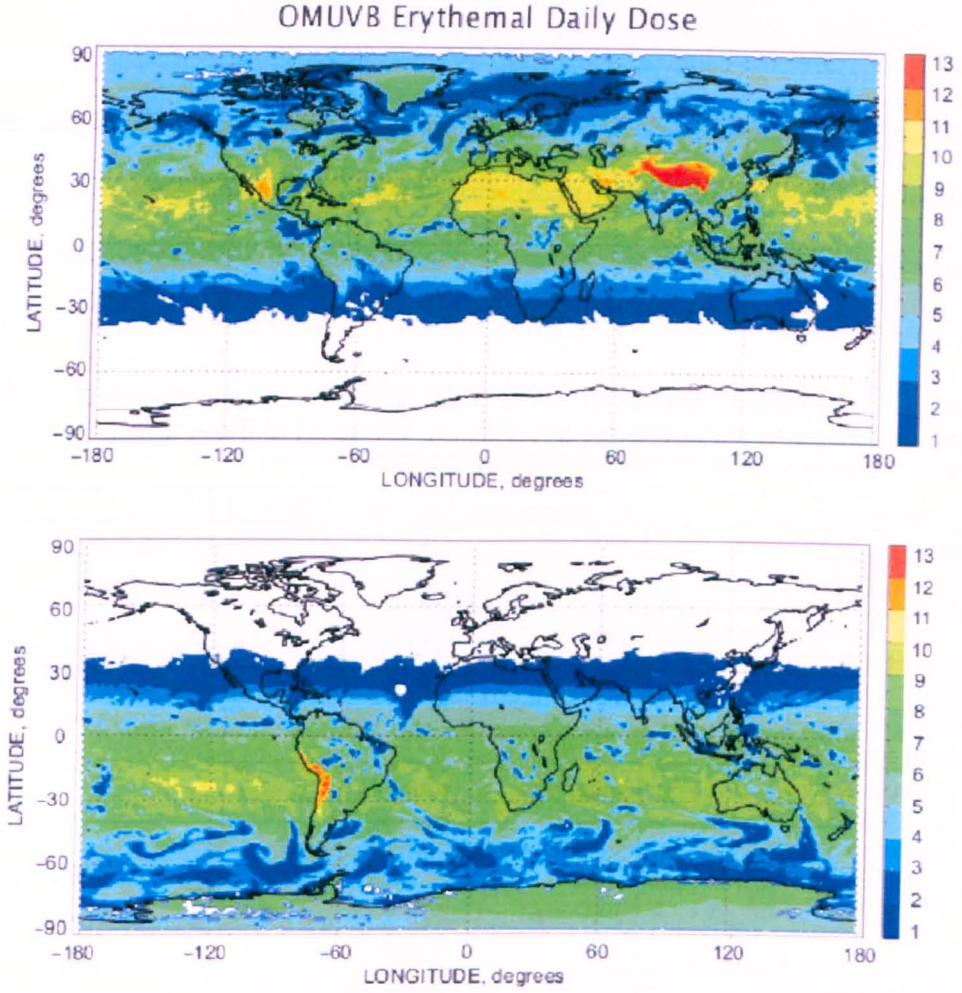

Figure 4.2 Global distribution of erythemal UV-B irradiance (kJ m^{-2}). Derived from the OMI satellite instrument for summer in a) northern hemisphere summer, and b) southern hemisphere. From: WMO, 2007. White pixels signify regions that no data are available for.

4.2.1.2 Altitude

UV-B flux is also found to vary greatly over altitudinal gradients, with significant increases in direct UV-B irradiance with increasing elevation (Blumthaler *et al.*, 1992; Sullivan *et al.*, 1992; Kudish *et al.*, 1997; Rozema *et al.*, 1997; McKenzie *et al.*, 2001, 2006). However, the rate of increase with altitude appears to be subject to a great deal of variation, as demonstrated by the range of values determined by various workers (Table 4.1). Such discrepancies may be attributed to the range of climatological factors that also play vital roles in surface UV-B flux at both local and regional scales (Section 4.2.3). For the purposes of this study an increase of

~15 % per 1000 m UV-B flux is applied as a reasonable mid-point approximation (Figure 4.3), calculated from the means of all minimum and maximum estimates within Table 4.1 (minimum mean = 12.8 % change/1000 m, maximum mean = 17.7 % change/1000 m).

Table 4.1 Published values of UV-B flux variation over altitudinal gradients expressed as percentage change per 1000 m. Range of altitude under investigation in each study is also provided (where appropriate).

Location	Alt. change (m)	% change/1000 m	Author
Haleakala, Maui, Hawaii	3000	4.3 - 4.9	Sullivan *et al.* (1992)
Neve Zohar & Beer Sheva, Isreal	690	10.2 - 17.3	Kudish *et al.* (1997)
Hradec Králové & Milešovka, Czech Republic	549	4.0 - 8.0	Dubrovský *et al.* (2000)
Vail, Colorado	1066	26.0 - 33.0	Rigel *et al.* (1999)
Davos, Weissfluhjoch & Jungfraujoch, Switzerland	1968	5.0 - 35.0	Schmucki & Philipona (2002)
Innsbruck, Austria & Jungfraujoch, Switzerland	2999	18.0	Blumthaler *et al.* (1997)
Antofagasta to Sairecabur, Andes, Chile.	5500	8.0 - 10.0	Piazena (1996)
Wank mountain, Alps, Germany	1000	24.0	Blumthaler *et al.* (1994)
Sajama volcano, Oruro, Bolivia	700	29.7 - 37.5	González *et al.* (2007)
Brianon, French Alps & Brussels, Belgium	1195	4.0 - 5.0	Pachart *et al.* (1999)
Lauder, New Zealand & Mauna Loa, Hawaii	3000	7.0	McKenzie *et al.* (2001)
Innsbruck, Austria & Jungfraujoch, Switzerland	2999	19.0	Blumthaler *et al.* (1992)
Model	-	6.3	Long *et al.* (1996)
Collated data - Review	-	5.0 - 23.0	Bais *et al.* (2007)

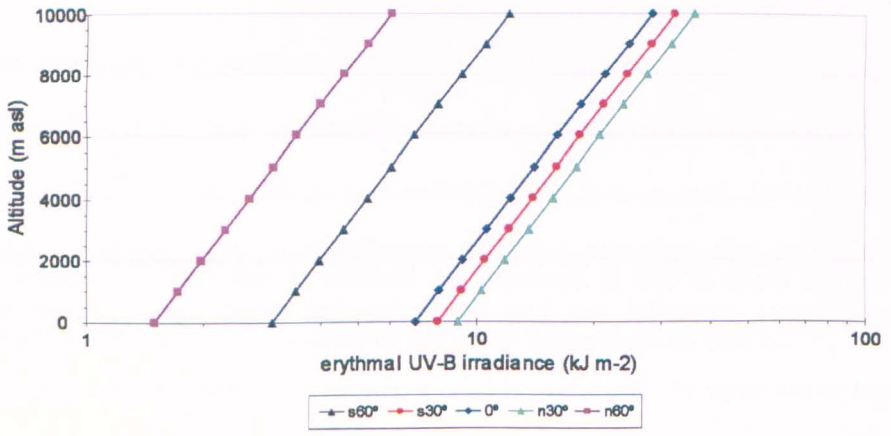

Figure 4.3 Idealised erythemal UV-B irradiance altitudinal profiles calculated using 15% change in UV-B radiation per 1000 m, as assumed in this work. Surface UV-B irradiance is estimated from OMI satellite-derived data (Figure 4.2). Profiles are calculated for 0º, 30º and 60º in both hemispheres.

4.2.1.3 Albedo

Regional and local scale surface radiation flux can also be modified by surface albedo of the surrounding area. Whilst this is a significant factor when considering visible light wavelengths (and longer wavelengths), UV-B flux is not affected to the same extent. In fact, most surfaces have a UV-B albedo of < 0.1 (Calbó *et al.*, 2005), with the most notable exceptions being surfaces covered in snow and/or ice. Increased UV-B albedo has the effect of enhancing the UV-B flux at a particular location giving rise to health concerns such as snow blindness and greater risk of sun burn (erythma), two conditions commonly reported to affect those participating in mountaineering and winter sports. The effect of albedo on UV-B may be compounded by the presence of clouds whereby UV-B radiation is reflected between the two high albedo surfaces of the snow and underside of the clouds, thus causing a greater enhancement of surface UV-B flux (Renaud *et al.*, 2000; Calbó *et al.*, 2005).

The present work does not investigate any regions where surface UV-B albedo is expected to be high or to vary significantly between regions; therefore surface albedo is unlikely to be an important factor in influencing any biochemical response in *Lycopodium* spores analysed here.

4.2.1.4 Ozone

Changes in UV-B flux across the globe and through time can be partly attributed to variations in total column ozone abundance. Spatial variation in total column ozone is dictated by regions of ozone production and regions where significant quantities of ozone are destroyed. It is observed that ozone is generated in the stratosphere at tropical latitudes and is transported polewards (Barry & Chorley, 1998), resulting in a distinct latitudinal gradient (Figures 1.3 and 4.4). This latitudinal variation coincides with that of surface UV-B (Figure 4.2).

Whilst the tropics are the source region for ozone, measurements show that these latitudes experience the lowest total column ozone concentrations (Figure 4.4), and are found to have been relatively unaffected by significant ozone depletion events (WMO, 2006). Conversely, polar regions normally experience relatively high ozone column values (Rex *et al.*, 2004) but are subject to great variation through time due to seasonal variation (see Chapter 1).

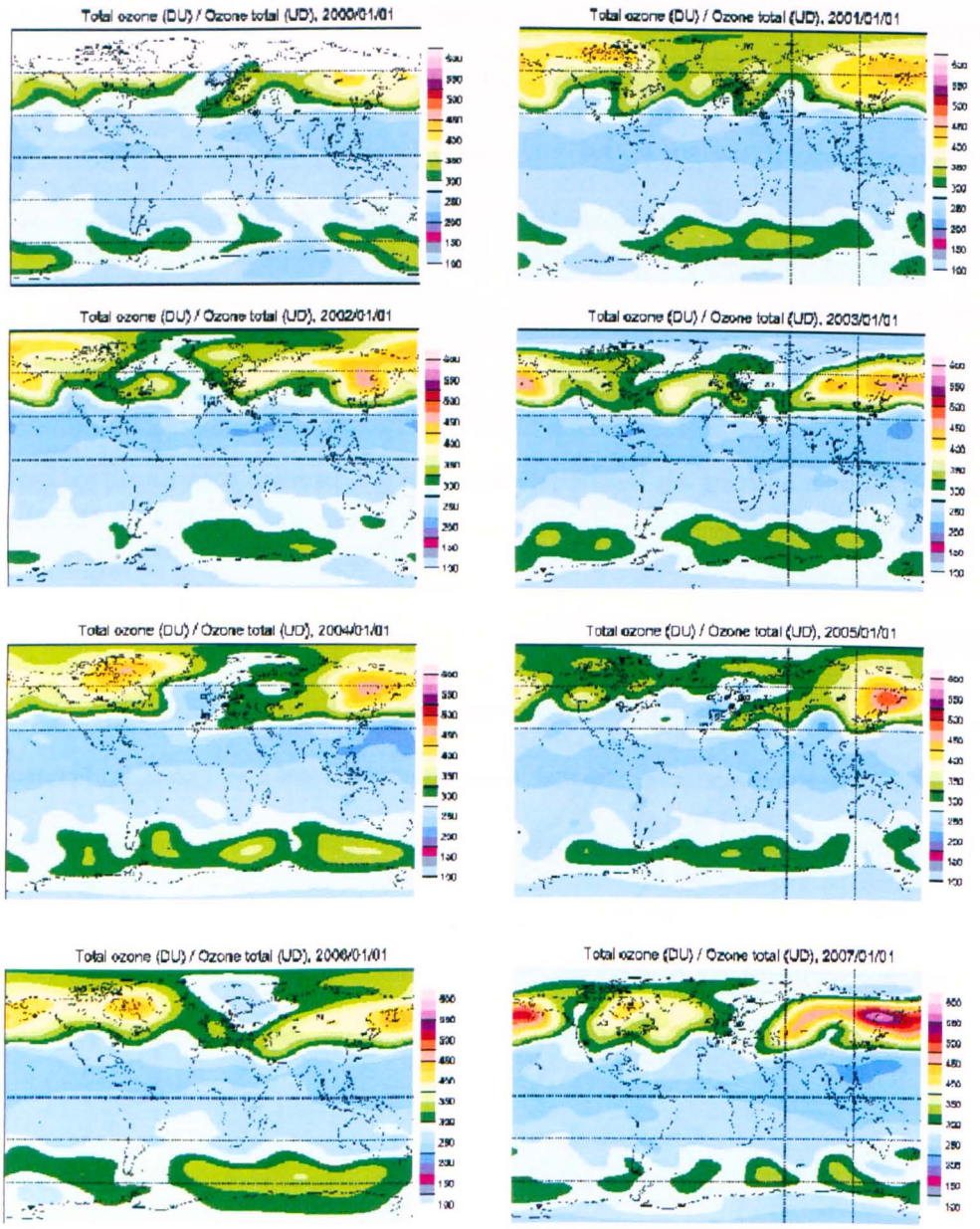

Figure 4.4 Annual average global total column ozone maps for the period 2000-2007. Increased ozone abundance is clearly visible in polar regions, with substantially less ozone at tropical latitudes. From: http://exp-studies.tor.ec.gc.ca/cgi-bin/selectMap

4.2.1.5 Aerosols

Aerosols occur in both the stratosphere and troposphere that act to reduce the flux of UV-B to the surface *via* absorption and scattering processes (Calbó *et al.*, 2005). Background levels of aerosol are thought to be maintained by natural and anthropogenic emissions of sulphur in the form of sulphur dioxide (SO_2), carbonyl sulphide (OCS) and dimethyl sulphide (DMS) (Barry & Chorley, 1998; Penner *et al.*, 2001; Myhre *et al.*, 2004; Deshler *et al.*, 2006), and are frequently perturbed by volcanic eruptions, which enhance the sulphate loading of the atmosphere, and thus increase the total column aerosol optical depth (AOD) (Toon & Pollack, 1976; Bluth *et al.*, 1997; Self, 2006; Stothers, 2007).

Tropospheric aerosols are highly variable through both time and space (Forster & Ramaswamy, 2007), being heavily influenced by atmospheric input from fuel burning, volcanic eruptions, biomass burning, mineral dust and sea salt aerosols (Toon & Pollack, 1976) (Figure 4.5). As already mentioned, due to the high variability of tropospheric aerosols, it is difficult to define the global aerosol climatology in more detail than broad generalisations. Regions that are heavily industrialised are a significant aerosol source; this is particularly evident in the northern hemisphere. Biomass burning can be seen to play a major role in AOD over the South American continent (Figure 4.5). Dust from the African continent is transported from the west coast across the Atlantic Ocean, and aerosols derived from sea salt are apparent at higher latitudes, in particular, around the Southern Ocean (Forster & Ramaswamy, 2007). Whilst tropospheric AOD may vary greatly on short time scales (days to weeks), over the course of a growing season for the plant investigations undertaken in the present work it is most likely that such changes in AOD will not have a significant impact upon the results.

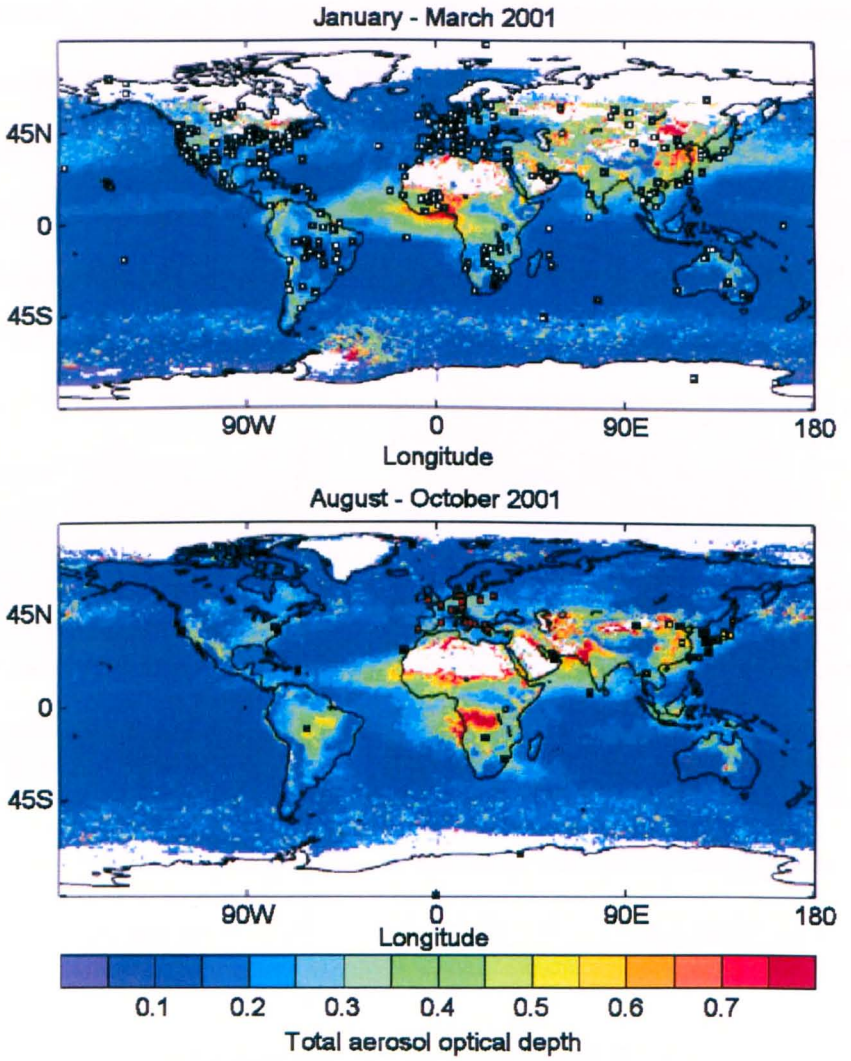

Figure 4.5 Global total column optical depth derived from satellite and ground-based measurements. From: Forster & Ramaswamy (2007). White pixels signify regions that no data are available for.

A relatively stable stratospheric aerosol layer was first observed by Junge *et al.* (1961a, 1961b) with peak concentration at 5-10 km above the local tropopause (as defined by an inversion in atmospheric temperature; see Chapter 1 [Figure 1.2]) (Rosen *et al.*, 1975), often referred to as the Junge layer (Hofmann & Rosen, 1981; Shallcross *et al.*, 2003). The most significant aspect of this finding was that aerosols were present at all times, including periods of relative quiescence with respect to volcanic activity and testing of atomic weapons (Junge & Manson, 1961; Rosen *et al.*, 1975; Toon & Farlow, 1981), suggesting that a natural equilibrium

maintains a background aerosol layer (Deshler *et al.*, 2006). There is no evidence that peak concentrations differ significantly across latitudes in an unperturbed atmosphere (Lazrus & Gandrud, 1974); the only observable change is the height at which the Junge layer occurs. At equatorial and tropical latitudes greatest aerosol concentration occurs at 20-25 km altitude (tropopause = ~15 km), whilst in polar regions the Junge layer is found in the range 15-20 km altitude (tropopause = ~10 km) (Rosen *et al.*, 1975; Barry & Chorley, 1998). The relatively uniform concentration observed across all latitudes has been attributed to strong and efficient vertical mixing of this portion of the atmospheric column, combined with a reasonable residence time of sulphate aerosols to allow such mixing (at least 1 year) (Lazrus & Gandrud, 1974).

4.2.1.5.1 Volcanic influence on stratospheric aerosols

The significance of volcanic eruptions to the stratosphere is a function of both explosivity, as denoted by the volcanic explosivity index (VEI, Newhall & Self, 1982), and global position of the eruption. Global location plays an important role because the height of the tropopause varies with latitude (Barry & Chorley, 1998), thus an eruption with VEI = 4 may be stratospherically significant at high latitudes, where the tropopause is at a lower altitude, whilst an eruption of equal magnitude may not have any stratospheric impact at lower latitudes (i.e. higher tropopause, therefore unable to reach the stratosphere).

Volcanic activity has the greatest influence on stratospheric aerosol concentration, most notably by the direct injection of volcanic sulphur into the stratosphere, which can lead to enhancements of aerosol concentration by more than an order of a magnitude (Hofmann & Rosen, 1981; Deshler *et al.*, 2006). To date, only two eruptions of stratospheric significant have occurred since technology has been advanced enough to provide a comprehensive analysis of the atmospheric impacts. These eruptions are the 1982 eruption of El Chichón (March, VEI = 5), Mexico and 1991 eruption of Mount Pinatubo (April, VEI = 6),

Philippines, although limited atmospheric data also exists for Agung, Indonesia (February 1963, VEI = 5) and Augustine, Alaska, USA (January 1976, VEI = 4) (Siebert & Simkin, 2002-present).

4.2.1.6 Astronomical & solar cycles

On long time-scales (thousands to millions of years) changes in the orbital parameters of the Earth give rise to regular, predictable trends in solar radiation reaching the Earth. The three elements of Earth's orbit are eccentricity, obliquity and precession of the equinoxes. Eccentricity describes the Earth's elliptical path around the Sun, which varies from a maximum eccentricity to nearly circular with a quasi-periodic cycle of ~ 95,000 years. Obliquity is the angle of axial tilt of the Earth with a period of ~ 41,000 years. Finally, precession of the equinoxes describes the regular 'wobble' of the Earth's axis, superimposed upon the obliquity cycle and has a mean period of ~ 21,700 years. Inter-play of these three factors results in a dynamic, complex pattern of insolation (incoming solar radiation) (Bradley, 1999; Wilson *et al.*, 2000; Burroughs, 2001). However, the total impact upon UV-B is on the order of a few percent (Loutre *et al.*, 2004) and the time-frame under consideration in the present work is so short by comparison that insolation can be regarded as constant.

Solar output has been measured in recent times and shows variations in relation to the number of sunspots, with a period of 11 years (Bard & Frank, 2006). Whilst total solar output is observed to vary by ~ 0.1 %, the heterogeneous nature of variation across the full spectra of solar irradiance results in UV-B wavelength radiation varying by as much as 1 % over the 11 year period (Burroughs, 2001; Bard & Frank, 2006). A systematic change of just 1 % is unlikely to adversely impact upon the results presented below.

4.2.2 Climatological and local-scale influences on UV-B flux

4.2.2.1 Cloud cover

UV-B flux may be modulated by other atmospheric parameters that readily vary on spatial and temporal scales, in particular cloud cover. Cloud cover for a given region will be subject to influence from, *inter alia*, global weather patterns, climatological changes, seasonal variation and orographic effects (Roe, 2005; Calbó *et al.*, 2007). The general consensus is that cloud cover acts to attenuate UV-B radiation throughout the atmospheric column *via* scattering caused by the presence of ice crystals and/or water droplets that constitute clouds, reducing UV-B flux by 10 to 40 % (summarised in Calbó *et al.*, 2007), although it must be noted that some caveats to this generalisation exist. First, cloud cover is only found to attenuate UV-B if the direct solar beam is obscured; if the direct component is not completely obscured, reflection of the radiation between Earth's surface and the underside of clouds may actually enhance incident UV-B at the surface (McKenzie *et al.*, 1991; Bais *et al.*, 1993; Sabburg & Wong, 2000). Second, cloud type is thought to exert an influence upon the transmissivity of the atmosphere. Vertically extensive convective-type cumulus clouds are most likely to block incoming UV-B when obstructing the direct solar beam, thus reducing atmospheric transmissivity. However, such cumulus clouds may also counteract UV-B reductions by the ability to effectively reflect the small amount of UV-B radiation that does penetrate the cloud layer, either *via* breaks in cloud cover, or at the edges of the cloud layer (Estupiñán *et al.*, 1996). Thinner clouds (e.g. cirroform) may exert an undetectable influence upon incoming UV-B (Estupiñán *et al.*, 1996; Calbó *et al.*, 2007). Finally, the position of clouds within the atmospheric column also appears to play a vital role in the degree of UV-B attenuation experienced at the surface. Lubin & Frederick (1991) present data that suggest clouds occurring at a high altitude are more effective attenuators of UV-B than clouds at lower levels, however, it should be noted that this trend may also incorporate a small amount of observational error caused by visual effects of differing altitudes of cloud (particularly

cirroform clouds); cloud cover extent is more difficult to observe when the clouds are at higher altitudes.

Whilst clouds are recognised as a dynamic, transient influence on UV-B surface flux, mean cloud cover for a particular region is identified to be reflected in inter-annual variations of UV-B flux (Frederick *et al.*, 1989). It is most likely that changes in seasonal averages may also impact UV-B flux to a degree that is detectable by the biochemical proxy described in this thesis.

4.2.2.2 Tree canopy

A localised effect that is found to modulate incident surface UV-B, and of possible significance to ground-level plants such as those considered in this study, is canopy cover provided by overhead vegetation (Grant, 1997; Grant *et al.*, 2002; Gies *et al.*, 2007; Chapter 2). The isolated effect of overlying canopy cover, i.e., when all other factors are equal, is to reduce incoming UV-B radiation, with greatest shading found under canopies of > 50% coverage (Grant *et al.*, 2002). Even a small proportion of canopy cover produces significant shifts in UV-B experienced assuming direct beam sunlight is obscured by the vegetation (Grant *et al.*, 2002; Gies *et al.*, 2007).

Complications arise when additional factors are considered simultaneously, for example, canopy cover combined with cloud cover. As highlighted above (Section 4.2.2.1), cloud cover generally acts to reduce incident UV-B radiation, as does canopy cover, however, given particular cloud conditions UV-B may be enhanced at ground-level *via* diffusive processes, which can cancel out the shading effect of a tree canopy (Grant & Heisler, 2006).

UV-B transmissivity of tree canopies is also related to solar zenith angles; hence it depends upon season, time of day and latitudinal position. High solar zenith angles may render the

overlying canopy ineffective because the direct solar beam may not be intercepted by the canopy at all. In forested areas, marginal locations will experience highly variable incident UV-B where the effective density of canopy is reduced and is dependent upon sun position. Locations in the centre of the forest will receive a more stable, but substantially lower UV-B flux due to the consistently dense canopy cover with a very limited ability of radiation reaching the ground from the sides (Figure 4.6) (Grant *et al.*, 2002).

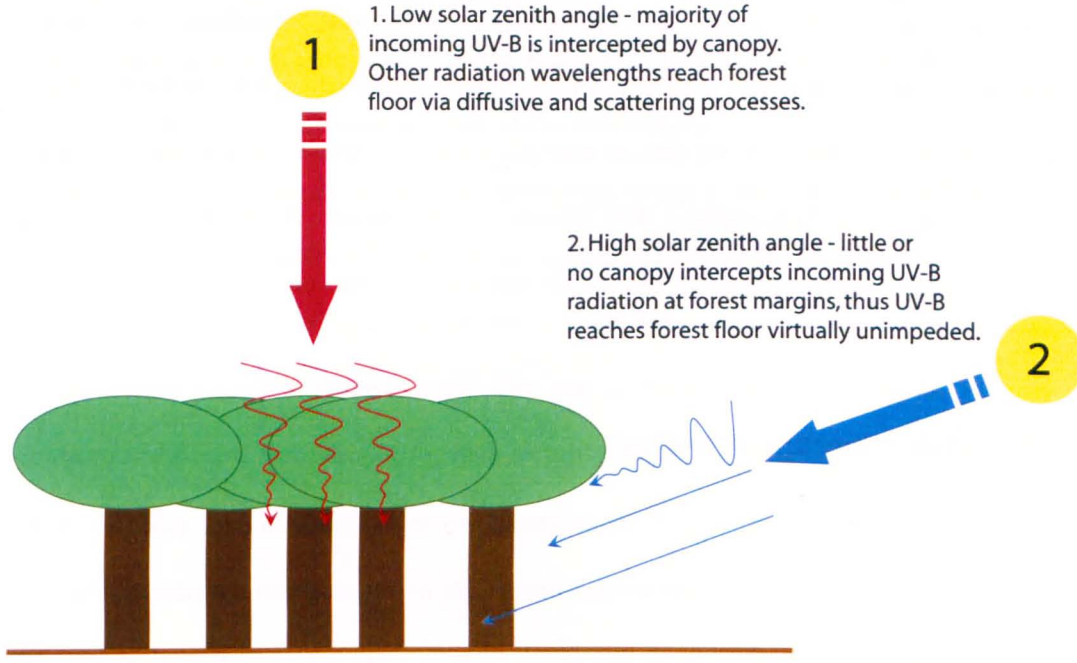

Figure 4.6 Schematic representation of solar beam pathways with respect to vegetation canopy. Two extreme scenarios are depicted: high and low zenith angles that demonstrate the influence tree canopies can have upon UV-B reaching the forest floor, and how the canopy can be ineffectual at latitudes where maximal diurnal solar input occurs with a high solar zenith angles (i.e. high latitudes).

The remainder of this chapter investigates the application of the biochemical proxy described in Chapter 2 to spores that are expected to have been subject to differing UV-B conditions, due to variations through time and/or space of some of the above mentioned atmospheric parameters. This is achieved first by exploring changes in spore chemistry caused by variations in UV-B due to differences in spatial positioning, in particular, elevation. The second stage is to investigate whether spore collections with long-term records can be exploited to track changes in UV-B, and hence ozone through time.

4.3 Experimental

4.3.1 Sample preparation and collection

Herbarium samples were hand picked from specimens held in collections at the Natural History Museum, London (Southeast Asia), the Botanical Museum, University of Copenhagen (Greenland) and Kew Gardens, London (Malaysia and India). Herbaria collections are generally stocked by botanical expeditions to various regions of the globe, thus collections are dependent upon when such expeditions take place and as a result are inherently sporadic in temporal resolution. In accordance with Chapter 2 and Appendix A, all samples were solvent extracted using acetone in order to remove the majority of labile components prior to analysis.

4.3.2 FTIR microspectroscopy

FTIR microspectroscopy was conducted in accordance with the method detailed in Appendix A. A Continuum IR-enabled microscope fitted with a 15x reflachromat objective lens and nitrogen-cooled MCT-A detector is interfaced with the bench unit to provide microscopic analysis capability. Analysis was conducted using a microscope aperture of 100 x 100 μm at 500 scans per sample with a resolution of 4 data points per reciprocal centimetre (cm^{-1}). Background spectra were collected immediately after every sample spectrum. Each analysis was replicated five times per sample.

4.4 Results

4.4.1 Spatial variations of UV-B flux

Two small sets of samples were collected from herbarium specimens in order to confirm the reproducibility of results by Watson *et al.* (2007). The samples are recorded to span elevational gradients of 83-750 m asl (India, 6 samples) and 100-1000 m asl (SE Asia, 3 samples). Such

elevations are of a comparable scale to those in the study of Watson *et al.* (2007). Given the relationship between increasing elevation and UV-B radiation (Section 4.2.1.2), it is expected that plant chemistry will alter in to order to provide greater UV-B protection, and this aspect of the work tests this presumption.

4.4.1.1 South-East Asia

Interrogation of *Lycopodium annotinum* spores from SE Asia reveals that those collected from higher elevations exhibit a stronger aromatic absorbance band than those collected from lower elevations (Table 4.2). Statistical analysis of the two samples collected from lower elevations (100 m and 150 m a.s.l.) shows that the spore aromaticity is not statistically different, or at least there is no discernable difference in the sample means for the given limited sample size (Table 4.3). However, comparison of the low elevation spore samples with the sample collected from higher elevation shows that the aromaticity of both lowland samples is significantly different from that of the high elevation sample, as demonstrated by the p-values obtained (Table 4.3). One limitation of this sample set is that the samples were not collected during the same year; hence inter-annual variations may influence these results.

Although of limited sample size, this sample set provides further evidence that there is a discernable difference in spore wall chemistry across an elevational gradient that relates to a systematic change in UV-B input. By comparison of two closely spaced samples, it is shown that spore aromaticity is essentially the same, whilst a greater vertical distance between samples results in a clear difference in spore chemistry.

Table 4.2 Spore chemistry of *L. annotinum* across an elevational gradient in SE Asia. Samples obtained from the herbarium collection held at the Natural History Museum, London. S.E. is standard error of mean; *n* is total number of FTIR spectra analysed; Lat. = latitude; Long. = longitude.

Sample	Year	Altitude	Mean spore chemistry (aromatic/OH)	S.E.	*n*	Lat.	Long.
SA1	1993	100	1.192	0.077	5	S 06° 45`	E 100° 07`
SA2	1998	150	1.238	0.044	5	S 04° 40`	E 117° 29`
SA3	1992	1000	1.693	0.091	5	-	-

Table 4.3 Test for differences in means of SE Asian samples. P-values (two-tail) obtained by comparison of paired means from Table 2 (t-test: paired two sample for means). Significance is set at the <0.05 level.

	SA1	SA2	SA3
SA1	-	0.878	<0.001
SA2	0.878	-	0.033
SA3	<0.001	0.033	-

4.4.1.2 India

Samples (*L. annotinum*) obtained from plant specimens collected in India show a similar overall trend in spore chemistry with elevation, albeit with a smaller degree of variation in aromaticity observed from minimum to maximum elevations (Table 4.4); this is most likely a result of the smaller elevational range covered by this sample set (83 m - 750 m a.s.l.). The lower variation between minimum and maximum elevations is clarified by statistical analysis of the sample means; comparison of means shows that there is no significant difference in spore chemistry across the entire elevation profile. However, graphical representation of the data does suggest that there is at least an increasing trend in spore aromaticity with elevation (Figure 4.7). Lack of statistical significance when compared with the results from the SE Asia samples is due to approximately equal standard error of means of the two sets of samples, but the Indian samples have a much smaller range in aromatic/OH ratio, thus the size of error has a greater influence on significance. Effects of inter-annual variations on UV-B radiation can be excluded from the Indian sample set because all samples were collected in a single year.

Table 4.4 Spore chemistry of *L. annotinum* across an elevational gradient in India. Samples obtained from collections held in the herbarium at Kew Gardens, London. S.E. is standard error of mean; *n* is total number of FTIR spectra analysed; shading? = indicates whether the collection site is likely to have been affected by shading effects.

Sample	Year	Altitude	Mean spore chemistry (aromatic/OH)	S.E.	*n*	Location	Shading?
K24	1985	83	1.025	0.063	5	Pathanamthitta	Y
K28	1985	267	1.043	0.047	5	Coimbatore	N
K17	1985	333	1.013	0.084	5	Kothayar	?
K18	1985	383	0.866	0.054	5	Iyerpadi	N
K14	1985	433	1.005	0.044	5	Upper Kothayar	?
K21	1985	750	1.132	0.080	5	Idukki	Y

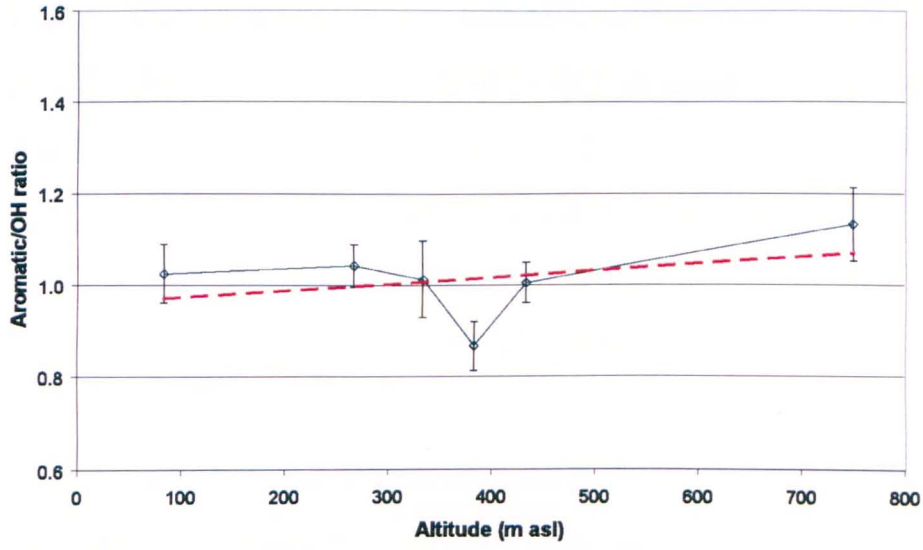

Figure 4.7 Elevation profile of spore chemistry in India. An overall increasing trend (dashed red line) in spore chemistry with increasing elevation can be seen, with a considerable excursion at central elevations (shown by solid blue line), most likely due to shading effects from inhabited areas and/or vegetation. Error bars are standard error.

An interesting feature of the Indian profile is that at central elevations (~330 to ~430 m a.s.l.) there is a sharp excursion in spore aromaticity from the overall trend. The locations where the central elevation samples were collected from are all moderately populated areas with relatively dense vegetation, whilst those samples collected from the extremities of the profile are from areas of open land. A potential consequence of increased habitation of the area (i.e. more buildings) and presence of vegetation will be to increase potential of shading effects on the

growing plants, thus reduce UV-B input and the resultant aromatic-based chemistry (see also Chapter 2).

4.4.2 Temporal variations of UV-B flux

4.4.2.1 Malaysia

A suite of *L. annotinum* spores collected in Malaysia constitute a short time-series (Table 4.5), incorporating samples bracketing the eruption of Mount Pinatubo in the Philippines (April 1991), and thus may provide an opportunity to test whether the proposed proxy can be used to successfully track changes in UV-B flux as a result of ozone perturbations by volcanic activity. All of the samples here are from essentially equatorial positions ($\leq 4°$ N), therefore unperturbed background ozone levels are expected to be relatively stable and low (Section 4.2.1.4).

The most prominent feature of this time-series is the low inter-annual variability for the majority of the period under consideration. Such an observation is in good agreement with the recognised stability of the ozone column in this region, where UV-B will also be expected to remain relatively stable. There does not appear to be any evidence for the ozone depleting effect of the Mt. Pinatubo eruption in this spore chemistry record; there may be a number of explanations for this. The first possibility is that the proxy proposed here is not sensitive enough to detect shifts in UV-B due to ozone depletion on this scale. However, this is unlikely because it has been estimated that in tropical regions, ozone depletion immediately after the 1991 eruption of Mt. Pinatubo was approximately 5-8 % (Hoffman *et al.*, 1994; Randel *et al.*, 1995; Coffey, 1996). As already demonstrated in this chapter, changes of ~ 15 % or less in UV-B flux, i.e. in relation to a change in elevation, are detectable using this proxy, thus the change in UV-B arising from a depletion of 5-8 % ozone should be discernable in this dataset. A second possibility is that the temporal sampling resolution is not sufficient in

order to pick up a volcanically-induced signal. Mt. Pinatubo erupted in June 1991, which is during the northern hemisphere summer, and the ozone depletion effect took a number of months to become apparent (Hoffman *et al.*, 1994; Randel *et al.*, 1995; Coffey, 1996), thus it is highly likely that any samples from 1991 did not experience any altered UV-B levels as a result of the eruption. Unfortunately there were no samples in this set collected during 1992 – the year most likely to show a significant volcanically-induced ozone effect. The next year in the sample set is 1993, but ozone levels may well have recovered sufficiently by this time to render the changes in ozone abundance undetectable using this chemical proxy. A final, but less likely possibility is that these samples are from a region that is too far south of the eruption to have been significantly affected; Mt. Pinatubo resides at ~ 15° N, whilst the samples from Malaysia were collected at a maximum of ~ 4° N. Another factor that may be playing a role is the superimposition of differing elevations of sample collection sites on to the time series. More than 1000 m difference in elevation exists in this dataset, which may be sufficient to adversely impact upon the success of this proxy in this situation.

Table 4.5 Spore chemistry of samples collected over the period 1988 to 1996 from various locations in Malaysia. Samples obtained from the herbarium collection held at Kew Gardens, London. S.E. is standard error of mean; *n* is total number of FTIR spectra analysed. Samples marked with an asterisk are from the same year and location, thus have been combined when presented in Figure 4.8.

Sample	Year	Altitude	Mean spore chemistry (aromatic/OH)	S.E.	*n*	Location
K44	1988	?	0.869	0.041	5	Ladan, Biawak
K38	1990	?	1.175	0.065	5	Lubang Biran, Sri Aman
K48*	1991	1125	0.843	0.080	5	NE of Gunong Retak
K50*	1991	1125	1.081	0.070	5	NE of Gunong Retak
K40	1993	150	0.938	0.033	5	Lubok Antu
K34	1995	50	0.826	0.097	5	East Kalimantan
K33	1996	110	0.845	0.073	5	East Kalimantan

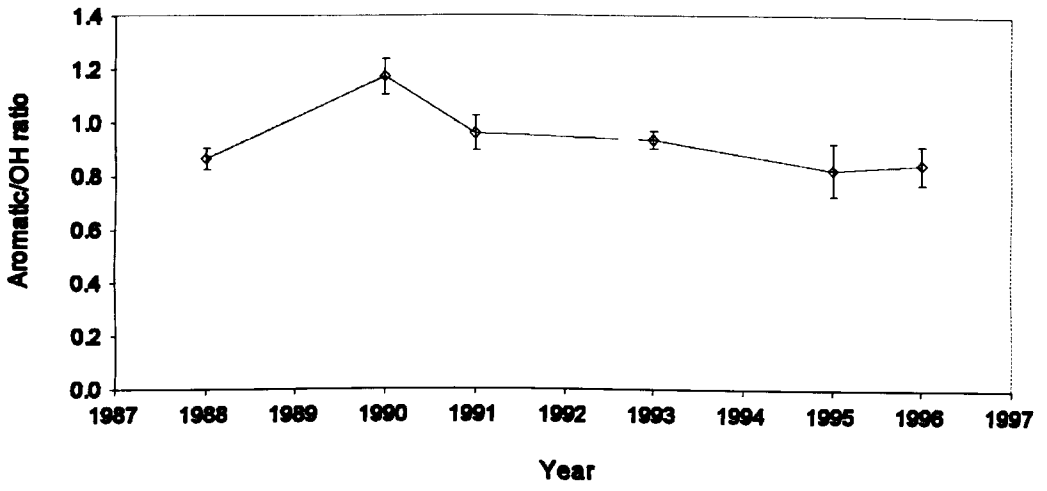

Figure 4.8 Time series of spore chemistry from samples collected in Malaysia during the period 1988 to 1996. Error bars are standard error.

4.4.2.2 Greenland

L. annotinum spores sourced from Greenland represent the greatest time range of all of the sample sets in this work, spanning nearly ninety years. Temporal resolution of this data is almost annual for periods of a decade in some cases (i.e. 1970s – 8 out of 10 years recorded). Table 4.6 lists the spore chemistry ratios, as well as geographical position and in cases where available, mean annual total ozone column from a nearby TOMS overpass site (Sondrestrøm, Greenland; 67° N 52° W, 300 m a.sl.). Graphical representation of this data reveals spore aromaticity to vary greatly throughout the period under consideration (Figure 4.9), particularly after 1960 where sampling density increases.

Changes observed in spore chemistry over this time period may reflect the changes in UV-B radiation in this region as a result of inter-annual variations in ozone. In order to test whether spore chemistry is recording changes in UV-B in relation to ozone abundance those years with both spore chemistry and ozone data available have been compared (Figure 4.10). In total, data for eight years is available spanning a range of nearly 40 D.U., thus providing a reasonable spread of data points to perform a reliable linear regression. All but one datum

falls within the 0.99 confidence intervals, with the remaining point lying on the lower confidence interval. Overall, the data suggest that there is an inverse relationship ($R^2 = 0.707$) between spore aromaticity and mean annual total ozone column abundance in this dataset, as is expected. Such an interpretation adds weight to the argument that spore chemistry can be used as a tool for tracking total ozone column through time *via* alterations in the UV-B transmissivity of the atmosphere.

Table 4.6 Spore chemistry of samples collected over the period 1906 to 1993 from Greenland. All samples were collected from elevations less than 400 m a.s.l. Samples obtained from the herbarium collection held at the University of Copenhagen, Denmark. S.E. is standard error of mean; *n* is total number of FTIR spectra analysed. Mean spore chemistry values are mean values as measured in *n* number of spectra; in some cases multiple samples are available from a single year, these have been combined and are signified by a larger *n* value than the majority of years.

Year	Mean spore chemistry (aromatic/OH)	S.E.	*n*	Lat.	Long.	Ozone (D.U.)
1906	0.790	0.046	5	65 36	51 44	-
1914	0.796	0.057	5	-	-	-
1937	0.827	0.073	5	61 10	48 28	-
1950	0.894	0.063	10	-	-	-
1954	0.890	0.052	5	-	-	-
1957	0.887	0.053	5	60 27	44 32	-
1961	0.729	0.092	5	60 40	51 04	-
1962	0.750	0.017	20	69 15	46 48	-
1963	0.764	0.020	5	60 49	47 57	-
1964	0.884	0.052	5	60 20	44 17	-
1968	0.739	0.040	10	62 54	49 25	-
1970	0.891	0.039	5	60 20	44 06	-
1971	0.724	0.026	5	62 54	49 53	-
1973	0.906	0.061	5	64 21	50 27	-
1974	0.645	0.080	5	61 10	45 25	-
1975	0.627	0.076	10	69 46	48 00	-
1977	0.847	0.032	5	65 35	51 44	-
1978	0.998	0.026	5	60 59	46 01	-
1979	0.788	0.038	15	65 02	51 20	354.56
1981	0.686	0.042	10	69 40	52 05	-
1982	0.799	0.031	10	-	-	368.09
1983	0.867	0.017	5	-	-	349.08
1987	0.795	0.027	5	61 11	45 48	354.91
1988	0.856	0.023	5	67 35	53 08	350.67
1991	0.796	0.027	5	66 56	53 40	357.06
1992	0.826	0.063	5	68 49	52 12	356.75
1993	0.913	0.021	5	60 09	45 15	334.33

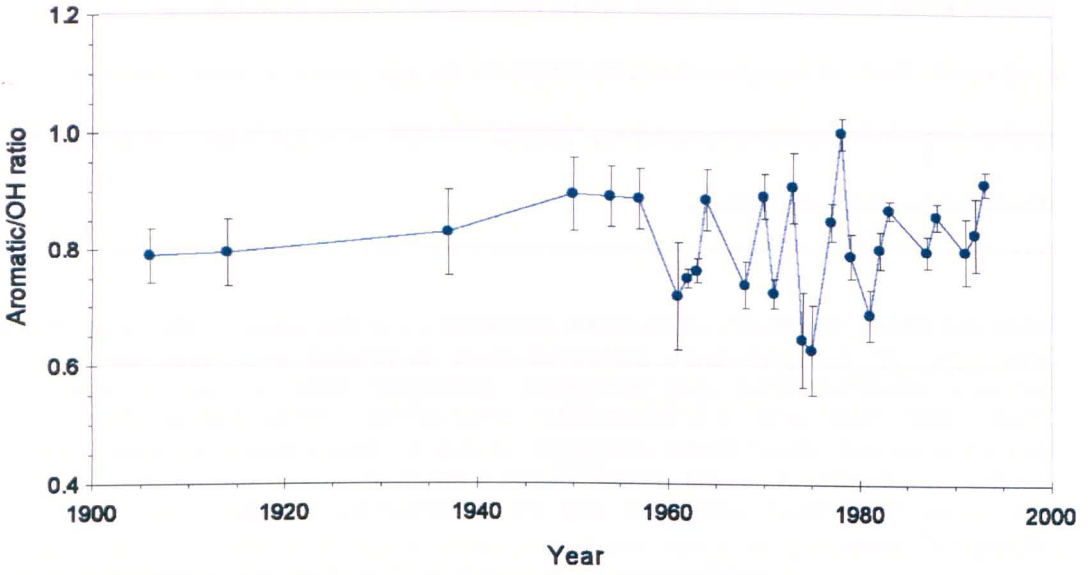

Figure 4.9 Time series plot of spore chemistry ratio from Greenland for the period 1906-1993. Error bars are standard error.

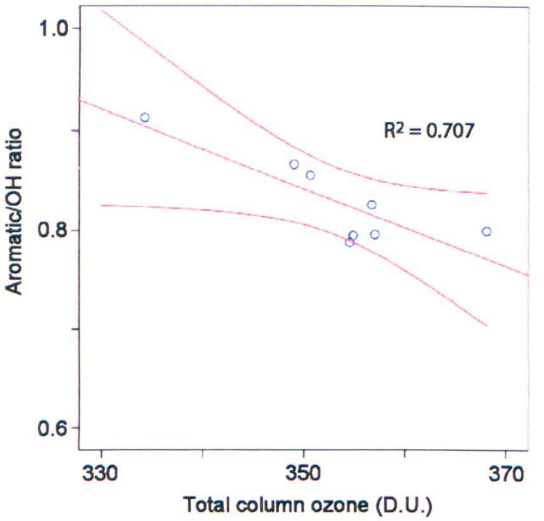

Figure 4.10 Regression of spore aromaticity versus annual total column ozone in Greenland. Eight years have both spore chemistry and ozone data are available (during the period 1979-1993). Mean confidence intervals are at the 0.99 level. Ozone data is from the TOMS instruments at a single overpass site (Sondrestrøm, 67ºN 52.62º W, 300 m a.s.l.). Pearson correlation coefficient = -0.841 at the 0.01 significance level; F = 14.447, p = <0.01.

By application of the linear equation derived from the inverse relationship between spore chemistry and total ozone column (y = -178.74x + 501.53) to the observed spore chemistry in the Greenland samples, it is possible to propose a reconstruction of mean annual total ozone column abundance for the period 1906-1993 (Figure 4.11). This reconstruction uses the final

eight years in the period 1979 to 1993 where both spore chemistry and ozone abundance coincide to retrospectively drive the estimates of ozone abundance prior to 1979. Consequently the observed linear relationship between spore chemistry and ozone results in ozone estimates to be essentially a mirror image of the spore chemistry throughout this time series. As expected from the correlation coefficient of the linear regression in Figure 4.10, the years used to derive the calculation in the time series of Figure 4.11 demonstrate a strong resemblance between TOMS ozone data and that reconstructed from spore chemistry.

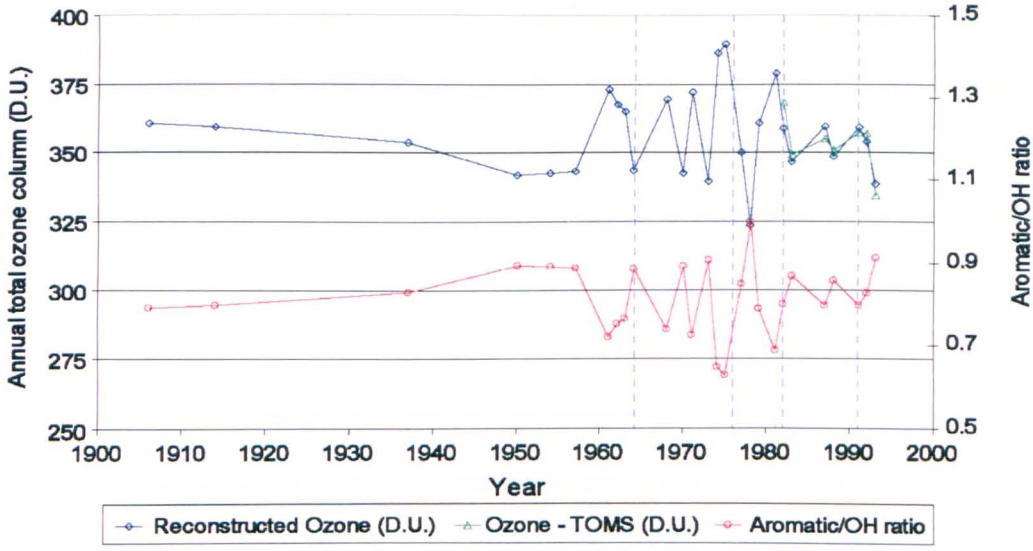

Figure 4.11 Proposed reconstruction of mean annual total ozone column derived from spore chemistry for the period 1906-1993. TOMS data for calibration of the linear regression are included as green triangles for comparison with reconstructed ozone. Marked in dashed vertical lines are the years of significant northern hemisphere eruptions; 1963 – Agung; 1976 – Augustine; 1982 – El Chichón; 1991 – Mt. Pinatubo.

The period prior to 1960 in the time series is not particularly instructive due to the low sample density, but after 1960 the sample resolution improves, lending itself to the investigation of the effect of known ozone depletion induced changes in UV-B radiation on spore chemistry. Marked by dashed lines on Figure 4.11 are the years of volcanic eruptions of sufficient size and explosivity that are either known to, or are likely to have had an impact upon stratospheric ozone chemistry *via* the injection of sulphate aerosols in to the stratosphere (see Section 4.2.1.5.1). A speculative look at the relative positioning of the eruptions in time in

relation to the reconstructed ozone record suggests that the 2-3 year period after the year of eruption experiences lower ozone abundances than the years immediately preceding the eruptions. Whilst this interpretation shows great potential for the successful reconstruction of past ozone abundance using spore chemistry, the considerable variation during periods of relative volcanic quiescence suggests that the background noise inherent in this dataset is significant, in some cases as large as, or even greater than the possible volcanic effects. For example, the difference in reconstructed ozone between 1971 and 1973, a period without any notable volcanic activity, is ~ 30 D.U., whereas the period spanning the eruption of El Chichón in 1982 (i.e. 1981 versus 1983) also shows a difference in reconstructed ozone of ~ 30 D.U. On the other hand, the period bracketing the 1976 eruption of Augustine (Alaska) shows a substantial shift in spore chemistry, and consequent reconstructed ozone abundance, with a change of ~ 70 D.U. between the years 1975 to 1978. It is worth noting that Augustine is the only volcano of the four under consideration here that is located at high latitude, thus it is a possibility that the Greenland ozone reconstruction may be reflecting localised effects of the eruption. Of the four eruptions considered here, Mt. Pinatubo (mid-1991 eruption) has the greatest amount of atmospheric data available, but unfortunately plant specimens are not available after 1993 from this region; samples from the period 1994-1996 would have provided additional information about background noise in the spore chemistry signal in order to constrain any ozone related changes.

4.5 Synthesis

The reconstruction of ozone concentration over Greenland for the period 1906-1993 (Figure 4.11) is a reasonable first estimate, however, for more recent ozone changes, i.e. post-1979, it is not a truly independent record because the spore chemistry-ozone relationship has been calibrated using data from these years. In order to generate a more independent relationship between spore chemistry and ozone, additional data taken from the other sample sets in this chapter are collated to produce a hemispheric calibration. The resultant linear regression is

shown in Figure 4.12. The advantages of this approach are that the range in ozone column under consideration is much broader (~ 250 to ~ 360 D.U.) due to latitudinal variation in atmospheric ozone abundance and therefore a greater range in spore chemistry. To construct this hemispheric-wide regression careful selection criteria were adhered to when filtering the data. First, due to the effect of altitude on UV-B only samples that fell in the range 100 to 1000 m a.s.l. were selected. Second, only samples that were collected from a tangible, recorded location were included in the dataset, and finally satellite-derived ozone data must be available for a recognised TOMS overpass site within a reasonable distance from each sample site. As a result of the selection criteria a number of points from each of the datasets presented above have been discarded; the majority of which are from the altitudinal profiles due to falling outside of the permitted elevation range. The outcome of combining datasets in this manner is a semi-independent regression, suitable for application to a spore chemistry dataset.

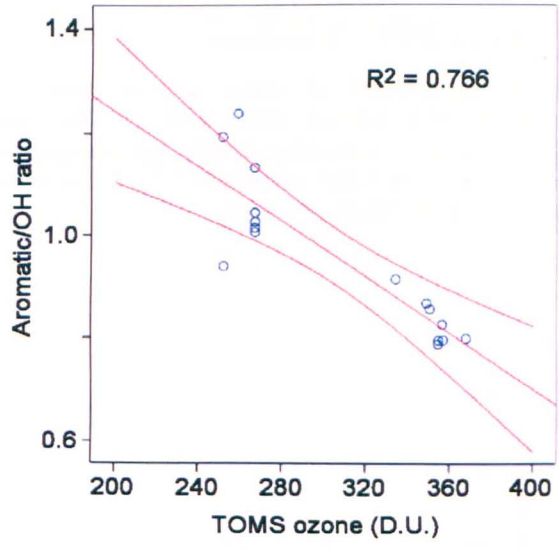

Figure 4.12 Regression of spore aromaticity versus annual total column ozone. Only points where both spore chemistry and ozone data are included. These data incorporate sample information from India, Malaysia, SE Asia and Greenland. Mean confidence intervals are at the 0.99 level. Ozone data is from the TOMS instruments at a single overpass sites nearest to the location of sample collection. Pearson correlation coefficient = -0.875 at the 0.01 significance level; F = 45.920, p = <0.01.

Reconstruction of ozone for the period 1906 to 1993 can be repeated using the revised semi-independent calibration of spore chemistry versus total ozone column abundance of Figure

4.12 to give the time series presented in Figure 4.13. Comparison of the post-1979 reconstructed data with TOMS data for the same period exhibits a good fit (Figure 4.14), with most of the reconstructed ozone data falling within error of the measured TOMS data (Figure 4.13), suggesting that the remainder of the reconstructed record is reliable.

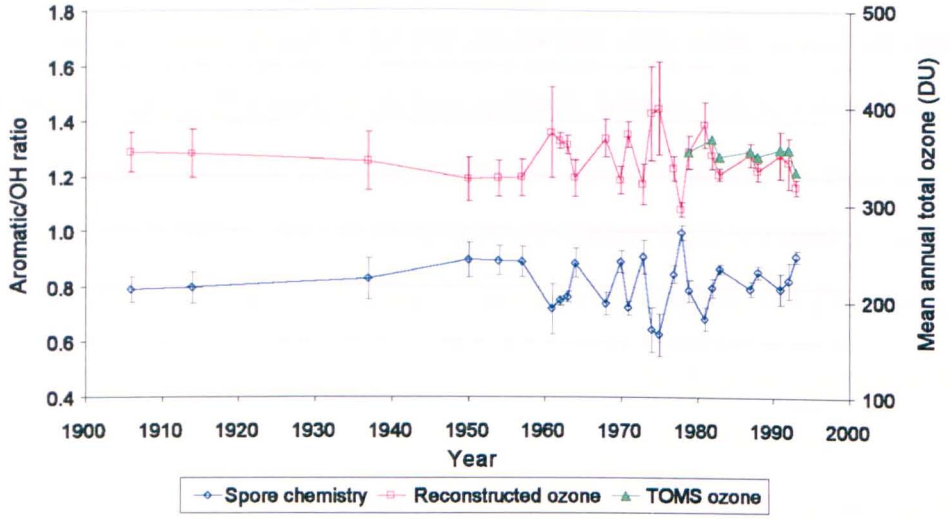

Figure 4.13 Revised reconstruction of mean annual total ozone column derived from spore chemistry for the period 1906-1993. TOMS data (Figure 4.10) are included as green triangles for comparison with reconstructed ozone. Error bars for the reconstructed ozone have been calculated from the variance represented by the standard error of the spore chemistry data.

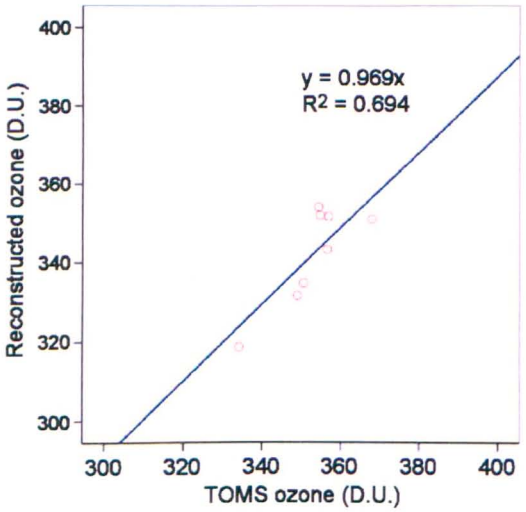

Figure 4.14 Linear regression of TOMS ozone versus reconstructed ozone abundance. Pearson correlation coefficient = 0.841 at the 0.01 significance level; F = 14.449, p = <0.01.

The reconstructed ozone time series proposed here represents the first spore chemistry-based proxy for mean annual total ozone column abundance, *via* the interactions of ozone with UV-B radiation.

4.6 Discussion & Conclusions

From the results presented here it is possible to tentatively conclude that spore chemistry records changes in UV-B radiation in relation to a number of environmental factors. A number of different UV-B regimes have been investigated where incident UV-B is known to systematically change, with promising results.

Elevational gradients appear to exhibit a positive relationship with spore aromaticity due to the increase in UV-B with altitude. Samples from both SE Asia and India show positive trends in chemistry across substantial elevational profiles, a finding that confirms previous work (Watson *et al.*, 2007). An interesting point is highlighted by the Indian profile, which demonstrates that caution should be exercised when obtaining samples from herbarium collections; the details of the specimen collection location may be poorly recorded, concealing the presence of significant vegetative canopy cover or proximity to inhabitancy that may adversely alter the influence of incoming radiation.

Time series of preserved samples provide the opportunity to investigate the UV-B and corresponding ozone abundance of the past. In the case of Malaysia, the relatively stable ozone experienced at this latitude appears to result in very little variation in spore chemistry, however, the limited sample resolution of this dataset may be obscuring the true picture. This region is expected to have shown some ozone depletion related to the eruption of Mt. Pinatubo in 1991, but samples were not collected during the key years of interest (1992 and 1993), thus a valuable piece of the puzzle is missing. The time series obtained from Greenland holds the greatest promise for the future of this biochemical proxy. Successful

application of the proxy has enabled the proposal of a reconstruction of past ozone for the Greenland region back to the beginning of the 20th century. Whilst this evidence shows strong potential for the proxy, questions about the amplitude of noise within the time series still remain. These questions will only be answered once a higher time resolution sample set can be sourced, ideally at annual resolution, containing multiple samples per year and combined with environmental data, such as cloudiness, site-based UV-B measurements and precipitation.

4.7 Summary of Findings

• Positive trends are found to exist between spore chemistry and altitude, where altitude has a positive relationship with UV-B radiation.

• Collation of spore chemistry data from a number of regions around the world has enabled a calibration of spore chemistry versus mean total annual ozone abundance to be generated.

• Changes in spore chemistry have been successfully used, in so far as the short timescales permit, to reconstruct an ozone record for Greenland for the period 1906-1993.

• Whilst the analyses presented here provide evidence in favour of the further development of this novel biochemical proxy, limitations still exist. First, any ozone/UV-B reconstructions will be limited by the resolution of samples available; ideally annually spaced samples should be used to ensure changes in spore chemistry are as accurate as possible. Second, whenever possible multiple samples from an individual year (or in the case of spatial relationships, individual sampling site) should be used; this will enable the inherent noise within a time series to be quantified.

This chapter has provided a basis for analysis of spore chemistry with a view to understanding past changes in surface UV-B radiation, and its relationship with environmental factors that modulate surface UV-B, in particular total ozone column abundance. The next chapter takes

this novel proxy and attempts to apply it to samples on a geological timescale in order to investigate the applicability to the more distant past than dealt with in this chapter.

4.8 References

Bais, A.F., Zerefos, C.S., Meleti, C., Ziomas, I.C. & Tourpali, K. (1993) Spectral measurements of solar UVB radiation and its relations to total ozone, SO_2, and clouds. *Journal of Geophysical Research* **98**(D3), 5199-5204.

Bais, A.F. & Lubin, D. (2007) Surface ultraviolet radiation: Past, present and future, in: *Scientific assessment of ozone depletion: 2006.* World Meteorological Organisation global ozone research and monitoring project – Report No. 50. Geneva, Switzerland.

Bard, E. & Frank, M. (2006) Climate change and solar variability: What's new under the sun? *Earth and Planetary Science Letters* **248**, 1-14.

Barry, R.G. & Chorley, R.J. (1998) *Atmosphere, weather and climate (7th ed.).* Routeldge, London, UK.

Blumthaler, M., Ambach, W. & Rehwald, W. (1992) Solar UV-A and UV-B radiation fluxes at two alpine stations at different altitudes. *Theoretical and Applied Climatology* **46**, 39-44.

Blumthaler, M., Webb, A.R., Seckmeyer, G., Bais, A.F., Huber, M. & Mayer, B. (1994) Simultaneous spectroradiometry: A study of solar UV irradiance at two altitudes. *Geophysical Research Letters* **21**(25), 2805-2808.

Blumthaler, M., Ambach, W. & Ellinger, R. (1997) Increase in solar UV radiation with altitude. *Journal of Photochemistry & Photobiology B: Biology* **39**, 130-134.

Bluth, G.J.S., Rose, W.I., Sprod, I.E. & Krueger, A.J. (1997) Stratospheric loading of sulphur from explosive volcanic eruptions. *Journal of Geology* **105**(6), 671-683.

Bradley, R.S. (1999) *Paleoclimatology: Reconstructing climates of the Quaternary.* Academic Press, San Diego, USA.

Burroughs, W.J. (2001) *Climate change: A multidisciplinary approach.* Cambridge University Press, Cambridge, UK.

Calbó, J., Pagès, D. & González, J-A. (2005) Empirical studies of cloud effects on UV radiation: A review. *Review of Geophysics* **43**, RG2002, doi:10.1029/2004RG000155.

Coffey, M.T. (1996) Observations of the impact of volcanic activity on stratospheric chemistry. *Journal of Geophysical Research* **101**(D3), 6767-6780.

Deshler, T., Anderso-Sprecher, R., Jäger, H., Barnes, J., Hofmann, D.J., Clemesha, B., Simonich, D., Osborn, M., Grainger, R.G. & Godin-Beekman, S. (2006) Trends in the

nonvolcanic component of stratospheric aerosol over the period 1971-2004. *Journal of Geophysical Research* **111**, D01201, doi:10.1029/2005JD006089.

Dubrovský, M. (2000) Analysis of UV-B irradiances measured simultaneously at two stations in the Czech Republic. *Journal of Geophysical Research* **105**(D4), 4907-4913.

Estupiñán, J.G., Raman, S., Crescenti, G.H., Streicher, J.J. & Barnard, W.F. (1996) Effects of clouds and haze on UV-B radiation. *Journal of Geophysical Research* **101**(D11), 16807-16816.

Forster, P. & Ramaswamy, V. (2007) Changes in atmospheric constituents and in radiative forcing (Chapter 2), In: *Climate Change 2007: The Physical Science Basis. Contribution of working group I to the fourth assessment report of the intergovernmental panel on climate change* (Eds. S. Solomon, D. Qin, Z. Chen, M. Marquis, K.B. Averyt, M. Tignor & H.L. Miller). Cambridge University Press, Cambrdige, UK.

Frederick, J.E., Snell, H.E. & Haywood, E.K. (1989) Solar ultraviolet radiation at the Earth's surface. *Photochemistry & Photobiology* **50**(8), 443-450.

Gies, P., Elix, R., Lawry, D., Gardner, J., Hancock, T., Cockerell, S., Roy, C., Javornickzy, J. & Henderson, S. (2007) Assessment of the UVR protection provided by different tree species. *Photochemistry & Photobiology* **83**, 1465-1470.

Grant, R.H. (1997) Biologically active radiation in the vicinity of a single tree. *Photochemistry & Photobiology* **65**(6), 974-982.

Grant, R.H., Heisler, G.M. & Gao, W. (2002) Estimation of pedestrian level UV exposure under trees. *Photochemistry & Photobiology* **75**(4), 369-376.

Grant, R.H., Heisler, G.M. (2006) Effect of cloud cover on UVB exposure under tree canopies: Will climate change affect UVB exposure? *Photochemistry & Photobiology* **82**, 487-494.

González, J.A., Gallardo, M.G., Boero, C., Cruz, M.L. & Prado, F.E. (2007) Altitudinal and seasonal variation of protective and photosynthetic pigments in leaves of the world's highest elevation trees *Polylepis tarapacana* (Rosaceae). *Acta Oecologica* **32**, 36-41.

Hofmann, D.J. & Rosen, J.M. (1981) On the background stratospheric aerosol layer. *Journal of the Atmospheric Sciences* **38**, 168-181.

Hofmann, D.J., Oltmans, S.J., Komhyr, W.D., Harris, J.M., Lathrop, J.A., Langford, A.O., Deshler, T., Johnson, T., Torres, A. & Matthews, W.A. (1994) Ozone loss in the lower stratosphere over the United States in 1992-1993: Evidence for heterogeneous chemistry on the Pinatubo aerosol. *Geophysical Research Letter* **21**(1), 65-68.

Junge, C.E., Chagnon, C.W. & Manson, J.E. (1961a) Stratospheric aerosols. *Journal of Meteorology* **18**, 81-108.

Junge, C.E., Chagnon, C.W. & Manson, J.E. (1961b) A world-wide stratospheric aerosol layer. *Science* **133**, 1478-1479.

Junge, C.E. & Manson, J.E. (1961) Stratospheric aerosol studies. *Journal of Geophysical Research* **66**(7), 2163-2182.

Kudish, A.I., Evseev, E. & Kushelevsky, A.P. (1997) The analysis of ultraviolet radiation in the Dead Sea basin, Israel. *International Journal of Climatology* **17**(15), 1697-1704.

Lazrus, A.L. & Gandrud, B.W. (1974) Stratospheric sulphate aerosol. *Journal of Geophysical Research* **79**(24), 3424-3431.

Levelt, P.F., Hilsenrath, E., Leppelmeier, G.W., van den Oord, G., Bhartia, P.K., Tamminen, J., de Haan, J.F. & Veefkind, J.P. (2006) *IEEE Transactions on Geoscience and Remote Sensing* **44**(5), 1199-1208.

Lindfors, A., Holmgren, B. & Hansen, G. (2006) Long-term erythemal UV at Abisko and Helsinki estimated using total ozone, sunshine duration, and snow depth. *Proceedings of SPIE*, **6362**. doi: 10.1117/12.689742.

Long, C.S., Miller, A.J., Lee, H-T., Wild, J.D., Przywarty, R.C. & Hufford, D. (1996) Ultraviolet index forecasts issued by the national weather service. *Bulletin of the American Meteorological Society* **77**(4), 729-748.

Loutre, M-F., Paillard, D. Vimeux, F. & Cortijo, E. (2004) Does mean annual insolation have the potential to change the climate? *Earth and Planetary Science Letters* **221**, 1-14.

Lubin, D. & Frederick, J.E. (1991) The ultraviolet radiation environment of the Antarctic peninsula: The roles of ozone and cloud cover. *Journal of Applied Meteorology* **30**, 478-493.

McKenzie, R.L., Matthews, W.A. & Johnston, P.V. (1991) The relationship between erythemal UV and ozone, derived from spectral irradiance measurements. *Geophysical Research Letters* **18**(12), 2269-2272.

McKenzie, R.L., Johnston, P.V., Smale, D., Bodhaine, B.A. & Madronich, S. (2001) Altitude effects on UV spectral irradiance deduced from measurements at Lauder, New Zealand, and at Mauna Loa Observatory, Hawaii. *Journal of Geophysical Research* **106**(D19), 22845-22860.

McKenzie, R.L., Bodeker, G., Scott, G., Slusser, J. & Lantz, K. (2006) Geographical differences in erythemally-weighted UV measured at mid-latitudes USDA sites. *Photochemical & Photobiological Sciences* **5**, 343-352.

Myhre, G., Berglen, T.F., Myhre, C.E.L. & Isaksen, I.S.A. (2004) The radiative effect of the anthropogenic influence on the stratospheric sulphate aerosol layer. *Tellus* **56B**, 294-299.

Newhall, C.G. & Self, S. (1982) The volcanic explosivity index (VEI): An estimate of explosive magnitude for historical volcanism. *Journal of Geophysical Research* **87**, 1231-1238.

Pachart, E., Lenoble, J., Brogniez, C., Masserot, D. & Bocquet, J-L. (1999) Ultraviolet spectral irradiance in the French Alps: Results of two campaigns. *Journal of Geophysical Research* **104**(D14), 16777-16784.

Penner, J.E., Andreae, M., Annegarn, H., Barrie, L., Feichter, J., Hegg, D., Jayaraman, A., Leaitch, R., Murphy, D., Nganga, J. & Pitari, G. (2001) Aerosols, their direct and indirect effects, in: *Climate Change 2001: The scientific basis. Contribution of working group I to the third assessment report of the intergovernmental panel on climate change* (eds. J.T. Houghton, Y. Ding, D.J. Griggs, M. Noguer, P.J. van der Linden, X. Dai, K. Maskell & C.A. Johnson). Cambridge University Press, Cambridge, UK. pp. 289-344.

Piazena, H. (1996) The effect of altitude upon the solar UV-B and UV-A irradiance in the tropical Chilean Andes. *Solar Energy* **54**(2), 133-140.

Randel, W.J., Wu, F. & Russell, J.M. (1995) Ozone and temperature changes in the stratosphere following the eruption of Mount Piantubo. *Journal of Geophysical Research* **100**(D8), 16753-16764.

Renaud, A., Staehelin, J., Fröhlich, C., Philipona, R. & Heimo, A. (2000) Influence of snow and clouds on erythemal UV radiation: Analysis of Swiss measurements and comparison with models. *Journal of Geophysical Research* **105**(D4), 4961-4969.

Rex, M., Salawitch, R.J., von der Gathen, P., Harris, N.R.P., Chipperfield, M.P. & Naujokat, B. (2004) Arctic ozone loss and climate change. *Geophysical Research Letters* **31**, L04116, doi:10.1029/2003GL018844.

Rigel, D.S., Rigel, E.G. & Rigel, A.C. (1999) Effects of altitude and latitude on ambient UVB radiation. *Journal of the American Academy of Dermatology* **40**, 114-116.

Roe, G.H. (2005) Orographic precipitation. *Annual Review of Earth and Planetary Sciences* **33**, 645-671.

Rosen, J.M., Hofmann, D.J. & Laby, J. (1975) Stratospheric aerosol measurements II: The worldwide distribution. *Journal of the Atmospheric Sciences* **32**, 1457-1462.

Rozema, J., Chardonnens, A., Tosserams, M., Hafkenscheid, R. & Bruijnzeel, S. (1997) Leaf thickness and UV-B absorbing pigments of plants in relation to an elevational gradient along the Blue Mountains, Jamaica. *Plant Ecology* **128**, 151-159.

Sabburg, J. & Wong, J. (2000) The effect of clouds on enhancing UVB irradiance at the earth's surface: A one year study. *Geophysical Research Letters* **27**(20), 3337-3340.

Schmucki, D.A. & Philipona, R. (2002) Ultraviolet radiation in the Alps: The altitude effect. *Optical Engineering* **41**(12), 3090-3095.

Self, S. (2006) The effects and consequence of very large explosive volcanic eruptions. *Philosophical Transactions of the Royal Society: A* **364**, 2073-2097.

Shallcross, D.E., Wang, K-Y. & Dimmer, C.H. (2003) *Handbook of atmospheric science: Principles and applications* (eds. C.N. Hewitt & A.V. Jackson). Blackwell Science Ltd., Oxford, UK

Siebert, L. & Simkin, T. (2002-) *Volcanoes of the world: An illustrated catalogue of Holocene volcanoes and their eruptions.* Smithsonian Institution, Global Volcanism Program Digital Information Series, GVP-3. http://www.volcano.si.edu/world/. Date accessed: 18/01/2008.

Stothers, R.B. (2007) Three centuries of observation of stratospheric transparency. *Climatic Change* **83**, 515-521.

Sullivan, J.H., Teramura, A.H. & Ziska, L.H. (1992) Variation in UV-B sensitivity in plants from a 3000m elevational gradient in Hawaii. *American Journal of Botany* **79**(7), 737-743.

Tanskanen, A., Krotkov, N.A., Hermna, J.R. & Arola, A (2006) Surface ultraviolet irradiance from OMI. *IEEE Transactions on Geoscience and Remote Sensing* **44**(5), 1267-1271.

Toon, O.B. & Pollack, J.B. (1976) A global average model of atmospheric aerosols for radiative transfer calculations. *Journal of Applied Meteorology* **15**, 225-246.

Toon, O.B. & Farlow, N.H. (1981) Particles above the tropopause: Measurements and models of stratospheric aerosols, meteoric debris, nacreous clouds, and noctilucent clouds. *Annual Review of Earth and Planetary Sciences* **9**, 19-58.

Watson, J.S., Sephton, M.A., Sephton, S.V., Self, S., Fraser, W.T., Lomax, B.H., Gilmour, I., Wellman, C.H., Beerling, D.J. (2007) Rapid determination of spore chemistry using thermochemolysis gas chromatography-mass spectrometry and micro-Fourier transform infrared spectroscopy. *Photochemical & Photobiological Sciences* **6**, 689-694.

Wilson, R.C.L., Drury, S.A. & Chapman, J.L. (2000) *The great ice age: Climate change and life.* Routledge, London, UK.

WMO (World Meteorological Organisation) (2007) *Scientific assessment of ozone depletion: 2006.* World Meteorological Organisation global ozone research and monitoring project – Report No. 50. Geneva, Switzerland.

5 Application of proxy to ancient datasets

5.1 Introduction

Five major mass extinctions have occurred during the Phanerozoic Eon (~ 570 Ma to the present), resulting in substantial reductions in global biodiversity (Sheldon & Skelton, 1993; Lunine, 1999). These "big five" extinctions are defined in the geological record by the rapid loss of families of organisms with significant taxonomic effect. Numerous causes have been proposed for such global loss of diversity, including catastrophic asteroid or comet impacts, extreme changes in Earths' climate, such as the onset of major ice ages, or sustained, large-scale volcanic activity (Alvarez *et al.*, 1980; Raup & Sepkoski, 1982; Crowley & North, 1988; Rampino & Stothers, 1988; Stothers, 1993; Wignall, 2001; Courtillot & Renne, 2003). Considering the hypothesis that volcanic activity may be related to mass extinctions, Visscher *et al.* (2004) proposed that the end-Permian extinction event may have been due to perturbation of the atmosphere caused by multiple phases of eruption of the Siberian Traps, resulting in ozone depletion and commensurate increases in UV-B radiation. The development of a proxy for ozone depletion *via* the chemical response to incident UV-B radiation in the previous chapters of this study lends itself to testing such a theory.

The intention of this chapter is to investigate the applicability of the biochemical proxy described and tested on modern samples in previous chapters to geological samples. In particular, to investigate whether lycopsid spores extracted from lithological units spanning the Permian-Triassic boundary (251 ±0.4 Ma; Gradstein *et al.*, 2004) record changes that might be related to UV-B flux, hence if volcanically-induced perturbations of UV-B radiation could have been an important driving factor in the end Permian extinction (Beerling *et al.*, 2007).

5.2 History of research

5.2.1 The end-Permian ecological crisis

As a mass extinction event the Permo-Triassic boundary (PTB) is of unrivalled magnitude in the geological record. Estimates of global marine biodiversity spanning the PTB reveal that 57 % of taxonomic families had become extinct by the end of the Permian period (Sheldon & Skelton, 1993; Figure 5.1); later calculations suggest as many as 96 % of species were lost at this time (Renne *et al.*, 1995; White, 2002; Grard *et al.*, 2005). In addition to the substantial reduction in marine diversity, terrestrial ecosystems are also found to have suffered greatly, with losses estimated to be in the region of 70 % of terrestrial vertebrate families (Renne *et al.*, 1995; Retallack 1995). The loss of marine biota is thought to have occurred over a period of ~ 5 million years, whilst the impact upon terrestrial systems is likely to have taken longer (Holser & Magaritz, 1992), however, the duration of the extinction is still open to debate, with other estimates suggesting the process was much more rapid, perhaps even less than 1 million years (Bowring *et al.*, 1998; White, 2002). There is evidence that terrestrial flora also decreased in numbers, with only a limited range of diversity continuing for a considerable period after the PTB and pre-PTB levels of diversity not being reached again until 7 million years later in the early Triassic (~ 244 Ma; Retallack, 1995; White, 2002). Whatever the outcome of further studies regarding the absolute duration and relative timing of extinction of different groups, the general view is that marine fauna declined rapidly whilst the impact upon terrestrial flora and fauna was a much slower process.

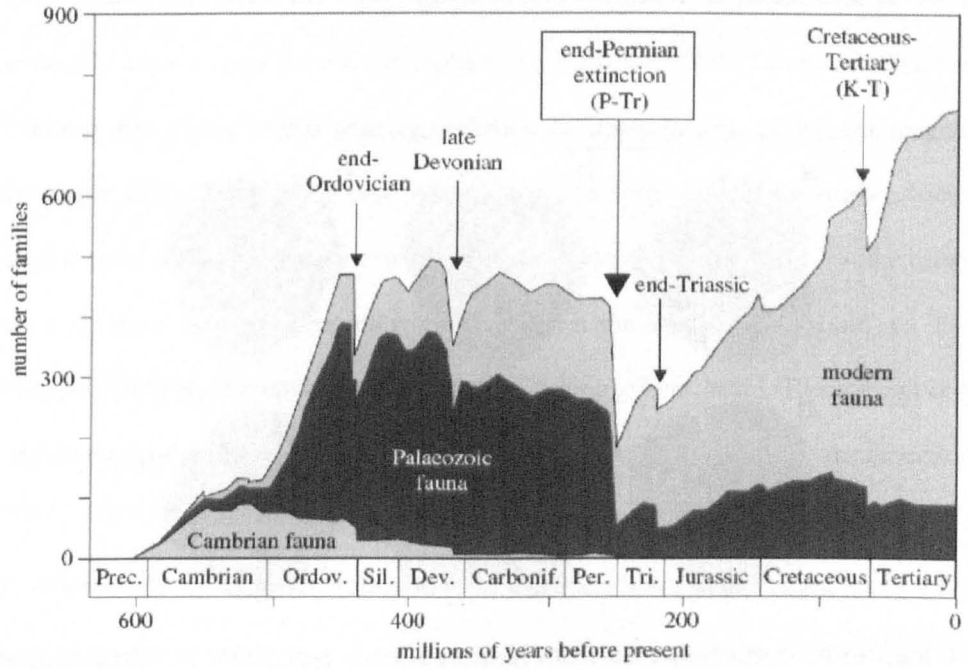

Figure 5.1 Palaeozoic faunal diversity plot with the "big five" mass extinctions highlighted. Clearly the end-Permian extinction experienced the greatest loss in biodiversity. From: White (2002).

Palynological studies of PTB sediments have identified mutated *Lycopod* spores where separation of the spores in a late stage of development has failed to occur limiting their ability to perform their reproductive role. When the spores form, they develop in a tetrad configuration joined in a way that obscures the triradiate germinal aperture (Figure 5.2), which is essential for further plant development; such a formation pattern does not present a problem to spore that separate normally, but is clearly a potential disadvantage for mutant tetrad spores that fail to separate (Visscher *et al.*, 2004). UV-B radiation is a known agent of mutagenesis and has been suggested as a possible global-wide cause of mutations observed in flora (Visscher *et al.*, 2004). An extension of this idea is that a global change in UV-B radiation could exert stress on ecosystems resulting in a decline in biodiversity, with only the most resilient organisms surviving, which can then go on to re-colonise the broader environment unhindered by competitive stress. One potential cause of such a dramatic shift in surface UV-B at this time is large-scale volcanic activity.

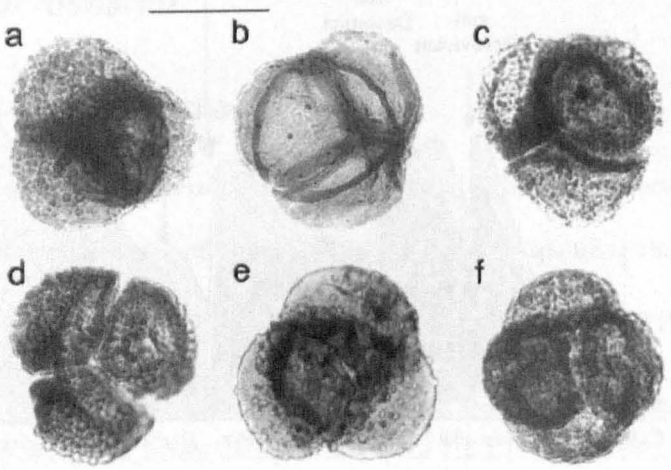

Figure 5.2 Permian microspores from heterosporous lycopsids in tetrad formation. From: Visscher *et al.* (2004).

5.2.2 Permo-Triassic volcanism

A key influence in the shift from marine to terrestrial-based life is thought to be the development of an oxygenated atmosphere, which led to the build up of ozone in the atmosphere. Prior to ~ 2.5 billion years ago Earths' atmosphere was anoxic, thus there was no ozone layer absorbing incoming UV-B radiation. As outlined in Chapter 1, UV-B radiation can have detrimental consequences for living organisms, thus is thought to have severely restricted the inhabitability of terrestrial environments. However, once atmospheric ozone concentrations had reached sufficient levels to provide an effective shield against UV-B (an "external filter") the transition of life from sea to land became more amenable (Lunine, 1999).

The stratospheric ozone layer during the Permian period would have performed the same function as the present day ozone layer, with the exception that it would not have been subject to the stresses imparted upon it today by anthropogenic ozone-depleting emissions; only natural influences would have exerted any pressure on the atmospheric equilibrium. Therefore ozone abundance would have been primarily driven by the total abundance of diatomic oxygen (O_2) as a precursor/equilibrium partner to ozone (O_3), and naturally occurring perturbations to the atmosphere, such as those caused by volcanic activity.

Whilst volcanic activity on the scale experienced in the historical period has, at times, had a considerable impact upon Earths' atmosphere (i.e. Pinatubo, 1991; Tambora, 1815; Santorini, 17th century BC; Toba, 74,000 years ago (Francis & Oppenheimer, 2004)), the magnitude of these events pale into insignificance when compared with the activity further back in the geological past, particularly the extrusion of large igneous provinces (LIP – the term "large igneous province" is used here interchangeably with the term "flood basalt" to describe a voluminous, prolonged eruption of basaltic composition). One such LIP eruption occurred in the latter stages of the Permian period in what is now Siberia, giving rise to the Siberian Traps.

Vast volumes of material are brought to the surface during the eruption of LIPs over prolonged periods of time, both in terms of gas and solid phase material (Bryan & Ernst, 2008). In the case of the Siberian Traps it is estimated that somewhere in the range of 1.5-4 x 10^6 km^3 of material was erupted over the course of less than 1 million years (Renne *et al.*, 1995; Courtillot *et al.*, 1999; Grard *et al.*, 2005; Beerling *et al.*, 2007), although the duration may well have be shorter than this (100-600 thousand years; Kamo *et al.*, 2003). Whilst the Siberian Traps are not of an uncommon magnitude or duration for flood basalts (Courtillot *et al.*, 1999), this formation does show some features that could potentially make this the most significant eruption in the Phanerozoic eon for global climate change (Campbell *et al.*, 1992). Geochemical evidence suggests the magma source was very sulphur-rich, where the sulphur could ultimately reach the stratosphere and form sulphate aerosols; a key influence on ozone depletion (Campbell *et al.*, 1992; Chapter 1). It has been proposed that the eruption of the Siberian Traps also released a substantial volume of halogenated compounds into the atmosphere that could then proceed in ozone-destroying reactions on the surface of the freshly formed sulphate aerosols. Such halogen-containing compounds are not an integral feature of the magma itself, but are thought to have originated from coal-bearing beds and evaporite deposits that the magma passed through *en route* to the surface (Visscher *et al.*, 2004; Beerling *et al.*, 2007). The existence of these organic- and halogen-rich deposits is indicated by

the regional geology (Kontorovich *et al.*, 1997; Melnikov *et al.*, 1997; Czamanske *et al.*, 1998). Finally, it has been calculated that as much as 20 % (by volume) of the entire volcanic sequence comprises of tuffs, suggesting significant pyroclastic activity as a result of unusually high explosivity (Campbell *et al.*, 1992; Beerling *et al.*, 2007). Increased explosivity provides a mechanism whereby a greater proportion of erupted material (i.e. sulphur and halogenated compounds) may reach higher altitudes, thus potentially being injected into the stratosphere. Based on the available evidence, is it very likely that the eruption of the Siberian Traps had a significant impact upon the atmosphere, and is likely to have been a contributing factor towards the contemporaneous mass extinction.

Given the time-frame of eruption of the Siberian Traps has been constrained to $\leq$ 1 million years duration (Renne *et al.*, 1995; Courtillot *et al.*, 1999; Grard *et al.*, 2005; Beerling *et al.*, 2007), the minimum duration of extinction suggested by Holser & Magartiz (1992) of $\geq$ 5 million years does not appear to be compatible. It is therefore much more likely that a realistic duration of extinction is of the order proposed by Bowring *et al.* (1998) and White (2002), i.e. 1 million years or less.

The preservation of the plant microfossils in the geological record can be exceptional under specific conditions, thus they have the potential to be a source of geochemical information that may reveal whether changes in surface UV-B played a role in the end Permian ecological crisis. The scope of this chapter is to investigate the viability of fossilised spores for the application of the novel geochemical UV-B proxy proposed earlier in this work. This will be achieved by testing the proxy against a period in geological history thought to be subject to environmentally significant shifts in surface UV-B radiation following substantial volcanic activity, e.g. the end-Permian eruption of the Siberian Traps.

5.3 Experimental

5.3.1 Sample preparation

A suite of samples comprising apiculate and laevigate megaspores were separated, hand picked and identified from sediments collected in the Salt Range and Surghar Range, Western Pakistan (C.H. Wellman, *personal communication*) that span the Permo-Triassic boundary, totalling approximately 365 m of stratigraphic column. The complete sequence runs from the Chhidru Formation in the Upper Permian through to the Tredian Formation of the Middle Triassic (Balme, 1970; Figure 5.3).

5.3.2 FTIR microspectroscopy

FTIR microspectroscopy was conducted in accordance with the method detailed in Appendix A. A Continuum IR-enabled microscope fitted with a 15x reflachromat objective lens and nitrogen-cooled MCT-A detector is interfaced with the bench unit to provide microscopic analysis capability. Analysis was conducted using a microscope aperture of 100 x 100 μm at 500 scans per sample with a resolution of 4. Background spectra were collected immediately after every sample spectrum. Each analysis was replicated three times per sample, where a sample constitutes a single megaspore.

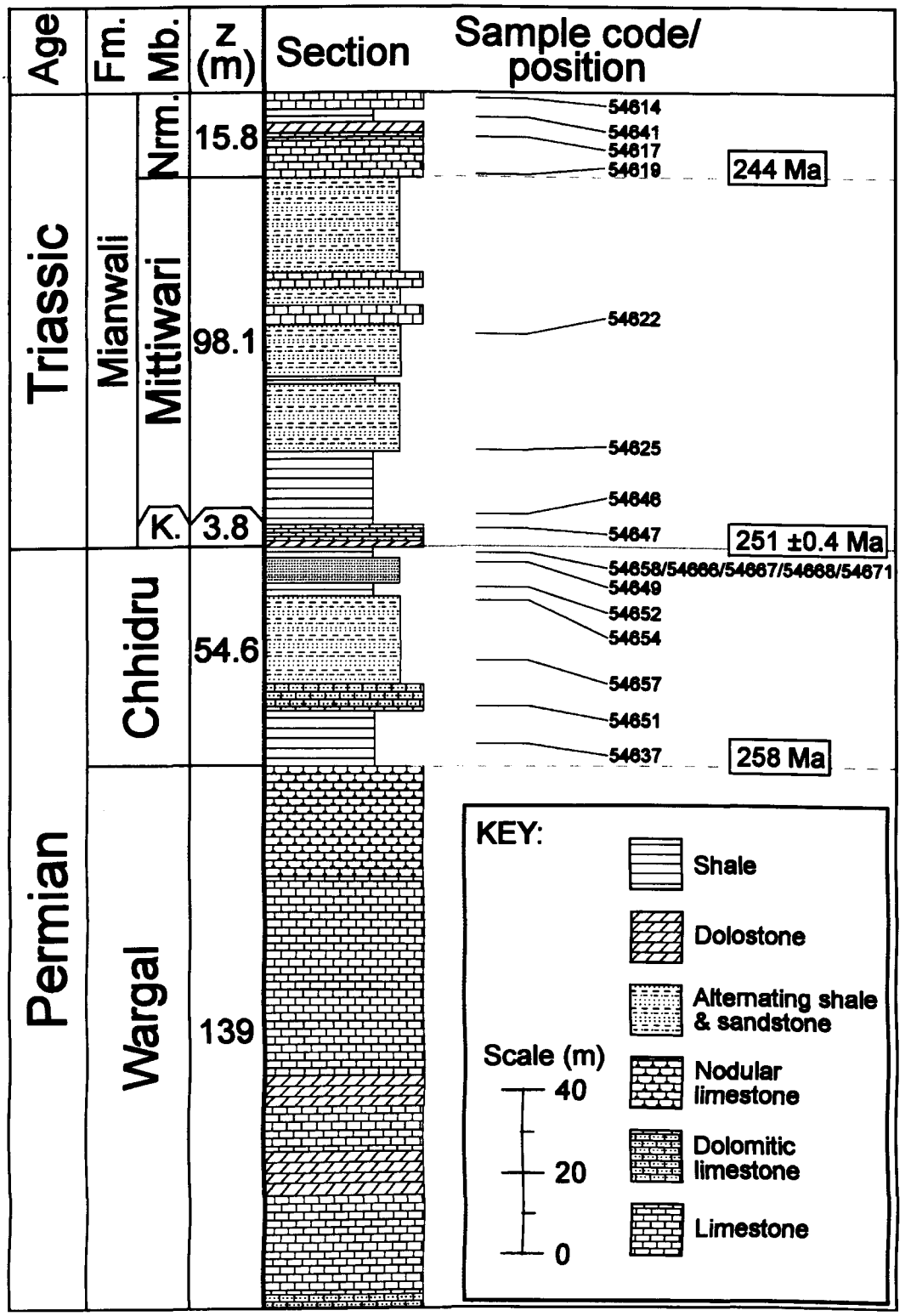

Figure 5.3 Generalised stratigraphy spanning the Permo-Triassic boundary in the Salt Range, Pakistan. Stratigraphic position of samples is provided. Adapted from Balme (1970), Wignall & Hallam (1993) and Hassan *et al.* (1999).

5.4 Results

5.4.1 Permo-Triassic Lycopsids of the Salt Range, Pakistan

Spectra obtained using FTIR microspectroscopy identify a number of functional groups within the fossilised megaspores (Figure 5.4), revealing spore chemistry that is functionally similar, but not identical to the modern-day samples analysed in Chapters 2, 3 and 4. The functionality of the fossilised megaspores is set out in the section below in wavenumber order, from high wavenumber to low. All interpretation of FTIR spectra are in accordance to those of Rouxhet *et al.* (1980) and Williams & Fleming (1980).

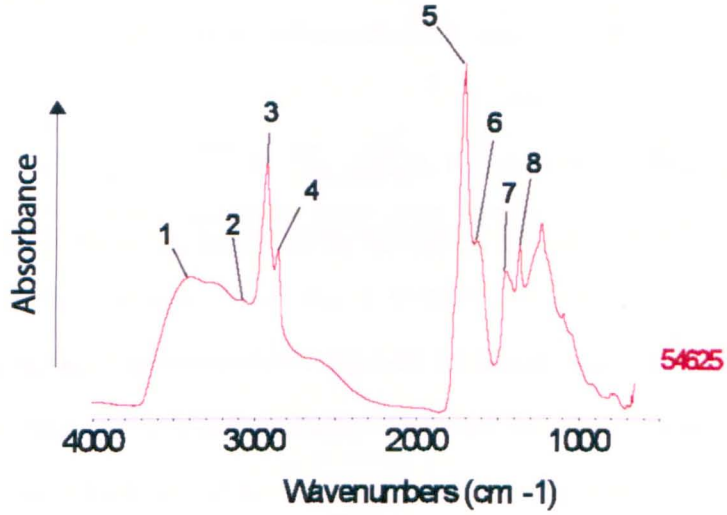

Figure 5.4 FTIR band assignments. 1. *ν*(OH); 2. *νs*(C=C); 3. *νs*(CH_2 + CH_3); 4. *νas*(CH_2 + CH_3); 5. *ν*(C=O); 6. *νs*(C=C); 7. *ν*(CH_2 + CH_3); 8. *ν*(CH_3).

5.4.1.1 Infrared spectra band assignments

A clear absorption band is observed in the region 3700-3100 cm^{-1} (Figure 5.4, label 1), indicative of the presence of hydroxyl (OH) groups. As seen in the modern-day samples, the positioning and broad nature of the band suggests that the hydroxyl groups are bound into the structure of the spore wall rather than being due to 'free' hydroxyl groups, such as in water. The broadness of band also identifies that the hydroxyl groups may be involved in hydrogen bonding.

The presence of a weak band at ~ 3060 cm^{-1} (Figure 5.4, label 2) suggests that there are C-H stretching vibrations associated with C=C bonds in the structure of the fossil sporopollenin. However, it is unclear as to whether such C=C bonds represent unsaturated carbon chains, or if they are C=C bonds within an aromatic ring. The positioning of the band appears to be too high to be attributed to aromatic moieties because aromatic C=C bonds are expected to show absorption bands nearer to 3030 cm^{-1}. Carbon double bonds associated with unsaturated compounds are expected to absorb in the region of 3020-3100 cm^{-1} due to the C-H bond stretching adjacent to C=C bonds. In this case it appears that unsaturated aliphatic compounds are the most likely cause of the absorption band at 3060 cm^{-1}.

Two strongly absorbing bands appear at 2925 and 2850 cm^{-1} (Figure 5.4, labels 3 and 4), representing symmetrical and anti-symmetrical stretching of C-H bonds within alkyl groups. Unlike the modern-day samples, the fossil spores show a greater definition of absorbance bands in this region. Alkyl bands in the region 2800-3000 cm^{-1} can be further assigned according to exact positioning of the bands. Absorption at 2926 and 2853 ± 10 cm^{-1} are due to symmetrical and anti-symmetrical stretching of C-H bonds in CH_2 groups, respectively, whilst the corresponding vibrational modes of CH_3 groups occur at the higher wavenumber positions of 2962 and 2872 cm^{-1}. Spectra obtained from the fossil spores show the alkyl absorbance bands at 2927 and 2856 cm^{-1}, suggesting that CH_2 groups are the dominant cause of the alkyl vibrations. The trough between the bands at 2927 and 2856 cm^{-1} is relatively shallow and the higher wavenumber limb of the 2927 cm^{-1} band shows signs of a 'shouldering' effect in some samples (Figure 5.5, e.g. 54614, 54625, 54636, 54658), indicating that absorption bands due to CH_3 groups are present, but are overprinted by the dominant CH_2 absorbance.

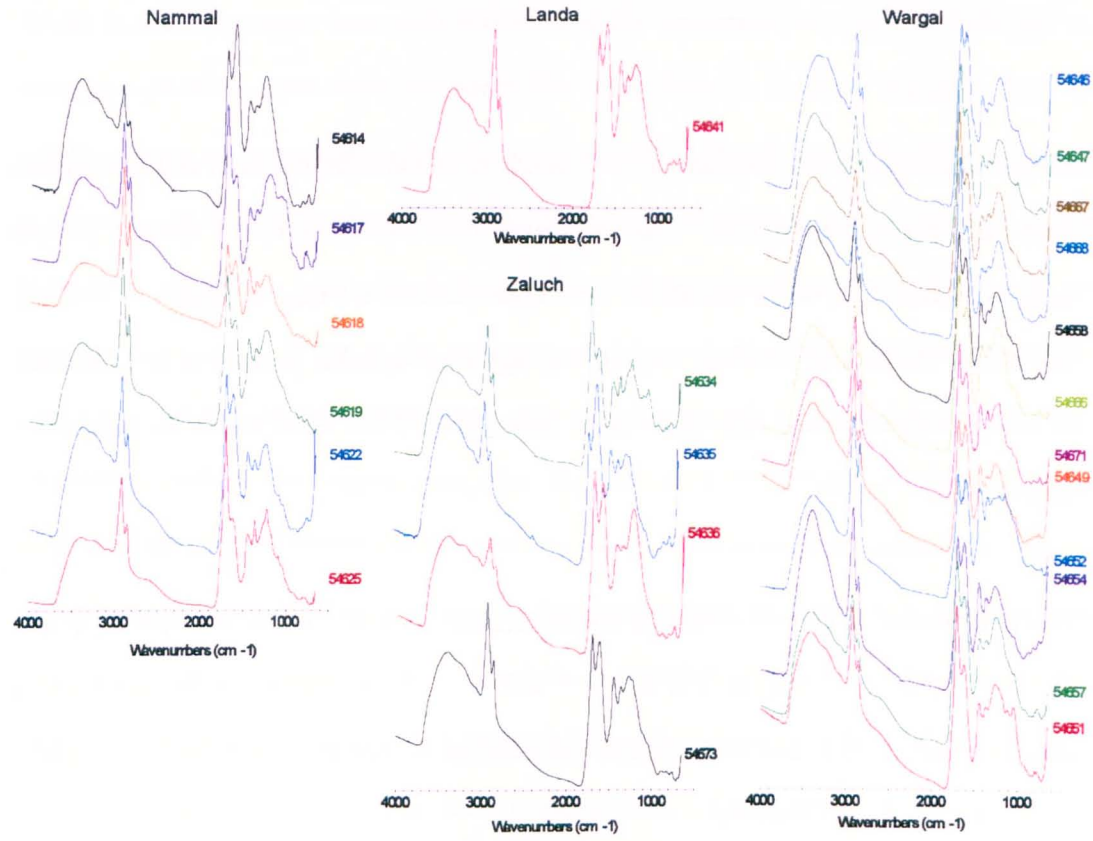

Figure 5.5 FTIR spectra obtained from Salt Range PTB lycopsid megaspore samples. Sample codes are provided for reference to Figure 5.3.

A prominent feature of spectra obtained from all samples is a strongly absorbing band at 1700-1710 cm^{-1} (Figure 5.4, label 5). Such a feature is typical of carbonyl group (C=O) stretching vibrational modes. In this case the wavenumber corresponds with carbonyl bonds forming carboxylic acid functional groups that are involved in the hydrogen bonding of hydrogen bonded dimers. Additional weight is added to the argument that hydrogen bonded dimers are present by the occurrence of a shoulder band observable in the majority of spectra in the region of 2500-2700 cm^{-1} (Figure 5.5). The feature in the 2500-2700 cm^{-1} region is associated with hydroxyl stretching that is involved in dimer hydrogen bonding. The possibility also exists that this carbonyl absorbance is due to ester linkages as observed in modern-day sporopollenin, giving rise to the biopolymeric structure, however, the position of the absorption band occurs at slightly too low a wavenumber to be conclusively assigned as an ester linkage.

Further evidence for the presence of C=C bonds is provided by the band at approximately 1620 cm^{-1} (Figure 5.4, label 6). This absorbance band falls close to the division between aromatic related C=C bonds and alkene C=C bonds; as with the band located at ~ 3060 cm^{-1} (see above), the band at 1620 cm^{-1} exhibits too high a wavenumber position to be attributable to aromatic C=C bonds, thus more likely represents a C=C bond within an unsaturated carbon chain.

The final feature of interest shown by the fossil sample spectra are the absorption bands at 1450 and 1360 cm^{-1} (Figure 5.4, labels 7 and 8). These bands can be attributed to deformations of CH_2 and CH_3 groups (anti-symmetric bending), and only CH_3 groups (symmetric bending), respectively.

5.4.1.2 Interpretation of infrared spectra

It is apparent from analysis with FTIR microspectroscopy that the sporopollenin within fossilised spore samples is dominantly, if not exclusively aliphatic in nature, rather than the aliphatic-aromatic copolymer that is seen in extant and historical material. Alkane-related absorbencies are strong throughout the sample set, with convincing evidence in favour of the presence of C=C bonds within aliphatic structures, rather than aromatic moieties.

The positioning and occurrences of O-H and C=O absorbencies suggest that hydrogen-bonding is playing an important role within the structure of fossilised sporopollenin, particularly the possibility that hydrogen bonded dimers are present. Based on the evidence presented here, it is likely that fossilised sporopollenin retains a polymeric structure as seen in extant sporopollenin.

Previous research conducted by Yule *et al.* (2000) incorporated infrared analysis of modern-day and fossilised lycopsid spores. Their interpretations of the infrared spectra are generally

similar to those presented here, with exception of the assignment of a band at 1520 cm^{-1} to nitrogen-containing compounds for which this study finds no evidence for (refer back to Chapter 2 for a more detailed discussion), and attribution of bands in the 750-900 cm^{-1} region to aromatic-related C-H bending vibrations. Assignment of bands in the 700-900 cm^{-1} region to aromatic moieties is valid only if there is also evidence elsewhere within the spectra for aromatic compounds, which in the case presented here there is not sufficient, conclusive evidence to suggest aromatic compounds play a significant role in fossilised sporopollenin. Absorbance within this region may also be due to C=C bonds in other chemical environments, such as alkene compounds, for which there is evidence within the spectra shown here. Finally, a band at 1630 cm-1 is attributed by Yule *et al.* (2000) to aromatic-related C=C bonds, but as outlined above, this study finds no convincing evidence that suggests the band can be reliably attributed to the presence of aromatic compounds. It is for these reasons that the band assignments given here differ to those of Yule *et al.* (2000).

A key point of interest is the distinct lack of any strong aromatic-related absorbency within the fossilised samples, such as the band observed in modern-day material positioned at 1520cm^{-1}; this observation highlights a fundamental difference between fossil and modern sporopollenin of related plant species/genera. Whilst there is evidence of carbon-carbon double bonds within the structure of fossil sporopollenin, it appears that they are not associated with aromatic ring structures. This poses a problem for the successful application of the proposed aromatic-based UV-B proxy. If there are no, or only very few aromatic moieties bound within the structure of fossil sporopollenin then the proxy becomes untenable. Comparison with extant material suggests that it is likely that aromatic compounds may have once contributed to the structure of sporopollenin. Two questions arise from this conundrum; firstly, how can we be sure that aromatic moieties were present in the sporopollenin of the fossil material during life? And secondly, if the fossil sporopollenin did once contain aromatic compounds

as observed in modern-day material, what processes have occurred in order to bring about the difference in resultant chemistry?

5.5 Conclusions

From the evidence presented here it can be concluded that the geochemical proxy proposed earlier in this work cannot be applied to fossilised lycopsid samples due to substantial changes in the fundamental chemistry of sporopollenin. Retention of sufficient morphological features of the megaspores enabling identification to genus level leads to the expectation that the chemistry will also be relatively unaltered; however, this is clearly not the case here. The presence of a polymer comprising almost exclusively aliphatic moieties renders an aromatic-based proxy unusable for this degree of maturity of organic material. As a result of the apparent change in spore chemistry from an aliphatic-aromatic copolymer to a dominantly aliphatic polymer, the question as to whether eruption of the Siberian Traps perturbed the global atmosphere leading to changes in stratospheric ozone and surface UV-B remains unanswered.

Comparison of the FTIR spectra obtained in this study with previous work by Yule *et al.* (2000) reveals great similarities between genuine fossil samples and artificially matured samples of *Lycopodium clavatum*. This comparison suggests that changes in sporopollenin chemistry proceed under relatively mild diagenetic conditions, although the findings reported here do not directly support those of other studies with regards the technical details, i.e. spectral interpretation (Yule *et al.*, 2000).

5.6 Summary of findings

• Fossil Lycopsid spores are chemically distinct from their modern-day counterparts, despite excellent preservation of morphological features.

• A dominantly aliphatic polymer appears to constitute the sporopollenin of fossil spores, rather than a combination of aliphatic and aromatic components found in extant material.

• The geochemical proxy under evaluation in the present work is not applicable to these spore samples of Permo-Triassic age due to the substantial chemical differences observed; a lack of aromatic moieties within fossil sporopollenin renders aromatic-content analysis inoperable.

The similarities exhibited by fossil and artificially matured samples provide an avenue to investigate some of the changes that organic material undergo during burial within sediments, as well as the opportunity to reconcile the differences in chemical interpretation found between the two sets of data. With this in mind Chapter 6 will attempt to elucidate the details of such chemical changes by performing artificial maturation experiments on modern-day spores similar to the experiments of Yule *et al.* (2000) and Marshall *et al.* (1991).

5.7 References

Alvarez, L.W., Alvarez, W., Asaro, F. & Michel, H.V. (1980) Extraterrestrial cause for the Cretaceous-Tertiary extinction. *Science* **208**, 1095-1108.

Balme, B.E. (1970) Palynology *of Permian and Triassic strata in the Salt Range and Surghar Range, West Pakistan.* University of Kansas special publication No. 4. pp. 306-453.

Beerling, D.J., Harfoot, M., Lomax, B. & Pyle, J.A. (2007) The stability of the stratospheric ozone layer during the end-Permian eruption of the Siberian Traps. *Philosophical Transactions of the Royal Society: Series A* **365**, 1843-1866.

Bowring, S.A., Erwin, D.H., Jin, Y.G., Martin, M.W., Davidek, K. & Wang, W. (1998) U/Pb zircon geochronology and tempo of the end-Permian mass extinction. *Science* **280**, 1039-1045.

Bradley, R.S. (1999) *Paleoclimatology: Reconstructing climates of the Quaternary* (2nd ed.). Academic Press Ltd., London, UK.

Bryan, S.E. & Ernst, R.E. (2008) Revised definition of Large Igneous Provinces (LIPs). *Earth Science Reviews* **86**, 175-202.

Campbell, I.H., Czamanske, G.K., Fedorenko, V.A., Hill, R.I. & Stepanov, V. (1992) Synchronism of the Siberian Traps and the Permian-Triassis Boundary. *Science* **258**, 1760-1763.

Chaloner, W.G. (1999) Taxonomic and nomeclatural alternatives, in; *Fossil plants and spores: Modern techniques* (eds. Jones, T.P. & Rowe, N.P.). Geological Society, London, UK.

Courtillot, V., Jaupart, C., Manighetti, I., Tapponnier, P. & Besse, J. (1999) On causal links between flood basalts and continental breakup. *Earth & Planetary Science Letters* **166**, 177-195.

Courtillot, V.E., & Renne, P.R. (2003) On the ages of flood basalt events/Sur l'âge des trapps basaltiqes. *Comptes Rendus Geoscience* **335**, 113-140.

Crowley, T.J. & North, G.R. (1988) Abrupt climate change and extinction events in the Earth history. *Science* **240**, 996-1002.

Czamanske, G.K., Gurevitch, A.B., Fedorenko, V. & Simonov, O. (1998) Demise of the Siberian plume: Paleogeographic and paleotectonic reconstruction from the prevolcanic and volcanic record, north-central Siberia. *International Geology Review* **40**, 95-115.

Einsele, G. (2000) *Sedimentary basins: Evolution, facies, and sediment budget* (2nd ed.). Springer-Verlag Publishing, Berlin, Germany.

Francis, P.W. & Oppenheimer, C. (2004) *Volcanoes* (2nd ed.). Oxford University Press, Oxford, UK.

Gerrienne, P., Meyer-Berthaud, B., Fairon-Demaret, M., Streel, M. & Steemans, P. (2004) *Runcaria*, a middle Devonian seed plant precursor. *Science* **306**, 856-858.

Gradstein, F.M., Ogg, J.G., Smith, A.G., Agterberg, F.P., Bleeker, W., Cooper, R.A., Davydov, V., Gibbard, P., Hinnov, L.A., House, M.R., Lourens, L., Luterbacher, H.P., McArthur, J., Melchin, M.J., Robb, L.J., SHergold, J., Villeneuve, M., Wardlaw, B.R., Ali, J., Brinkhuis, H., Hlgen, F.J., Hooker, J., Howarth, R.J., Knoll, A.H., Laskar, J., Monechi, S., Plumb, K.A., Powell, J., Raffi, I., Röhl, U., Sadler, P., Sanfilippo, A., Schmitz, B., Shackleton, N.J., Shields, G.A., Strauss, H., van Dam, J., van Kolfschoten, T., Veizer, J. & Wilson, D. (2004) *A Geologic timescale 2004*. Cambridge University Press, Cambridge, UK.

Grard, A., François, L.M., Dessert, C., Dupré, B. & Goddéris, Y. (2005) Basaltic volcanism and mass extinction at the Permo-Triassic boundary: Environmental impact and modelling of the global carbon cycle. *Earth & Planetary Science Letters* **234**, 207-221.

Guildford, W.J., Schneider, D.M., Labovitz, J. & Opella, S.J. (1988) High resolution solid state ^{13}C NMR spectroscopy of sporopollenins from different plant taxa. *Plant Physiology* **86**, 134-136.

Hassan, S., Ishiga, H., Roser, B.P., Dozen, K. & Naka, T. (1999) Geochemistry of Permian-Triassic shales in the Salt Range, Pakistan: implications for provenance and tectonism at the Gondwana margin. *Chemical Geology* **158**, 293-314.

Hemsley, A.R., Chaloner, W.G., Scott, A.C. & Groombridge, C.J. (1992) Carbon-13 solid state nuclear magnetic resonance of sporopollenins from modern and fossil plants. *Annals of Botany* **69**, 545-549.

Holser, W.T. & Magaritz, M. (1992) Cretaceous/Tertiary and Permian-Triassic boundary events compared. *Geochimica et Cosmochimica Acta* **56**, 3297-3309.

Kamo, S.L., Czamanske, G.K., Amelin, Y., Fedorenko, V.A., Davis, D.W. & Trofimov, V.R. (2003) Rapid eruption of Siberian flood-volcanic rocks and evidence for coincidence with the Permian-Triassic boundary and mass extinction at 251 Ma. *Earth & Planetary Science Letters* **214**, 75-91.

Killops, S.D. & Killops, V.J. (2005) Introduction to organic geochemistry (2nd edition). Blackwell Publishing, Oxford, UK.

Kontorovich, A.E., Khomenko, A.V., Burshtein, L.M., Likhanov, I.L., Pavlov, A.L., Staroseltec, V.S. & Ten, A.A. (1997) Intense basic magmatism in the Tunguska petroleum basin, eastern Siberia, Russia. *Petroleum Geoscience* **3**, 359-369.

de Leeuw, J.W., Versteegh, G.J.M. & van Bergen, P.F. (2006) Biomacromolecules of algae and plants and their fossil analogues. *Plant Ecology* **182**, 209-233.

Lowe, J.J. & Walker, M.J.C. (1997) *Reconstructing Quaternary environments* (2nd ed.). Pearson Education Ltd., Harlow, UK.

Lunine, J.I. (1999) *Earth: Evolution of a habitable world.* Cambridge University Press, Cambridge, UK.

Marshall, J.E.A. (1991) Quantitative spore colour. *Journal of the Geological Society of London* **148**, 223-233.

Martin, P.S. & Gray, J. (1962) Pollen analysis and the Cenozoic. *Science* **137**, 103-111.

Melnikov, N.V., Knomenko, A.V., Kuznetsova, E.N. & Zhidkova, L.V. (1997) The effect of traps on salt redistribution in the Lower Cambrian of the western Siberian Platform. *Geologiya i Geofizika* **38**(8), 1339-1345.

Rampino, M.R. & Stothers, R.B. (1988) Flood basalt volcanism during the past 250 million years. *Science* **241**, 663-668.

Raup, D.M. & Sepkoski, J.J. (1982) Mass extincitions in the marine fossil record. *Science* **215**, 1501-1503.

Renne, P.R., Zichao, Z., Richards, M.A., Black, M.T. & Basu, A.R. (1995) Synchrony and causal relations between Permian-Triassic boundary crises and Siberian flood volcanism. *Science* **269**, 1413-1416.

Retallack, G.J. (1995) Permian-Triassic life crises on land. *Science* **267**, 77-80.

Rouxhet. P.G., Robin, P.L & Nicaise, G.B. (1980) Characterisation of kerogens and their evolution by infrared spectroscopy, in; *Kerogen*, (ed. B. Durand), Editions Techniq, Paris. pp. 163-190.

Scott, A.C. (2002) Coal petrology and the origin of coal macerals: a way ahead? *International Journal of Coal Geology* **50**, 119-134.

Sephton, M.A. (1997) Organic compounds in meteorites. PhD thesis, The Open University.

Sheldon, P. & Skelton, P. (1993) Phylogenetic patterns, in; *Evolution: A biological and palaeontological approach* (ed. P. Skelton). Addison-Wesley Publishing Company, Wokingham, UK. pp. 743-842.

Stankiewicz, B.A., Briggs, D.E.G., Michels, R., Collinson, M.E., Flannery, M.B. & Evershed, R.P. (2000) Alternative origin of aliphatic polymer in kerogen. *Geology* **28**(6), 559-562.

Stothers, R.B. (1993) Flood basalts and extinction events. *Geophysical Research Letters* **20**(13), 1399-1402.

Tissot, B.P. & Welte, D.H. (1984) *Petroleum formation and occurrence* (2nd ed.). Springer-Verlag Publishing, Berlin, Germany.

Vandenbroucke, M. & Largeau, C. (2007) Kerogen origin, evolution and structure. *Organic Geochemistry* **38**, 719-833.

Visscher, H., Looy, C.V., Collinson, M.E., Brinkhuis, H., van Konijnenburg-van Cittert, J.H.A., Kürschner, W.M. & Sephton, M.A. (2004) Environmental mutagenesis during the end-Permian ecological crisis. *Proceedings of the National Academy of Sciences of the United States of America* **101**, 12952-12956.

Watson, J.S., Sephton, M.A., Sephton, S.V., Self, S., Fraser, W.T., Lomax, B.H., Gilmour, I., Wellman, C.H., Beerling, D.J. (2007) Rapid determination of spore chemistry using thermochemolysis gas chromatography-mass spectrometry and micro-Fourier transform infrared spectroscopy. *Photochemical & Photobiological Sciences* **6**, 689-694.

White, R.V. (2002) Earth's biggest 'whodunnit': Unravelling the clues in the case of the end-Permian mass extinction. *Philosophical Transactions of the Royal Society: Series A* **360**, 2963-2985.

Wignall, P.B. & Hallam, A. (1993) Griesbachian (earliest Triassic) palaeoenvironmental changes in the Salt Range, Pakistan and southeast China and their bearing on the Permo-Triassic mass extinction. *Palaeogeography, Palaeoclimatology, Palaeoecology* **102**, 215-237.

Wignall, P.B. (2001) Large igneous provinces and mass extinctions. *Earth Science Reviews* **53**, 1-33.

Williams, D.H. & Fleming, I. (1980) Spectroscopic methods in organic geochemistry. McGraw-Hill, London.

Yule, B.L., Roberts, S. & Marshall, J.E.A. (2000) The thermal evolution of sporopollenin. *Organic Geochemistry* **31**, 859-870.

6 Diagenesis of sporopollenin in fossil spores

6.1 Introduction

The current state of understanding of the structure and composition of sporopollenin is based on analysis performed on disparate species of both angiosperm and gymnosperm origin, with much information gleaned from a combination of extant and fossil sporopollenin. However, knowledge of sporopollenin structure and composition is limited due to the highly resistant nature of sporopollenin, resulting in the finer details of sporopollenin composition remaining relatively inaccessible. Much debate about compositional analysis currently exists because of the many different approaches taken to extract the chemical information; many methods require harsh chemical treatments in order to access the structural information, which may alter the composition observed in the final analysis.

It is apparent from the analysis presented in previous chapters (particularly Chapter 2 and 5) that fossil lycopsid spores do not possess the same spore-wall chemistry as extant *Lycopodium* species. This difference in modern and fossil spore chemistry is likely to be a key factor in the lack of consensus on sporopollenin structure that currently exists.

By artificially simulating an incremental range of conditions experienced by sediments and associated organic matter it is possible to gain an insight into chemical transformations that occur in natural systems when organic matter is buried. Such an approach will enable observations of time slices through the burial-maturation process with respect to sporopollenin, and shed light on the mechanism by which sporopollenin alters that renders it inoperable as a source of geological geochemical proxy information.

6.2 History of Research

6.2.1 Sedimentary organic matter

A recent comprehensive review (Vandenbroucke & Largeau, 2007) estimates that only 0.1-1 wt % of living biomass eventually becomes sedimentary organic matter whilst the rest of the original biomass is removed from the burial process by degradation mediated by chemical, physical and biological agents. Sedimentary organic matter is referred to broadly as kerogen, although this term has a very wide range of definitions (Einsele, 2000; Killops & Killops, 2005), but for the purposes of this study, kerogen can be defined as "insoluble macromolecular organic matter dispersed in sedimentary rocks" (see Vandenbroucke & Largeau, 2007 for a discussion on the development of the definition and the current state of knowledge regarding kerogens). As such, the formation and the point at which organic matter can be regarded as a kerogen is justifiably poorly constrained, where the process of becoming kerogen can be better described as a continuum from living biomass to fossil macromolecular organic matter, or on a molecular level, from a biopolymer to a geopolymer (Einsele, 2000).

Kerogens have received considerable attention from the organic geochemistry community primarily because they are closely linked to the formation of hydrocarbon reserves; *via* maturation and alteration processes economically important coals, oils and gases are generated from kerogens. Throughout the Phanerozoic two main contributors to kerogens are identified: algae, and since the Silurian period, higher plants. The result of such prolonged burial and maturation of organic matter is the global-wide occurrences of hydrocarbon reserves. To put the scale of kerogen abundance into context, as a carbon sink kerogens are estimated to hold ~ 10^{19} kg of global carbon, thus are a substantial carbon sink, especially when compared with estimates of total current living biomass, which is of the order of ~ 10^{15} kg of global carbon (Vandenbroucke & Largeau, 2007). Interestingly some kerogens have been identified to be almost exclusively comprised of aliphatic constituents, despite the almost

certain presence of aromatic moieties in the starting material (Stankiewicz *et al.*, 2000), suggesting *in situ* alteration of the organic matter *via* defunctionalisation, loss of oxygen and increase in relative amounts of CH_2 and CH_3 groups (i.e. diagenesis (Yule *et al.*, 2000). Further changes in chemistry occur when the "oil-window" is reached (i.e. catagenesis), including thermal cracking and structural reorganisation (Tissot & Welte, 1984; Einsele, 2000; Yule *et al.*, 2000), however, organic matter obtained from this grade of source rock may well be too chemically altered to be of use for the investigation of aromaticity.

6.2.2 Recalcitrant polymers in sediments

Plant-derived microfossils (pollen and spores) are found throughout the geological record since the late-Ordovician (Wellman *et al.*, 2003) and are widely used to gain an insight into the climate of the past (Martin & Gray, 1962; Lowe & Walker, 1997; Bradley, 1999). Preservation of spore/pollen morphology in ancient sediments enables identification of organisms to genus level in the majority of examples; species- or family-level identification is not possible if no extant relation exists because of the low preservation potential of entire macrofossils (i.e. whole plants and/or associated plant parts) in order to fully characterise a particular family/species (Martin & Gray, 1962; Chaloner, 1999). Whilst fossilised plant material is of interest for understanding plant evolution and palaeo-environmental analysis, it is also a significant source of organic matter locked in the sedimentary record.

A number of biopolymers (or biomacromolecules) are found to be preserved in sediments as 'organic matter' and are attributed to a biological origin. All of these biopolymers are characterised by the following features: high molecular weight; comprise of aromatic and/or aliphatic monomers; monomers are joined *via* ester and/or ether bonds; and most biopolymers serve a structural purpose in plants, algae and other organisms, as well as often performing secondary functions too (de Leeuw *et al.*, 2006; Vandenbroucke & Largeau, 2007).

Examples of the most common types of biopolymers preserved as sedimentary organic matter are listed in Table 6.1.

Table 6.1 Common biopolymers found to be present as sedimentary organic matter, their dominant biological sources and the resultant kerogen type formed after catagenesis. Information from: Tissot & Welte, 1984; Einsele, 2000; Killops & Killops, 2005; de Leeuw *et al.*, 2006; Vandenbroucke & Largeau, 2007.

Biopolymer	Source	Kerogen type
Algaenan	Algae cell wall	Liptinite (type I)
Chitin	Arthropod cuticle	Exinite (type II)
Sporopollenin	Spore and pollen cell wall	Exinite (type II)
Lignin	Vascular plant cell wall	Vitrinite (type III)
Suberin	Plant roots	Vitrinite (type III)

The mechanism by which highly resistant polymeric macromolecules are retained in sediment has been a contentious issue. It was originally thought that macromolecules found in fossilised material were simply selectively preserved components of the original biological source, i.e. the components that resisted chemical attack and degradation. Such components were thought to have already been present in the living material, albeit in very low concentrations that after time became concentrated as a result of the surrounding, less resistant organic material being removed (Tegelaar *et al.*, 1989; Derenne *et al.*, 1991; Baas *et al.*, 1995). Later work disputed selective preservation as the sole mechanism resulting in the occurrence of resistant macromolecules in sediment, proposing *in-situ* repolymerisation processes were taking place that altered the chemical identity of the macromolecules observed in fossil material (Hemsley *et al.*, 1992; Stankiewicz *et al.*, 1997, 2000; Mösle *et al.*, 1998; Briggs, 1999; Gupta *et al.*, 2007a,b,c). Evidence for such polymerisation processes has been provided by the comparison of extant, fossilised and artificially matured material. If selective preservation acting in favour of resistant macromolecules was the only process occurring when organic material was incorporated into sediments, the same macromolecules present in the original material would be expected to be present in the resultant fossilised material. Geochemical analyses in the work cited above have shown this not to be the case. The most enlightening examples of this can be drawn from chitin and lignin; these biopolymers generally

contain very few or no aliphatic monomers (Nimz, 1974; Stankiewicz *et al.*, 2000) however, analyses of fossil examples exhibit the presence of a highly aliphatic resistant macromolecule (Hemsley *et al.*, 1992; Stankiewicz *et al.*, 1997). It is clear that the presence of an aliphatic polymer is irreconcilable with the lack of aliphatic polymer in the starting material, suggesting selective preservation cannot be invoked as the only mechanism that gives rise to resistant sedimentary macromolecules.

Decompositional investigations performed on sporopollenin have demonstrated that significant defunctionalisation occurs during simulated diagenesis/catagenesis. Extant spores/pollen were either subject to thermal maturation conditions that bear resemblance to conditions experienced during burial in sediments (Marshall, 1991; Yule *et al.*, 2000) or underwent chemical decomposition *via* repeated acidic methanolysis (Bubert *et al.*, 2002). The most prominent observation is the loss of oxygen-containing functional groups (carbonyls) shown by an overall reduction in oxygen content (Yule *et al.*, 2000; Bubert *et al.*, 2002); such a result was not found by Marshall (1991) due to oxidation effects during experimental heating. Other changes observed include a relative increase in carbon abundance (Marshall, 1991; Bubert *et al.*, 2002), an increase in the relative proportion of CH_2 and CH_3 groups (Yule *et al.*, 2000), and the rapid loss of hydrogen between 206 to 212 °C (Marshall, 1999). Given that sporopollenin is just one of a number of highly-resistant biopolymers that exist in the plant and animal kingdoms, it is very likely that the other resistant biopolymers also have the tendency to demonstrate similar trends to sporopollenin under thermal/chemical decomposition conditions.

By considering the lack of consistency between biopolymers found in fossil material and the precursor extant organisms in conjunction with evidence for defunctionalisation of biopolymers under thermal/chemical decomposition regimes, it is possible to hypothesise an alternative mechanism for the occurrence of aliphatic-rich polymers in sediments. Stankiewicz

et al. (2000) suggest a two-stage process whereby selective preservation first concentrates extant resistant biopolymers; in this case a chitin-protein complex within arthropod cuticle that lacks an aliphatic polymer. The second step is the *in-situ* alteration/polymerisation of the recalcitrant chitin material, during which some components are likely to be removed. This second step leads to the formation of an aliphatic polymer not present in the starting material. Whilst the study described above investigated chitin, by analogy it is most probable that the same processes act upon other biopolymers. Thus the resistant, aliphatic polymers observed in fossil samples are in fact polymers of a geological origin (a 'geopolymer') rather than resistant biopolymers, as originally hypothesised.

The major biopolymer component of the exine (outer wall) of lycopsid spores is sporopollenin. A number of possible compositions have been suggested for the structure of sporopollenin, as well as the proposition that more than one type of sporopollenin exists (de Leeuw *et al.*, 2006; Vandenbroucke & Largeau, 2007; Chapter 2). The current state of understanding of sporopollenin structure and likely compositional models has already been considered in Chapter 2 (Section 2.2), therefore only a summary of such information is provided here. Essentially three compositional models exist for extant sporopollenin: an entirely aliphatic biopolymer, where all monomeric components are single-chain fatty acids; an exclusively aromatic biopolymer, with all monomeric components showing a close relation to the cinnamic acids; and finally, a mixed-composition model, where both aliphatic and aromatic moieties contribute to the overall structure (Guildford *et al.*, 1988; Scott, 2002; Blokker *et al.*, 2005; Killops & Killops, 2005; de Leeuw *et al.*, 2006; Vandenbroucke & Largeau, 2007). It is the third model that has been adopted in this study based on the coincidence of both aliphatic and aromatic compounds in spore samples analysed by pyro-/thermochemolysis-GC-MS as well as evidence from FTIR microspectroscopy for both aliphatic and aromatic moieties (Watson *et al.*, 2007; Chapter 2). Evidence that led to the proposal of the aliphatic-only model of sporopollenin was obtained partly from analogous fossil samples that were thought to be

representative of modern-day sporopollenin composition (Scott, 2002; de Leeuw *et al.*, 2006); as already discussed (Section 6.2.2), such evidence may well be flawed if diagenetic effects on the chemistry are taken into account.

6.2.3 Laboratory simulation of diagenetic conditions

The combination of elevated temperature and pressure under non-oxidising conditions experienced during burial of sediments and the entrained organic material is responsible for the generation of hydrocarbons (Einsele, 2000). The first recognition that heat and pressure were vital components in hydrocarbon generation came about in the late 19th and early 20th centuries (see Stranges (1984) for a detailed account of the history of this topic). Numerous methods exist for the artificial simulation of the processes that occur during burial and the resultant diagenetic changes; here the focus will be upon thermal maturation experiments whereby samples are subject to elevated temperatures and pressures for a known duration (e.g. Marshall, 1991; Stankiewicz *et al.*, 2000). Other methods used to investigate similar processes to diagenesis employ chemical degradation techniques, as mentioned above (e.g. Bubert *et al.*, 2002), although these are not strictly reproducing true diagenetic conditions; they merely result in analogous consequences to diagenesis.

The majority of thermal maturation studies now follow roughly similar experimental designs, taking into account that these experiments are rapid analogue models of sedimentary burial. Key factors to control in such experiments are temperature, pressure, time and type of system (open or closed?). System types can be either open or closed (in the physical sense, rather than the chemical use of such terminology), thus open systems are exposed to oxidising conditions, resulting in oxidation of the material under investigation; open systems were generally used in earlier experiments (Landais *et al.*, 1994), or are purged with an inert gas (Schenk *et al.*, 1990), although may also occur unintentionally (Marshall, 1991). Closed systems ensure oxidation of the sample cannot occur during the heating process and are

conducted using a sealed 'bomb', or sealed glass/gold tubes (Landais *et al.*, 1994; Sephton, 1997; Stankiewicz *et al.*, 2000; Gupta *et al.*, 2007c). One drawback of the closed system approach is that it is not truly representative of the real world because the samples are considered entirely in isolation without any possibility of exchange of material with surrounding sediment. However, it has been suggested that chemical exchanges with external material within the sediment is not necessary to effect changes (de Leeuw *et al.*, 2006; Gupta *et al.*, 2007a,c).

The underlying chemical reactions that occur during organic maturation can be suitably described by a first order Arrhenius equation, which suggests time and temperature may be treated as a time-temperature pair, whereby high temperature-short duration experiments should produce results equivalent to a low temperature-long duration experiment. However, this may not necessarily be an accurate assumption as primary and/or secondary cracking reactions may also take place during heating at higher temperatures when samples are in sealed vessels (Landais *et al.*, 1994). In spite of these possible complications, the general time-temperature relationship can be summarised as: assuming equal duration of heating conditions, samples exposed to higher temperatures will be of greater maturity than those exposed to lower temperatures.

6.3 Experimental

6.3.1 Sample preparation

Commercially available *Lycopodium clavatum* spores (Fluka) underwent soxhlet extraction for a period of 24 hours with a dichloromethane:methanol mixture of 93:7 (by volume). After solvent extraction a subset of *L. clavatum* spores were saponified to remove ester-bound labile components in 1M KOH in methanol (boiling) for 2 hours. 1M HCl (extracted with hexane) was added in order to neutralise the sample. Spores were then washed to neutral pH with

distilled water, and dried in air before a second soxhlet extraction. Finally *L. clavatum* spores (either solvent extracted or solvent extracted-saponified) were loaded into clean borosilicate tubes (100 mm x 6 mm (o.d.), 4 mm (i.d.)) and flame-sealed under vacuum (10^{-3} mbar).

6.3.2 Thermal maturation heating procedure

The sealed borosilicate tubes were heated within an oven for 48 hours across a range of temperatures (100, 150, 200, 250, 300, 350 and 400 °C). After heating, the tubes were opened, rinsed and sonicated for 3 minutes with 1 ml of toluene:methanol mixture (9:1 by volume). This was repeated three times and superannuate collected each time. The spores were allowed to air dry in the tubes and then transferred to vials. Once in the vials another two extractions using toluene were performed to investigate the composition of material expelled from sporopollenin structure. Superannuate from these final two extraction was added to the superannuate from the rinsing of the borosilicate tubes. An aliquot of the solvent extract was blown to dryness in a vial in a stream of dry nitrogen and 20 µl BSTFA:TMCS (99:1; Supelco) with 10 µl pyridine (Fluka). After the drying process, the vial was sealed and heated for 20 minutes at 80 °C.

6.3.3 Pyrolysis/Thermochemolysis-GC-MS

GC-MS analyses were obtained using an Agilent Technology 6890 gas chromatograph coupled to a 5973 mass spectrometer. The GC injector was maintained at a temperature of 270 °C and operated in split mode (10:1) with a column flow rate of 1.1 ml min^{-1}. The GC column used was a BPX5 column (SGE, 30 m length, 0.25 µm film thickness and 0.25 mm internal diameter). The GC oven was held at 50 °C for one minute, then ramped at a rate of 5 °C min^{-1} to 310 °C; this temperature was held for a duration of nine minutes. Mass spectra were acquired in electron impact mode (70 eV) from 50 to 500 amu.

Artificially matured spore samples were prepared for pyrolysis-GC-MS by loading them into quartz pyrolysis tubes that were plugged at each end with quartz wool. Pyrolysis was performed using a CDS Pyroprobe 1000 (CDS Analytical) fitted with a 1500 valve interface. The Pyroprobe was integrated with the GC-MS introduction system and held at 250 °C. Pyrolysis was conducted by ramping up the temperature to 610 °C at a rate of 20 °C ms^{-1} and then held at this temperature for 15 s. Helium was used as the carrier gas.

Samples were prepared for thermochemolysis-GC-MS by loading into quartz pyrolysis tubes in the same manner as for pyrolysis-GC-MS. Once loaded, 10 µl of 25% tetra-methyl-ammonium-hydroxide (TMAH) in methanol was added to the sample. Samples were left for 12 hours to allow the methanol to evaporate. Thermochemolysis uses the same introduction method as pyrolysis with the CDS Pyroprobe interface valve held at 250 °C. A ramping rate of 20 °C ms^{-1} was used to reach 300 °C, which was then held for 15 s in a helium gas flow. The GC oven was held at 35 °C for ten minutes, then ramped to 310 °C at a rate of 5 °C min^{-1} and held at this temperature for nine minutes.

6.3.4 FTIR microspectroscopy

Samples were analysed in accordance with the method detailed in Chapter 2 and Appendix A. A Continuum IR-enabled microscope fitted with a 15x reflachromat objective lens and nitrogen-cooled MCT-A detector is interfaced with the bench unit to provide microscopic analytical capability. Analysis was conducted using a microscope aperture of 100 x 100 µm at 500 scans per sample with a resolution of 4 data points per reciprocal centimetre (cm^{-1}). Background spectra were collected immediately after every sample spectrum. Each analysis was replicated five times per sample.

Data analysis of spectra obtained from artificially matured *Lycopodium* spores diverges from that presented in previous chapters. Aromaticity in artificially matured spores is expressed as

an aromatic/aliphatic ratio, due to the significant reduction in the hydroxyl group observed in samples heated to higher temperatures. Reduction of the OH infrared absorbance band would detrimentally interfere with the aromatic signal obtained from samples if the hydroxyl ratio method of earlier chapters were to be applied here. Instead an aromatic/aliphatic ratio allows comparison of the relative balance between aromatic and aliphatic moieties in relation to maturity, which may be an important factor highlighted by previous studies (Stankiewicz *et al.*, 2000; Gupta *et al.*, 2007a,b,c). Aromaticity of artificially matured spores was calculated using the following equation:

Equation 6.1 Normalisation of aromatic abundance to total aliphatic abundance.

$UV_{ab} = aro_{1520} / (CH_{2925} + CH_{2850})$

Where UV_{ab} is the abundance of UV-absorbing aromatic compounds, aro_{1520} is the measured intensity of the aromatic FTIR response, and $(CH_{2925} + CH_{2850})$ is the combined intensity of the aliphatic C-H stretching bands. Use of this ratio will demonstrate changes in both aromatic and aliphatic sporopollenin components. Determination of the aromatic/aliphatic balance will enable the tracking of aliphatic content that has been found to undergo significant relative changes in other biopolymers during maturation.

6.3.5 Attenuated Total Reflectance-FTIR spectroscopy

In order to ensure the quality of data obtained using FTIR microspectroscopy, the complementary technique of Attenuated Total Reflectance (ATR)-FTIR was employed to perform a single analysis on each sample. ATR-FTIR operates by passing an infrared beam through a diamond crystal cell whilst the sample is held in direct contact with one surface of the diamond cell. ATR-FTIR analysis was performed at Imperial College, London on a Thermo Nicolet 6700 bench unit, fitted with an EverGlo IR source, KBr beamsplitter and DTGS detector. ATR functionality was enabled by the loading of a SMART Orbit ATR module into the sample compartment. Analysis was performed over 256 scans at a resolution of 4 across a range of 4000-500 cm^{-1} wavenumber.

6.4 Results

6.4.1 Non-saponified spores

6.4.1.1 Pyrolysis-GC-MS

Pyrolysis-GC-MS of unheated *L. clavatum* spores reveals a strong presence of derivatives of the aromatic compounds ferulic acid and *p*-coumaric acid. The carboxylic acids *n*-$C_{16:0}$ and *n*-$C_{18:1}$ are the primary aliphatic components in the chromatogram (Figure 6.1). Also present are the methyl esters of the *n*-$C_{16:0}$ and *n*-$C_{18:1}$ acids. Heating within the range 100-200 °C does not significantly alter overall spore chemistry or the relative balance between aromatic and aliphatic compounds.

At 250 °C it is apparent that a suite of *n*-alkane/alkene doublets (C_8 to C_{20}) are present; these persist and become more prominent throughout the higher maturation temperatures to 350 °C. However, such *n*-alkane/alkene doublets are notable by their absence at lower heating temperatures (no heating to 200 °C). After heating at 350 °C aliphatic *n*-alkane/alkene doublets are the dominant features of the chromatograms. Derivatives of ferulic acid and *p*-coumaric acid make a considerable contribution to the chromatogram at 250 °C, but at 300 °C and 350 °C aromatic moieties are much less prevalent.

Analysis of the products solvent extracted from artificially matured spores after heating reveals the components that are liberated from the sporopollenin structure during heating. Between 100 °C and 250 °C chromatograms are dominated by *n*-$C_{16:0}$ and *n*-$C_{18:1}$ carboxylic acids, with minor contributions from *n*-$C_{16:1}$ and *n*-$C_{18:0}$ carboxylic acids (Figure 6.2). Methyl esters of both *n*-$C_{16:1}$ and *n*-$C_{18:0}$ are also present. At 100-150 °C no traces of aromatic compounds are observed. Not until a heating temperature of 200 °C is used are aromatic compounds found in the liberated component, albeit as a very small proportion of the total.

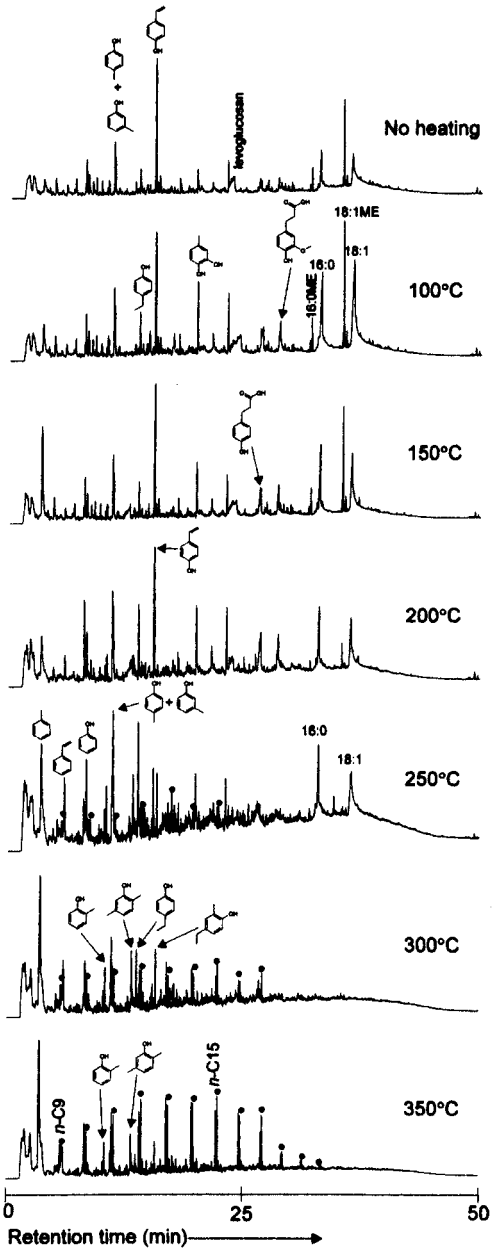

Figure 6.1 Pyrolysis-GC-MS total ion chromatograph of *L. clavatum* spores after thermal maturation and solvent extraction.

With increasing temperature to 350 °C the *n*-$C_{18:0}$ carboxylic acid becomes increasingly more important than the *n*-$C_{18:1}$ acid, with prominence shifting in the temperature step between 250 °C and 300 °C. *n*-$C_{16:0}$ remains a key feature throughout the temperature series up to 350 °C. Other changes that occur at the 350 °C step are the development of a homologous suite of shorter chain *n*-alkanoic (C_{10} to C_{20}) acids and *n*-alkanes (C_{14} to C_{20}), and two interesting peaks

corresponding to *n*-C_{15} and *n*-C_{17} alkanes. Odd numbered carbon compounds are not found in the original spore material; therefore it is most likely that the *n*-C_{15} and *n*-C_{17} alkanes are caused by decarboxylation of the *n*-C_{16} and *n*-C_{18} carboxylic acids. At 400 °C the *n*-C_{15} and *n*-C_{17} alkanes are the most abundant products with *n*-C_{16} and *n*-C_{18} carboxylic acids reduced to very low abundances (Figure 6.2).

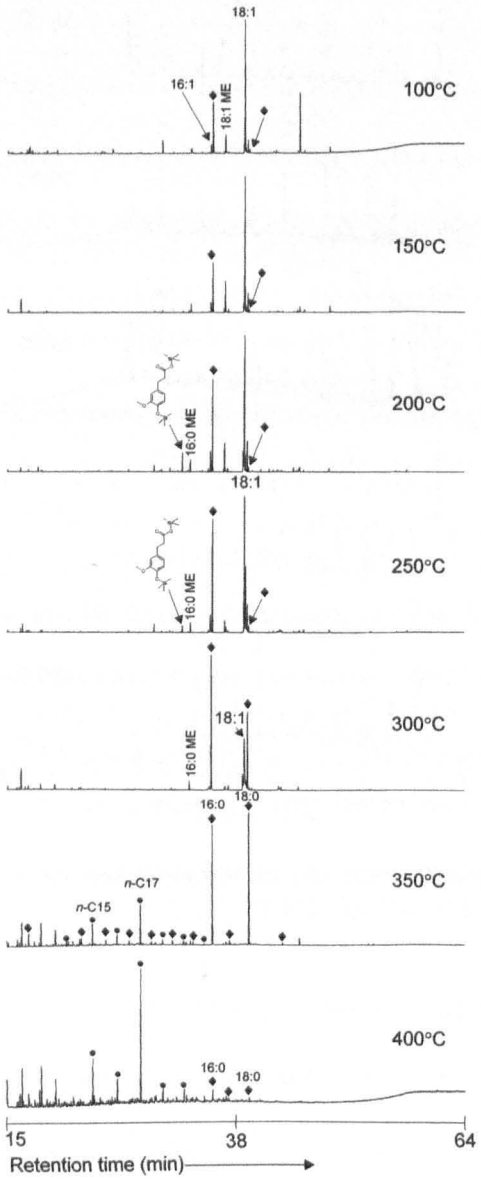

Figure 6.2 GC-MS total ion chromatograph of solvent extracted material from *L. clavatum* spores after thermal maturation and solvent extraction.

6.4.1.2 Thermochemolysis-GC-MS

Thermochemolysis liberates methyl esters of a number of alkanoic carboxylic acids and aromatic products from the unheated spore samples. Coincident with the results of pyrolysis-GC-MS performed on these samples, *n*-$C_{16:0}$ and *n*-$C_{18:1}$ carboxylic acids are the most abundant products, with *n*-$C_{16:1}$ and *n*-$C_{18:0}$ making a smaller contribution to the chromatogram. The other main thermochemolysis products from the unheated spores are methyl esters of ferulic acid and *p*-coumaric acid (Figure 6.3).

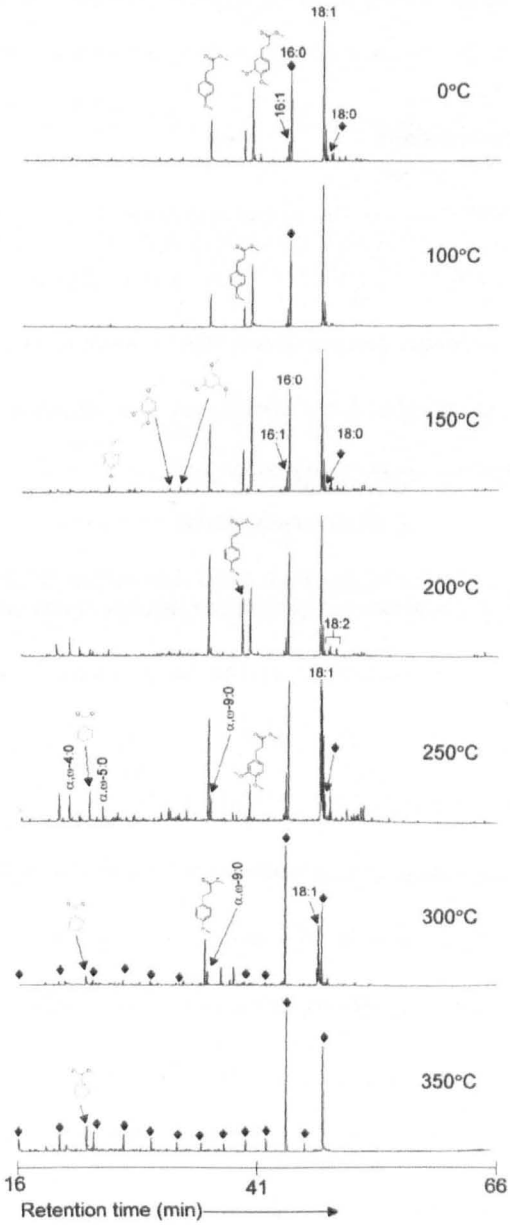

Figure 6.3 Thermochemolysis-GC-MS chromatograms of *L. clavatum* spores after thermal maturation and solvent extraction.

In the heating range 100 °C to 250 °C there are no significant changes in the thermochemolysis products. At 300 °C to 350 °C a series of *n*-acids are expelled from the structure of sporopollenin (C_6 to C_{18}), with $C_{16:0}$ and $C_{18:0}$ as the most abundant products. As seen in the pyrolysis data, the step between 250 °C and 300 °C exhibits a shift in dominance from $C_{18:1}$ to $C_{18:0}$ in the *n*-acids. Benzoic acid is observed in chromatograms from 250 °C upwards.

6.4.1.3 FTIR Microspectroscopy

All absorption band assignments for the unheated samples (0 °C) are identical to those of modern-day spores discussed in Chapter 2. Immediately apparent from Figure 6.4 are the distinct spectral changes at higher temperatures, with a general simplification of the spectra with increased maturity. Throughout the sample set is a strong presence of aliphatic C-H stretching modes located in the region 2800-3000 cm^{-1}.

Additional features are observed in samples from higher temperature experiments in the region 3000-3100 cm^{-1} that are concealed by the broad hydroxyl stretching band in lower temperature samples. Three previously unseen bands can be seen in samples from 200 °C upwards and occur at approximately 3080, 3049 and 3025 cm^{-1}. At 400 °C this set of bands becomes poorly defined, amassing into a single broad band rather than three distinct bands. The most likely causes of absorption in this region are C-H stretching bonds associated with aromatic ring structures or C=C double bonds (Williams & Fleming, 1980) however, it is not possible to determine whether these bands can be assigned exclusively to either functional group. These bands are clearly only visible due to the significant reduction in the otherwise prominent OH stretching band.

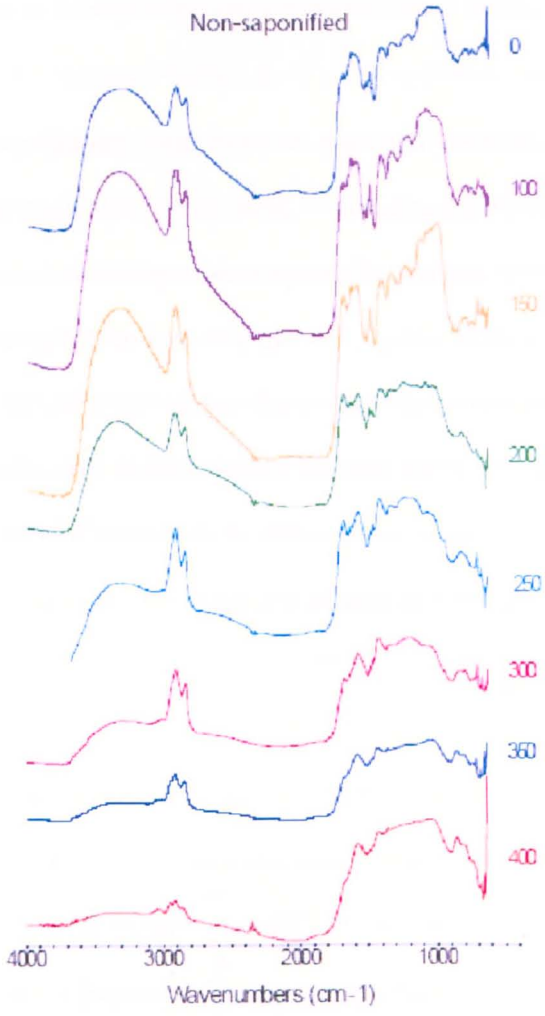

Figure 6.4 FTIR spectra obtained from non-saponified *L. clavatum* spores after solvent extraction and heating. Maturation temperature is given on the right hand side of each column in ºC.

Another feature not accessible in lower temperature samples is the division of the aliphatic-related C-H stretching bands located in the region 2800-3000 cm^{-1} into bands that are assignable to CH_2 and CH_3 groups. CH_2 and CH_3 groups each exhibit two vibrational modes in this region due to anti-symmetric and symmetric stretching modes. Methyl (CH_3) groups produce bands at slightly higher wavenumbers with characteristic absorbencies occurring at 2962 and 2872 cm^{-1}, corresponding to anti-symmetric and symmetric modes, respectively. CH_2 groups are found to absorb at 2926 and 2853 cm^{-1} for anti-symmetric and symmetric stretching modes, respectively (Rouxhet *et al.*, 1980). Closer inspection of the spectrum collected from the sample heated to 300 °C (Figure 6.5) shows the more prominent aliphatic

bands to be positioned at ~ 2925 and ~ 2854 cm^{-1}, relating to CH_2 groups, but with substantial band shoulders occurring at ~ 2958 and ~ 2871 cm^{-1} corresponding to methyl groups. Whilst the bands due to CH_2 groups remain greater in intensity, i.e. there are more CH_2 groups present than CH_3 groups, the bands due to methyl groups appear to be of only slightly lower intensity, indicating that methyl groups are relatively more abundant in the mature samples than in the lower maturity samples where the difference between CH_2 and CH_3 band intensity is much more pronounced. A shift in the balance of relative intensities of CH_2 and CH_3 groups suggests a general shortening of carbon chains, and possibly an increase in methylation of compounds.

The band observed in the region of 1710 cm^{-1} in unheated samples is attributed to carbonyl (C=O) bonds most likely as saturated ester linkages (Williams & Fleming, 1980; Chapter 2). With increasing maturity the band at ~ 1710 cm^{-1} dramatically reduces in intensity. Such a reduction indicates the loss of carbonyl groups with increasing temperature. Coincident with this reduction in carbonyl groups, as briefly mentioned above, there is a significant reduction in hydroxyl groups, as shown by the decrease in intensity of the band at centred ~ 3300 cm^{-1}. The reduction in hydroxyl and carbonyl groups highlights a decrease in the oxygen-containing functional groups found in unheated spores; this is an observation also made previously by Yule *et al.* (2000) and Bubert *et al.* (2002) in sporopollenin, and is a typical feature of increasing maturation of kerogen (Einsele, 2000).

The absorption band at ~ 1520 cm^{-1} that has been assigned to aromatic compounds as the basis of the geochemical proxy under evaluation in this thesis is clearly visible in the unheated samples, as would be expected from analysis of modern-day, unaltered spore samples (Chapters 2, 3 and 4). Up to 150 °C the band at 1520 cm^{-1} remains relatively unperturbed, but further increases in maturity reduces band intensity and appears to shift to lower wavenumbers (~1495 cm^{-1}). At 200 °C the band is still present in spectra, although the clarity

of the band does appear to be degrading and alternative bands becoming evident at 1503 and 1494 cm^{-1} (Figure 6.5); it is unclear whether these newly apparent, lower wavenumber bands are due to absorption by aromatic ring structures, although aromatic rings are also found to absorb at these frequencies (Williams & Fleming, 1980). From 250 °C the absorption band at 1520 cm^{-1} is no longer discernable from the surrounding spectral line and the bands at 1503 and 1494 cm^{-1} reduce in intensity from 300 °C until at 400 °C there are no distinguishable spectral features that can be assigned to aromatic moieties, suggesting that the aromatic components evident in less mature samples are no longer present, or are below the detectable limit in this region, in these highly mature samples.

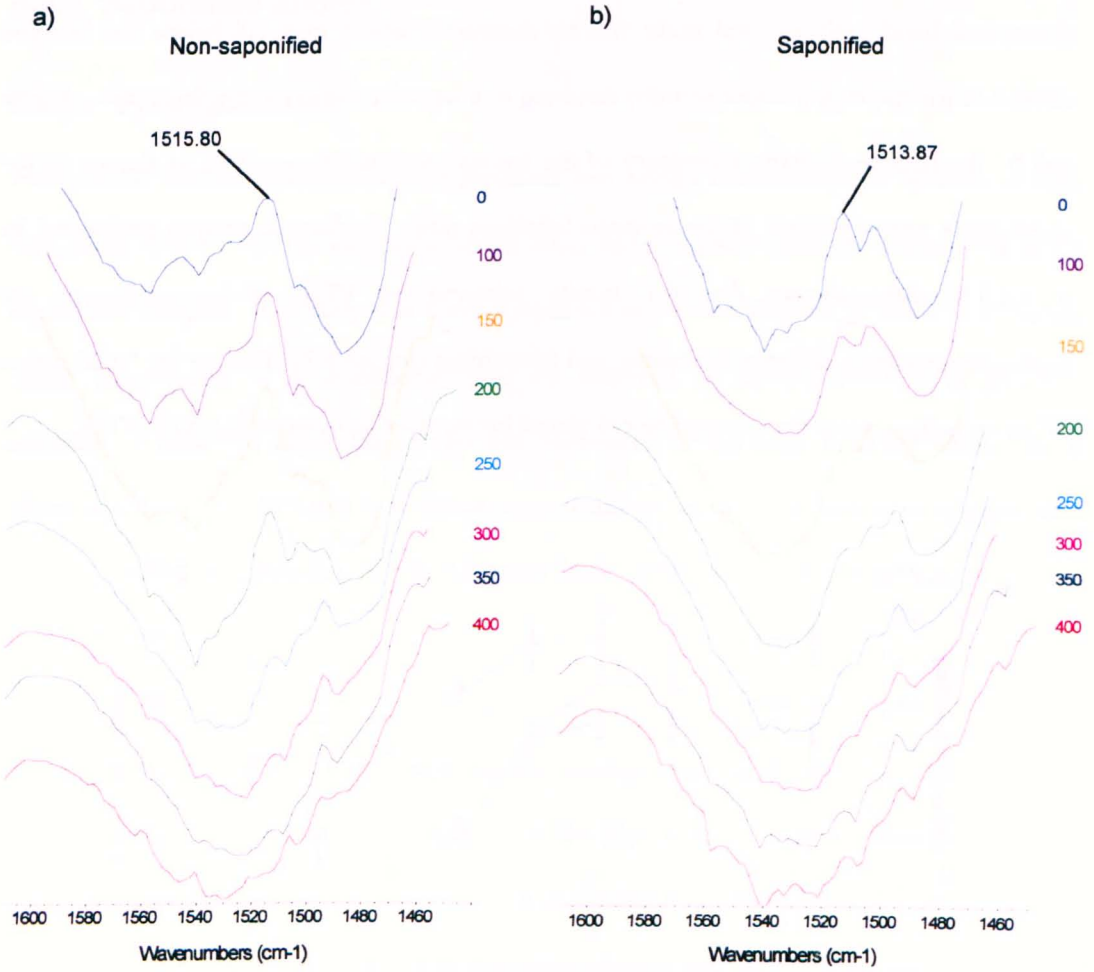

Figure 6.5 Zoom view of ~ 1520 cm^{-1} band in a) non-saponified, and b) saponified *L. clavatum* spore samples. The band position is labelled in both unheated samples. Reduction in band intensity is apparent after heating to 250 ºC and upwards, as well

as a possible shift in band position towards lower wavenumbers. Maturation temperature is given on the right hand side of each column in ºC.

Degradation of the FTIR aromatic signal is represented in Figure 6.6 by the ratio of aromatic peak intensity to total aliphatic content. Figure 6.6 contains information not only about aromaticity of the artificially fossilised spores, but also the relative abundance of aliphatic compounds. It is clear that the aromatic/aliphatic ratio remains essentially constant up until 200 °C and then rapidly declines at 250 °C. Beyond 250 °C aromatic/aliphatic values are negative due to the lack of discernible aromatic bands in the spectra; without a measurable absorption band, only spectral noise will be measured, which may fall below the baseline calculated for the region under scrutiny resulting in a negative value for the final ratio. Above 300 °C the relative aliphatic abundance of the spores continues to increase, as shown by the increasingly negative trend of the aromatic/aliphatic ratio. Additional analysis performed by ATR-FTIR demonstrates that the results achieved by FTIR microspectroscopy are reproducible using a different technique and instrument (Figure 6.7). Due to the 'bulk' nature of the technique, error bars cannot be calculated for samples analysed using ATR-FTIR.

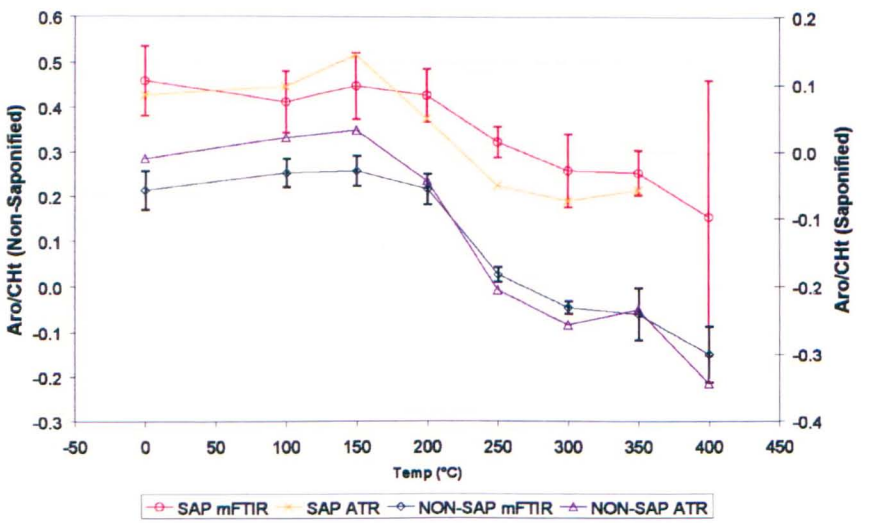

Figure 6.6 Aromatic:aliphatic ratio in artificially matured *L. clavatum* spores across step-wise increments of maturation temperature. Note the offset of scale on the y-axes. CHt = total aliphatic abundance. Error bars are 2σ.

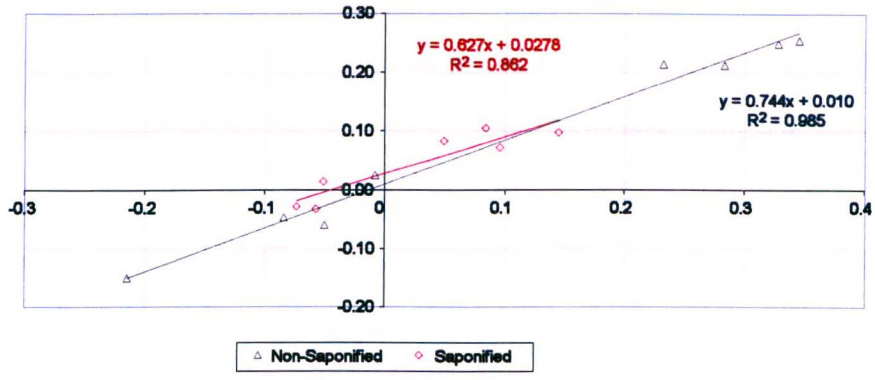

Figure 6.7 Graphical representation of relationship between ATR and microspectroscopy techniques for the analysis of artificially matured *Lycopodium* spores when measuring aromatic/CHt ratio. Slope of line are almost identical between sample sets if scatter of points is taken into consideration.

6.4.2 Saponified spores

6.4.2.1 Pyrolysis-GC-MS

Pyrolysis-GC-MS of saponified spores produces very similar chromatograms to those of non-saponified spores, with the exception of the *n*-C_{16} and *n*-C_{18} acids that are not present in the saponified samples. It is likely that these *n*-acids are major contributors to the loosely bound 'labile' components of sporopollenin, thus are removed by saponification. The pyrolysis products of unheated saponified spores are dominated by aromatic moieties, almost all of which appear to be derivatives of ferulic or *p*-coumaric acids. The unheated samples also show a number of compounds that are most likely artefacts of the saponification process (Figure 6.8).

No significant chemical changes occur during heating steps up to 200 °C, where aromatic compounds remain the primary products. At 250 °C a series of *n*-alkane/alkene (C_8 to C_{20}) doublets are detectable, with a suite of aromatic products still dominating the signal. At 300 °C the *n*-alkane/alkene doublets become more prominent, and finally reach intensities comparable to those of the aromatic components at 350 °C.

6.4.2.2 Thermochemolysis-GC-MS

Thermochemolysis-GC-MS was performed on unheated saponified spores for comparison with non-saponified spores. As shown by the pyrolysis-GC-MS data, the thermochemolysis products are almost exclusively aromatic derivatives, with only a minor contribution from *n*-acids ($C_{16:0}$, $C_{18:0}$ and $C_{18:1}$). The low abundance of aliphatic material indicates that it is the aliphatic components that are removed by saponification; however, some remain, suggesting there is a fraction of aliphatic material that is occluded within sporopollenin (Figure 6.9). The presence of residual aliphatics is the most probable source of the *n*-alkane products shown in the pyrolysis-GC-MS chromatograms after heating.

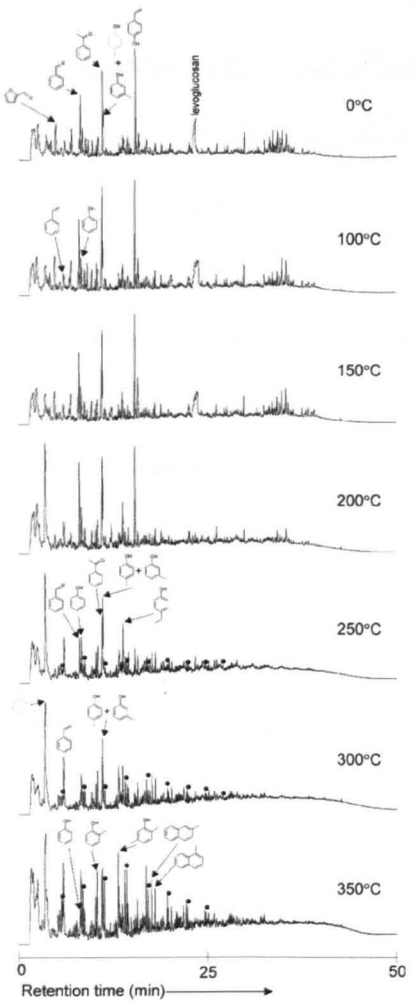

Figure 6.8 Pyrolysis-GC-MS total ion chromatograph of *L. clavatum* spores after saponification, thermal maturation and solvent extraction.

6.4.2.3 FTIR microspectroscopy

Saponified spores show very similar IR spectra to the non-saponified spores, and also exhibit the same trends (Figure 6.10). The greatest difference between saponified and non-saponified spore spectra is the definition of the absorbance bands; saponified samples show features with greater clarity, probably due to the added power of saponification to remove any residual non-sporopollenin components. Of interest to the present work, the aliphatic bands in the region 2800-3000 cm^{-1} do not show the clear division into CH_2- and CH_3-specific bands until a maturation temperature of 400 °C is reached. The band at 1520 cm^{-1} is not as clearly defined in the saponified samples as it is in the non-saponified samples. The poorer definition of the aromatic band may be due to some aromatic components being removed during saponification; however, the aromatic response does not appear to be significantly affected by this. Figure 6.6 shows the aromatic/aliphatic ratio for comparison with that of the non-saponified spores. It is clear that there is good agreement between the trends in aromaticity of both saponified and non-saponified spores. Again, ATR-FTIR data are displayed for saponified samples to demonstrate the reproducibility of these results. The saponified sample heated to 400 °C does not have a datum because there was insufficient sample to obtain an acceptable ATR-FTIR spectrum; this is borne out by the unusually large errors shown by the FTIR microspectroscopy data at this temperature. For this reason, the saponified sample heated to 400 °C can be disregarded.

The greatest change in functionality of the saponified spores compared with non-saponified samples is the reduction of the carbonyl peak at ~ 1720 cm^{-1} that has been attributed to ester linkages. During saponification ester linkages are broken, thus removing any relatively loosely bound material from the periphery of sporopollenin.

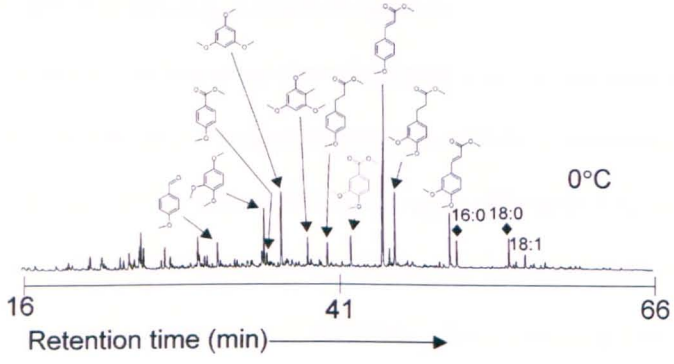

Figure 6.9 Thermochemolysis-GC-MS chromatograms of *L. clavatum* spores after saponification, thermal maturation and solvent extraction.

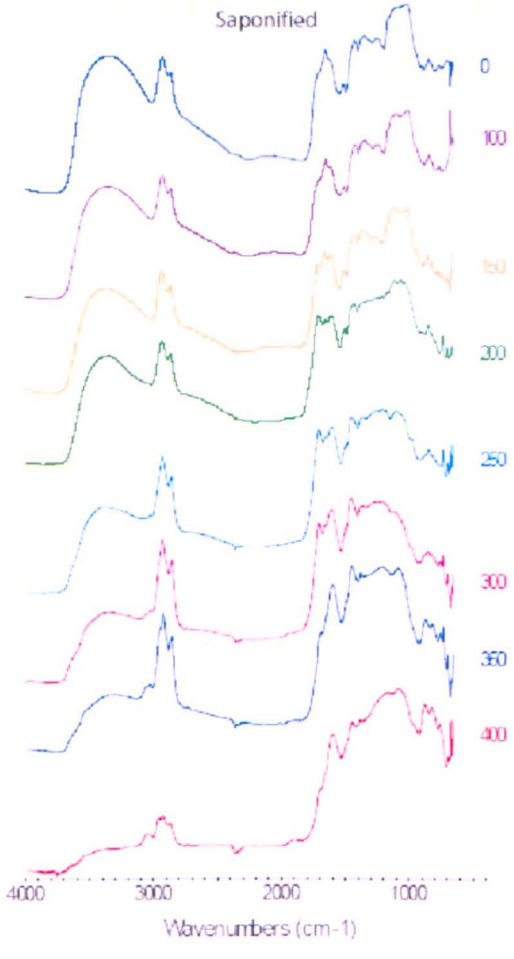

Figure 6.10 FTIR spectra obtained from saponified *L. clavatum* spores after solvent extraction and heating.

6.4.3 Discussion of artificial maturation results

All analyses performed show an overall trend towards a 'geopolymer' that is highly aliphatic, with low aromaticity and reduced oxygen content commensurate with increasing maturity. Both FTIR and GC-MS results show a consistent relative increase in aliphatic abundance with increasing temperature in non-saponified samples, as well as a trend towards the shortening of carbon chains lengths in heated products. Such an increase in aliphatic abundance is consistent with the evidence reported in other studies that have observed either an increase in aliphatic structural components, or the formation of an aliphatic biopolymer during thermal maturation (Hemsley *et al.*, 1992; Stankiewicz *et al.*, 1997, 2000; Yule *et al.*, 2000; Gupta *et al.*, 2007a,b,c).

The shift towards a dominant aliphatic structure suggests a reduction in diversity of compound classes, i.e. most geopolymer components are *n*-alkanes/alkenes, therefore with respect to compound class, the geopolymer is becoming more uniform in composition.

It must be noted that aromatic pyrolysis/thermochemolysis products appear to be present in all samples, with a very low amount contributing to the solutes extracted after heating (Section 6.4.1.1). Whilst this may appear contradictory to the notion that the resultant geopolymer is highly aliphatic, it is most likely that any aromatic moieties are not easily distinguishable due to the extraction procedure that employs toluene. Despite this, both FTIR and GC-MS data show a continued decrease in relative aromatic abundance in relation to maturity. It may be argued that the disappearance of the aromatic absorbance band in the FTIR spectra is due to condensation reactions involving aromatic rings to form polyaromatic compounds. Such a conclusion can be discounted because GC-MS data do not provide any evidence of polyaromatic molecules.

6.4.4 Comparison with fossil samples

The chemistry of thermally matured spores show a strong resemblance to that of fossilised spores presented in Chapter 5; this is particularly apparent when comparing FTIR spectra from the two sample types (Figure 6.11). In both cases aliphatic related CH_n absorption bands in the region 2800-3000 cm^{-1} are strong features, although appear to have greater dominance in the natural fossil samples than found in the artificial samples. Carbonyl groups play a significant role in the structure of fossilised spores, probably as ester linkages between monomers. Non-saponified spores show analogous carbonyl groups that are likely to be performing the same role in ester bonds. Artificially matured saponified samples do not exhibit the same extent of ester bound material because much would have been removed prior to heating. None of the high temperature artificial ($\geq$ 250 °C) or natural fossil spores show any aromatic absorbance in the 1510 cm^{-1} region, suggesting that this may be a critical threshold for preservation of aromatic structures within sporopollenin and is reflected by the sharp drop in aromatic content in Figure 6.6 at this temperature.

Included in Figure 6.11 for reference are examples of spectra obtained from modern-day *Lycopodium* species. *L. clavatum* was used in these artificial maturation experiments, whilst *L. annotinum* has been investigated elsewhere within this work (Chapter 2, 3 and 4). Comparison of these closely related, yet distinct species demonstrates that chemically, sporopollenin composition is identical across both species, adding credence to the applicability of these experimental findings to other *Lycopodium* species, as is the case when comparing artificial heating results with natural spores samples. Fossil spores are not necessarily of the same species as the modern-day spores; therefore inter-species effects on sporopollenin chemistry have the potential to interfere with results. However, any inter-species effects can most likely be discounted because of the chemical similarities between species shown here.

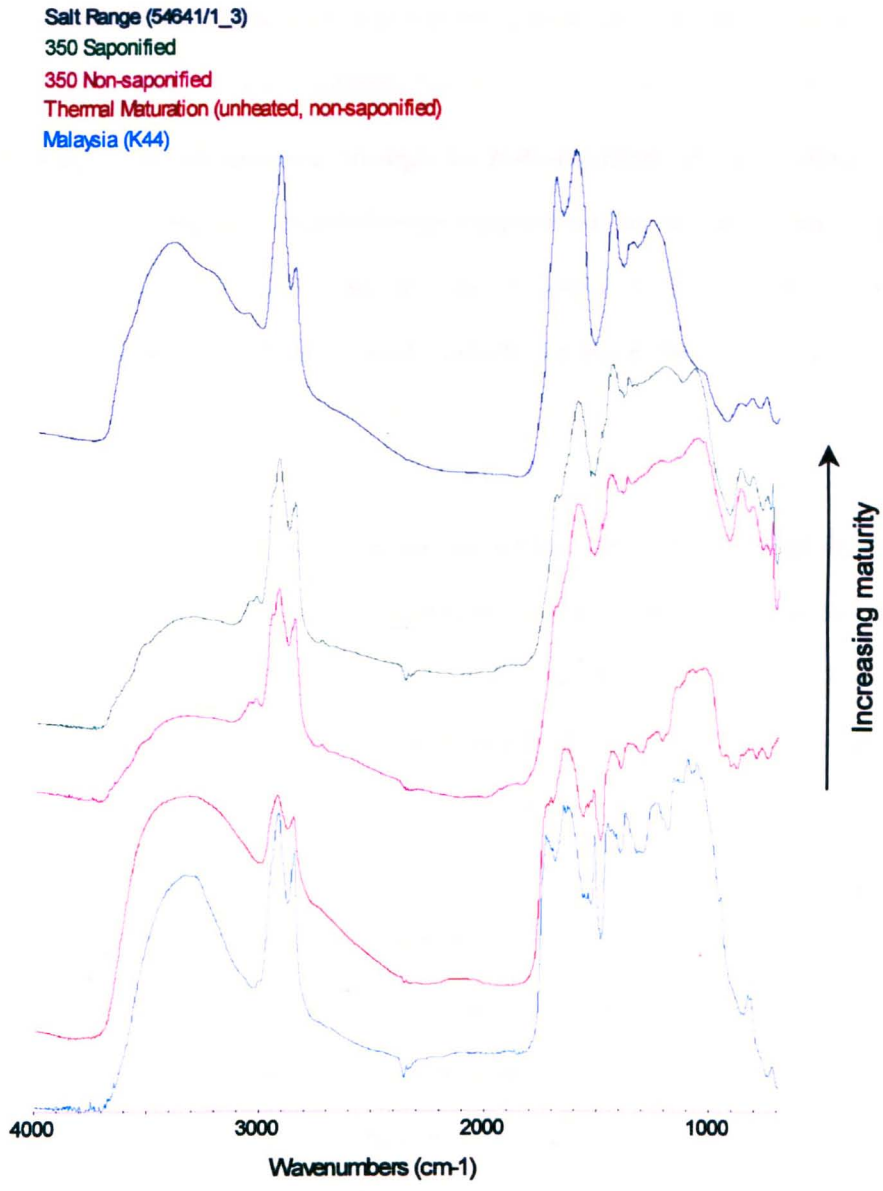

Figure 6.11 Comparison of FTIR spectra of modern, artificially matured and fossil spores. Spores obtained from modern-day *L. annotinum* (Malaysia, Chapter 4), unheated non-saponified *L. clavatum*, heated (to 350 ºC) saponified, and non-saponified *L. clavatum*, and a natural fossil (Lycopsid; Salt Range, Pakistan, Chapter 6). Spectra from modern *L. annotinum* and *L. clavatum* are indistinguishable from each other. Both saponified and non-saponified artificially matured samples show a strong resemblance to the natural fossil sample from the Salt Range (Permo-Triassic boundary, ~ 251 Ma).

6.5 Conclusions

Diagenesis, whether it is a natural process following sedimentation and burial or if it is simulated in the laboratory, is found to cause significant changes to the chemistry of organic matter, such as *Lycopodium* spores. Such changes can be recognised by: 1) a relative increase in

aliphatic content, i.e. the polymerisation of aliphatic components into a geopolymer; 2) stripping of functional groups, particularly oxygen-containing groups (carbonyls, hydroxyl) and aromatic groups; and 3) increased order of the polymer whereby the nature of the components becomes more uniform, allowing fewer possible combinations of polymer to exist.

The most probable source of the aliphatic geopolymer is the hydrolysable 'labile' component of sporopollenin – the loosely bound (*via* ester linkages) aliphatic, fatty acid monomers. Spore samples that have not undergone saponification, i.e. ester linkages left intact prior to heating, show a greater proportion of final aliphatic material at the highest maturation temperatures (Figure 6.1) because there are abundant aliphatic moieties available for polymerisation. Saponified samples contain proportionally fewer aliphatic monomers from the beginning and as a result the balance between residual aromatic structures and aliphatic components is approximately equal at the highest level of maturity (350 °C, Figure 6.8). The most convincing explanation is that the loosely bound aliphatic components are stripped from the biopolymer and polymerise whilst the original biopolymer is degraded; the newly formed aliphatic polymer is probably broken down further, thus producing chain lengths of aliphatic products in the GC-MS chromatograms that are shorter than the original *n*-acids present in the unheated spores (C_{16} and C_{18}).

By comparison with natural fossil material (Figure 6.11) it is apparent that the recalcitrant nature of geopolymers found throughout the sedimentary record is not only due to the resistant properties of the original biopolymer, but are a characteristic of the newly formed aliphatic geopolymer. The resistance to degradation of the initial biopolymer simply aids the process of selective preservation that enables concentration of resistant biopolymer material.

The evidence shows that the formation of aliphatic geopolymers is perfectly feasible given an initial co-polymer such as sporopollenin, however, it is important to bear in mind two important facts that will inevitably cloud the results presented here. Firstly that natural systems are not closed systems as simulated here, but are open systems with much potential for exchange of material between many different components of the sediment, including a broad variety of other resistant biopolymers (lignin, chitin, suberin, algaenan), thus natural samples are highly likely to incorporate some components from these other sources. The power of this study has been to demonstrate that the formation of the aliphatic geopolymer is *possible* in a closed system. Secondly, sporopollenin constitutes a proportionally very small fraction towards total organic matter in sediments, where lignin is the most abundant biopolymer by far (Killops & Killops, 2005). Therefore the changes seen in sporopollenin here are likely to have minimal, if any, effect on the overall composition of the kerogen ultimately formed by diagenesis. However, the trends in changes observed in sporopollenin provide weight to the generalised mechanism of the chemical changes to biopolymers taking place during diagenesis that influence the evolution of kerogens.

6.6 Summary of Findings

• Highly aliphatic geopolymers may be formed *in situ* from a mixed aromatic/aliphatic biopolymer as a starting material without any additional input from external sources.

• Alteration during maturation of the organic matter occurs *via* defunctionalisation and repolymerisation.

• Stripping of aromatic monomers from the original biopolymer to produce a dominantly aliphatic geopolymer provides an explanation for the proxy being evaluated in this study to be unsuccessful when applied to fossilised spores, as found in Chapter 5.

• Use of artificial maturation experiments to mimic the processes occurring in natural systems has proven to be a powerful tool for probing diagenetic alteration of organic matter, as

measured by the many chemical similarities between artificially matured and fossilised spore samples.

• Comparison of data presented here with those of other studies shows that various biopolymers, irrespective of the initial monomeric composition, may ultimately form a highly aliphatic, resistant geopolymer.

The evidence presented here has provided an insight into the chemical changes that occur during burial and subsequent diagenesis of organic matter trapped in sediments. It is critical for those conducting work on the boundaries of palynology and organic geochemistry to bear in mind that the apparently pristine appearance of fossilised spores may in fact conceal a much altered chemistry from that expected.

This Chapter marks the end of the investigation of spatial and temporal changes in spore wall chemistry in relation to UV-stress, thus it is the aim of the next Chapter to draw together conclusions from this work and suggest future directions that this research may take.

6.7 References

Baas, M., Briggs, D.E.G., van Heemst, J.D.H., Kear, A.J. & de Leeuw, J.W. (1995) Selective preservation of chitin during the decay of shrimp. *Geochimica et Cosmochimica Acta* 59(5), 945-951.

Blokker, P., Yeloff, D., Boelen, P., Broekman, R.A. & Rozema, J. (2005) Development of a proxy for past surface UV-B irradiation: A thermally assisted hydrolysis and methylation py-GC/MS method for the analysis of pollen and spores. *Analytical Chemistry* 77(18) 6026-6031.

Bradley, R.S. (1999) *Paleoclimatology: Reconstructing climates of the Quaternary* (2nd ed.). Academic Press Ltd., London, UK.

Briggs, D.E.G. (1999) Molecular taphonomy of animal and plant cuticles: selective preservation and diagenesis. *Philosophical Transaction of the Royal Society of London, B* 354, 7-17.

Bubert, H., Lambert, J., Steuernagel, S., Ahlers, F. & Wiermann, R. (2002) Continuous decomposition of sporopollenin from pollen of *Typha angustifolia* L. by acidic methanolysis. *Zietschrift Naturforsch* 57c, 1035-1041.

Chaloner, W.G. (1999) Taxonomic and nomeclatural alternatives, in; *Fossil plants and spores: Modern techniques* (eds. Jones, T.P. & Rowe, N.P.). Geological Society, London, UK.

Derenne, S., Largeau, C., Casadevall, E., Raynaud, J.F., Berkaloff, C. & Rousseau, B. (1991) Chemical evidence of kerogen formation in source rocks and oil shales via selective preservation of thin resistant outer walls of microalgae: Origin of ultralaminae. *Geochimica et Cosmochimica Acta* 55, 1041-1050.

Einsele, G. (2000) *Sedimentary basins: Evolution, facies, and sediment budget* (2nd ed.). Springer-Verlag Publishing, Berlin, Germany.

Guildford, W.J., Schneider, D.M., Labovitz, J. & Opella, S.J. (1988) High resolution solid state ^{13}C NMR spectroscopy of sporopollenins from different plant taxa. *Plant Physiology* 86, 134-136.

Gupta, N.S., Briggs, D.E.G., Collinson, M.E., Evershed, R.P., Michels, R. & Pancost, R.D. (2007a) Molecular preservation of plant and insect cuticles from the Oligocene Enspel Formation, Germany: Evidence against derivation of aliphatic polymer from sediment. *Organic Geochemistry* 38, 404-418.

Gupta, N.S., Briggs, D.E.G., Collinson, M.E., Evershed, R.p., Michels, R., Jack, K.S. & Pancost, R.D. (2007b) Evidence for the in-situ polymerisation of labile aliphatic organic compounds during the preservation of fossil leaves: Implications for organic matter preservation. *Organic Geochemistry* 38, 499-522.

Gupta, N.S., Michels, R., Briggs, D.E.G., Collinson, M.E., Evershed, R.P. & Pancost, R.D. (2007c) Experimental evidence for the formation of geomacromolecules from plant leaf lipids. *Organic Geochemistry* 38, 28-36.

Hemsley, A.R., Chaloner, W.G., Scott, A.C. & Groombridge, C.J. (1992) Carbon-13 solid state nuclear magnetic resonance of sporopollenins from modern and fossil plants. *Annals of Botany* 69, 545-549.

Killops, S.D. & Killops, V.J. (2005) Introduction to organic geochemistry (2nd edition). Blackwell Publishing, Oxford, UK.

Landais, P., Michels, R. & Elie, M. (1994) Are time and temperature the only constraints to the simulation of organic matter maturation? *Organic Geochemistry* 22(3-5), 617-630.

de Leeuw, J.W., Versteegh, G.J.M. & van Bergen, P.F. (2006) Biomacromolecules of algae and plants and their fossil analogues. *Plant Ecology* 182, 209-233.

Lowe, J.J. & Walker, M.J.C. (1997) *Reconstructing Quaternary environments* (2nd ed.). Pearson Education Ltd., Harlow, UK.

Marshall, J.E.A. (1991) Quantitative spore colour. *Journal of the Geological Society, London* 148, 223-233.

Martin, P.S. & Gray, J. (1962) Pollen analysis and the Cenozoic. *Science* 137, 103-111.

Mösle, B., Collinson, M.E., Finch, P., Stankiewicz, B.A., Scott, A.C. & Wilson, R. (1998) Factors influencing the preservation of plant cuticles: A comparison of morphology and chemical composition of modern and fossil examples. *Organic Geochemistry* 29(5-7), 1369-1380.

Nimz, H. (1974) Beech lignin: Proposal of a constitutional scheme. *Angewandte Chemie International Edition* 13(5), 313-321.

Rouxhet. P.G., Robin, P.L & Nicaise, G.B. (1980) Characterisation of kerogens and their evolution by infrared spectroscopy, in; *Kerogen*, (ed. B. Durand), Editions Techniq, Paris. pp. 163-190.

Schenk, H.J., Witte, E.G., Littke, R. & Schwochau, K. (1990) Structural modifications of vitrinite and alginite concentrates during pyrolytic maturation at different heating rates. A combined infrared, ^{13}C NMR and microscopical study. *Organic Geochemistry* 16(4-6), 943-950.

Scott, A.C. (2002) Coal petrology and the origin of coal macerals: a way ahead? *International Journal of Coal Geology* 50, 119-134.

Stankiewicz, B.A., Briggs, D.E.G., Evershed, R.P., Flannery, M.B. & Wuttke, M. (1997) Preservation of chitin in 25-million-year-old fossils. *Science* 276, 1541-1543.

Stankiewicz, B.A., Briggs, D.E.G., Michels, R., Collinson, M.E., Flannery, M.B. & Evershed, R.P. (2000) Alternative origin of aliphatic polymer in kerogen. *Geology* 28(6), 559-562.

Stranges, A.N. (1984) Friedrich Bergius and the rise of the German synthetic fuel industry. *Isis* 75(4), 643-667.

Tegelaar, E.W., de Leeuw, J.W., Derenne, S. & Largeau, C. (1989) A reapparisal of kerogen formation. *Geochimica et Cosmochimica Acta* 53, 3103-3106.

Tissot, B.P. & Welte, D.H. (1984) *Petroleum formation and occurrence* (2nd ed.). Springer-Verlag Publishing, Berlin, Germany.

Vandenbroucke, M. & Largeau, C. (2007) Kerogen origin, evolution and structure. *Organic Geochemistry* 38, 719-833.

Visscher, H., Looy, C.V., Collinson, M.E., Brinkhuis, H., van Konijnenburg-van Cittert, J.H.A., Kürschner, W.M. & Sephton, M.A. (2004) Environmental mutagenesis during the end-Permian ecological crisis. *Proceedings of the National Academy of Sciences of the United States of America* 101, 12952-12956.

Watson, J.S., Sephton, M.A., Sephton, S.V., Self, S., Fraser, W.T., Lomax, B.H., Gilmour, I., Wellman, C.H., Beerling, D.J. (2007) Rapid determination of spore chemistry using

thermochemolysis gas chromatography-mass spectrometry and micro-Fourier transform infrared spectroscopy. *Photochemical & Photobiological Sciences* 6, 689-694.

Wellman, C.H., Osterloff, P.T. & Mohiuddin, U. (2003) Fragments of the earliest land plants. *Science* 425, 282-285.

Williams, D.H. & Fleming, I. (1980) Spectroscopic methods in organic geochemistry. McGraw-Hill, London.

Yule, B.L., Roberts, S. & Marshall, J.E.A. (2000) The thermal evolution of sporopollenin. *Organic Geochemistry* 31, 859-870.

7 General discussion and summary

7.1 Summary

The intent of this thesis was to evaluate the feasibility of exploiting the chemical composition of the biopolymer sporopollenin as a novel geochemical proxy for passive monitoring of past UV-B radiation. The evaluation process was summarised in the form of a series of questions at the end of Chapter 1, where each question has been addressed in turn by sequential chapters. The questions posed are reiterated below and findings of relevant chapters summarised in answer to the questions.

Can these biochemical monomers of sporopollenin be readily identified/quantified with current analytical instrumentation?

A key goal in the development of this geochemical proxy was the ability to access equivalent information locked within spores using different analytical techniques, namely obtaining, quickly and efficiently, a measure of the relative abundance of aromatic UV-absorbing compounds within the structure of sporopollenin. By comparing the chemical composition of sporopollenin characterised by pyrolysis-GC-MS and thermochemolysis-GC-MS analysis with the infrared absorbance spectra generated using FTIR microspectroscopy in Chapter 2, chemical features that are exclusive to the UV-B absorbing pigments can be isolated. Aromatic rings are found to be exclusive to the UV-B pigments, thus by isolating the infrared signal due to aromatic structures it is possible to track relative changes in abundance of the UV-B pigments. The power of FTIR microspectroscopy lies in the analytical speed, enabling sample throughput that far outweighs that of GC-MS techniques. In addition FTIR has the advantages of being inexpensive and completely non-destructive. The success of FTIR microspectroscopy is highlighted by the ability of FTIR to measure changes in sporopollenin

aromaticity across the known UV-B regimes experienced in the differing shade conditions of a forest canopy.

Does the chemical composition of spore/pollen exine vary in relation to UV-B flux?

Manipulation of UV-B under experimental conditions was intended to provide a calibration for the aromatic-based response to UV-B radiation. A positive trend was found to exist between UV-B flux to the spore-bearing plant and the aromatic content of the spores in Chapter 3. The associated errors, however, were large relative to the measured differences, reducing the statistical power of the analysis. The reasons for such large errors are unclear, but may be linked to the influence of additional environmental factors on plant growth such as precipitation, temperature and cloudiness, as well as changes in other wavelengths of radiation that were not measured. Whilst aromatic pigments have been shown to be the only compounds that are effective absorbers of UV-B radiation present in sporopollenin, it remains a possibility that other wavelength radiation may be exerting an influence. Two potential wavelengths ranges that may also be important are photosynthetically active radiation (PAR) and UV-A, but radiation at these wavelengths was not controlled within the experimental design. Kotilainen *et al.* (2008) demonstrate that the action spectra of radiation may play a role in influencing the abundance of metabolites in two species of tree, thus adding weight to the idea that other UV wavelengths need to be considered in conjunction with UV-B in future work.

Inter-annual variations in spore aromaticity were apparent when an entire year of experimentally grown samples were analysed as a single set. Compared against precipitation data, aromatic abundance in spores decreases with increases in summer precipitation. The explanation offered for this relationship is that the area under consideration falls within a rain shadow caused by the adjacent mountains; hence changes in precipitation are most likely

reflecting changes in frequency of cloudiness. Thus growing seasons (summer) with higher precipitation are more likely to also incur increased cloud cover and frequency of cloudy days, therefore reducing the surface UV-B flux experienced by the plants.

Can the proposed chemical proxy be successfully applied to determine past UV-B flux?

Natural variations in UV-B flux provide a more realistic assessment of the strength of the proposed geochemical proxy because there are no controls on other environmental factors that may play a role in determining spore aromaticity; therefore the aromatic signal obtained encompasses the UV-B environment in its entirety. UV-B radiation gradients are known to occur across latitudes and over changes in elevation, changing by approximately -2 % per 1° latitude polewards and ~ +15 % per 1000 m increase in elevation. Aromatic abundance measured using FTIR shows that spatial changes in UV-B flux result in a corresponding change in spore chemistry.

The development of a broad latitude calibration of spore chemistry versus stratospheric ozone abundance, where ozone measurements are thought to have a negative correlation with UV-B enables the extension back in time of this geochemical proxy, assuming that spore samples are available from known locations. By applying this calibration to samples collected from herbarium samples spanning the majority of the 20th century it has been possible to estimate stratospheric ozone over Greenland for the period 1906-1993. Features characteristic of volcanically related ozone depletion appear to occur in the reconstructed record of Greenland ozone during the 2-4 year period immediately after stratospherically significant eruptions. The record of stratospheric ozone over Greenland presented here is the first effort to reconstruct ozone using a geochemical proxy of this kind.

How far back in time can this proxy be reliably used?

It is possible that volcanic eruptions may be identifiable in the Greenland record presented in Chapter 4, but the evidence is not yet conclusive; a much more significant eruption would allow confidence to be placed in the Greenland reconstruction. In order to investigate an eruption of such unimaginable scale that will have undoubtedly had a global wide impact on atmospheric and terrestrial systems, it is necessary to go back to geological aged events. The Permo-Triassic boundary is known to have witnessed the greatest loss of biodiversity in Earth's history, attributed in part to the eruption of the Siberian Traps. Whilst spore sample exist on either side of the Permo-Triassic boundary, the chemical signature of the spores appears to be substantially different to that of modern-day spores, critically, the aromatic signal present in modern/recent spores is no longer present in fossil samples. Without a measurable aromatic component in fossil sporopollenin, it is not possible to apply the geochemical proxy presented here. This finding marks an upper boundary to the applicability of this proxy given the well preserved morphological features of the spores analysed. In order to extract information from fossilised spores, organic matter must be of a very low maturity in order to ensure success, for example, based on the analyses presented in Chapter 6 material of maturity equivalent to ~ 250 Ma in age is beyond current capabilities, and in fact most likely over-estimates the potential useful timeframe of this proxy by a substantial amount.

Spores present what appears to be, an ideal opportunity to observe the UV-B regime of the past because the excellent preservation of spores suggests minimal chemical processes have taken place that may lead to alterations of the spore chemistry. However, this is misleading; despite distinguishable morphological features common to fresh spores, spore chemistry in artificially matured spores differ considerable from their modern-day, unaltered counterparts. Tracking the chemical changes through various stages of simulated maturity revealed that two key changes occur. Firstly, sporopollenin undergoes defunctionalisation whereby all

functional groups are stripped out of the biopolymer, including oxygen containing groups (carbonyls, hydroxyls) and aromatic ring structures. Secondly, the remaining components of sporopollenin, which are mostly unbranched aliphatic compounds, repolymerise to form a new polymer with a highly aliphatic nature. Repolymerisation of these aliphatic components is also evident, as shown by the shortening of carbon chain length of *n*-alkanes/alkenes in samples of greater maturity.

As a result of defunctionalisation and repolymerisation of sporopollenin components, a new polymer is formed, but because it has been formed by geological processes rather than biological processes, it is now a geopolymer. In a natural setting the reconfiguration of sporopollenin would have occurred in an entirely open system where free exchange of material with the surrounding sediment would have been possible, as has been proposed as an important source of resistant aliphatic geopolymers in the past (Gupta *et al.*, 2007). Here it is shown that an open system is not necessary in order to form an aliphatic geopolymer, providing an alternative route by which highly resistant geopolymers may form. It is likely that the trends in alteration observed in sporopollenin are common to other biopolymers that are incorporated into sediments. Thus, other biopolymers will also undergo defunctionalisation and repolymerisation processes, including a significant loss of oxygen-containing groups, a relative increase in aliphatic content and shift towards a more uniform composition with respect to class of monomers comprising the geopolymer.

7.2 Future work

7.2.1 Technical developments

Considering the microscopic analytical capability of FTIR microspectroscopy, there is potential for further technique development, in particular the possibility of performing analysis on individual spores. In the present work groups of between six and twelve spores

have been analysed as a single datum. Analysis on single spores would allow an alternative method of quantification of the various absorbance bands by enabling functional group abundance to be reported on a 'per spore' basis.

7.2.2 Species-specific chemical variability

Lycopodium are abundant throughout the geological record and have a very wide geographical distribution in the present day, however, palynological research covers a great variety of genera/species. The wealth of palynological resources available could provide the opportunity to develop this proxy for UV-B to span multiple species, thus increasing the applicability and reliability of the proxy substantially and investigate any chemical variability that may exist between species.

7.2.3 Diagenetic alteration of biopolymers

Sporopollenin has been used here as a model biopolymer in order to assess the impact of diagenetic processes on spore wall chemistry. Other studies have also already investigated decomposition of other naturally occurring biopolymers, but the degradation techniques and experimental set-ups vary from study to study. In order to generate a fully generalised scheme of the chemical changes observed in natural biopolymers, a range of simultaneous artificial maturation experiments should be conducted on a number of biopolymers (chitin, cutin, lignin suberin, algaenan). Trends likely to be observed include reduction in oxygen-containing functional groups, increase in aliphatic components even when none are present in the original material, and a reduction in aromatic content.

7.2.4 Other changing environmental parameters

As demonstrated in Chapters 4 and 5, factors other than stratospheric ozone can modulate the UV-B flux experienced at the surface. This presents the opportunity to apply the proxy developed here to investigate other environmental/climatic parameters by changing the variable factor. One such environmental factor is cloudiness. Isolation of UV-B changes due to cloud cover may be possible by investigating a region of variable cloudiness over time, in a relatively ozone stable global position. Equatorial and tropical regions offer relatively stable ozone columns, therefore are a prime region to target for studying other UV-B climatic parameters.

7.2.5 Constraining an applicable time-frame

A final avenue to be explored with this technique is the definition of the time frame in which it may be applied. Clearly the Permo-Triassic boundary is beyond the scope of the technique, however, thermal maturation studies also presented here suggest that the signal may be retained under considerable diagenetic conditions (up to ~ 200 °C experimental temperature). Retention of the aromatic proxy signal at milder levels of diagenesis is promising because it is almost certain that the proxy will remain applicable on the order of 10^3 to 10^5 years, enabling investigation of known environmental shifts such as interactions between UV-B flux and glacial-interglacial periods. The potential exists for the proxy to remain viable for millions of years, assuming mild enough burial conditions are prevalent.

7.3 References

Gupta, N.S., Briggs, D.E.G., Collinson, M.E., Evershed, R.P., Michels, R. & Pancost, R.D. (2007) Molecular preservation of plant material and insect cuticles from the Oligocene Enspel Formation, Germany. Evidence against derivation of aliphatic polymer from sediment. *Organic Geochemistry* **38**, 404-418.

Kotilainen, T., Tegelberg, R., Julkunen-Titto, R., Lindfors, A. & Aphalo, P.J. (2008) Metabolite specific effect of solar UV-A and UV-B on alder and birch leaf phenolics. *Global Change Biology* **14**, 1-11.

8 Appendices

8.1 Appendix A

8.1.1 FTIR analysis to investigate spore wall chemistry

8.1.1.1 What is FTIR?

Fourier Transform Infrared (FTIR) spectroscopy is commonly used to determine chemical functionality (which functional groups are present) and broad structural features of molecules. Chemical bonds absorb energy in the form of photons and will begin to vibrate if the frequency of the absorbed photon matches the frequency of one of the molecule vibrational modes. As a result of this energy absorption, the chemical bond is raised to a higher vibrational energy level. Bond vibrational modes can be grouped into two types; stretching, and deformation vibrations. Stretching modes manifest as elongation and shrinking of bonds, whilst deformation modes can occur as various scissoring, wagging, twisting and rocking motions. The wavelength of infrared energy absorbed by a bond is determined by three factors: reduced mass across the bond, strength of the bond, and mode of vibration, where reduced mass accounts for the mass of the atoms at each end of the bond and bond strength is represented as the bond force constant, k. Interplay between these three factors and interactions between chemical bonds at adjacent positions within a molecule result in chemical bonds absorbing at characteristic wavebands of the IR spectrum. At the most basic level, infrared spectroscopy allows the identification of chemical bonds within a sample; however, much more information can be gleaned from IR spectra. An idea of molecular structure can be obtained, for example, by looking for bonds in typical skeletal group such as CH_2 groups in a hydrocarbon chain, or bonds that typically form bridges between potentially independent monomers, such as ester and ether linkages, identifiable by the occurrence of a carbonyl (C=O) group. The power of FTIR is held in the characteristic absorbencies of chemical

bonds in particular functional group environments, which leads to the ability to 'fingerprint' molecules based on their IR spectra. Final output from FTIR spectroscopy is a suite of spectra that can be mathematically analysed to determine differences in relative abundance of specific functional groups or chemical bonds and allows certain groups, once characterised, to be tracked.

The underlying principle of FTIR analysis is that a known spectrum of IR radiation is input to the sample, thus any wavelengths that have been reduced or removed from in the spectrum when the IR beam reaches the detector must be due to absorption by chemical bonds within the sample. The proportion of IR radiation absorbed is essentially proportional to the relative abundance of chemical bond/group present within the sample; hence if a particular spectral band increases in intensity across a suite of samples it is a fair interpretation that the functional group that absorbs in that region is increasing in abundance. A caveat to be considered when tracking changes in intensity of spectral bands is that not all functional groups/chemical bonds absorb IR radiation to the same degree; some bonds are strong absorbers of energy, whilst others are weak absorbers.

FTIR spectra report either the proportion of IR radiation transmitted through the sample (in percentage) indicating the regions in which less IR radiation reaches the detector by values < 100 %. Alternatively the signal is converted instantaneously by OMNIC software to absorbance units are represented as peaks showing the spectral regions that are absorbed. Absorbance is the chosen format for FTIR spectra within this thesis for ease of visualisation of changes in absorbance where absorbance bands are represented as spectral peaks, thus a larger peak demonstrates greater abundance the corresponding functional group.

Coupling FTIR spectroscopy with microscopy enables an analytical technique that operates in the same way as FTIR but with the added advantage that the microscope magnifies the

infrared beam for analysis, allowing greater accuracy in beam positioning and substantially smaller samples sizes to be investigated. Sample size can be reduced from ~0.1-0.2 g of sample used in traditional FTIR analysis down to individual grains or groups of spores (between ~6 and ~20) covering an area of up to 100 x 100 μm.

FTIR microspectroscopic analysis was conducted using a Thermo Nicolet Nexus FTIR bench unit, fitted with a KBr beam splitter and a MCTA detector. To alleviate atmospheric interference signals within spectra the entire system including microscope stage was purged with air of constant composition (CO_2 and H_2O) generated by a purge unit. Data processing of resultant spectra was performed using OMNIC software (Thermo Fisher Scientific) and spectral peak measurements using TQ Analyst (Thermo Fisher Scientific).

In order to isolate the IR spectrum obtained from an individual sample it is necessary to collect a background spectrum, which is then automatically removed from the sample spectrum by the OMNIC software. A background spectrum is collected by running the FTIR without a sample within the IR beam, thus records only information about the interference of ambient air with the IR beam. Background spectra are collected in different ways, and at different time intervals, dependent upon the particular technique being used (See below).

Two sub-techniques of FTIR were adopted during this project: transmission FTIR (t-FTIR) and Attenuated Total Reflectance FTIR (ATR-FTIR). The choice of technique used was determined by the type, size and opacity of the sample under investigation.

8.1.1.2 Transmission FTIR

8.1.1.2.1 Parameter selection

A Continuum IR microscope operating with a 15x IR cassegrain reflachromat objective lens is attached to the FTIR bench unit, through which the IR beam passes. The microscope has an adjustable aperture for the IR beam, with a usable range of ~10 x ~10 μm, up to 100 x 100 μm. Optimal signal to noise is achieved using larger aperture sizes, although this is not always possible and is dependent upon sample size. In all analyses presented in this thesis an aperture of 100 x 100 μm was used with as much of the aperture area filled with spore samples. User defined parameters are listed in Table 8.1 below.

Table 8.1 Parameter set-up for transmission FTIR analysis.

Wavenumber range	4000 – 650 cm-1
Resolution	4 wavenumbers
Number of scans (sample & background)	500
Interferogram mirror velocity	1.8988 cm s-1
Phase correction	Mertz
Apodization	Hepp-Genzel

Background spectra were collected immediately after each sample to ensure that any minor changes in background air composition were compensated for by the background correction process. The number of scans used for the analyses was chosen based on the need for high quality spectra, whilst maintaining a high throughput of samples. Signal-to-noise ratios of blank spectra were compared to find the optimum quality/time efficient setting (Figure 8.1), where blank spectra are obtained using identical set-ups with no samples placed under the microscope for both sample and background spectra. Five hundred scans per analysis were chosen because the signal-to-noise ratio was sufficiently low whilst remaining a rapid technique and any further increases in scan number did not result in a substantially improved signal-to-noise ratio without incurring a great increase in analysis duration.

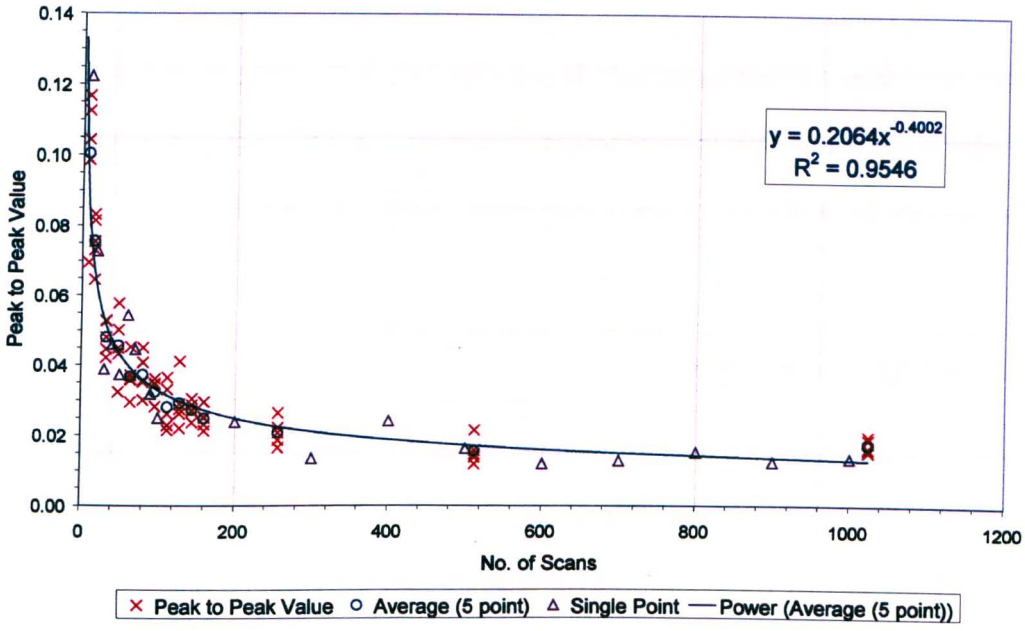

Figure 8.1 Plot of signal-to-noise (peak to peak) as a function of number of scans. Increasing scan number reduces the signal-to-noise, with progressively greater increases of number of scans required in order to return equivalent improvements in signal-to-noise ratio.

The choice of spectral resolution is determined by sample type and detail of spectra required. Higher resolution enables greater definition of infrared absorbance bands within the spectra, thus allowing individual bands to be identified that are closely spaced together, however, greater resolution can increase signal-to-noise ratios and result in longer collection times. Generally, the highest resolutions (0.25-0.5 wavenumbers) are used for analysis of gas samples, resolutions in the range 1-2 wavenumbers are used for liquid samples, and resolutions of 4-32 wavenumbers for solid samples, where a resolution of 4 wavenumbers results in data spacing of one point in every four wavenumbers.

In all transmission FTIR analyses presented within this thesis samples are placed on top of sodium chloride (NaCl) discs to allow easy mounting and manipulation; NaCl is the chosen material for these disks because it does not absorb in the infrared spectral range.

The basis criteria for analysis using FTIR microspectroscopy are that samples must be small enough to attain a sensible focus beneath the microscope and that enough infrared beam can pass through the sample for sufficient beam energy to reach the detector.

8.1.1.2.2 Spectral analysis

All FTIR spectra generated were analysed using TQ Analyst software (Thermo Fisher Scientific), which calculates intensity of absorbance bands *via* an automated process. The automated spectral analysis is a two-step procedure; first, the spectral bands, or as presented in this thesis peaks, are manually defined by the operator using peak height and/or peak area tools within OMNIC. A baseline is defined beneath the peak under investigation using baseline anchor points that remain at fixed wavenumbers throughout all spectra analysed, as presented in Table 8.2, where either peak area or maximum peak height are quoted in relation to the baseline.

Table 8.2 Baseline definition parameters for automated spectral analysis. x_{max} and x_{min} define the upper and lower points along the x-axis (wavenumber) where the baseline anchor points occur. Peak max. region is the region within which the peak of interest occurs along the x-axis.

Peak	Baseline anchor points		Peak max. region (cm^{-1})
	x_{max} (cm^{-1})	x_{min} (cm^{-1})	
OH (3300 cm^{-1})	3999.71	2237.06	3354.22 – 3143.45
Aromatic (1520 cm^{-1})	1581.37	1488.80	1525.44 – 1515.80

The second step is to define the region within which the maximum peak height or full width at half height (FWHH) occurs (Table 8.2). IR absorbance peaks are liable to small variations in peak position due to slight differences in chemistry between samples and instrumental effects, thus it is important to define a region for TQ Analyst to search within rather than a fixed position. In the case of measuring peak height a region is selected that will contain the

maximum height of only the peak of interest. Peak area measurements used fixed region points because the region anchor points defined the FWHH rather than a maximum value. Once manually defined these parameters are used by TQ Analyst to perform identical analysis on all spectra input. Such an automated method is preferred over a manual method because the analysis is free of any operator subjectivity.

To compare values obtained using peak height and peak area methods spectra collected from the samples discussed in Chapter 2 were analysed as a test dataset. The results of this comparison show that there is no discernable difference between the outputs from either peak height or peak area (Figure 8.2), resulting in a positive linear relationship. On the basis of finding no difference in quality of data the peak height method was selected for all further analysis of spectra due to ease of method set-up and time efficiency when performing the analysis.

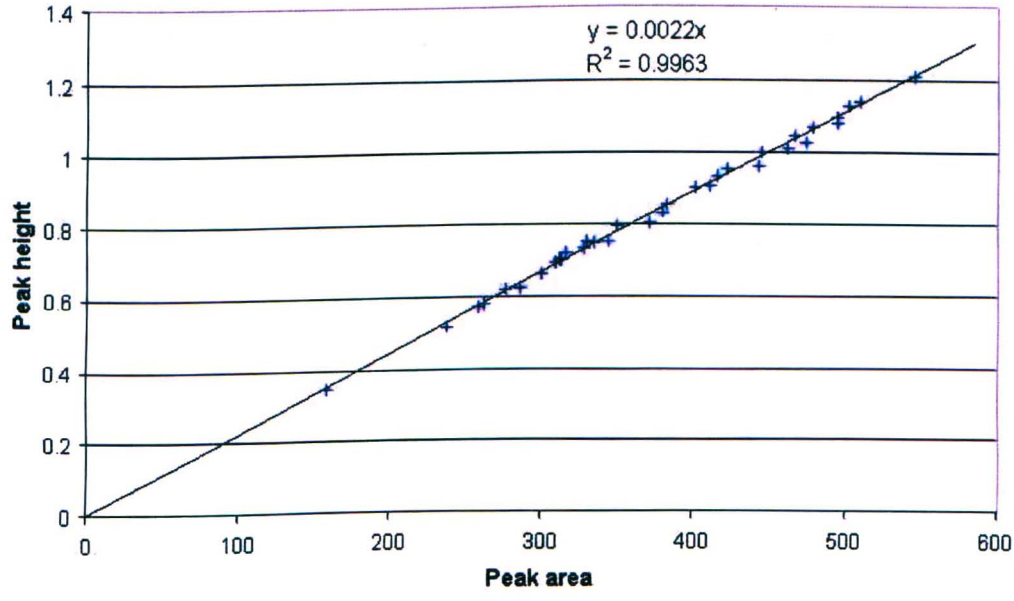

Figure 8.2 Linear relationship between peak area and peak height as measured by TQ Analyst.

8.1.1.2.3 Data analysis

In order to ensure data collected from spectra were reliable and robust, reproducibility was tested by repeated measurements. Statistical analysis performed on repeat analyses (n = 110) of the same group of spores reveals that measurement both OH and aromatic absorbance bands return an essentially normal distribution (Figure 8.3 and Table 8.3).

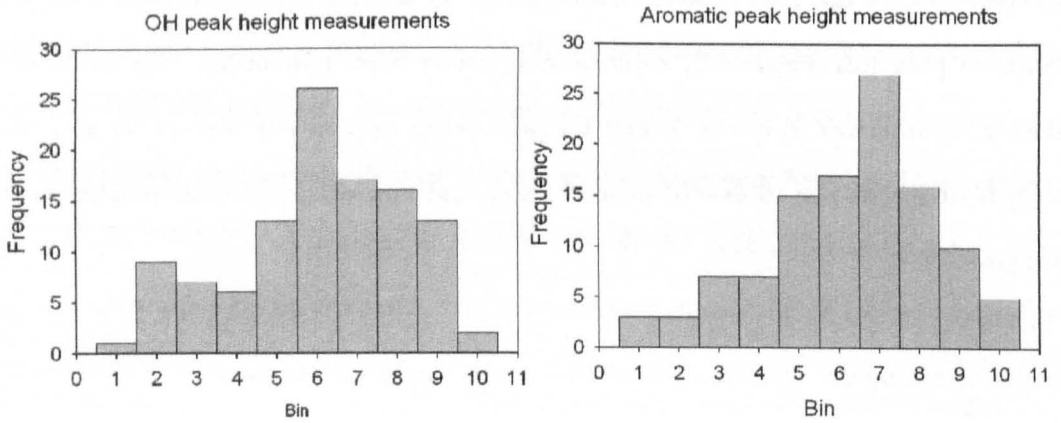

Figure 8.3 Distribution of OH and Aromatic measurements made by TQ Analyst.

Table 8.3 Descriptive statistics for repeat measurements of OH and aromatic absorbance bands.

	OH (3300 cm^{-1})	Aromatic (1520 cm^{-1})
Mean	0.817	0.872
Min	0.811	0.819
Max	0.821	0.911
2σ	0.004	0.040
n	110	110
Kurtosis	-.0198	-0.099
Skewness	-0.549	-0.531

Thus, it is reasonable to assume that all other samples will show a normal distribution in measurements and can be treated as such, as a result five repeats measurements performed on

randomly selected groups of spores is deemed appropriate to obtain a representative sample of the total population.

8.1.1.3 ATR-FTIR

Artificially matured spores proved to be too opaque for analysis using FTIR microspectroscopy; therefore an alternative technique was required to access the same information. Attenuated total reflectance (ATR)-FTIR provides the opportunity to obtain IR spectra from samples that do not allow sufficient transmission of the IR beam. Table 8.4 gives details of the analytical parameters used for ATR-FTIR analysis.

Table 8.4 Parameter set-up for ATR-FTIR analysis.

Wavenumber range	4000 – 650 cm-1
Resolution	4 wavenumbers
Number of scans (sample & background)	256
Interferogram mirror velocity	1.8988 cm s-1
Phase correction	Mertz
Apodization	Hepp-Genzel

ATR-FTIR requires a larger quantity of sample for each individual analysis to be performed, however, this increase if total sample mass gives greater precision at a lower number of scans. For ATR-FTIR analyses, a total of three repeat measurements were sufficient to obtain reliable results.

8.1.1.4 GC-MS

GC-MS analysis was carried out using an Agilent Technology 6890 gas chromatograph coupled to a 5973 mass spectrometer. The GC injector was held at 270 °C and operated in split mode (10:1) with a column flow rate of 1.1 ml/min. Separation was performed on a BPX5 column (SGE; 30 m length, 0.25 mm internal diameter and 0.25 μm film thickness). The GC oven temperature was held for 1 min at 50 °C and ramped to 310 °C at a rate of 5 °C

min $^{-1}$ and held at this for 9 min. Mass spectra were acquired in electron impact mode (70 eV) from 50 to 500 amu.

8.1.1.5 Py-GC-MS

Heated spores were placed in quartz pyrolysis tubes, previously cleaned by roasting in air to 450 °C and plugged at either end with quartz wool. Samples were pyrolysed using a CDS Pyroprobe 1000 (CDS Analytical) fitted with a 1500 valve interface held at 250 °C and coupled to a GC-MS. Following heating to 610 °C at a rate of 20 °C ms $^{-1}$ the sample was held at this temperature for 15 s in a flow of helium. GC-MS analysis was as for the solvent extracts.

8.1.1.6 Thermochemolysis-GC-MS

Heated spores were placed in quartz pyrolysis tubes, which were plugged with quartz wool at each end. The loaded sample then had 10 µl of 25% tetramethylammonium hydroxide (TMAH) in methanol added and the methanol allowed to evaporate for 12 hours. Samples were heated using a CDS Pyroprobe 1000 fitted with a 1500 valve interface held at 250 °C (CDS Analytical, Oxford, PA) and coupled to a GC-MS. Following heating to 300 °C at a rate of 20 °C ms $^{-1}$ the sample was held at this temperature for 15 s in a flow of helium. GC-MS conditions were as for the solvent extract and Py-GC-MS except the GC oven temperature program was 10 min at 35 °C and ramped to 310 °C at a rate of 5 °C min $^{-1}$ and held at this for 9 min.

8.2 Appendix B

8.2.1 Precipitation in the Abisko valley and surrounding region.

Table 8.5 Annual precipitation in the Abisko valley and surrounding region used in Figure 3.1.

Location	Altitude	Longitude	Latitude	ppt. (mm)	Source
Andenes	10	16 09	69 18	1060	Kirchhefer *et al.* (2001)
Kleiva	23	15 17	68 39	1397	
Borkenes	36	16 11	68 46	820	
Gibostad	12	18 04	69 21	900	
Tromsø	100	18 56	69 39	1031	
Riksgränsen	508	18 08	68 25	1001	Hammarlund *et al.* (2002)
Katterjåkk	500	18 10	68 25	848	
Abisko	388	18 42	68 20	322	
Torneträsk	393	19 43	68 13	472	
Björkliden	474	18 40	68 24	652	Ridefelt & Boelhouwers (2006)
Tarfala Research Station	1130	18 35	67 55	950	Hock & Holmgren (1996)
Kiruna	500	20 13	67 51	498	Dove & Boustead (2001)
Vouskkujárvi	348	19 06	68 20	308	Bigler *et al.* (2002)
Narvik stn 84790	23	17 33	68 25	855	Meteorologisk instituut
Ankenes stn 84450	99	17 22	68 25	862	
Bjørnfjell stn 84900	550	18 04	68 25	940	
Skjomen-Slettjord stn 84170	6	17 19	68 17	680	
Svolvær (Lofoten Islands)	10	14 31	68 16	1500	Wikipedia

8.2.2 References

Bigler et al. (2002) The Holocene 12(4), 481-496

Dove & Boustead (2001) Proceedings of the 2001 Automotive and Transportation Technology Congress and Exhibition (ATTCE), Barcelona, Spain, 1st-3rd Ocotober 2001, pub. SAE v.8, pp.1-4 "A new approach to acidification in LCA"

Hammarlund et al. (2002) The Holocene, 12(3), 339-351

Hock & Holmgren (1996) Geografiska Annaler series A, 78(2-3) 121-131

Kirchhefer et al. (2001) The Holocene, 11(1) 41-52

Meteorologisk instituut met.no (http://met.no/) Date accessed: 13/04/2007

Ridefelt & Boelhouwers (2006) Permafrost and Periglacial Processes 17, 253-266

Wikipedia (http://en.wikipedia.org/wiki/Geography_of_Norway) Date accessed: 13/04/2007

8.3 Appendix C

8.3.1 Modelling UV-B irradiance at Abisko-Naturvetenskapliga using photosynthetically active radiation.

UV-B measurements are unavailable for the experimental growing period of 2004-2006 from ANS (Figure 8.3). In order to provide a sub-seasonal resolution dataset PAR was used as a proxy from which to estimate UV-B flux. Two sets of data were used to reconstruct UV-B flux; the first are daily PAR measurements recorded by the automated weather station based at ANS, and the second are PAR and UV-B measurements collected as part of the ELDONET project with an instrument based at ANS (Häder *et al.*, 2007).

The ELDONET instrument has been recording UV-B and PAR at ANS for eight years (Häder *et al.*, 2007) (up to 2006), and has been in continuous operation for all three years of the growth experiment conducted at ANS (Chapter 3). Visual inspection of the UV-B data collected during the period 2004-2006 shows that 2005 and 2006 have incomplete or irregular records (Figure 8.4); data collected in the PAR waveband also show an identical pattern suggesting that there were instrumental problems affecting both 2005 and 2006 datasets. However, data collected in 2004 show a bell-shaped, or even Gaussian distribution throughout the year, as would be expected given the daylight regime in this arctic region (Figure 8.4). As a result, only data collected in 2004 are reliable measures of the UV-B flux during any of the experimental years under consideration. This poses a problem because knowledge of UV-B flux during 2005 and 2006 is also essential to understand the chemical response for these years within the growth experiment. In order to address this problem PAR was used to estimate UV-B flux. It should highlighted from the outset that this is not an ideal approach because UV-B and PAR can behave independently of one another and are altered by environmental factors in different ways, but no other information concerning UV-B for this period exists. As mentioned in Chapter 3, the ANS UV-B instrument based within the automatic

meteorological station was out of operation for the period 2004-2006 due to failure and subsequent repair and calibration.

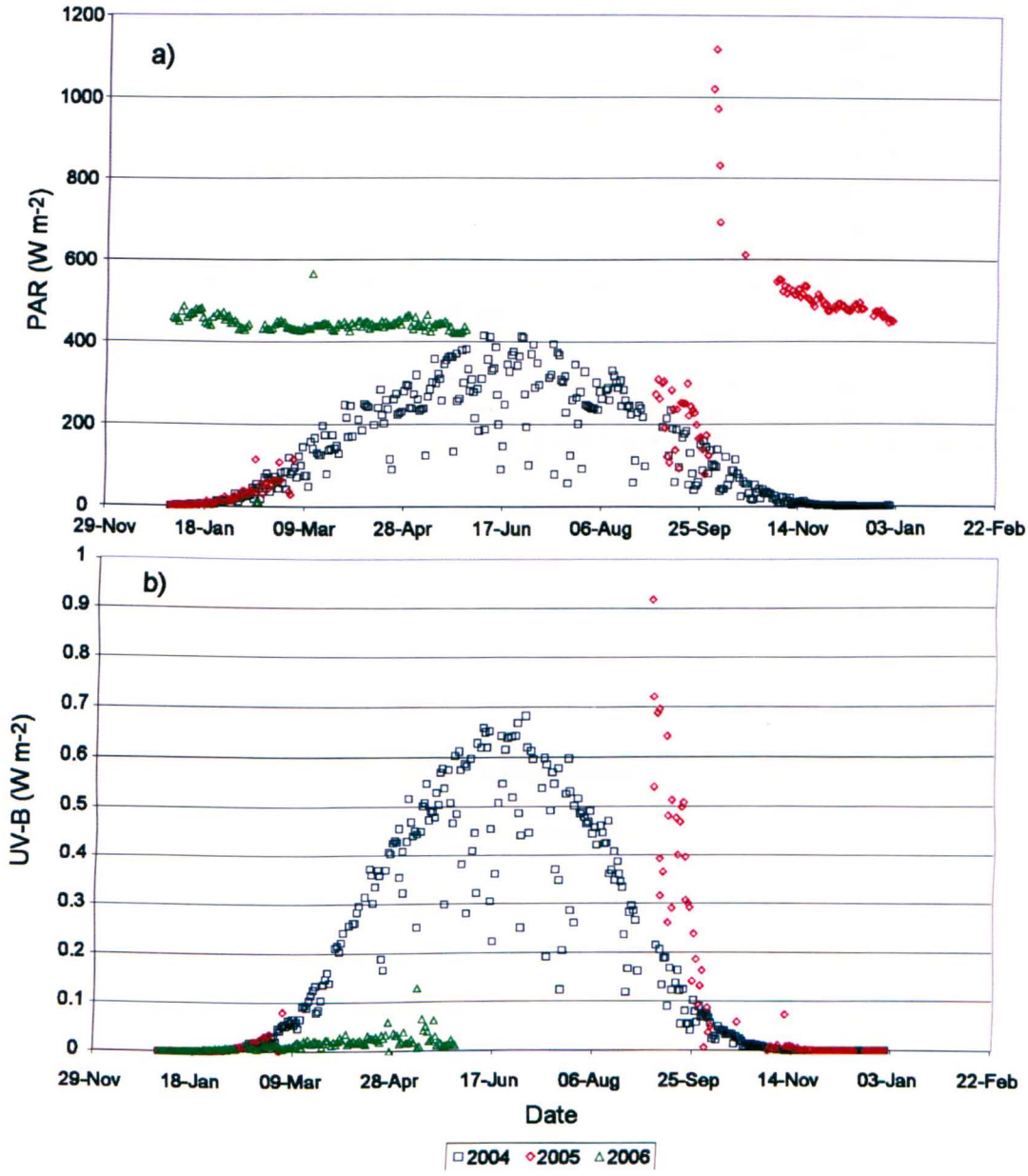

Figure 8.4 ELDONET measurements of a) PAR, and b) UV-B for 2004-2006.

Comparison of UV-B and PAR data collected by ELDONET reveals a relatively strong positive relationship (Figure 8.5) suggesting that an acceptable estimate of UV-B can be obtained from PAR records.

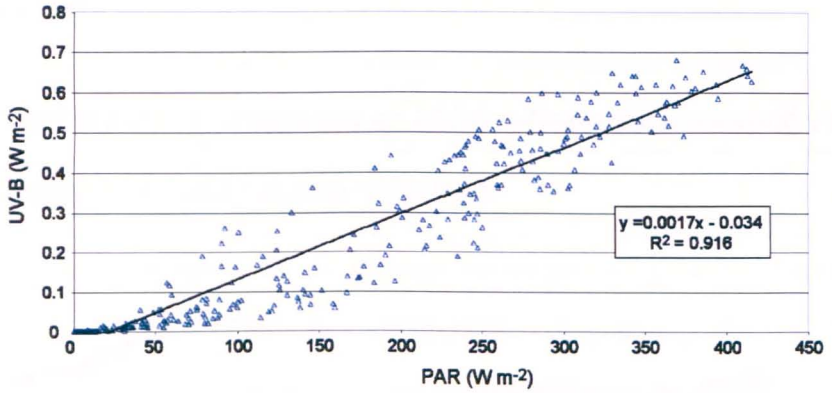

Figure 8.5 Linear regression of ELDONET UV-B and PAR flux. Data recorded by the ELDONET instrument during 2004 show a strong positive relationship (Figure 8.4). Pearson correlation coefficient = 0.957 at the 0.01 significance level; F = 3664.161, *p* = <0.01.

As demonstrated in Figure 8.4, only a single year (2004) of usable UV-B and PAR data are available from the ELDONET instrument however, ANS maintains continuous monitoring program of PAR that spans the period 1985-present, including years 2004-2006 (Figure 8.6). Comparison of UV-B data from ELDONET and PAR data from the ANS meteorological station provides further evidence of a reasonable relationship between PAR and UV-B (Figure 8.7) that may be exploited to reconstruct UV-B flux for the duration of the growth experiment. Figure 8.7 demonstrates that data from different monitoring networks can be cross-compared.

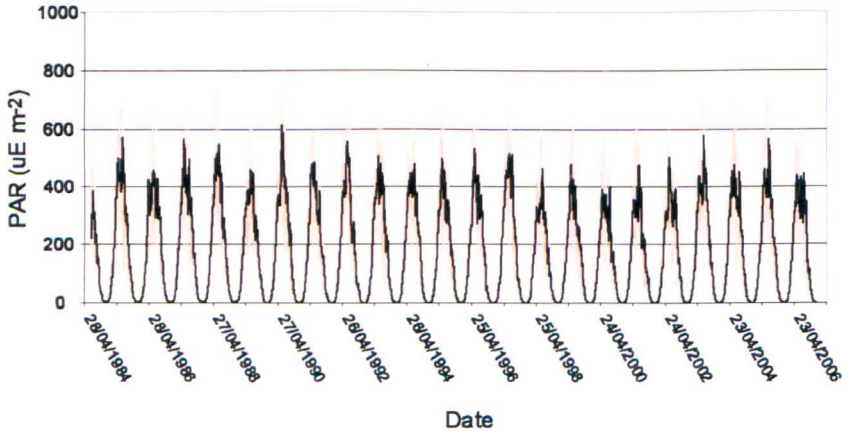

Figure 8.6 Continuous record of PAR at ANS for the period 1984-present. Black line is 14-day running mean; orange line is daily data to demonstrate range of variability.

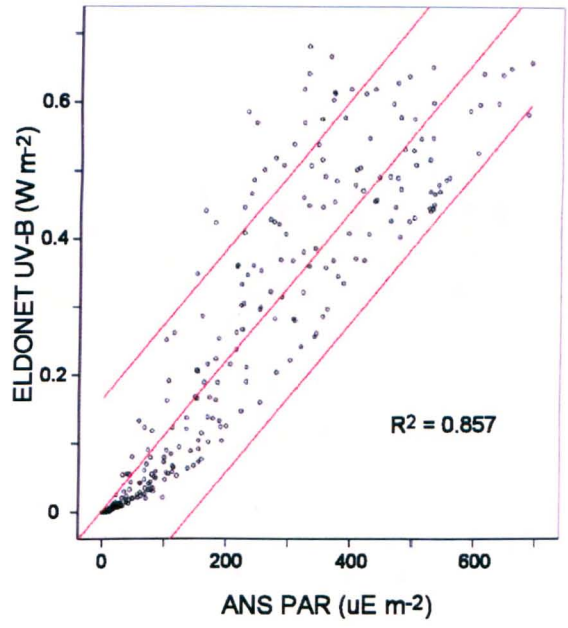

Figure 8.7 Scatter plot of ELDONET UV-B and ANS PAR data showing linear relationship for the year 2004. 95% confidence limits are shown for reference. Pearson correlation coefficient = 0.925 at the 0.01 significance level; F = 2023.622, *p* = <0.01.

Using the slope equation derived from the linear trend line of Figure 8.7 it is possible to reconstruct UV-B flux from the ANS PAR record following the relationship shown. The equation is of the form:

Equation 8.1 Slope equation derived from Figure 8.7.

$y = 0.0011016709x + 0.0028358308$

where x is ANS PAR for the period 1985-2006 and y is the resultant reconstructed UV-B (UV-Bmod). The output from this simple model is shown in Figure 8.8 with a 14-day running average to remove the influence of any short-term meteorological phenomena that may obscure results.

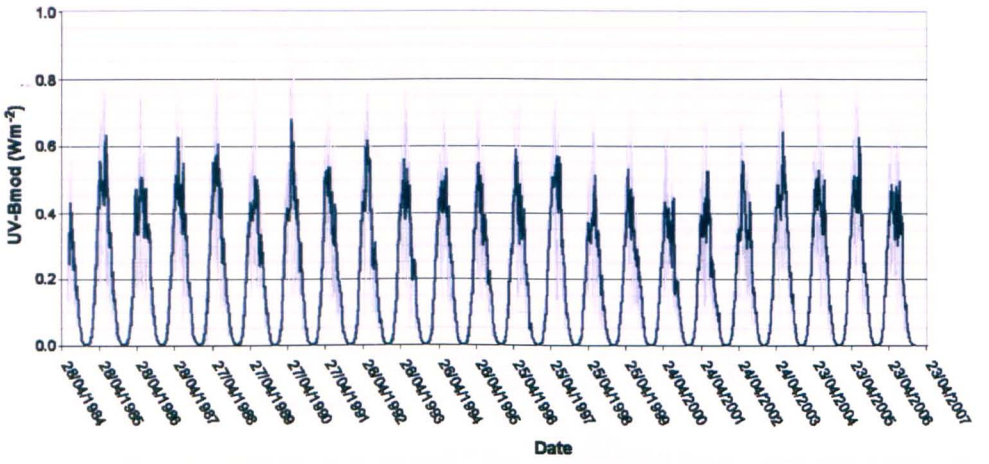

Figure 8.8 Reconstruction of UV-B flux using ANS PAR data for the period 1984-2007. Light grey line are daily data, dark blue trend line is a 14-day running mean.

Retrospective comparison of reconstructed UV-B against the measured ELDONET UV-B for 2004 returns a reasonable fit, suggesting that the model presents an adequate estimation of measured UV-B flux for the period considered (Figure 8.9). The linear trend line of Figure 8.8 is close to a 1:1 ratio, with a reasonably strong R^2 value (0.846). This modelling approach enables investigation of UV-B flux on sub-seasonal timescales that was not possible using previously published modelling data (Lindfors *et al.*, 2006) whilst providing a reasonable fit with the Lindfors *et al.* data (Figure 8.10).

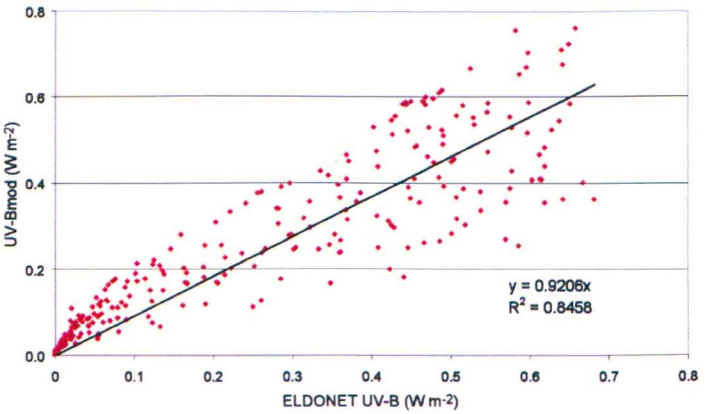

Figure 8.9 Comparison of measured UV-B (ELDONET) with UV-B flux reconstructed from PAR data (UV-Bmod). Linear trend line is forced through the origin. Pearson correlation coefficient = 0.925 at the 0.01 significance level; F = 2023.608, p = <0.01.

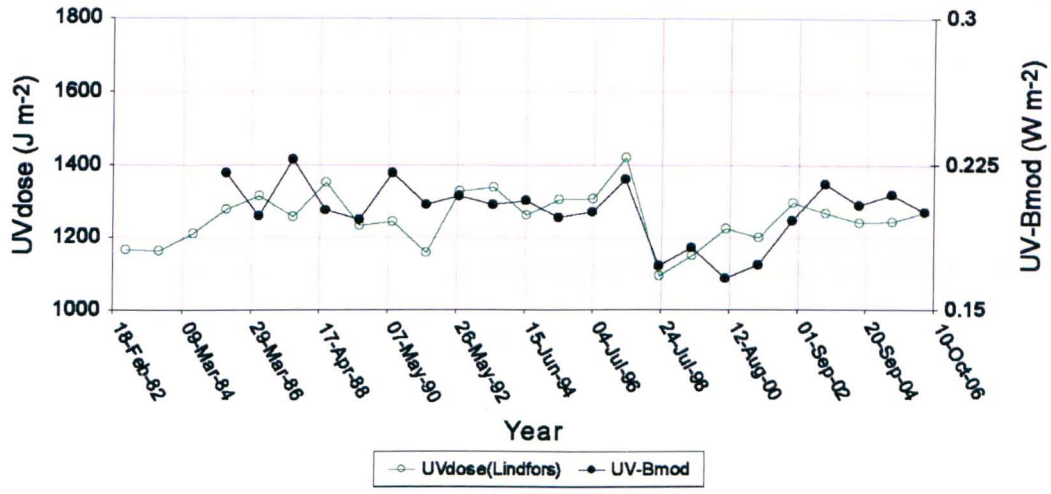

Figure 8.10 Comparison of UV-Bmod reconstruction with Uvdose reconstruction of Lindfors *et al.* (2006).

8.4 Appendix D

8.4.1 Growing season total ozone column calculations, Abisko.

Häder *et al.* (2007) obtain a mean value of 333 D.U. for total ozone column for the period 1997-2005, where a total of 58 % of days were included in their analysis after non-clear sky days were removed. Using freely available data from the various satellite-borne TOMS instruments monthly mean total ozone column values above ANS were calculated for eight months of the year. The remaining four months of the year occur during the winter; 24-hour darkness and the angle of incidence of the satellite prevent detection of ozone during this period. Daily total ozone column data throughout the period 1997-2005 were reduced to monthly mean values (March to October) (Table 8.5).

Table 8.6 Monthly mean total ozone column values derived from TOMS instruments for the area around ANS.

Month	1997	1998	1999	2000	2001	2002	2003	2004	2005
January	0	0	0	0	0	0	0	0	0
February	0	0	0	0	0	0	0	0	0
March	352	378	448	345	442	405	331	369	343
April	325	416	395	370	407	365	382	346	406
May	369	390	382	341	365	341	384	374	380
June	340	350	332	352	343	331	349	353	347
July	299	331	323	308	321	310	296	303	316
August	281	319	313	291	300	278	286	283	291
September	283	272	269	265	276	262	277	266	293
October	283	275	274	262	268	265	262	240	260
November	0	0	0	0	0	0	0	0	0
December	0	0	0	0	0	0	0	0	0
Annual Mean	317	341	342	317	340	320	321	317	330
Growing season mean	314	332	324	311	321	304	318	316	325
Min	281	272	269	262	268	262	262	240	260
Max	369	416	448	370	442	405	384	374	406
% change over year	80.4%	72.8%	61.2%	75.9%	60.6%	65.4%	79.2%	65.0%	75.8%
Overall annual mean	327								
Overall growing season mean	319								

The final value of 327 D.U. for the overall total ozone column depth for the period 1997-2005 is in good agreement with that of Häder *et al.* (2007), with the advantage that these data presented here allow investigation of monthly means rather than seasonal or annual means.